Hyaluronic acid 3D microenvironments for diabetes treatment

Fernanda Zamboni

Publication date

01-01-2021

Document Version
1

Hyaluronic Acid 3D Microenvironments for Diabetes Treatment

Author

Fernanda Zamboni

A THESIS IS SUBMITTED FOR THE DEGREE OF DOCTOR OF PHILOSOPHY

AT

SCHOOL OF ENGINEERING, UNIVERSITY OF LIMERICK, IRELAND

SUPERVISOR

Dr Maurice N. Collins

Stokes Laboratories, School of Engineering, Bernal Institute, University of Limerick, Ireland

Postgraduate Scholarship 2015, Irish Research Council

Submitted to the University of Limerick, Ireland, 10th May 2021

Declaration

I declare the substance of this dissertation is the original work of the author and due reference and acknowledgment has been made, where necessary, to the work of others.

No part of this dissertation has been submitted in candidature for any previous degree.

_____

Fernanda Zamboni

Abstract

Diabetes mellitus is characterized by hyperglycaemia. The origin of type 1 diabetes mellitus (T1DM) arises from loss of pancreatic β cells in response to an autoimmune reaction. This results in a state of absolute insulin deficiency. The current state of the art research in T1DM involves developing a strategy to protect pancreatic β cells from immune system attack while restoring physiological insulin responsiveness to blood glucose variations for transplantation. This thesis aims to develop a new immunoprotective microenvironment based on hyaluronic acid (HA) for insulin-producing cells to treat T1DM. Therefore, biomaterial development is fundamental to the success of creating an immunoprotective microenvironment. This project investigates new routes to chemically modify and crosslink HA. Bis(β-isocyanatoethyl) disulphide (BIED) has been synthesised to crosslink HA of low and high molecular weight (0.1 and 1.2 MDa, respectively) through the formation of urethane bonds. Chemical, physical, mechanical, and biological characterization of the HA hydrogels were performed. Results show that 0.1 MDa gels have higher crosslinking densities and consequently, higher tensile and storage loss moduli. Both high and low molecular weight gels show biocompatibility. Gels maintain cell viability and they do not incite activation of the immune system as observed by low GM-CSF and TNFα cytokine secretion. Moreover, results show that 1.2 MDa gels have increased bacteriostatic activity against *Staphylococcus aureus*. Subsequently, reduction of the disulphide bond of these hydrogels resulted in new HA derivates bearing thiol groups and pyridine groups. A novel cell encapsulation technique was then developed, utilising the latest cell surface modification methodologies, and conformal multilayer deposition of these HA derivates via a disulphide exchange mechanism in physiological conditions. Pancreatic beta cells from the MIN-6 lineage were encapsulated and displayed normal function with improved immunoprotection *in vitro*. Female mice from the black 6 (C57BL/6) strain were induced with diabetes by five consecutive low dose streptozotocin (STZ) injections. Following diabetes induction, mice were transplanted with surface engineered MIN-6 and encapsulated MIN-6 cells under the kidney capsule. Due to sex dimorphism and hormonal variances, female mice showed to be more resistant to the inducing effects of STZ, where hyperglycaemia was achieved in 48% of the cohort. Moreover, single-cell encapsulation

did not revert hyperglycaemia after transplantation due to the lack of cell-cell interactions Overall, materials research from benchwork to final animal testing showed great potential of HA derivates for cell encapsulation and protection of pancreatic beta cells for T1DM treatment.

Acknowledgements

First and foremost, I would like to express my sincere gratitude to my supervisor, Dr Maurice N. Collins, for all the support, guidance, and patience demonstrated throughout the course of my PhD. Dr Collins always made himself available for his students, and he would always give the best advice in order to help if any difficulties were encountered during the project. I would also like to thank Dr Collins for mentoring my own development as an early career scientist. He always encouraged me to be the best that I can be and taught me to always thrive for excellence.

I would like to extend my appreciation to the 3B's Research Group in Portugal, in especial to Dr Joaquim Miguel Oliveira. The time I spent at the 3B's was extremely important for me to learn so many different research skills and analytical techniques.

I would like to thank the brilliant people that I had the opportunity to collaborate during the development of this project, such as co-workers, staff, laboratory technicians and students. To name a few, I would like to acknowledge Dr Mario Culebras, Dr Eric Dalton and Mrs Fionnuala O'Connell from the Stokes Labs, Dr Elizabeth Ryan, Mr David Egan, Mr Clive Considine, and Mrs Catherine Johnson. Additionally, I would also like to thank the Irish Research Council (IRC) for funding this project.

I would like to thank the unconditional support that I received from my beloved family and from my dearest friends. I would like to express my deepest gratitude to my parents, Marzelena and Fernando, and to my siblings, Amanda and Ângelo, for always supporting me on the pursuit of my dreams, even when it meant leaving home to move abroad.

I would like to thank my mother-in-law Mrs Kathleen Cahill, for receiving me into her house with open arms during the course of this 5 years. Last but not least, I would like to thank my (now) husband, Dónal, for his never-ending patience and support. He was always by my side to celebrate my achievements, but most importantly, he was always there to cheer me up and encourage me to overcome all the difficult times when experiments were not going well. I dedicate this work to you all.

“Os livros não mudam o Mundo, quem muda o Mundo são as pessoas, os livros só mudam as pessoas”

Mario Quintana

“Imíonn an tuirse ach fanann an tairbhe”

Old Irish Seanfhocail

Table of Contents

List of Figures

List of Tables

List of Abbreviations

Abbreviation	Meaning
A	Permeation Surface Area
AB	Alamar Blue
ACR	Albumin to Creatine Ratio
ADP	Adenosine Diphosphate
AFM	Atomic Force Microscopy
ANOVA	Analysis of Variance
APC	Antigen-presenting Cells
APTES	3-Aminopropyltriethoxisilane
ATCC	American Type Culture Collection
ATP	Adenosine Triphosphate
ATR	Attenuated Total Reflectance
BIED	Bis(β-isocyanatoethyl) Disulphide
C_D	Concentration of Donor Solution
CGM	Continuous Glucose Monitoring
CNF	Carbon Nanofiber
CO_2	Carbon Dioxide
CoA	Coenzyme A
Cp	Factor
CSII	Continuous Subcutaneous Insulin Infusion
D_2O	Deuterium Oxide
Da	Dalton (unit)
DAISY	Diabetes Autoimmunity Study in the Young
DAMP	Damage-associated Molecular Pattern
DAPI	4,6-Diamidino-2-phenylindole
DiPiS	Diabetes Prediction in Skåne
DKA	Diabetes Ketoacidosis
DMA	Dynamic Mechanical Analysis
DMEM	Dulbecco's Modified Eagle Medium
DMPA	2-2-dimethoxy-2-phenylacetophenone
DMSO	Dimethyl Sulphoxide
DPPE	Dipalmitoyl-glycerol-phosphatidyl Ethanolamine
DSC	Differential Scanning Calorimetry
DTT	Dithiothreitol
ECACC	European Collection of Authorized Cell Cultures
ECM	Extra Cellular Matrix
EDTA	Ethylenediaminetetraacetic Acid Disodium Salt Dihydrate
ELISA	Enzyme-linked Immunosorbent Assay
ENDIA	Environmental Determinants of Islet Autoimmunity
ERK	Extracellular Signal-regulated Kinase
FBR	Foreign Body Reaction
FBS	Foetal Bovine Serum
FGF-2	Fibroblast Growth Factor 2
FITC	Fluorescein Isothiocyanate
FT-IR	Fourier-Transformed Infrared Spectroscopy
G'	Storage Modulus
G''	Loss Modulus
GADA	Glutamic Acid Decarboxylase Antibody

GAG	Glycosaminoglycan
G-CSF	Granulocyte Colony Stimulating Factor
GLP-1	Glucagon-like-peptide 1
GLUT2	Glucose Transporter Type 2
GLUT4	Glucose Transporter Type 4
GM-CSF	Granulocyte Macrophage Colony Stimulating Factor
GWAS	Genome-wide Association Studies
H_2O_2	Hydrogen Peroxide
H_2SO_4	Sulfuric Acid
HA	Hyaluronic Acid
HA-PD	Pyridine-modified Hyaluronic Acid
HARE	Hyaluronic Acid Receptor for Endocytosis
HAS	Hyaluronan Synthase
HA-SH	Thiolated-Hyaluronic Acid
HbA1c	Glycated Haemoglobin
HCl	Hydrochloric acid
HDAC3	Histone Deacetylase 3
HLA	Human Leucocyte Antigen
HMW	High Molecular Weight
HYAL	Hyaluronidase
Hz	Hertz (unit)
IA	Insulin Antibody
IAA	Insulin Auto Antibody
IBMIR	Immediate Blood-mediated Inflammatory Reaction
ICA	Islet Cell Antibody
IDF	International Diabetes Federation
IEQ	Islet Equivalent
IFNγ	Interferon Gamma
IgG	Immunoglobulin G
IL	Interleukin
iPS	Induced Pluripotent Stem Cells
K	Cantilever Spring Constant
kPa	Kilo Pascal (unit)
LADA	Late onset autoimmune diabetes of adults
LAP	Lithium phenyl-2,4,6-trimethrylbenzoylphosphinate
LB	Luria Bertani Broth
L-b-L	Layer-by-Layer
LDH	Lactate Dehydrogenase
LMW	Low Molecular Weight
LYVE-1	Lymph Vessel Endothelial Hyaluronan Receptor 1
M	Molar (unit)
Mal	Maleimide
Mal-PEG-NHS	Maleimide propionyl-polyethylene glycol-n-hydroxy succinimide ester
Mc	Molecular Weight Between Crosslinks
MCP-1	Monocyte Chemoattractant Protein-1
MENA	Middle East and North Africa
MGR	Mean Growth Rate
MHC	Major Histocompatibility Complex
MIDIA	Norwegian Environmental Triggers of Type 1 Diabetes
mm	Millimetre (unit)
mM	Milli Molar (unit)

MMP	Matrix Metalloproteinase
MRGI	Mean Relative Growth Index
MRI	Magnetic Resonance Imaging
MSC	Mesenchymal Stem Cell
MWCO	Molecular Weight Cut-off
N	Newton (unit)
NAC	North America and the Caribbean
Nampt	Nicotinamide Phosphoribosyl Transferase
NHS	N-hydroxyl Succinimide
nm	Nanometre (unit)
NMR	Nuclear Magnetic Resonance Spectroscopy
NO	Nitric Oxide
NPH	Neutral Protamine Hagedorn
OP	Optical density
P	Permeability coefficient
PAI-1	Plasminogen activator-inhibitor-1
PAMP	Pathogen-associated Molecular Pattern
PANAM	Poly(amidoamine)
PBS	Phosphate Buffered Saline
PC	Phosphorylcholine
PD	Pyridine
PECAM	Platelet Endothelial Cell Adhesion Molecule
PEG	Polyethylene Glycol
PEGDA	Polyethylene Glycol Diacrylate
PEI	Poly(ethylenimine)
PET	Positron-emission Tomography
PKC	Protein Kinase C
PLL	Poly-L-Lysine
PM	Plasma Membrane
PMNs	Polymorphonuclear Cells
ppm	Parts per million (unit)
PRR	Pattern Recognition Receptor
psi	Pressure (unit)
PSomes	Polymersomes
PVA	Polyvinyl Alcohol
PVP	Portal Venous Pressure
PVT	Portal Venous Thrombosis
QD	Quantum Dot
Q_M	Experimental Swelling Ratio
RHAMM	Hyaluronan-mediated Motility Receptor
ROS	Reactive Oxygen Species
RPM	Revolution per Minute
RPMI	Roswell Park Memorial Institute
RT	Room Temperature
S^-	Thiolate anion
SACA	South America and Central America
S_c	Central Sulphur
sCR-1	Soluble Complement Receptor 1
SD	Standard Deviation
SEM	Scanning Electron Microscope
SH	Thiol
S_{lg}	Leaving Sulphur

SN_2	Bimolecular Nucleophilic Substitution
SPECT	Single Photon Emission Computed Tomography
SPIO	Superparamagnetic Iron Oxide
STZ	Streptozotocin
T1DM	Type 1 Diabetes Mellitus
T2DM	Type 2 Diabetes Mellitus
TEDDY	The Environmental Determinants of Diabetes in the Young
TF	Tissue Factor
TGFβR1	Transforming Growth Factor Beta Receptor 1
TLR	Toll-like Receptor
TMB	Tetramethylbenzidine
TNFα	Tumour Necrosis Factor Alpha
TRIGR	Trial to Reduce Insulin Dependent Diabetes Mellitus in Genetically at Risk
TSG-6	Tumour necrosis factor stimulated gene 6
UK	United Kingdom
US	Ultrasound
USA	Unites States of America
UV	Ultraviolet
V	Volts (unit)
V_1	Molar volume of PBS
V_A	Volume of Acceptor Solution
VDCC	Voltage-gated Calcium Channel
VEGF	Vascular Endothelial Growth Factor
VIGR	Viruses in Genetically at Risk
WHO	World Health Organization
Zp	Deflection of Cantilever
°C	Degree Celsius (unit)
µm	Micrometre (unit)
ξ	Mesh Size
ρs	Density of PBS
ρρ	Density of the polymer
υ	Specific Volume of Dry Polymer
χ	Flory Polymer Solvent Interaction Parameter

Chapter 1: Introduction

1.1.Introduction

In this chapter an outline of the background information on the architecture of the pancreas, insulin metabolism and regulation with emphasis in beta cell functionality and its importance in diabetes mellitus pathogenesis is discussed.

1.2.Architecture of the Pancreas

Diabetes mellitus is a disease that primarily affects the pancreas. The pancreas is a glandular organ that exerts two functions, one involves exocrine cells (acinar and ductal) organized in acini, and the other involves endocrine cells organized in small islets (islets of Langerhans). The exocrine component of the pancreas occupies over 95% of the organ and it produces enzymes such as trypsinogen, pancreatic lipase and amylase that help with food digestion (Grapin-Botton, 2005). Pertaining to the endocrine component, pancreatic islets consist of five distinct cellular types which are responsible for the synthesis and secretion of distinct peptide hormones involved in the metabolism regulation (Figure 2.1).

Glucagon, insulin, somatostatin, ghrelin, and pancreatic polypeptide are secreted by the α cells, β cells, δ cells, ε cells and PP cells, respectively (Sakata et al., 2019). However, the pancreatic islets are not just comprised of the endocrine cells (mentioned above), they also contain numerous other cell types, such as vascular cells, other stromal cells, immune cells, and neural elements (Jansson et al., 2016). Stromal and immune cells play a key role in the development of diabetes and β cell obliteration, which will be discussed in more depth over coming chapters.

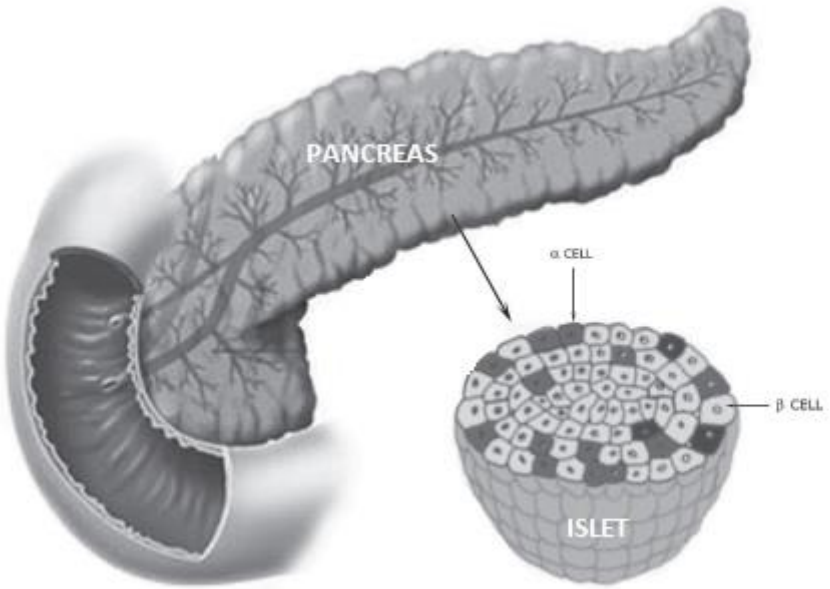

Figure 2.1. Structure of the human pancreas: Endocrine pancreas, islet of Langerhans.

Each islet contains approximately 1,000 β cells, accounting for 60% of all cells in the islet. The remaining 40% of cells are divided in α cells (30%) and the remaining 10% includes the δ cell, ε cell and PP cells (Da Silva Xavier, 2018). However, cell composition is known to vary according to pancreatic anatomical location and also changes amongst different species (shown in Table 1.1). Moreover, the proportion of different hormone-producing cells in the pancreas also differs between males and females of the same species. Studies suggest that islets from women have an average of 6% more β cells than islets from men (Gannon et al., 2018).

Table 1.1: A comparison between mouse and human pancreas (Dolensek et al., 2015)

Scale	Property	Mouse	Human
Organ	Anatomical shape	Diffuse/dendritic, lobular, soft	Solitary, compact, firm
	Ducts	Main duct joins with the bile duct proximal to the entry into duodenum	Main duct joins with the bile duct proximal at the point of entry into duodenum
		Numerous accessory ducts	A single accessory duct
Tissue	Diameter of lobules	0.5-1.5 mm	1-10 mm

	Diameter of islets	Single cells to 500-700 µm	Single cells to 500-700 µm
	Number of islets	1,000-5,000	1,000,000-15,000,000
	Location of islets	Random, interlobular	Uniform, intralobular
	Microvascular pattern	Insulo-venous system prevails, insulo-acinar system also present	insulo-acinar system prevails
	Order of perfusion	Centre-to-periphery (66%), polar	Most likely polar
Cells	% of β and α cells	β cells: 60-80%	β cells: 50-70%
		α cells: 10-20%	α cells: 20-40%
	Microarchitecture of islets	Mantle islets predominate	Trilaminar islets predominate
	Sympathetic fibres	Scarce innervation of exocrine tissue	Rich innervation of exocrine tissue
		In contact with α cells and vascular smooth muscle cells	In contact with vascular smooth muscle cells
	Parasympathetic fibres	Scarce innervation of exocrine tissue	Rich innervation of exocrine tissue
		In contact with all types of endocrine cells	In contact with β and δ cells, possibly α cells.

1.3.Insulin Structure

In the present study, focus is given to the β cell and its product, insulin, owing to its important role in the regulation of carbohydrate, fat and protein metabolism (Wu et al., 2015). The insulin gene encodes a precursor peptide known as preproinsulin, which contains a N-terminal signal peptide (24 amino acids), a C peptide (30 amino acids) and insulin (Figure 1.2). Before being secreted by the β cells, insulin first loses the N-terminal signal peptide sequence which converts preproinsulin into proinsulin. Then proinsulin is enzymatically cleaved and converted into insulin and free C peptide, the latter being co-secreted with insulin in equimolar amounts (Ashcroft and Ashcroft, 1992).

Insulin, the active hormone, has a molecular weight of 5.8 kDa. It consists of two polypeptide chains, an A chain (21 amino acids) and a B chain (30 amino acids),

connected by two interchain disulphide bridges between cysteine residues at A7-B7 and A20-B19 positions with one intrachain disulphide bridge at residues A6-A11 (Ryle et al., 1955, Brown et al., 1955, Sanger et al., 1955).

Insulin, at a concentration of 40 mM, is stored in granules within the pancreatic β cells (Zhuo et al., 2013). A mouse pancreatic β cell is reported to contain as many as 13,000 insulin granules. However, only 1% of these granules are readily accessible to be released, whereas the remaining granules are stored as reservoirs (Pagliuca and Melton, 2013).

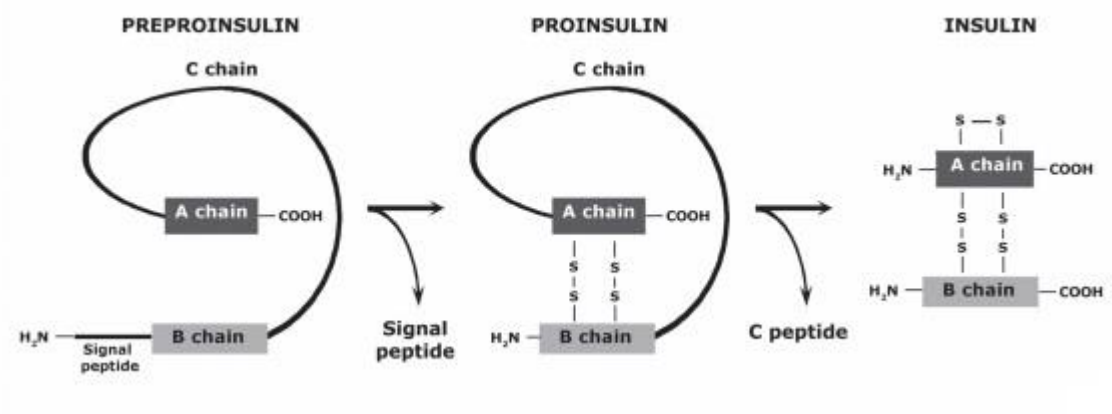

Figure 1.2. Insulin hormone: signal sequence (preproinsulin), C peptide (proinsulin), A and B chains (insulin).

1.3.1. Insulin Secretion Mechanism

Carbohydrates are a most important source of energy, and insulin plays a key role in glucose homeostasis. Glucose absorption in the intestine increases blood glucose concentration (above 7-10 mM), which increases insulin secretion by the release of gastrointestinal hormones such as glucagon-like-peptide 1 (GLP-1). In the pancreas, β cells sense the higher blood glucose levels and transport glucose inwards via a facilitated diffusion process mediated by a transmembrane protein called GLUT2. Inside the β cell, glucose is metabolized by entering the oxidation pathway and generates energy in the form of adenosine triphosphate (ATP). Higher intracellular ATP concentration will stimulate the exocytosis of insulin into the blood stream (Figure 1.3) (Lehninger et al., 2013).

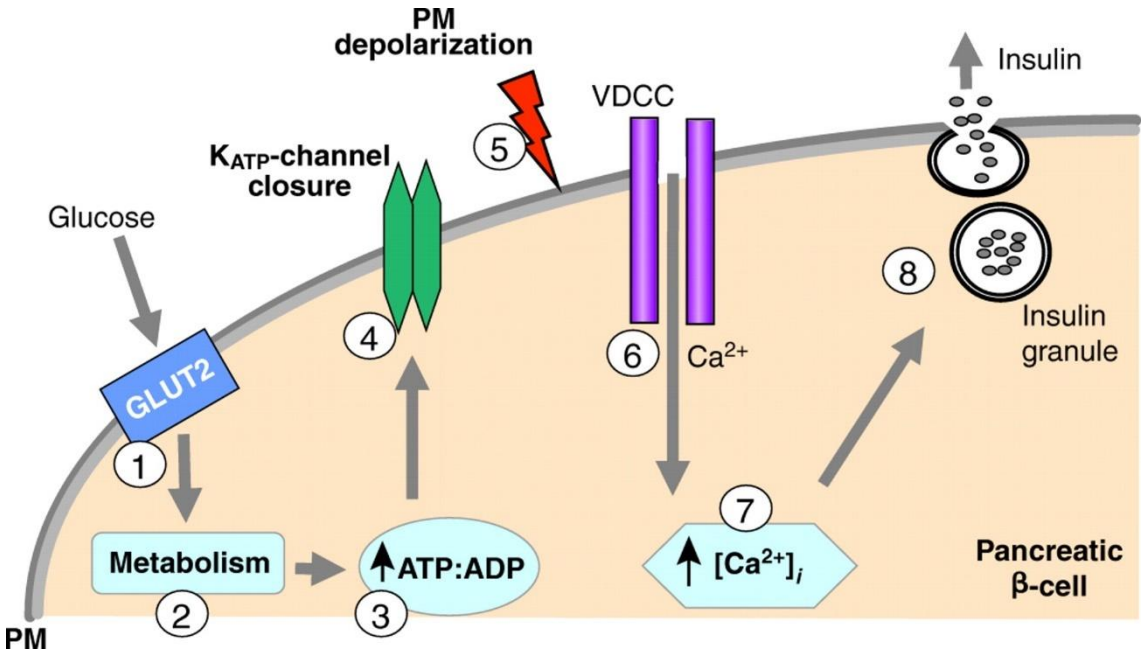

Figure 1.3. Action of glucose on insulin secreting β cells. [1] Uptake of glucose through GLUT2. [2-3] Glucose is metabolized to convert adenosine diphosphate (ADP) into the generation of ATP. [4] Increase in ATP induces the closure of K_{ATP} channels, followed by the depolarization of the plasma membrane (PM). [6-7] Aperture of voltage-gated calcium channel (VDDC) and influx of Ca^{2+}, which triggers the [8] release of insulin by exocytosis. (Wang and Thurmond, 2009).

1.3.2. Regulation of Carbohydrate Metabolism

Not all tissues are insulin sensitive (brain, kidneys, and intestine) but those that are (striate muscle and adipose tissue) will share specific insulin receptors on their cell membranes. The insulin-sensitive tissues will only take up glucose in the presence of insulin. This is due to a different glucose transporter that is insulin dependent, named type 4 (GLUT4). In these tissues, insulin binds to the insulin receptor of the cell membrane. This generates an intracellular cascade response that activates the translocation of GLUT4 from internal membrane vesicles to the plasma membrane (Figure 1.4) (Lehninger et al., 2013).

Only after GLUT4 is translocated in the plasma membrane, glucose uptake is performed. In the cytosol, glucose enters the glycolytic pathway to generate lactate. Most of the lactate produced in the muscle is then utilized by the liver and converted to glycogen, via gluconeogenesis. The conversion of lactate to glycogen in the liver and the continuous formation of lactate from glucose in the other tissues of the body represent the cyclical flow of carbon that has been termed as the Cori cycle (Ashcroft and Ashcroft, 1992).

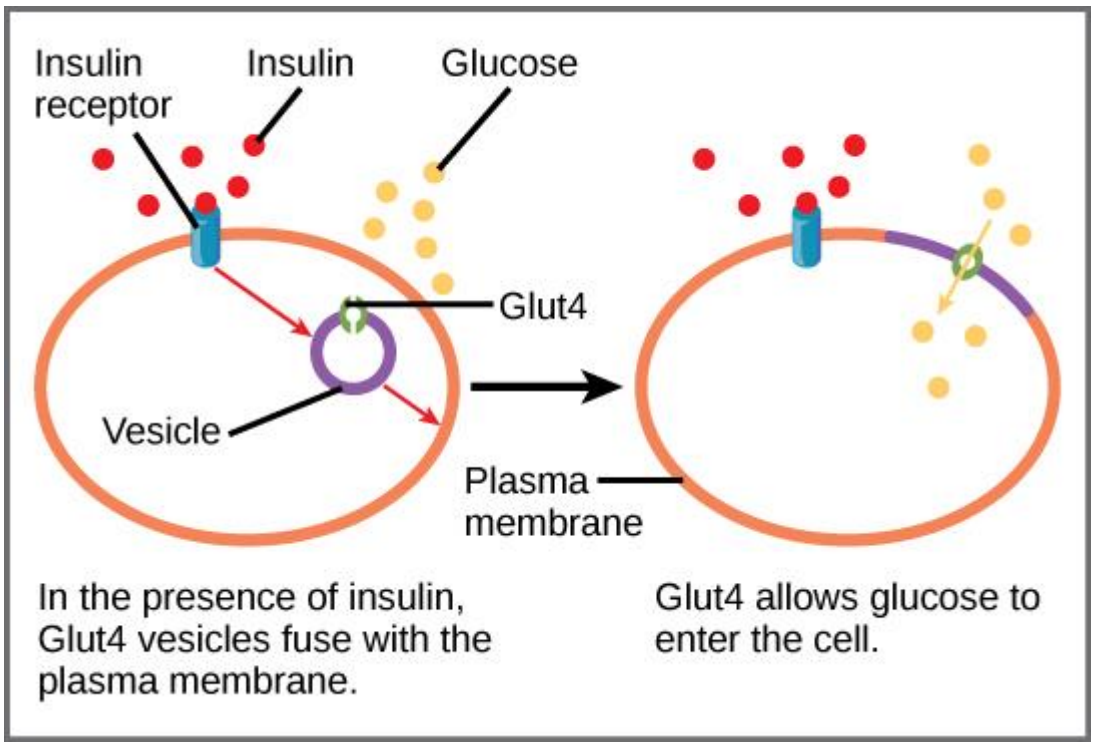

Figure 1.4. Insulin activates the translocation of GLUT4 protein to the cell membrane for the uptake of glucose on striate muscle and adipose tissues.

1.4.Autoimmunity

When the immune system experiences a biological imbalance, several chronic and acute inflammatory conditions can be triggered. For example, when the immune system loses the ability to differentiate between potentially harmful foreign antigens and self-antigens, the autoimmune response unfolds. In this case, autoreactive T cells escape detection by central tolerance mechanisms. Although several peripheral tolerance mechanisms exist as a safety mechanism such as anergy, deletion, T cell suppression through the induction of regulatory T cells (T regulatory), and anatomical barriers such as the blood-brain barrier (Kelly et al., 2017) to remove or suppress any such autoreactive T cells, in autoimmunity one or more of these also fail.

More than 80 autoimmune diseases have been diagnosed, with half of these considered rare. The auto immunological reactivity can be against any cell type, thus leading to diseases with different degrees of severity. It is estimated that autoimmune diseases, such T1DM, inflammatory bowel disease or rheumatoid arthritis affect 7.6–9.4% of the population worldwide (Gutierrez-Arcelus et al., 2016). Recent studies have shown that 76% of autoimmunity traits present a predominantly heritable influence, whereas 24% are mostly influenced by environment, such as diet and infections (Mangino et al.,

2017) (Figure 1.5). Furthermore, both innate and adaptive immune system alterations are associated with environmental factors (Hotamisligil, 2017), however the mechanisms of which these factors may regulate the homeostasis of the immune system are still poorly understood (Brodin and Davis, 2017).

Several studies suggest that the genetic mechanisms underlying autoimmune diseases are related to the major histocompatibility complex (MHC), such as the human leukocyte antigen (HLA) (Opdenakker et al., 2016) and the toll-like receptors (TLRs). These belon to the family of pattern recognition receptors (PRRs) that recognize a wide range of pathogen-associated molecular patterns (PAMPs) (Chen et al., 2016, Jimenez-Dalmaroni et al., 2016). In addition to these mechanisms, the genome-wide association studies (GWAS) have identified 90 shared genetic regions associated with celiac disease, rheumatoid arthritis, multiple sclerosis, and T1DM (Fortune et al., 2015).

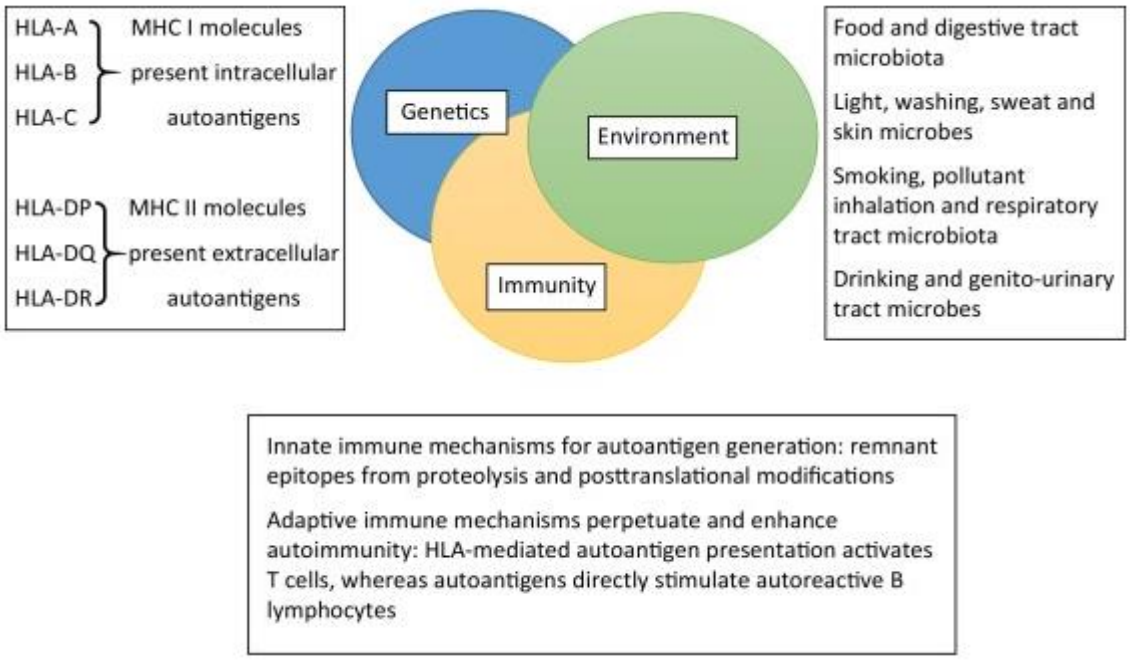

Figure 1.5. Genetic, Environmental, and Immunological Factors Impacting the Initiation and Progression of Autoimmune Diseases (reprinted with permission of (Opdenakker et al., 2016)).

1.5.Diabetes Mellitus

Diabetes mellitus is a disorder characterized by hyperglycaemia, where levels of blood glucose are persistently raised above the normal physiological range. This hyperglycaemic state arises from a complex interaction of genetic, environmental and lifestyle factors that impairs pancreatic β cell activity.

In 2014, the global economic burden of diabetes was estimated at approximately USD 612 billion, representing 11% of total global health expenditures (da Rocha Fernandes et al., 2016). The expenditure varies by region, age group, gender, and country's income level (Zhang et al., 2010).

Diabetes mellitus can be subdivided into two main subtypes, which differ from their aetiology. In T1DM, the destruction of pancreatic β cells in response to an autoimmune-mediated reaction eventually leads to a state of absolute insulin deficiency (Watkins, 2003). Whereas, in type 2 diabetes mellitus (T2DM), pancreatic β cells are not destroyed, but their responsiveness to glucose via the GLUT2 receptor is defective. Moreover, in T2DM, peripheral tissues have a reduced sensitivity to insulin uptake (known as insulin resistance), contributing to a higher glycaemic level in the blood (Watkins and Watkins, 2003).

T1DM has been effectively treated with exogenous insulin replacement following the discovery of insulin in 1922. Despite this, even with good metabolic control and considerable improvements in the quality and delivery of insulin, diabetes is associated with significant morbidity, mortality and overall reduced life expectancy. Microvascular complications associated with T1DM include retinopathy, nephropathy and neuropathy, while macrovascular complications include ischaemic heart disease, stroke and peripheral vascular disease. These complications further contribute to the financial burden of the health care system, emphasizing T1DM as an important public health matter (Zamboni and Collins, 2017).

In contrast, T2DM can be treated with an array of oral therapies in conjunction to lifestyle modifications to attain optimal glycaemic control. Initially, T2DM is treated with a monotherapy, usually using oral hypoglycaemic agents, such as metformin (Rhee et al., 2017). However, if normoglycaemia is not achieved, a polypharmacy approach is prescribed. The introduction of this oral combination therapy (multiple drug regimen) targets the control of hyperglycaemia through their different pharmacological mechanisms of action (Lavernia et al., 2015). These include insulin sensitizers, insulin secretagogues, thiazolidinediones, GLP-1 analogues, dipeptidyl peptidase-4 inhibitors, and others. If none of the above therapeutic regimens are able to control hyperglycaemia, exogenous insulin therapy is advised (Marín-Peñalver et al., 2016).

In this landscape, due to the immune-mediated aetiology of T1DM and the lack of treatment options to control hyperglycaemia, restricted only to exogenous insulin replacement therapy, the focus of this work is on the development of novel strategies to treat T1DM.

1.6.Pancreatic β Cell Replacement and Immunoisolation

Latest trends in T1DM treatment are shifting towards pancreatic β cell replacement, envisioning to restore physiological insulin responsiveness to blood glucose variations. Beta cell replacement strategies include the transplantation of islets and genetically engineered insulin secreting cells. Pancreatic islet transplantations infused through the portal vein of the liver (Edmonton Protocol) have demonstrated improved glucometabolic control, reduced hypoglycaemic episodes and cessation of complications resulting from diabetes (Maffi and Secchi, 2015). However, the major drawbacks associated with islet transplantation, like in any other organ transplant, include the shortage of donors and the danger associated with pharmacological immunosuppression. In this landscape, immunoisolation of cellular grafts has been proposed to avoid transplant rejection and diabetes reoccurrence (Lim and Sun, 1980).

When pancreatic β cells are immunoisolated within a semipermeable matrix, cells receive the essential nutrients and oxygen needed for their survival. Furthermore, they are protected from immune system recognition and rejection while restoring physiological insulin responsiveness to blood glucose variations (Figure 1.6). Thence, it is possible to perform allo- or xeno-transplants without immunosuppression.

Amongst all immunoisolation strategies, growing interest is being given to nano encapsulation of pancreatic β cells in ultra-thin coatings. The combination of surface engineering and the deposition of multiple layers of biomaterials through conformal coating provide effective mass transport while still conferring protection from the immune attack (Zamboni and Collins, 2017).

Various natural and synthetic materials have been used to encapsulate pancreatic β cells (table 3.1). Although alginate is still the gold standard for islet cell encapsulation and it is perceived as biocompatible (Krishnan et al., 2014, Calafiore et al., 2006), alginates with high mannuronic acid or impurity content are potentially immunogenic (Lee and Mooney, 2012). Moreover, the short-term stability of ionic-crosslinked alginate hydrogels, due to

the leaching of ions to the outer environment, demonstrates the need to study other biomaterials for cell encapsulating purposes.

In this scenario, polymers naturally present in the extra cellular matrix (ECM) of tissues seem to outperform other materials as they closely resemble the native environment and have a decisive effect on cellular signalling, immune regulation, and vascularization (Zamboni et al., 2018b). These biomaterials, like HA, collagen and others, form hydrogels with long-term stability and controllable permeability by customizing the polymeric concentration, the type of crosslinking agent or varying the polymeric molecular weight and monomeric ratio (Gasperini et al., 2014).

HA is a natural carbohydrate polymer of increasing significance to bioengineering and biomaterials science and is finding applications in wide ranging areas. HA properties, both physical and chemical, together with its versatile processability (in solution, film, or hydrogel forms), are extremely attractive for various technologies concerned with body repair (Collins and Birkinshaw, 2013a). In physiological conditions, HA is under constant remodelling and reorganization in response to the surrounding microenvironment. The degradation of HA into low molecular weight (LMW) fragments provides signalling cues known to promote angiogenesis and inflammation in the surrounding tissue, whilst high molecular weight (HMW) HA possess intrinsic anti-inflammatory, insulinotropic effects and antimicrobial properties (Zamboni et al., 2018a, Li et al., 2006).

The inherent property of HA is to promote angiogenesis and vascularization, along with the ability to modulate the immune response without the need of additional functionalization bearing therapeutic drugs or biological factors. This makes HA the material of choice to enable successful encapsulation of pancreatic β cells. Vascularization of encapsulated pancreatic cells is of primary importance for effective oxygenation and transportation of glucose and insulin in and out the capsule when these are transplanted in extravascular sites.

To date, there has never been any report on nanoencapsulation systems derived from HA conformal coatings for pancreatic β cell encapsulation. Several chemical modifications have been developed to protract HA degradation, and tailor its mechanical integrity. However, only a few chemical modifications can be safely exploited for cell encapsulation without hampering cell viability and without causing any cellular damage or cytotoxicity. Thiolation of HA is one of these cell-friendly HA modifications that can

create reversible crosslinking bonds via thiol/disulphide bond formation through a disulphide exchange mechanism. This method facilitates the sequential deposition of several polymeric layers on the surface of pancreatic islets to tailor optimal capsule performance. Disulphide exchange mechanism is a covalent crosslinking method that gives more robust and stable coatings. Covalently crosslinked layer-by-layer systems create stiffer coatings with increased Youngs modulus thereby, outperforming ionic crosslinking coatings (Amorim et al., 2020).

In this context, we developed a new cell encapsulation strategy to aid the treatment of T1DM. This work envisages the creation of a biofunctional engineered immunoprotective environment with the ambition of restoring insulin competence, making this the central argument for this project.

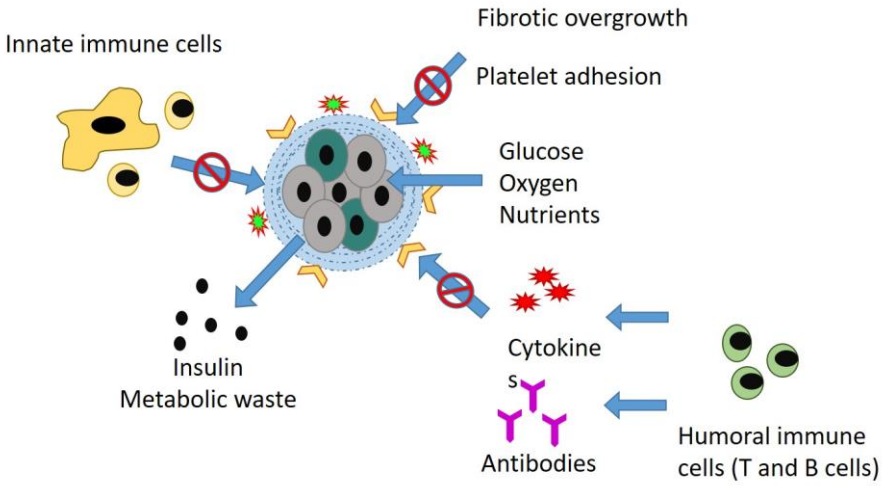

Figure 1.6. Encapsulation of insulin-producing cells within a semi-permeable hydrogel matrix allows nutrient, oxygen, and glucose diffusion while preventing immune cells, cytokines and antibodies activation and mediated-cell death.

1.7.Objectives

The project core aim is to develop a new immunoprotective microenvironment based on HA for the encapsulation of pancreatic β cells to aid the treatment of T1DM. The project is divided into 6 main objectives:

a) Materials development: selection (high vs. low molecular weight), synthesis of a novel biocompatible crosslinking agents (di-isocyanate compound) and the

utilization of the new di-isocyanate based crosslinker to crosslink HA and produce gels;

b) Biological characterization assessment of newly crosslinked HA hydrogels;

c) Chemical modification of HA to thiol-bearing and pyridine-bearing HA derivates for layer-by-layer (L-b-L) assembly and crosslinking;

d) Surface modification of pancreatic β cells through PEGlation for subsequent HA layer anchorage site;

e) Conformal encapsulation of pancreatic β cells using layered HA derivates; and

f) Transplantation of encapsulated cells into a T1DM animal model.

1.8.Thesis Outline

Chapters 2, 3 and 4 are an in-depth review of the literature on T1DM, cell encapsulation and HA, respectively, which are critical topics in this thesis. The following chapters compile the experimental work. As outlined in Figure 1.7. Chapters 5 and 6 were grouped into the experimental work package 1, while Chapter 7-8 and chapter 9 encompass experimental work packages 2 and 3, respectively.

For the attainment of the first objective of the project, chemical, physical, and mechanical characterizations of the novel synthesized di-isocyanate crosslinker, bis(β-isocyanatoethyl) disulphide (BIED), and HA derivates were performed. Technologies included freeze drying, scanning electron microscope (SEM), Fourier-transformed infrared (FT-IR) spectroscopy, solid-state proton nuclear magnetic resonance (NMR) spectroscopy, differential scanning calorimetry (DSC), dynamic mechanical analysis (DMA) rheometer, and atomic force microscopy (AFM). Results are compiled in Chapter 5.

Once these materials were fully characterized, biological assessments were carried out. For the achievement of the second objective, fibroblast lineages were used to evaluate cell proliferation and cytotoxicity, while macrophages were used to assess immunological response, via macrophage activation and production of pro-inflammatory cytokines. The antimicrobial activity of HA was also evaluated using *Staphylococcus aureus*. These results are compiled in Chapter 6.

Subsequently, objectives 3, 4, and 5 were achieved utilizing pancreatic β cells from the MIN-6 lineage, which were surface modified through PEGlation (Chapter 7). The evaluation of the cell encapsulation with the different HA derivates developed in the chapters 5 and 6 was assessed for cytotoxicity, cell proliferation, glucose challenge, and insulin release profile studies for both surface engineered and encapsulated cells. These results are compiled in Chapter 8.

For the achievement of the last objective, an *in vivo* study was performed, where encapsulated cells were transplanted into the kidney subcapsule of female mice of the black 6 (C57BL/6) strain. Prior to the transplantation, a T1DM model in mice was developed using five consecutive low-dose STZ injections. To access the successful transplantation of the cells, blood glucose levels were monitored, and histology was conducted to evaluate transplant rejection via localized immunological infiltration. These results are compiled in Chapter 9.

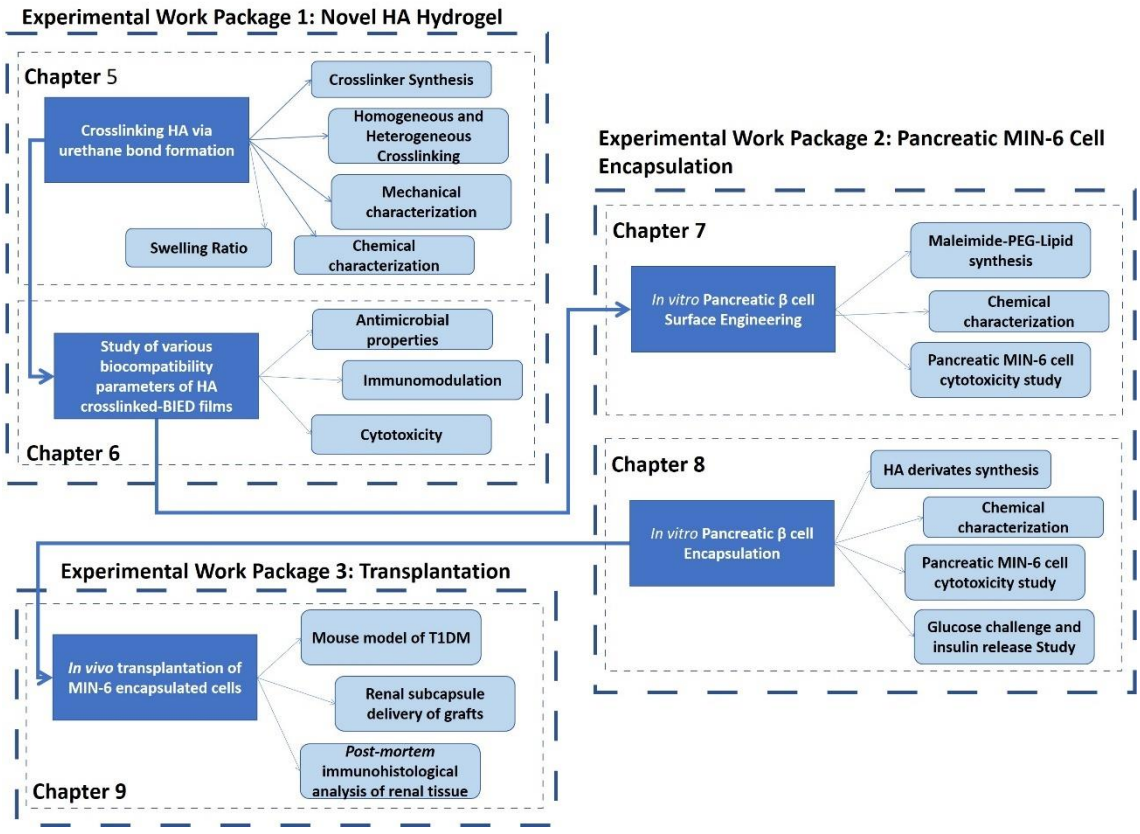

Figure 1.7. Thesis Outline

Chapter 2: Type 1 Diabetes Mellitus

2.1.T1DM Aetiology and Pathophysiology

T1DM is an autoimmune disease where selective destruction of pancreatic β cells leads to a state of absolute insulin deficiency. *Post-mortem* studies of pancreata showed that in recently diagnosed type 1 diabetics, patients displayed lymphocytic infiltration of islets, which is part of the autoimmune process (Willcox et al., 2009). The β cells are reduced in number and eventually disappear completely. Then, islets consist predominantly of α cells. It is, therefore, not surprising that patients are insulin dependent.

The peak of incidence is usually during early childhood (5-9 years of age) or during early teenage years and decreases drastically after 13 years of age (Harjutsalo et al., 2008). The early onset of diabetes in younger children is presumed to be due to premature exposure to environmental factors (Weets et al., 2002). These factors will be discussed in more depth in section 2.2. Nonetheless, it is worthwhile to mention that there is a further subtype of T1DM affecting an older demographic group known as Late Onset Autoimmune Diabetes of Adults (LADA) (Kapustin, 2008).

The currently accepted model of T1DM (Figure 2.1) describes it as a condition primarily occurring in people with an underlying genetic susceptibility, combined with disease-inciting environmental factors. This in turn triggers an autoimmune reaction in the pancreatic β cells, also known as insulitis. It can be identified by the presence of autoantibodies to the islet components in the blood. Hyperglycaemia and diabetes only become evident after more than 80% of the β cells are destroyed. The end result of this process results in complete loss of β cells and, therefore, loss of insulin production (Atkinson and Eisenbarth, 2001).

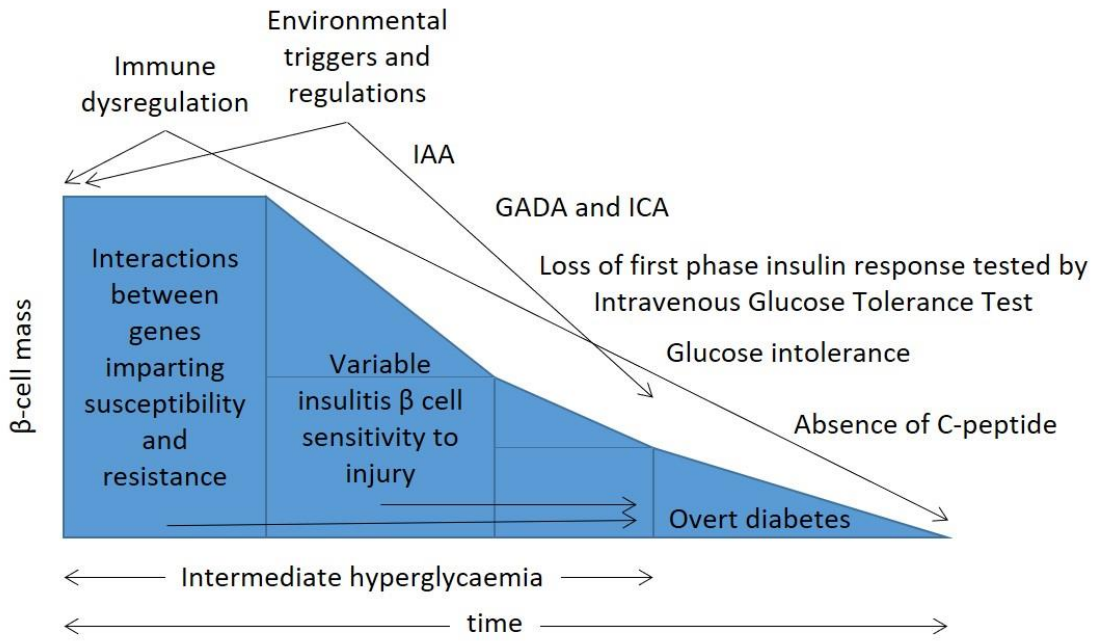

Figure 2.1. Modern model of the natural history of T1DM (Atkinson and Eisenbarth, 2001)

Susceptibility is highly associated with the HLA genes and linked to a lesser extent with other non-HLA genes. The HLA genes encode the MHC proteins. They are subdivided in three main classes: class I, class II and class III. Class I antigens are expressed in the cell membrane of all cells and they bind to CD8+ cells (T cytotoxic), being responsible for the cellular lyses associated with viral infection. Class II antigens are expressed on antigen-presenting cells and bind to CD4+ cells (T helper cells). Class III are associated with the action of the complement system (Heinonen et al., 2015). Class I (HLA-B8 and B15) and class II (HLA-DR3 and DR4) are associated with increased risks for T1DM. In contrast, class II (HLA-DR2) appears to protect against diabetes (Erlich et al., 2008).

In the period preceding the onset and diagnosis of T1DM, there is continual ongoing immune-mediated β cell destruction, with the remaining insulin secreting β cells preventing overt hyperglycaemia. This period is clinically silent and characterized by β cell stress, β cell destruction, insulitis, and autoimmunity (Eisenbarth, 1986). At this stage, biomarkers can be identified, such as islet cell antibodies (ICA), glutamic acid decarboxylase antibodies (GADA), insulin auto antibodies (IAA) and insulin antibodies (IA). People that have two or more antibodies have higher risk (up to 88%) of developing T1DM (Watkins et al., 2014).

Many diabetic patients develop circulating IAA and the majority of patients develop IA upon initiation of insulin treatment. IAA production is associated to HLA-DR3 and/or DR4, in contrast to IAA, it seems that high levels of IA are associated with the expression of HLA-DR4 and/or DR7.

The interstitial space that surrounds the islet during inflammation shows an infiltration of antigen-presenting cells, such as mononuclear cells (macrophages and dendritic cells). These cells express on their membrane surface HLA class II antigens. They also secrete high amounts of pro-inflammatory cytokines, such as interleukins (IL) and tumour necrosis factor alpha (TNFα). These cytokines in conjunction with interferon gamma (IFNɣ), produced by T cytotoxic and T helper cells, enable the immunological destruction of β cells (Chiarelli et al., 2019).

2.2.Environmental factors in T1DM

The development of T1DM cannot solely be explained by genetics alone. Environmental factors are also thought to contribute to the pathogenesis of T1DM. Many theories have been developed regarding environmental factors that could possibly trigger T1DM: viral infections, nutritional factors (breast feeding, cow's milk components and gluten), vaccinations, toxins (N-nitroso derivatives), drugs, psychological stress, maternal and intrauterine factors, lack of sunshine (vitamin D) and climatic influences (Tuomilehto, 2013).

Longitudinal studies have been conducted to assess environmental triggers in T1DM, such as the Babydiab/Babydiet, The Environmental Determinants of Diabetes in the Young (TEDDY), Trial do Reduce IDDM in Genetically-at-Risk (TRIGR), Viruses in the Genetically at Risk (VIGR), Norwegian Environmental Triggers of Type 1 Diabetes (MIDIA), Diabetes Prediction in Skåne (DiPiS), Diabetes Autoimmunity Study in the Young (DAISY), and Environmental Determinants of Islet Autoimmunity (ENDIA) (Ziegler et al., 2012) (Hagopian et al., 2006, Krischer, 2007) (Akerblom and Grp, 2011) (Yeung et al., 2012) (Tapia et al., 2015) (Larsson, 2008) (Frederiksen et al., 2013, Penno et al., 2013). Despite ongoing trials none of these environmental factors were proven to be associated with T1DM. Moreover, some studies show controversial and contradictory results.

2.3. T1DM Pathophysiology: ECM Remodelling

The ECM is the non-cellular component of all tissues, responsible for the provision of physical support to cells and for the regulation of diverse cell functions through biochemical and biomechanical cues. ECM is composed of water and fibrous-forming proteins, such as collagen, elastin, and fibronectin; glycoproteins; proteoglycans; and glycosaminoglycans (GAGs) (Theocharis et al., 2016). ECM composition varies from tissue to tissue, as a result of multiple signals, that dictate the ECM structure and its biomechanical properties.

The ECM is a very dynamic structure, which is continuously remodelled by matrix-degrading enzymes, in a controlled manner. When this balance is compromised, due to genetic abnormalities or in pathological conditions, matrix composition changes. This ECM change can promote critical implications on disease development and progression (Theocharis et al., 2016, Frantz et al., 2010).

In the pancreas, the pericellular membrane surrounds each acinar cell, pancreatic islet, and blood vessel, while the interstitial matrix is a thin layer subjacent to the peri-islet basement membrane. The interstitial matrix confers tensile strength and elasticity to tissues mainly due to the presence of fibrillar collagens. The basement membrane is a highly crosslinked sheet-like layer that provides an anchoring platform for epithelial cells, preventing them from rupture via the formation of hemidesmosomes (Bogdani et al., 2014). The basement membrane is composed of collagen (type IV), laminins (particularly, laminin 511) and proteoglycans. Laminins provide cell adhesion sites and transduce signals to cells that impact cell proliferation, migration, and differentiation, while collagen stabilizes the overall structure. While linker molecules interconnect collagen and laminin networks (Theocharis et al., 2016).

ECM remodelling plays an important role in T1DM pathogenesis by promoting immune cell activation, islet invasion and destruction of pancreatic β cells. The degradation of ECM components by proteases, such as matrix metalloproteinases (MMP), are responsible for the generation of ECM bioactive fragments (also called matrikines). These matrikines fine tune inflammatory responses by influencing the activity and/or function of both infiltrating and resident cells (Jiang et al., 2011). HMW HA (> 1000 kDa), present in normal pancreatic tissue becomes degraded into LMW HA (250 kDa) during the disease process (Li et al., 2006). These LMW HA fragments promote leukocyte

recruitment and adhesion by activating TLRs (Vigetti et al., 2014, Shakya et al., 2015). Moreover, HA fragments can be crosslinked into structures that impact leukocyte function by the interaction with a diverse group of HA-binding proteins, known as hyaladherins. HA-hyaladherin structures are stable complexes in solution and enhance or induce HA binding to the cell surface receptor CD44 on lymphocyte cell lines (Baranova et al., 2011).

Islet invasion starts with neutrophil diapedesis towards the pancreas. It occurs within the post-capillary venules that surround the islets, where haemodynamic shear forces are minimised. After passing through the capillary endothelium, leukocytes penetrate the peri-islet basement membrane before they gain access to the β cells. The transmigration of leukocytes through the peri-islet basement membrane is hypothesized to involve three mechanisms: a) the proteolytic digestion of the membrane; b) the use of mechanical force; and/or c) preferred basement membrane sites of variant composition (Bogdani et al., 2014). The variability in the composition of the basement membrane is mainly attributed to laminin, where α5 deficient regions facilitate leukocyte diapedesis (Hallmann et al., 2015).

In developing pancreatic islets, β cells are confirmed to express α1β1 receptors which are a specific type of laminin receptor. The α1β1 receptors are co-localized with collagen IV in the basal membranes of juxtaposed endothelial cells. The β cell α1β1 integrin interaction with collagen IV promotes β cell migration and potentiates insulin secretion (Kaido et al., 2004). However, upregulation of integrin α6β1 by leukocytes has been suggested to facilitate cell transmigration through the peri-islet basement membrane. Leukocyte migration through the interstitial matrix occurs via collagen-mediated actin-myosin system (Sorokin, 2010).

The proteoglycan composition of the peri-islet basement membrane has also been studied, showing the presence of heparan sulphate proteoglycans (Cheng et al., 2012a). Syndecan-4 (a membrane-associated heparan sulphate proteoglycan) is also observed on β cells. Interestingly, the inhibition of heparan sulphate degradation is shown to prevent destructive autoimmunity and the progression of T1DM (Ziolkowski et al., 2012).

2.4.Disease Incidence and Prevalence

The International Diabetes Federation (IDF) has estimated that the global prevalence of diabetes mellitus in 2015 for people aged between 20 and 79 years old was 8.8%, with over 414.7 million people diagnosed with the condition. By 2040 IDF estimates that this will increase to over 642 million people, with the overall prevalence increasing to 10.4% (Federation, 2015). The estimation of the number of people with diabetes in different regions worldwide is presented in table 2.1. The main driving forces for the increased diabetes incidence around the world are associated with unhealthy eating habits, obesity, and increasingly sedentary lifestyles (Patterson et al., 2014).

Table 2.1: Estimative of the number of people (aging from 20 to 79 years old) with diabetes in the year 2015 and 2040 (Federation, 2015).

	2015			2040		
IDF region	Population (million)	Diabetes (million)	Prevalence (%)	Population (million)	Diabetes (million)	Prevalence (%)
Africa	441	14.2	3.2	926	34.2	3.7
Europe	660	59.8	9.1	663	71.1	10.7
MENA*	387	35.4	9.1	635	72.1	11.4
NAC*	344	44.3	12.9	413	60.5	14.7
SACA*	315	29.6	9.4	411	48.8	11.9
Southeast Asia	926	78	8.5	1310	140	10.7
Western Pacific	1600	153	9.3	1800	215	11.9
Total	4720	414.7	8.8	6160	642	10.4

*ABBREVIATIONS: Middle East and North Africa (MENA); South American and Central America (SACA); North America and the Caribbean (NAC)

Currently, there are 1.9 billion children in the world, of those, 542,000 children (0-14 years old) have T1DM (Federation, 2015). Each year 86,000 new cases are diagnosed with an annual incidence increase of 3% (Patterson et al., 2009, Bessaoud et al., 2006). The United States of America currently has the highest number of children with diabetes in the world (84.100 children), with Finland being the country with the highest number of new cases of T1DM in children (62.3 new cases per 100.000 population per year) (table

2.2). Ireland is in 7th place, with an incidence of 26.8 new cases in every 100,000 children per year. The causes of the rapid change in the T1DM incidence rate are unknown, and they are unlikely to be due to shifts in genetic background alone. Hence, environmental agents are also presumed to contribute to this incidence increase (Patterson et al., 2014).

Table 2.2. Rank of countries for number of children with T1DM and rank of countries for number of new cases of kT1DM per 100000 children per year.

Top 5 countries for number of children with T1DM			Top 5 countries for new cases of T1DM in children		
Rank	Country	Number of cases	Rank	Country	Number of new cases/100000 children/year
1	USA*	84100	1	Finland	62.3
2	India	70200	2	Sweden	43.2
3	Brazil	30900	3	Kuwait	37.1
4	China	30500	4	Norway	32.5
5	UK**	19800	5	Saudi Arabia	31.4

*United States of America, **United Kingdom.

2.5.Diagnosis

T1DM symptoms include increased diuresis (polyuria) and nocturia, this is primarily because the renal threshold for glucose reabsorption is exceeded. Further symptoms include dehydration; polydipsia (thirst); weight loss; and fatigue. In the absence of more specific biological markers to define diabetes, the measurement of plasma glucose levels and glycated haemoglobin are the only diagnostic criteria established so far.

In insulin competent individuals, fasting plasma glucose levels are below 6.1 mmol.L^{-1} (normoglycaemia). Higher fasting glucose levels ranging from 6.1 to 6.9 mmol.L^{-1} are classified as intermediate hyperglycaemia and may be considered for diabetes prevention intervention (2020a). Note that fasting is defined as no caloric intake for at least 8 hours. Traditionally, diabetes is diagnosed when venous plasma glucose levels exceed 7 mmol.L^{-1}.

Summarized in table 2.3 are the glycaemic values used to diagnose diabetes as defined by the World Health Organization (WHO). Measurement of glycated haemoglobin (HbA1c) reflects the average plasma glucose level over a period of 12 weeks. This is an

excellent indicator of glucose control over time and is used in the monitoring of glycaemic control in patients with diabetes (Organization, 2011).

Table 2.3: WHO criteria values for T1DM diagnosis (WHO/IDF, 2006).

Diabetes mellitus	Venous plasma glucose
Fasting	≥7.0 mmol/L (126 mg.dL^{-1})
Random plasma glucose*	≥11.1 mmol/L (200 mg.dL^{-1})
Oral glucose tolerance test	≥11.1 mmol/L (200 mg.dL^{-1})
HbA1c	≥6.5%

*in presence of diabetes symptoms.

2.6.Secondary Complications

2.6.1. Ketoacidosis

Diabetic ketoacidosis (DKA) is a potentially life-threatening metabolic derangement that occurs from severe insulin deficiency in untreated T1DM (American Diabetes, 2013). After a meal containing carbohydrates, glucose accumulates to abnormally high levels in the blood. Since adipose tissue (an insulin-dependent tissue) is unable to take up glucose due to lack of insulin, adipose cells increase lipase activity in order to breakdown triacylglycerols.

The free fatty acid chains released after lipolysis are exported to the liver where they are oxidized into acetyl coenzyme A (CoA). Acetyl-CoA instead of entering the citric acid cycle, it is diverted to the formation of "ketone bodies". Acetoacetate is decarboxylated to give acetone or alternatively β-hydroxybutyrate. Acetone is released by the lungs and acetoacetate and β-hydroxybutyrate are transported by the blood to tissues other than liver (extrahepatic tissues), where they are converted to acetyl-CoA and oxidized in the citric acid cycle, providing energy to be used as fuel as a glucose substitute (Foster and McGarry, 1983).

The overproduction of acetoacetate and β-hydroxybutyrate leads to their accumulation in the blood and urine (ketosis) which can subsequently, decrease the blood pH level to as low as 6.8 (acidosis) (Owen et al., 1982). DKA is accompanied by dehydration, potassium depletion, respiratory compensation and metabolic acidosis, impaired consciousness, vomiting, leucocytosis and hypothermia (Gallo de Moraes and Surani, 2019).

2.6.2. Micro and Macrovascular Complications

Persistent hyperglycaemia over many years, incite well known secondary complications, such as retinopathy, neuropathy, and nephropathy. These complications considerably reduce life expectancy and quality of life of patients (Ramasamy et al., 2006). The toxic effects of hyperglycaemia might be explained by the formation and accumulation of glycosylated proteins and lipids which induce oxidative stress in target tissues (Feener and King, 1997).

Nearly all patients with T1DM develop retinopathy later in life. Retinopathy will eventually lead to complete eyesight loss and it is responsible to approximately 4.8% of all cases of blindness in the world (Resnikoff et al., 2004).

Neuropathy is a result of autonomic and peripheral nerve damage in patients with diabetes, which is one of the main causes for the diabetic foot. First small neural fibres are damaged by demyelination. The accumulative effect is most apparent in the long nerves, causing peripheral loss of sensation. The inability to sense trauma and abnormal pressure on skin can lead to skin ulcers and infections. Infections are treated with antibiotics but can lead to amputation in patients with more extensive gangrene or limited gangrene in presence with sepsis (Tesfaye, 2014).

Patients with diabetes can develop subsequent renal pathology, characterized by capillary closure and tissue ischaemia. The progression of renal disease occurs over many years leading to proteinuria, this typically occurs when the albumin to creatine ratio (ACR) is above 30 mg/mmol/L. Preventative treatment is by controlling the blood pressure, primarily with angiotensin-converting-enzyme inhibitors (enalapril and ramipril) or angiotensin-2 receptor antagonists (losartan and olmesartan) (Suissa et al., 2006). If there is progression to end stage renal failure, patients may end up requiring dialysis and / or renal transplantation (Smets et al., 1999).

2.6.3. Management of Secondary Complications

Diabetic patients are advised to maintain tight glycaemic control with the aim of keeping their HbA_{1C} levels below 7%, in order to reduce micro- and macrovascular complications. Five years following the diagnosis of T1DM, follow-up appointments are recommended annually for screening and assessment of the development and progression of nephropathy, retinopathy and polyneuropathy (2020f).

Adults with diabetes are also advised to perform at least 150 minutes a week of moderate-intensity aerobic activity (50–70% of maximum heart rate), in 3 days a week. Studies have shown that physical activity can improve glucose levels, reduce cardiovascular risk and prevent complications in diabetes (2020b).

2.7. Blood Glucose Monitoring

To maintain good glycaemic control, patients need to be attentive to their lifestyle and assess the response to their insulin therapy by measuring their blood glucose concentrations. This is routinely done by pricking the tip of a finger with a needle (or lancet) and placing the blood into a capillary strip containing an enzyme, such as glucose oxidase or glucose dehydrogenase. The glucose concentration is determined by either an electrochemical or colorimetric readout system (Heller and Feldman, 2008). New studies are being developed in order to produce more accurate and less inconvenient glucose monitoring sensors, such as non-enzymatic glucose sensors (Tian et al., 2014).

The American Diabetes Association guidelines suggest that people with T1DM should monitor blood glucose levels a minimum of three times a day, particularly prior to meals and snacks and also at bedtime (2020c). When low blood glucose is suspected, their blood glucose levels should be assessed prior to exercise and critical tasks such as driving. After the correction of low blood glucose, achieved usually by ingesting a sugary snack or drink, self-monitoring should be performed until normoglycaemia is achieved. Real-time continuous glucose monitoring (CGM) is also available through the measurement of interstitial glucose (which correlates with plasma glucose). CGM devices can be equipped with Bluetooth (for receiving readouts on a smartphone or smart watch). CGM are also equipped with alarms for hypo- and hyperglycaemic states which is beneficial for children and adolescents or patients with hypoglycaemia unawareness and/or frequent hypoglycaemic episodes (2020d).

2.8. Pharmacological Therapies in T1DM

Following the discovery of insulin in 1922, exogenous insulin replacement has been an effective treatment for T1DM which allows patients to maintain safe blood glucose levels and lead a relatively normal life (Banting and Best, 1922). Traditionally, insulin therapy is administered via subcutaneous injections, however other administration routes have also been studied, such as the respiratory route with the utilisation of inhalers (Mohanty and Das, 2017).

Insulin therapy has constantly changed over the decades, starting from early insulin extracts obtained from animal pancreas and advancing to the development of human insulin analogues by molecular biology manipulation. These human insulin analogues contain small changes in the amino acid sequence of insulin which implicates in major changes in their pharmacokinetic profiles (Mathieu et al., 2017).

2.8.1. Insulin Regimen

The goal of insulin replacement therapy is to achieve normoglycemia, where a fasting blood glucose should be between 90 and 120 mg/100 mL and a 2-hour postprandial value below 150 mg/100 mL (2020c). To achieve these glycaemic values, insulin is given in doses that are expressed in units. The convention is that one unit of insulin is responsible to reduce the concentration of 45 mg/100 mL blood glucose in a fasting rabbit. A healthy person produces normally between 18 and 40 units per day of insulin, which is 0.2-0.5 units/Kg/day. In T1DM patients, the average requirement of insulin is usually around 0.7 units/Kg/day (Hirsch, 2005). However, insulin requirements can be subject to change due to a number of situations, such as exercise, stress or illness.

The right technique to administer insulin injections are either at a 45° or 90° angle into a fold of skin pinched between fingers. The common areas to inject insulin in the body are the anterior thighs, dorsal arms, buttock, and abdomen. However, different injection sites have an influence on insulin absorption and consequently, on its pharmacokinetics (2020e).

Insulin preparations are classified according to their duration of action, known as short- and rapid-acting, intermediate, or long-acting insulins. The pharmacokinetic profiles vary among the insulins available (Figure 2.2).

A number of insulin regiments (such as split-mixed or basal/bolus) try mimicking normal pancreatic insulin secretion patterns. These regiments combine a single injection of an intermediate or long-acting insulin (mimicking low basal insulin rate) following multiple rapid or short-acting insulin injections (mimicking postprandial insulin rate) (Hilal-Dandan et al., 2014, Lechleitner and Hoppichler, 2011).

Non-diabetic subjects produce half of their insulin as a low basal rate and half in response to meals. The insulin response to meals occurs after 5 minutes and lasts for 2-3 hours following each meal. In T1DM patients the basal dose of insulin is around 40% to 60% of the total daily requirement which supresses lipolysis, proteolysis and gluconeogenesis.

The remaining dose is then divided in response to meals (Lechleitner and Hoppichler, 2011).

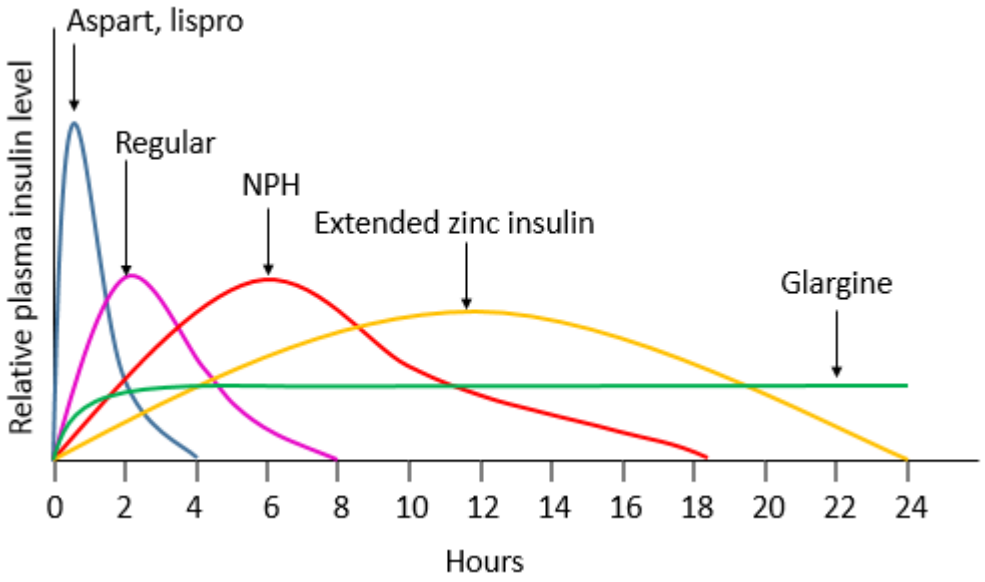

Figure 2.2. Approximate pharmacokinetic profile of rapid-acting (Aspart and Lispro), short-acting (Regular), intermediate-acting (Neutral Protamine Hagedorn-NPH, extended zinc insulin) and long-acting (Glargine) insulins.

2.8.2. Insulin Delivery Systems to Treat T1DM

Insulin pump therapy or continuous subcutaneous insulin infusion (CSII) is a method to deliver insulin at a steady state rate. It is a device the size of a pager that can be attached to the belt or placed in a pocket. The infusion is set as a slow, continuous rate throughout the day which is known as the basal infusion and/or to release larger amounts of insulin at mealtime or when blood glucose levels are high which is known as the bolus dose. The bolus dose is calculated using carbohydrate counting.

All insulin pumps available in the market are “smart pumps” and they have an on-board calculator which calculates and corrects the amount of bolus insulin to be injected for any given carbohydrate value. Latest-generation insulin open-loop pumps bring CGM features attached to the device. The type of insulin used in this device is rapid-acting insulin (Dajkovich and Barkley, 2015).

Insulin pump therapy is still expensive in comparison to conventional pen/syringe insulin administration, whilst in countries like Australia, Sweden and the UK insulin pump usage rates are below 20% (AIHW, 2012) (Steineck et al., 2015) (Ghatak et al., 2015). The

guideline recommendation for CSII use is intended for children under 12 years with T1DM if treatment with multiple daily injections is not practical or for any patient with T1DM if HbA1c targets are not achieved via multiple daily injections or if hypoglycaemia episodes are frequent and not controlled by multiple daily injections (2020d).

The overall advantages of insulin pumps are the reduction of hypoglycaemic episodes and improvement of HbA1c. However, the disadvantages are related to catheter infection and pump failure, which increases risk of DKA (Maede and Rushton, 2013, Woerner, 2014, Johnson et al., 2013).

While open-loop insulin pumps are available in the market, close-loop devices (artificial pancreas) integrated with CGM to infuse insulin accordantly are still only available in research. Tubeless pumps (patch pumps) are also being developed and they consist of a reservoir of insulin in a tiny pump attached to the skin which communicates with the smart calculator and glucose monitor via Bluetooth (Nicholls and Partridge, 2015, Alexander and Greene, 2009).

2.8.3. Common Problems Associated with Insulin Therapy

Alternation of the injection site is important to prevent lipohypertrophy. Lipohypertrophy is caused by the tropic action of insulin and it is a common problem in insulin-dependent diabetic patients. It can lead to functional disorders, such as pain, reduced local insulin efficacy, and aesthetic problems (Kordonouri et al., 2002).

Insulin therapy can also lead to potentially dangerous side effects. Hypoglycaemia is described as plasma glucose below 2.8 $mmol.L^{-1}$ in men or 2.6 $mmol.L^{-1}$ in women. Symptoms are autonomic in nature and include sweating, shaking, palpitations, anxiety, and neuroglycopenic effects, such as confusion, drowsiness, and slurred speech (McCrimmon and Sherwin, 2010). Patients rely on the presence of these symptoms to alert them of an hypoglycaemic episode, which can be in turn reduced by eating carbohydrates. However, hypoglycaemia can be sometimes overtreated, resulting in post hypoglycaemic hyperglycaemia, also known as the Somogyi effect (Gerich, 1988). Physical activity induce hypoglycaemia, for this reason patients are advised to reduce insulin intake after exercise (2020g).

2.9. Pancreatic Islet Transplantation

Since 1922, blood glucose levels have been effectively controlled via exogenous insulin replacement therapy (Banting et al., 1922). However, it still does not mimic the physiological pancreatic insulin secretion pattern, and therefore it can result in the occurrence of life threating hypoglycaemic episodes and increased risk of both micro and macrovascular complications (Virk et al., 2015, Steineck et al., 2015).

Nowadays, the treatment of T1DM is shifting towards the replacement of original islets via exogenous islet transplantation. Islet and whole organ transplantation are recommended for patients with renal failure who also require a kidney transplant or for those with life-threatening hypoglycaemic unawareness (Cahill et al., 2019).

In 2000, a multicentre study called the Edmonton Protocol developed a new immunosuppressive regimen that was shown to be safer and less toxic to islet transplanted patients with T1DM. This new regimen does not require the use of steroids and has reduced the use of calcineurin inhibitors (Shapiro et al., 2000). Follow-up data from 36 subjects showed that 16 patients were insulin independent for 1 year, 5 remained insulin independent for 2 years (Shapiro et al., 2006) however, only 2 patients remained insulin independent at 10 years post-transplantation (Brennan et al., 2016).

Initially, pancreatic islet transplantation was performed using surgical access such as laparotomy (Johnson et al., 1999), however nowadays the procedure is performed by minimally invasive techniques using percutaneous access and interventional radiology (Owen et al., 2003, Venturini et al., 2016, Madoff et al., 2016).

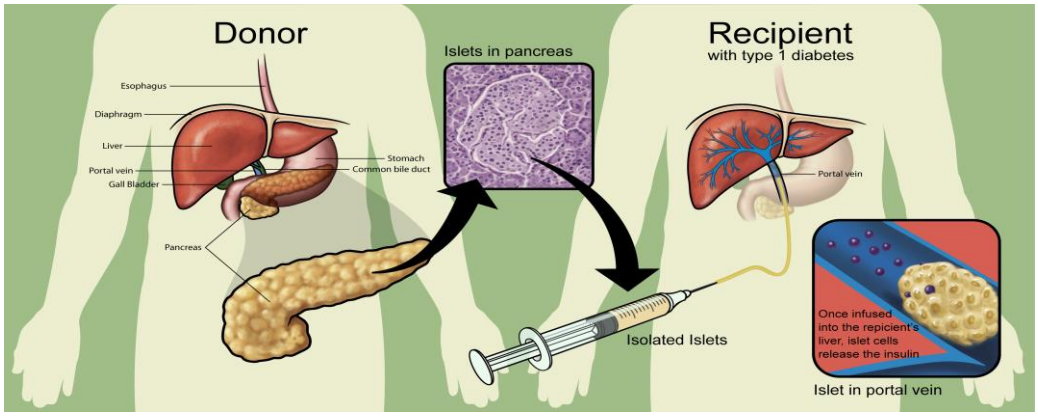

Figure 2.3: Schematic representation of pancreatic islet transplantation (Naftanel and Harlan, 2005)

For the transplantation of islets (shown in Figure 2.3), the successful isolation of the islets is regarded the most important step for achieving normoglycaemia. Notably, during isolation, cells lose their vascularized network and have their ECM disrupted, which reduces the viability of the harvested cells (Cheng et al., 2012a). The interaction between β cells and ECM is known to influence several aspects of islet functionality, including survival, proliferation, and insulin secretion (Theocharis et al., 2016).

It is calculated that the total number of islets to achieve insulin independency is about 200,000 islet equivalent (IEQ) (Weir, 2013). Therefore, for one single transplant recipient, approximately 2-3 donors are required to obtain enough viable cells. However, to overcome the shortage of donors, autologous and xenogeneic cellular sources incorporating cell modification and cell encapsulation strategies have been investigated (Zamboni et al., 2018b).

2.9.1. Percutaneous Islet Transplantation

Percutaneous transhepatic islet transplantation utilizes ultrasound (US) to locate a peripheral branch of the right portal vein, after which a catheter is placed under fluoroscopic guidance. This facilitates the even distribution of pancreatic islets into both lobes of the liver. The portal venous pressure (PVP) is measured prior, during and after islet infusion. PVP is maintained below 12 cm H_2O/20 mm Hg as higher PVP is directly associated to complications such as portal vein thrombosis (PVT) and excessive bleeding (Wilhelm et al., 2013). Islets are suspended in a sterile medium containing 200 mL of dextran and heparin (35 units/kg) to prevent the instant blood-mediated inflammatory reaction (IBMIR) and to reduce the risk of portal vein thrombosis (Baltzinger et al., 2016). Where one unit of heparin is an amount approximately equivalent to 0.002 mg of pure heparin. After completion of the infusion procedure, venous flow is assessed by a portogram to ensure no PVT or bleeding. Upon removal of the catheter from the portal vein, the tract is embolised with platinum fibred coils or Gelfoam® plugs to prevent haemorrhage (Park et al., 2014).

Studies have shown that tissue volume and islet size influences infusion safety for example tissue volumes <0.25 cm^3/kg of islets appear to decrease the risk of bleeding and PVT (Suszynski et al., 2014, Wilhelm et al., 2013). Allotransplanted islets have been reported to decrease risk for acute PVP when compared to auto-transplanted islets and this has been attributed to the high purification of allotransplanted islets (Kawahara et al., 2012).

2.9.2. Post-transplantation Complications

Next day post-operative imaging in the form of liver ultrasound, is utilised to assess for potential complications which include hepatic hematoma, bleeding and PVT (Bozkurt et al., 2013).Bleeding is reported to occur in 12% of the transplantations due to puncture of the parenchyma around the capsule of the liver or within the peritoneum. Thrombosis is reported to occur in 6% of all transplantation cases. Thrombosis can be potentially life-threatening, but the risk is reduced by the addition of heparin during the islet infusion (Owen et al., 2003).

The acute management of PVT requires the use of anticoagulation therapy, initially with low molecular weight heparin followed by warfarin if appropriate. The goal of anticoagulation is to prevent clot extension, intestinal infarction, and portal hypertension. The recommended duration of anticoagulation therapy does not exceed 6 months in patients without a known hypercoagulable state (Robertson and Hayes, 2015).

Hepatic steatosis (also known as fatty liver) is an extravascular complication of islet transplantation. It has been reported in 19% of cases as early as 6 months after islet transplantation using US (Low et al., 2015). The hepatic fat accumulation is hypothesised to occur in infusions of higher islet mass content or by localised islet cell over activity (Venturini et al., 2015b). Hepatic steatosis has been shown to persist for up to 5 years, however, there has been reported cases where this resolved spontaneously and cases of subsequent reoccurrence (Jackson et al., 2013).

2.9.3. Islet Transplant Rejection

After islet transplantation, patients achieve improved metabolic control and insulin independence. However, from all transplant patients only a few remain insulin independent after the first year of transplantation. A clinical study was conducted in 36 subjects showing that 16 patients were insulin independent for 1 year after transplantation

and 5 remained insulin independent at 2 years after transplantation (Shapiro et al., 2006). In long-term follow-up study, 7 participants were enrolled from those initial 36 subjects. All subjects demonstrated some islet function for at least 10 years, but only 2 patients remained insulin independent (Brennan et al., 2016).

Early loss of islet mass upon portal vein infusion, recurrence of insulitis (the hallmark of T1DM immunopathogenesis leading to immune-mediated β cell destruction), and islet allograft rejection contribute to graft failure overtime (Roep, 2020). In figure 2.4, the time frame of detrimental factors leading to early injury and late functional loss after islet transplantation is shown.

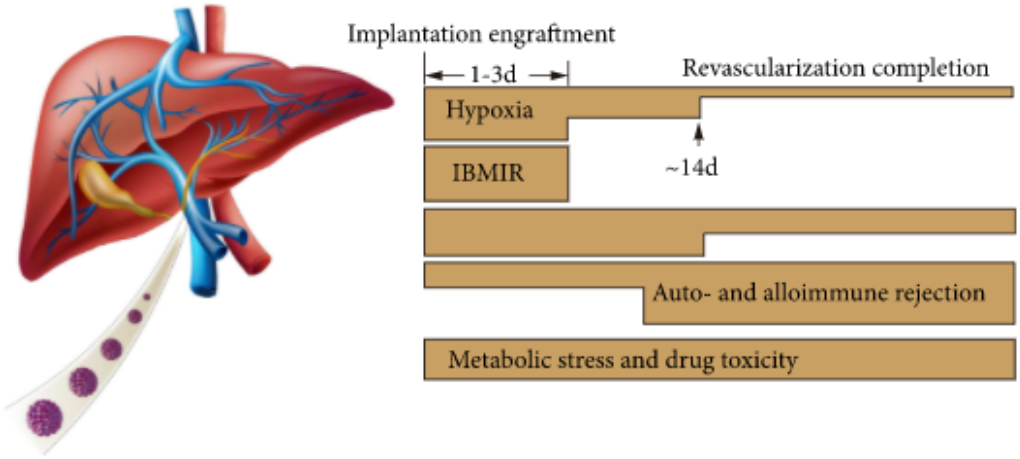

Figure 2.4. Fate of intrahepatic islets infused through the portal vein. Graft function is lost overtime due to hypoxia, immediate blood-mediated inflammatory reaction (IBMIR), auto- and alloimmune rejection (Li et al., 2018).

Early islet loss is a result of a severe hypoxic environment in the first several days after transplantation, where islets rely only on passive oxygen diffusion for survival (Li et al., 2018). Following transplantation, islets are also in direct contact with the ABO blood antigens, platelets, and the complement system, leading to IBMIR (Figure 2.5). Tissue factor (TF) present in the surface of islets interacts with factor VIIa and initiates the extrinsic coagulation cascade by the activation and deposition of platelets. This leads to the formation of thrombin and the formation of the fibrin clot. The activation of the complement proteins C3a and C5a leads to the recruitment and infiltration of polymorphonuclear cells (PMNs), such as neutrophils and eosinophils. The accumulation of immunoglobulins and complement proteins, such as C3, C4 and C9, on the surface of transplanted islets also indicates that the classical complement activation pathway may be involved in IBMIR (Kanak et al., 2014).

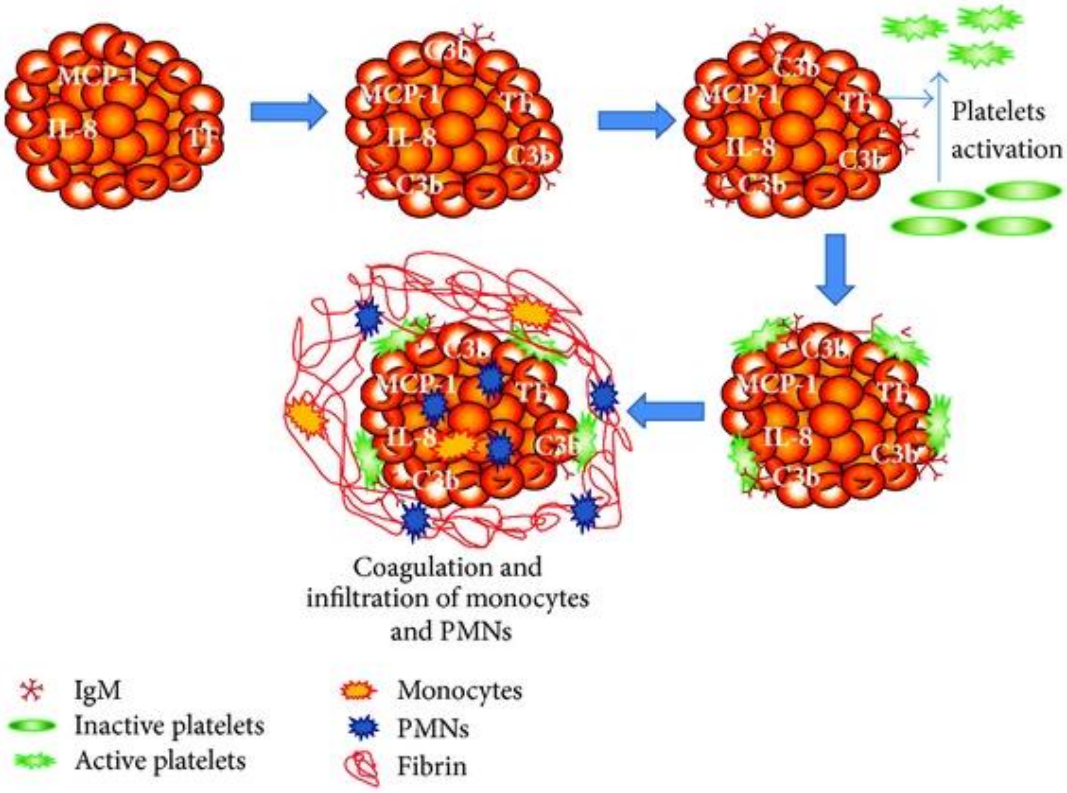

Figure 2.5. Mechanisms of the instant blood-mediated inflammatory reaction (Kanak et al., 2014).

Alloimmune rejection of islet grafts is shown to be associated with granulocyte infiltration to the site of transplantation. Neutrophils and eosinophils are usually the first leukocytes to infiltrate transplanted organs and are a well-established marker of transplant rejection (Moberg et al., 2005, Weir et al., 2012). Fresh isolated islets express pro-inflammatory cytokines and chemokines such as IP-10, IL-8 and monocyte chemoattractant protein-1 (MCP-1) that upon transplantation are known to attract leukocytes, neutrophils and macrophages to the transplantation site, respectively (Kanak et al., 2014). Moreover, T-cell alloreactivity plays an important role in transplant rejection (Gras et al., 2011). Indirect alloantigen recognition occurs when allogeneic MHC molecules from graft cells are taken up and processed by recipient APCs and subsequently presented to alloreactive T cells (Figure 2.6). Direct allorecognition, by contrast, uses donors' own APCs to present allogenic MHC molecules to recipients alloreactive T cells (Davis, 2004).

T-cell alloreactivity also instigates further leukocyte activation and recruitment. Once alloantigens are recognize by CD4+ Thelper17 cells, they promote neutrophilia via the

production of IL-17 cytokine (Crawford et al., 2020). IL-17 is a potent driver for neutrophil infiltration and production of granulopoietic cytokines such as granulocyte macrophage colony stimulating factor (GM-CSF) and granulocyte colony stimulating factor (G-CSF), which further promote macrophage activation (Scozzi et al., 2017).

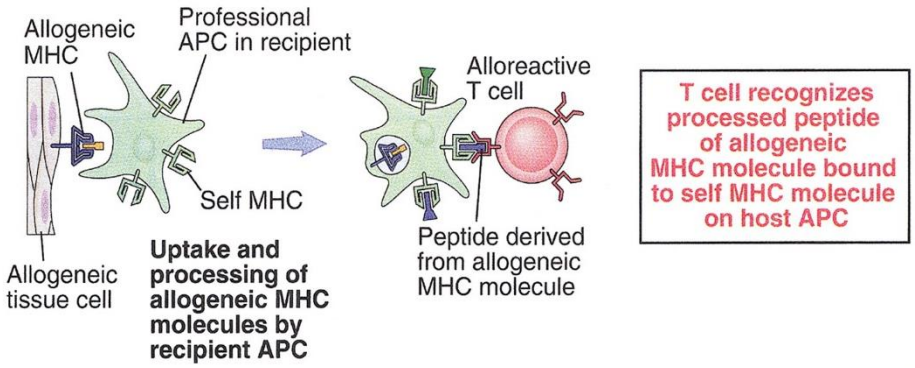

Figure 2.6. Indirect T-cell alloreactivity (Davis, 2004).

2.10. Future Treatments for T1DM

A bioartificial endocrine pancreas is proposed as a future alternative to current treatment options. This bioengineering approach could theoretically provide an inexhaustible source of bio-engineered insulin-producing cells to treat patients with insulin-secretion deficiency. These bio-engineered insulin-producing cells have the potential to also enhance graft survival and decrease transplant rejection by the combination of a number of strategies brought together by regenerative medicine. The conceptual triad for tissue engineering in T1DM is depicted in Figure 2.7.

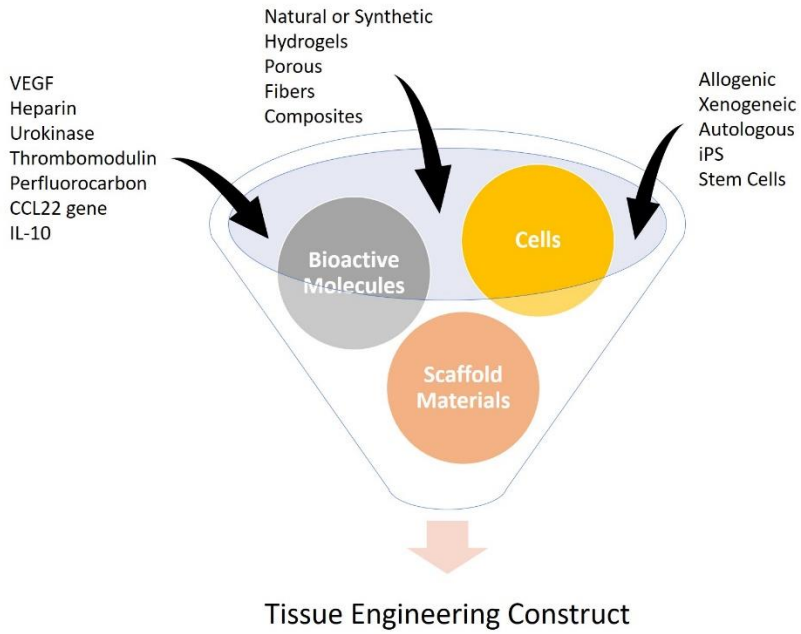

Figure 2.7. Tissue engineering an insulin-secreting cellular graft for T1DM treatment.

In the next chapter, a detailed review of the recent achievements and challenges encountered in the development of pancreatic β cell encapsulation and immunoisolation strategies will be presented. These strategies are sought to protect β cells from the host immune system following transplantation in order to avoid rejection and diabetes reoccurrence.

Chapter 3: Cell-based Regenerative Medicine in T1DM

The following chapter presents an in-depth review of literature. The contents of this chapter are adapted from the review article published in the International Journal of Pharmaceutics.

Zamboni, F. and M.N. Collins, Cell Based Therapeutics in Type 1 Diabetes Mellitus. Int J Pharm, 2017. 521(1-2): p. 346-356.

DOI: 10.1016/j.pmatsci.2018.04.003

3.1. Cell-based Therapy in T1DM

Due to lack of donors (under 10,000 organ donors in the USA per year), whole organ and islet transplantation is not a viable option for diabetes treatment (Scharp and Marchetti, 2014). To overcome the shortage of donors, it is necessary to address the ability to expand cells from human (auto and allografts) or animal sources (xenografts).

Endogenous sources of β cells in humans arise in the pancreas. In developmental pancreas, most β cells originate from the differentiation of pancreatic precursor cells (duct cells which present pancreatic transcription factor PDX-1) (Szabat et al., 2012). Likewise, pancreatic stem cells can also differentiate into β cells. However, once terminally differentiated β cells are established, their turnover is very limited, and appears to be a largely post-mitotic process with very low rates of proliferation after the age of 20-30 years old (De Tata, 2014). Therefore, adult pancreatic β cells present a long lifespan with minimal proliferative capacity (Tuch; and Kannangara, 2008). To address this matter, a variety of immortal pancreatic cell lines for *in vitro* research were created (Skelin et al., 2010).

Xenogeneic islet sources, such as from pigs, are an interesting alternative to overcome the scarce availability of human pancreatic endocrine tissue (Dufrane and Gianello, 2012). Porcine pancreatic structure and physiology are compatible with human pancreas (Kinasiewicz et al., 2011). Moreover, porcine and human insulin are structurally similar, differing by only one amino acid (Brown et al., 1955). For xenogeneic islet transplantation, the isolation of neonatal porcine islets is preferred due to the structure and high isolation yield (Nagaraju et al., 2015). Concerns regarding xenograft safety, focused on the potential for the transfer of pathogens, such as porcine cytomegalovirus, with zoonotic capabilities to the transplant recipient and the strong immunological response against the xenograft have risen (van der Windt et al., 2012). Nevertheless, encapsulation technologies provide a way forward for these xenogeneic grafts (Ludwig and Ludwig, 2015).

3.1.1. Reprogramming non-Pancreatic Cell Sources into Insulin-Producing Cells

Stem cells are found in developing and adult tissue. Embryonic stem cells are pluripotent which means they can differentiate into cells representing the three germ layers:

endoderm, ectoderm and mesoderm. Differing from embryonic stem cells, adult stem cells are multipotent, and they differentiate into multiple cell lineages that constitute an entire tissue. Adult stem cells can be found in the bone marrow, adipose tissue, dental pulp, and umbilical cord blood (Sumi, 2011).

Adult somatic cells can be artificially induced into a pluripotent state, following exposure to certain reprogramming factors. The current generation of induced pluripotent stem (iPS) cells have shown to be functionally equivalent to embryonic stem cells. The main advantages of these cells come from their unlimited replication capacity and their ability to be reprogrammed or (trans)differentiate into insulin-producing cells (Figure 3.1). Several multi-step protocols are in place to differentiate stem cells into insulin-producing β cells (Tse et al., 2015). Cultured human iPS cells may take up antigens from xenogeneic materials causing humoral rejections of the graft. For this reason, xeno-free protocols have been proposed for cell reprogramming.

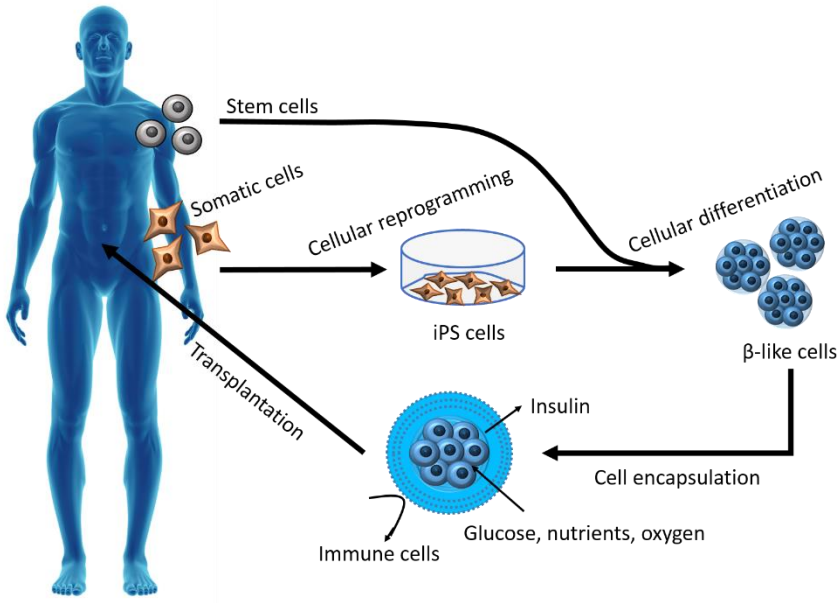

Figure 3.1. Autologous cell sources used to obtain pancreatic β cells in order to overcome the shortage of donors for transplantation in T1DM.

3.1.2. Immortal Pancreatic Cell Lines

Preliminary *in vitro* research can use a variety of immortal pancreatic cell lines, especially in order to overcome limited availability of primary β cells and donor variability. Most cells have a finite life span due to replicative senescence, but various transformation approaches have been used to produce continuous cell lines with an infinite life span. Methods such as induction of pancreatic tumour by irradiation or viral infection, and development of transgenic mice with targeted expression of recombinant oncogene in β cells have produced numerous immortal cell lines, such as RIN, HIT, β-TC and INS cells. However, just a few β cell lines show normal response to glucose concentrations in the physiological range, which include MIN-6 cells (Skelin et al., 2010).

3.2. Pancreatic β Cell Immunoisolation

Another issue encountered during islet transplantation is life-long systemic immunosuppressive drug therapy. These are required to suppress the host immune system from attacking both allografts and xenografts which may result in transplant rejection. An alternative approach to prevent graft failure and the need for immunosuppressants is β cell immunoisolation.

3.2.1. Transplantation Sites for Intravascular and Extravascular Devices

An optimal implantation site should provide easy access for implantation and removal, immune protection, a physiological route for insulin delivery, a sufficient blood and oxygen supply and enough space for a large volume of encapsulated islets and β cells (Zamboni and Collins, 2017).

Many implantation sites have been proposed as shown in Figure 3.2. Intravascular devices are normally implanted directly connected to the circulatory system, such as in the portal vein of the liver. Extravascular devices, on the other hand, have been reported to be implanted in sites such as the renal sub-capsule, subcutaneous spaces, peritoneal cavity, intramuscularly, spleen, gastrointestinal wall, bone marrow and immune privileged sites, such as testis and thymus (Cantarelli et al., 2013, Merani et al., 2008a).

For example, the liver remains the gold standard in clinical studies, as it provides close contact between the islet graft and the host's blood stream, ensuring a rapid graft oxygenation and exchange of insulin and glucose. However, the infusion of islets into the portal vein of the liver can cause hepatic thrombosis and liver ischemia due to the limited

available volume for implantation (Venturini et al., 2015a). Intrahepatic islet infusion also presents high risk of graft failure via the IBMIR (Cantarelli et al., 2013). Consequently, this method also requires anticoagulation therapy to decrease the incidence of blood clots and IBMIR.

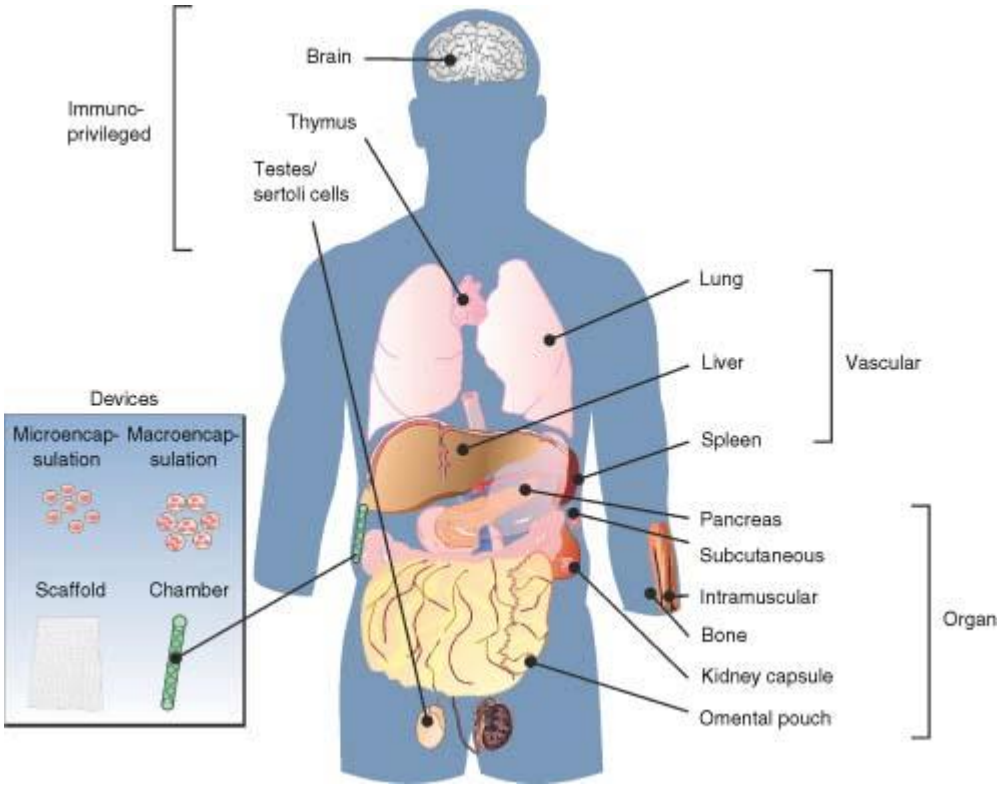

Figure 3.2. Transplantation sites for islet grafts (Merani et al., 2008b).

The kidney capsule has been a preferred site for experimental islet transplants in mice because the surgical procedure is relatively easier and less invasive than through the portal vein. Moreover, transplantation under the kidney capsule is easier to monitor and to retrieve by nephrectomy for both histological studies and proof of function of the islets (Cantarelli et al., 2013). Unlike the liver, the kidney capsule is an extravascular site. The impact on graft oxygenation may pose a limitation within the kidney sub-capsule. However, it may also confer a degree of immune privilege, as it is not directly exposed to non-specific immune response mediated predominantly by innate and inflammatory events, found in intra-liver islet engraftment (Cantarelli et al., 2013).

3.2.2. Pancreatic Beta Cell Encapsulation

Cell encapsulation is a method developed to protect pancreatic β cells from the immune system using a permselective matrix. This matrix will prevent immune cells, cytokines, and antibodies to reach β cells while promoting the diffusion of nutrients, oxygen,

glucose, and insulin (Figure 1.1). Many cell encapsulating approaches have been developed, such as macroencapsulation, microencapsulation and ultra-thin or nanoencapsulation (Figure 3.3). This section will give and overview on macro and micro devices but focus will be mainly on nanoencapsulation strategies, such as L-b-L and conformal encapsulation (Zamboni and Collins, 2017).

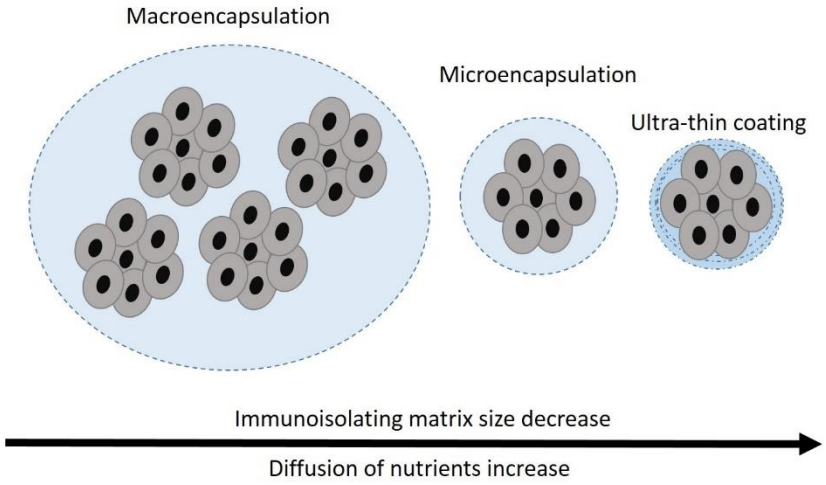

Figure 3.3. Encapsulation strategies for pancreatic islets.

3.2.2.1. Macroencapsulation

Macroencapsulation devices are generally large capsules that can measure several centimetres in length. These devices can be fabricated from various materials and with various geometries, such as tubular chambers, hollow fibres and planar devices (Giraldo et al., 2010). The large size of the capsule enables the encapsulation of many embedded cells, generally implanted in extra-vascular sites such as the peritoneal cavity (Song and Roy, 2016).

Macroencapsulation research began in 1933, when insulinoma tissue was inserted into permselective membranes to determine the role of vascularization or its absence on transplanted tissue (Bisceglie, 1934). Since then, numerous macro-devices have been reported, with some already available in the market, such as TheraCyte and ViaCyte. TheraCyte devices utilize bi-layered polytetrafluoroethylene membranes, to facilitate neovascularization, and to provide immune protection (Lee et al., 2009). ViaCyte uses a semipermeable membrane (branded as “Encaptra”) to encapsulate pancreatic progenitor cells for *in vivo* differentiation (Ernst et al., 2019).

These devices can be easily implanted and removed with minimal risk. On the other hand, their major drawbacks are related to islet cell aggregation and limited oxygen and nutrient diffusion. These factors may lead to compromised islet viability and eventual graft failure. Another limitation associated with such devices is their delayed insulin secretion in response to abrupt changes in glucose concentrations (Skrzypek et al., 2017). The time lag created by these devices directly affect the physiological kinetics of insulin.

3.2.2.2. Microencapsulation

Microcapsules incorporate individual or small groups of islets in a spherical hydrogel polymer with a stable mechanical structure. Different methods, such as drop extrusion, and microfluidic flow, can produce wide capsule size diameters ranging from 2,000 μm to as low as 200 μm, respectively (Giraldo et al., 2010). Ideally, microcapsule size should not exceed 300 μm, as this facilitates more effective inward diffusion of oxygen and nutrients (Steele et al., 2014). However, a decrease in capsule size as small as 300 μm has also been shown to induce a progressively stronger fibrotic response (Ernst et al., 2019).

Several considerations favour microcapsules over macrocapsules. The spherical geometry and low volume of microcapsules offer better oxygen and nutrient transport due to a higher surface area-to-volume ratio. Moreover, the small diameter of these capsules requires less invasive surgery, being achieved by simple injection into the desired implantation site (Kang et al., 2014). Within the peritoneal cavity, larger (800 μm) hydrogel capsules remain free-floating in the peritoneal fluid while smaller (500 μm) capsules aggregate and adhere to peritoneal organs (Ernst et al., 2019).

A variety of animal models used for islet transplantation with or without encapsulation has been reported (Sakata et al., 2012). For example, Souza et al. compared the transplantation of free islets and encapsulated islets in rodents showing that encapsulated islets transplanted into the peritoneal cavity were functional for an average of 100 days without the use of immunosuppressant drugs. While non-encapsulated islets were transplanted into the liver and they lasted for an average of 167 days with the use of immunosuppression drugs (Souza et al., 2011). In 2006, one of the first studies in humans, reported allogenic islet transplantation in alginate microcapsules (Calafiore et al., 2006).

A downside of microencapsulation is the difficulty associated with retrieving the capsules (if not impossible) following implantation. Moreover, traditional methods of islet microencapsulation can still result in diffusional limitations associated with capsule size,

The mean diameter of islets is on average 150 μm and the total number of islets to achieve insulin independency is 200,000 IEQ. After microencapsulation, the total volume of one encapsulated islet cell can increase dozens of times. If 1000 IEQ is contained in 1 cm^2, the volume of the implant will measure up to 400 cm^2, making the peritoneal cavity the only viable for site for transplantation (Weir, 2013).

In addition, microencapsulation can result in inadequate or incomplete coating of the islets. These islets protruding from the capsule are not immunoisolated and can thus trigger the immune attack leading to graft rejection (Zhang and He, 2011).

3.2.2.3. Nanoencapsulation

Ultra-thin coatings using L-b-L assembly or conformal polymerization directly modify the surface of islets to enhance transport and mechanical properties (Zamboni and Collins, 2017). These coatings aim to cover each islet with a uniform thickness rather than controlling the overall capsule diameter like in microencapsulation.

L-b-L deposition of oppositely charged biomaterials is achieved by the sequential adsorption of complementary multivalent molecules, such as polymeric electrolytes, nanoparticles, and proteins on the islet or β cell surface (Oliveira et al., 2016). Alternatively, a conformal coating technique based on the interfacial polymerization of biomaterials to form a thin (< 500 nm) and cross-linked coating network on the surface of islets and β cells can be employed (Zhi et al., 2013). This cyclic stepwise deposition method can tailor the final number of layers and coating thickness, thus, dictating the permeability and robustness of the coating (Silva et al., 2016a). The development of this thin nano-sized membrane minimizes graft size and volume, thereby enabling graft transplantation into sites such as the renal capsule and the liver (Yang and Yoon, 2015).

A serious consideration for electrostatic L-b-L assembly design is cytotoxicity of the polymer. It has been widely observed that polycations impair cell viability (Ernst et al., 2019). The instability of ionic interactions in L-b-L polyelectrolyte membranes are acknowledge to be prone to consumption, degradation and loss of selective permeability (Calafiore, 2018). However, cytotoxic by-products released during conformal chemical crosslinking could potentially disrupt the integrity of cell membrane, causing cell death.

3.2.3. Surface Engineering the Plasma Membrane of β Cells

Researchers are now using surface engineering approaches in order to manipulate the cellular membrane through the attachment of biomolecules to cell surface proteins or by anchoring biomolecules to the phospholipid bilayer and these studies are detailed in Table 3. There are two principal methodologies associated with the anchoring of biomolecules to cell surfaces. One is by chemical conjugation where amine groups of the cell surface proteins are chemically conjugated to linkers carrying bio-functional molecules and the second is by the physical insertion or adsorption of hydrophobic moieties such as fatty acid tails (that are conjugated to bio-functional molecules) into the lipid bilayer (Kim and Tae, 2015) as shown in Figure 3.4.

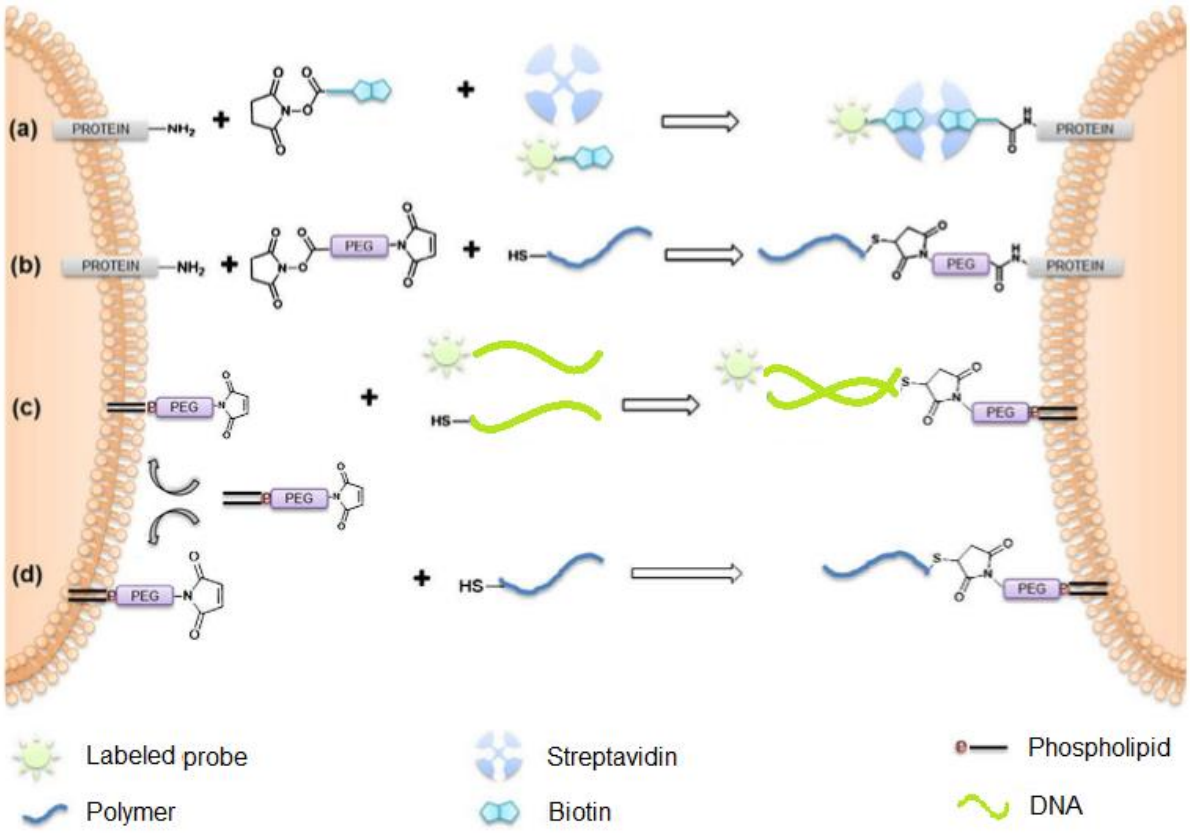

Figure 3.4. Schematic diagram of surface engineering by chemical conjugation (a and b) and physical insertion (c and d) (modified from (Kim and Tae, 2015)).

Table 3.1: Nanotechnologies for cell-based therapies in T1DM.

Method	Materials	Cell type	Outcome

Layer-by-layer assembly of multilayers	Chitosan (90-150 kDA) and alginate (75-100 kDa) bilayers with outermost layer of phosphorylcoline (PC)-modified chondroitin sulphate (20 kDa)	MIN-6 pseudoislets	Exclusion of antibody probe (150 kDa) using deposition of 2-3 bilayers. Decreased protein absorption due to PC-modified chondroitin sulphate (Zhi et al., 2010)
	PC-derivate chitosan and PC-derivate alginate with outermost layer of PC-modified chondroitin sulphate	Murine isolated islets	Preserved post implantation islet function for up to one month (Zhi et al., 2012)
	12 layers of cerium oxide nanoparticles/ alginate	Pancreatic β cells	The encapsulation promoted complete protection to the entrapped β cells from oxidative stress, with no significant changes in cellular metabolic activity, oxidant capacity, or insulin secretion dynamics, when compared to untreated controls (Abuid et al., 2019)
	15-30 kDa poly-L-lysine (PLL) and 60 kDa poly(ethylenimine) (PEI)	Rat Pancreatic islets	PLL/PEI polyelectrolyte multilayer allowed survival and function of encapsulated cells (Granicka et al., 2011)
	Multilayers of phosphatidine-functionalized poly(amidoamine) (PANAM) dendrimer, highly branched dicarboxyphenyl glycineamide-alginate and PEG	Pancreatic Islets	Bioorthogonal L-b-L encapsulation of pancreatic islets via hyperbranched polymers resulted in high coating efficiency and stability, as well as, islet viability and function (Gattas-Asfura and Stabler, 2013)
	three-layers of SH-6-arm-PEG-NHS, 6-arm-PEG-catechol and linear PEG-SH	Non-human primate pancreatic islets	L-b-L islets were transplanted in a xenorecipient (mice) showing 100% survival rate for

			150 days after transplantation in comparison to naked islet (poor survival time of 77.5 ± 42 days) (Haque et al., 2017)
Conformal polymerization of multilayers	Thiolated PVA and Pyridine-modified PVA	Murine isolated islets	(Teramura et al., 2007)
	PEG-block-PLA-based polymersomes (PSomes) crosslinked between bi-functional PSomes (NHS-/NH2-PSomes).	Neonatal porcine islet-like cell clusters	Nanoencapsulation did not affect insulin secretion (Kim et al., 2020)
	PANAM and alginate	Pancreatic rat islets	Encapsulated islets were viable and functional. Upon transplantation, encapsulated islets showed no foreign body responses (Gattás-Asfura et al., 2020)
	PEG-NHS covalently linked to PANAM-hyperbranched alginate	Rat isolated islets	(Gattas-Asfura and Stabler, 2013)
	Eight-arm 10-kDa PEG functionalized with vinyl sulfone crosslinked with alginate	Islets were isolated from C57BL/6 mice	PEG-ALG conformally coated islets allowed small transplant volumes in the renal subcapsular space and show good biocompatibility and functionality, as the graft reversed diabetes in an animal model (Tomei et al., 2014)
	Maleimide-PEG crosslinked with homobifunctional SH-PEG-SH at a 3:1 molar ratio	Stem cells-derived islets	Conformal coated cells displayed physiological insulin secretion and reversed diabetes in mice (Stock et al., 2020)

Cell surface biotinylation	Biotin-PEG-triphenylphosphine with co-immobilization of thrombomodulin via streptavidin-biotin interaction	Murine isolated islets	Decreased immediate post-transplant IBMIR (Wilson et al., 2010)
	Avidin-coated nanoparticles conjugated to biotin-PEG	Murine isolated islets	Islet functionality is not impaired by encapsulation and islet viability is prolonged *in vitro* and *in vivo* (Dong et al., 2012)
	Biotin-NHS, Biotin-hydrazide and Maleimide-PEG-biotin	Human, porcine and murine isolated islets	Murine islets are not necessarily predictive of human and porcine islet surface chemistry (SoRelle et al., 2015)
Cell surface PEGylation	Maleimide-PEG-phospholipid with co-immobilization of heparin and SR-1	Rat isolated islets	Prevented immediate post-transplant IBMIR (Luan et al., 2011)
	Maleimide-PEG-phospholipid with co-immobilization of urokinase and thrombomodulin	Hamster isolated islets	Prevented immediate post-transplant IBMIR (Chen et al., 2011a)
	Hybridization of PEG-phospholipid liposomes carrying anticoagulant (argatroban) to DNA	Murine isolated islet	Prevented immediate post-transplant IBMIR (Chen et al., 2011b)
	Gelatin-catechol covalently linked to 6 arm-PEG-phospholipid conjugated with 3 different PEG layers (6-arm-PEG-SH, 6-arm-PEG-catechol, and linear PEG-SH)	Porcine isolated islets	Improved stabilization of islets and prevention of immune cells infiltration (Haque et al., 2016)
Others	6 arm-PEG modified with catechol (Jeong et al., 2013, Jeong et al., 2011) and 8 arm-PEG-catechol covalently linked to heparin (Im et al., 2013)	Rat isolated islets	Surface-camouflaged islets inhibited host immune cell infiltration, activation and IBMIR

Heparin-conjugated Dihydroxyphenylalanine	Rat isolated islets	Improved intrahepatic islet xenograft survival to inhibit IBMIR (Jung et al., 2012)
Glycol-chitosan conjugated to polyaldehyde-modified heparin covalently linked to cell membrane amines	Murine isolated islets	The incorporation of 1-antitrypsin to the nanocoating exhibited effective anti-coagulant activities *in vitro* (Zhi et al., 2015)
Maleimide-4 arm-PEG-RGD with co-immobilization of Vascular Endothelial Growth Factor (VEGF)	Rat isolated islets	VEGF-islet coatings were transplanted to the small bowel mesentery of healthy rats and revascularized by 4 weeks (Phelps et al., 2015)

3.2.4. Nanocoating Functionalization

In association with surface engineering and ultra-thin cell encapsulation systems, many other strategies can be implemented to tackle IBMIR, poor graft vascularization and hypoxia. Gene delivery technology can complement cell engineered systems to mask the immunological response against islet grafts. Tracking probes are also being researched for non-invasive post-transplantation monitoring of graft fate. The representation of nanocoating strategies is shown in Figure 3.5.

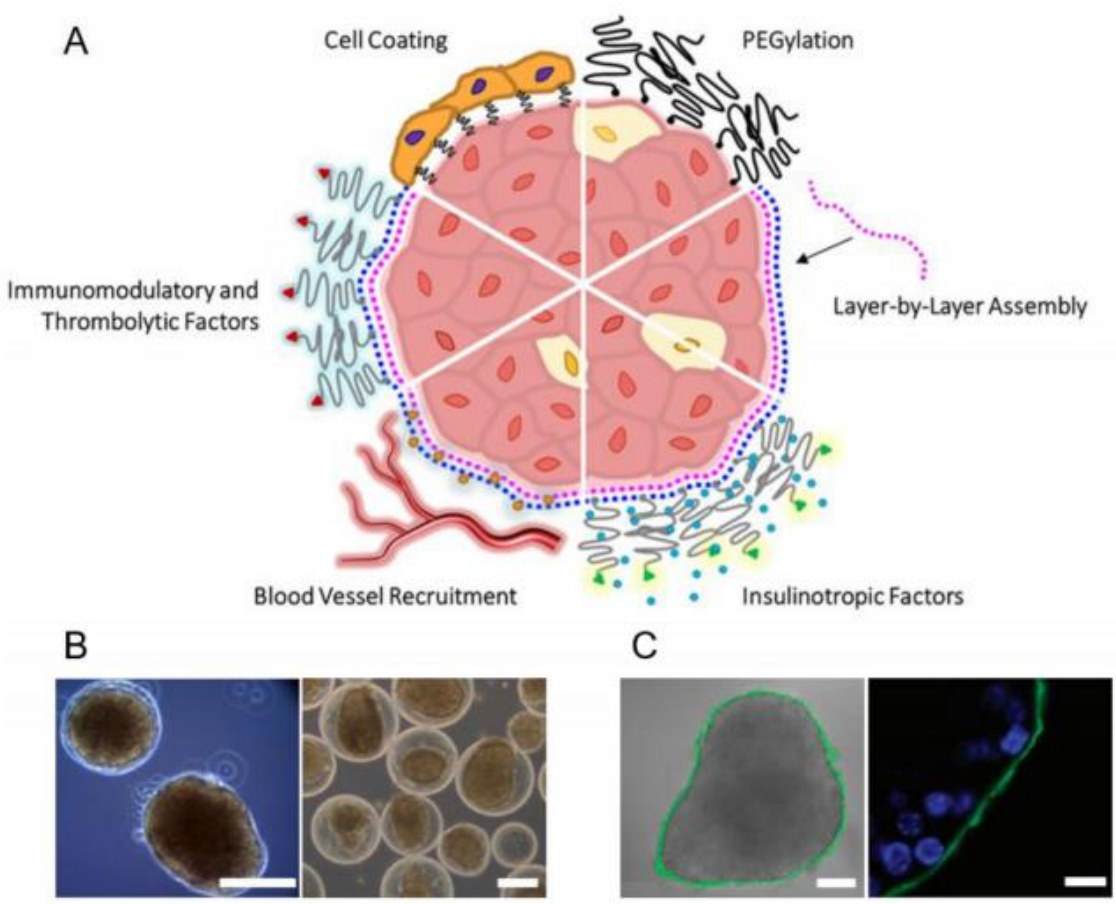

Figure 3.5. Bioengineering a nanoencapsulation system. A) Nano-thin coatings may be generated by (top right, proceeding clockwise): surface engineering (PEGylation); L-b-L or conformal assembly of alternating polymer layers deposited directly on the islet surface. Nano-coatings can be functionalized with (continuing clockwise): bioactive accessories such as insulinotropic agents including GLP-1 (green; insulin shown as blue circle); blood vessel recruiting factors (e.g. heparin, orange circles); immunomodulatory and thrombolytic agents (red; e.g. soluble complement receptor-1, thrombomodulin, urokinase, phosphorylcholine, heparin); or a cellular layer (e.g. endothelial cells, immunomodulatory cells). (B) Examples of conformal coating: phase contrast images of mouse islets conformally coated with a PEG-alginate composite gel (left) and rat islets conformally coated with a PEG-Matrigel composite gel. (C) Example of L-b-L nanocoating: brightfield image overlaid with confocal micrograph of 8-bilayer (PLL-g-PEG/ fluorescein-labelled alginate, green) coating; confocal micrograph showing coating localized on peripheral islet extracellular surface (Ernst et al., 2019).

3.2.4.1. Immobilisation of Therapeutic Agents

One unresolved issue is early graft loss due to inflammation triggered by blood coagulating on the surface of islets after transplantation. The blood coagulation and

complement systems are activated when islets are exposed to fresh blood in the portal vein, inducing IBMIR which results in graft loss (Teramura and Iwata, 2008). Systemic anticoagulation therapy to control these reactions after transplantation have successfully reduced islet loss; however, they are associated with an increased risk of bleeding. For this reason, incorporation of anti-inflammatory and antithrombotic agents for local release and control of coagulation and IBMIR have been investigated (Zhi et al., 2013). Immobilization of heparin (Im et al., 2013), urokinase and thrombomodulin (Chen et al., 2011a) on engineered cell surfaces has been reported to inhibit coagulation and complement activation, thereby reducing IBMIR. Curcumin, an anti-inflammatory drug, was co-encapsulated with pancreatic islets inside an alginate microcapsule, resulting in reduced fibrotic overgrowth (Dang et al., 2013).

3.2.4.2. Co-transplantation

Two separate studies in 2015 report the co-encapsulation of β cells with other cell types, such as mesenchymal stem cells (MSC) and hematopoietic stem cells with the objective of modulating host immune cells to provide immunotolerance (Schuetz and Markmann, 2015, Yoshimatsu et al., 2015, Oliveira et al., 2017). Other studies detail the co-encapsulation of pancreatic β cells with islet accessory cells, i.e. endothelial and perivascular cells, in order to the re-establish the vascular network of transplanted islets while minimising the occurrence of graft loss due to hypoxia and IBMIR (Del Toro-Arreola et al., 2016, Avolio et al., 2016, Kim et al., 2011, Li et al., 2013).

3.2.4.3. Vascularization strategies

Natural tissues and organs exhibit a 3D architecture which allows cell-to-cell and cell-to-ECM interactions. Survival of this large 3D architecture relies on blood perfusion within an intricate vascular network, delivering oxygen and nutrients while removing carbon dioxide (CO_2) and metabolites. The adequate vascularization of 3D tissue-engineered substitutes is a major engineering hurdle in creating artificial organs, as vascularisation is considered to be one of the greatest challenges in tissue engineering. Post-transplantation success of these tissue substitutes is highly dependent on the ability to promote rapid and stable neovascularization (formation of new blood vessels) to support the growth, function, and viability of the graft. Researchers rely on the increasing knowledge of angiogenic and vasculogenic processes to stimulate vascular network formation within 3D tissue constructs. The stimulation of the vascular network can be

performed by the incorporation of pro-angiogenic materials or growth factors on the development of cellular scaffolds.

In addition to the co-encapsulation of endothelial and perivascular cells, the incorporation of VEGF into the polymeric encapsulant accelerates proliferation and differentiation of nearby endothelial cells to produce a neovascular network within the graft at the transplantation site (Borg and Bonifacio, 2011). However, vascularization does not occur instantly after transplantation and other measures must be in place to provide early oxygen supply to the graft (Gholipourmalekabadi et al., 2016). Oxygen generating biomaterials are discussed below.

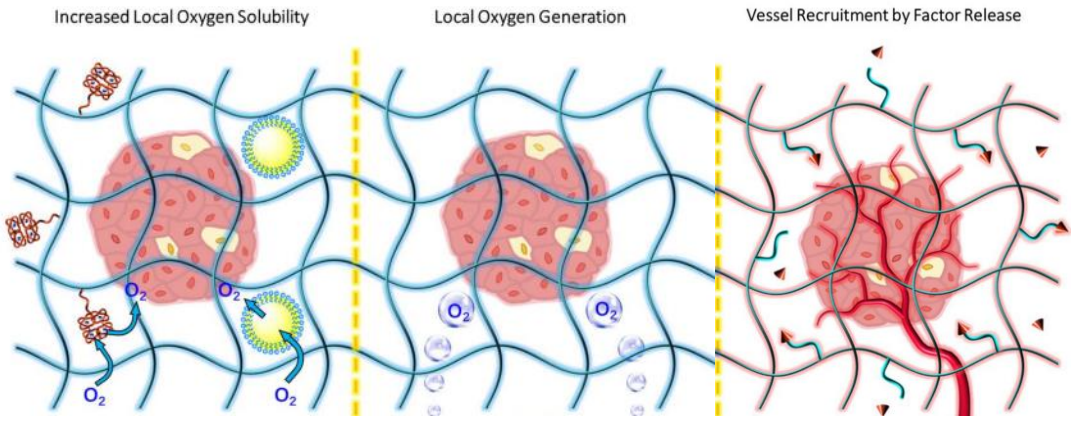

Figure 3.6. Oxygen-releasing systems for local and early oxygenation of pancreatic beta cell grafts and vascularization recruitment. Left: haemoglobin-conjugated (red) or perfluorocarbon (yellow) functionalized hydrogels; middle: peroxide particulates; and right: incorporation of growth factors, such as VEGF for the stimulation of vessel formation and recruitment (Ernst et al., 2019).

3.2.4.4. Oxygen-releasing Systems

In an attempt to address poor graft oxygenation oxygen-releasing systems have been proposed (Figure 3.6). These systems can be based on the use of peroxides, such as calcium peroxide (CaO_2), showing to prevent hypoxia-induced β cell death (Pedraza et al., 2012, Steg et al., 2016). Haemoglobin-based oxygen carriers and perfluorocarbon have been employed as blood substitutes (Jia et al., 2016). However, in 2014, *in situ* cell encapsulation of perfluorocarbonated-HA hydrogel was able to promote fibroblast cell growth under hypoxic conditions (Palumbo et al., 2014). Another oxygen-releasing system created exclusively for pancreatic islet transplantation, called Beta-O_2, utilises an

oxygen refuelled macro-chamber (called beta-air) that is composed of two compartments: one for islets and other for O_2 supply (Colton, 2014).

3.2.4.5. Gene Delivery Immunosuppressant Strategies

As discussed, targeting the immune system provides good outcomes in islet transplantation however caution must dictate as the immune system plays an important role in the surveillance of cancerous cells in the body and when our immune defences are lowered, opportunistic infections unfold. For this reason, the regulation of the immune system without the depletion of immune cells or the total ablation of the immune response is key for a balanced immunological function. With this in mind, we present the possibility of controlling the immune system using the transfection of genetic material to encode regulatory proteins for transient or permanent alteration of cell phenotype. For example, RNA-based gene therapy can reduce immunogenicity and mutagenesis and has proven to be more efficient than DNA-based gene therapy (Hill et al., 2016). For the transfection of genetic material, viral and non-viral vectors have been employed. Viral vectors (lentivirus, adenovirus and adeno-associated virus) are well suited to deliver genes that prevent islet immune rejection (Tian et al., 2007), but pose risks to recipients due to their inherent immunogenicity, to combat this they are co-administered with immunosuppressant agents (Foldvari et al., 2016). Non-viral gene carriers (such as lipids and positively charged polymers) are less efficient gene delivery agents than viruses but they possess higher packaging capacities.

Liposomes carrying CCL22 gene transfected in myocytes on the site of transplantation of islets increased local T regulatory cells accumulation and delayed islet graft rejection (Vagesjo et al., 2015). The cellular secretion of exosomes has also been investigated as potential nanocarriers of genetic material for gene delivery applications. Exosomes naturally deliver RNA from cell to cell and they can target specific cell types due to receptor-mediated interactions present in the exosome membrane. In this context, transfected hematopoietic stem cells derived from bone marrow delivered exosomes loaded with silencing RNA to pancreatic islets inducing down-regulation of Fas (Wen et al., 2016).

Gene therapy with IL-10 is of particular interest to investigators because IL-10, a cytokine synthesis inhibitor factor, has a critical role in modulating the immune system by down-regulating the expression of IL-17 and decreasing lymphocyte infiltration on islet grafts (Gower et al., 2014, Zhang et al., 2003). Furthermore, IL-10 also decreases the expression of IL-23 on dendritic cells, of which IL-23 is essential for the expansion and maintenance

of IL-17 producing T helper cells. In allogenic transplant rejection, dendritic cells are important immunological cell mediator types because they present alloantigen in the lymph node. This initiates the adaptive immune response by activating effector T helper cells that destroy the graft. As mentioned previously, dendritic cells also produce cytokines (IL-23) that inflict further injury and support the reactivity of alloreactive T cells. For these reasons, dendritic cells are the cell type targeted in gene delivery therapeutics for allograft immunotolerance (Fan et al., 2015).

3.2.4.6. Bioimaging Nanotechnology

Monitoring graft loss, which can occur secondary to immunological or non-immunological causes, either in the first phase after transplantation or in the later stages of a patient's life is a central issue in transplantation therapy. No imaging methodology currently exists to monitor viable islet mass after clinical intraportal islet transplantation, but imaging modalities have a prospective role in monitoring graft fate.

Due to the fact that islets are very small in size (50-600 μm in diameter), have a very low density (approximate 1%) and are localized deep in the abdomen, their specific imaging can be particularly challenging. Positon-emission tomography (PET), single photon emission computed tomography (SPECT) and MRI are all imaging techniques being applied to visualize post-transplanted islets.

PET and SPECT use radiolabelled tracers (Eter et al., 2015) and MRI uses superparamagnetic iron oxide (SPIO) (Malosio et al., 2015, Medarova et al., 2009, Hathout et al., 2009, Wang et al., 2013, Toso et al., 2008). When analysing the sensitivity of these imaging modalities for islets, MRI is shown to have poor islet sensitivity in comparison to other modalities because SPIOs are not efficiently taken up by islet cells. On the other hand, MRI shows better spatial resolution than PET and SPECT (McCall and Shapiro, 2012).

PET radiolabelled markers have been used to trace viable pancreatic islets (Jodal et al., 2017). A clinical study evaluated 8 human subjects that underwent intraportal islet transplantation using [^{11}C]5-hydroxytryptophan to trace viable islets. The marker uptake by the liver as a whole, or in defined hotspots, was correlated to measurements of islet graft function (Eriksson et al., 2016). Novel radiotracers such as radiolabelled exendin are under pre-clinical testing and they display high affinity to islets and are reported to be a promising tracer to visualize transplanted islets by SPECT. Radiolabelled exendin binds to GLP-1 receptor on islets. It was observed that radiolabelled exendin accumulated as

early as 3 days after transplantation and for up to 3 weeks post-transplantation which correlated to graft revascularization (Eter et al., 2015).

For encapsulated islets, SPIO ferumoxide (Feridex®) has been used to label alginate microcapsules. These magnetocapsules facilitated the graft monitoring by MRI over time and simultaneously provided immunoprotection to islets (Barnett et al., 2007). Labelling of islet cells with SPIO through DNA hybridization with the cell membrane was reported for monitoring of transplanted islets by MRI (Kitamura et al., 2013).

In 2015, quantum dots (QDs), inorganic semiconductor nanocrystals of groups II-VI, III-V or IV-VI, have been utilised as *in vivo* imaging probes in animal models (Liu et al., 2015). The main limitation of QDs is that they require a light excitation source that possess low tissue penetration capabilities (up to 1 cm deep) which restricts the detection of implants to subcutaneous depths (Iverson et al., 2016). To address this matter, self-illuminating QDs have been proposed. Bioluminescence resonance energy transfer (BRET) QDs have been conjugated to luciferase which induces QD emission (He and Ma, 2014). QDs were also attached to the cell membrane by biotin-avidin conjugation and by DNA hybridization (Wang et al., 2016a, Banerjee et al., 2016). This technology is still in its infancy and it will take considerable time before it reaches human clinical trials. Nevertheless, QDs present the potential application for the follow-up analysis of transplanted grafts in patients with T1DM.

3.3. Final Considerations

This chapter highlighted many tissue engineering strategies utilized for the development of bio-engineered insulin-producing cell constructs to treat T1DM. The summarized combination of the different approaches presented below is believed to offer an appropriate platform for the development of a cell-based therapy for T1DM:

a) Suitable cellular sources for pancreatic β cell replacement.

- Reprogramming autogenic cell types to create insulin-producing cells has the potential alone to mitigate transplant rejection. However, drawbacks are associated with genetic abnormalities and mutagenicity of the reprograming factors.

b) Suitable transplantation site should provide easy access for implantation and removal, immune protection, a physiological route for insulin delivery, a sufficient blood and oxygen supply and enough space for hosting the cellular graft

- Transplantation under the kidney capsule confers an appropriate confined space for the cellular transplant, it is relatively close to many blood vessels for appropriate oxygen supply and insulin delivery.

c) Suitable immunoisolation environment

- Nano encapsulation provides an appropriate environment for cellular grafts to re-establish ECM-cell interactions to improve graft functionality and survival

- Nano encapsulation provides an appropriate environment to prevent graft failure from immune-mediated rejection and the need for systemic immunosuppression

- Nano encapsulation also decreases graft size and volume for transplantation

- Effective immunoisolation environment is dependent on biomaterial selection

In the next chapter, a compilation of the most recent discoveries and findings associated with tailored HA structure/function relationships for cell encapsulation strategies will be discussed. The next chapter highlights HA's role in immunomodulation, vascularization and its anti-microbiological properties which are particularly critical to the reestablishment of pancreatic β cell functionality after isolation and encapsulation.

Chapter 4: Hyaluronic Acid in Tissue Engineering

The following chapter presents an in-depth review of literature. The contents of this chapter are adapted from the review article published in Progress in Materials Science.

Zamboni, F.; Vieira, S.; Reis, R. L.; Oliveira, J. M. and Collins, M. N. The Potential of Hyaluronic Acid in Immunoprotection and Immunomodulation: Chemistry, Processing and Function. Progress in Materials Science v. 97, p. 97-122, 2018.

DOI: 10.1016/j.pmatsci.2018.04.003

4.1.Background

HA owes its name to its transparent and bright appearance, named after hyaloid meaning "glassy" in Greek. HA was first described in the literature in 1918, when a new polysaccharide consisting of glucosamine and glucuronic acid was discovered (Levene and López-Suárez, 1918). A few years later, another independent publication reported the isolation of an extremely high molecular weight polysaccharide from the vitreous eye of cows (Meyer and Palmer, 1934). HA was initially produced by the extraction from various animal parts. However, the growing demand for HA shifted the production to microbiological sources. In 1937, Kendall et al. isolated HA from streptococci A and C (Kendall et al., 1937), which remains to date the most economical and reliable source for the industrial production of HA.

HA – the only non-sulphated GAG – is found in the ECM of many soft connective tissues, where it acts as a space filler, lubricant, and osmotic buffer (Clegg et al., 2013, Laurent et al., 1996). HA is anionic and contains alternate units of the disaccharide β-1,4-D-glucuronic acid-β-1,3-N-acetyl-D-glucosamine. The mutual repulsions between the carboxyl groups of the glucuronic acid moiety of HA causes it to swell forming a hydrated network. The associated plasticity of HA is highly important for tissue reorganization and embryonic development (Theocharis et al., 2016).

Among all GAGs, only HA is biosynthesized at the cell membrane and not within the Golgi apparatus. Moreover, HA is also the only GAG not covalently attached to proteoglycans (Theocharis et al., 2016). It binds either to its own synthases or to cell surface receptors (CD44 and RHAMM) (Acharya et al., 2008), being then involved in several cell function responses (Nasreen et al., 2002).

The size of HA depends on the relative activity of HA synthesizing and degrading enzymes. In mammals, there are three hyaluronan synthase (HAS) isoforms (HAS-1, 2, and 3) that mainly differ in their enzymatic ability to produce HA of different sizes. HA clearance *in vivo* starts when it binds to HA receptor for endocytosis (HARE) on the cell membrane (Pandey and Weigel, 2014). Then, HA is rapidly degraded by physiological enzymes called hyaluronidases (HYAL). The majority of HA degradation is obtained by HYAL-1 and HYAL-2, where they break the β1→4 glycosidic bond of HA to form LMW fragments that possess size-dependent functions (Stern, 2004). HYAL-1 is found in the lysosome and utilizes HA as a substrate to generate tetrasaccharides whereas HYAL-2

which is found in the plasma membrane (anchored by glycosilphosphatidyl-inositol) degrades HA to fragments of about 20 kDa (Stern, 2004).

HA is a material of increasing significance in bioengineering and biomaterials science due to both its physical and chemical properties, that can be processed in a versatile range of forms, such as in solution, film or hydrogel (Collins and Birkinshaw, 2008a, Collins and Birkinshaw, 2013b). Subsequently, there is no surprise why HA has found a variety of biomedical applications concerned with body repair, which include uses in cosmetics and cosmeceuticals (Bukhari et al., 2018), visco-supplementation (Bowman et al., 2018), wound healing (Graça et al., 2020), drug delivery systems (Choh et al., 2011), tissue engineering (Song et al., 2013), cell encapsulation (Peroglio et al., 2012) and microfluidics (Burdick and Prestwich, 2011).

4.1.1. Chemical Modifications of HA

As previously described, HA is readily degraded into bioactive fragments by enzymatic and hydrolytic degradation. The development of hyaluronidase inhibitors – such as hyaluromicyn – improve HA structural stability against enzymatic degradation (Kohi et al., 2016). Chemical modification and crosslinking strategies are used to decrease HA degradation by hydrolysis (Collins and Birkinshaw, 2007a). HA modification targets the following functional groups: the carboxylic acid of the glucuronic acid moiety or the hydroxyl of the N-acetylglucosamine moiety (Figure 4.1). Carboxylic acid functional groups can be modified by amidation, Ugi condensation or ester formation. While the hydroxyl groups can be modified by ether formation, hemiacetal formation using glutaraldehyde, ester formation, carbamate formation or oxidization (Schante et al., 2011).

These HA derivatives can be chemically crosslinked by covalent bonds, physically crosslinked using non-covalent interactions or by a combination of both methods (Collins and Birkinshaw, 2008b). The crosslinking process will form a 3D network able to retain large amounts of water – a hydrogel – with properties that resemble those of biological tissues, resulting in excellent biocompatibility (Collins and Birkinshaw, 2013a).

As aforementioned, several chemistries are available, and many others can be envisioned for HA modification and crosslinking. However, not all of them are suitable for cell encapsulation, due to the need for toxic reagents and/or harsh conditions that will hamper cell viability and functionality (Burdick and Prestwich, 2011). It is then necessary to use

HA systems that can be produced under physiological conditions, with proper gelation kinetics and also with processes that are free of toxic by-products (Xu et al., 2012).

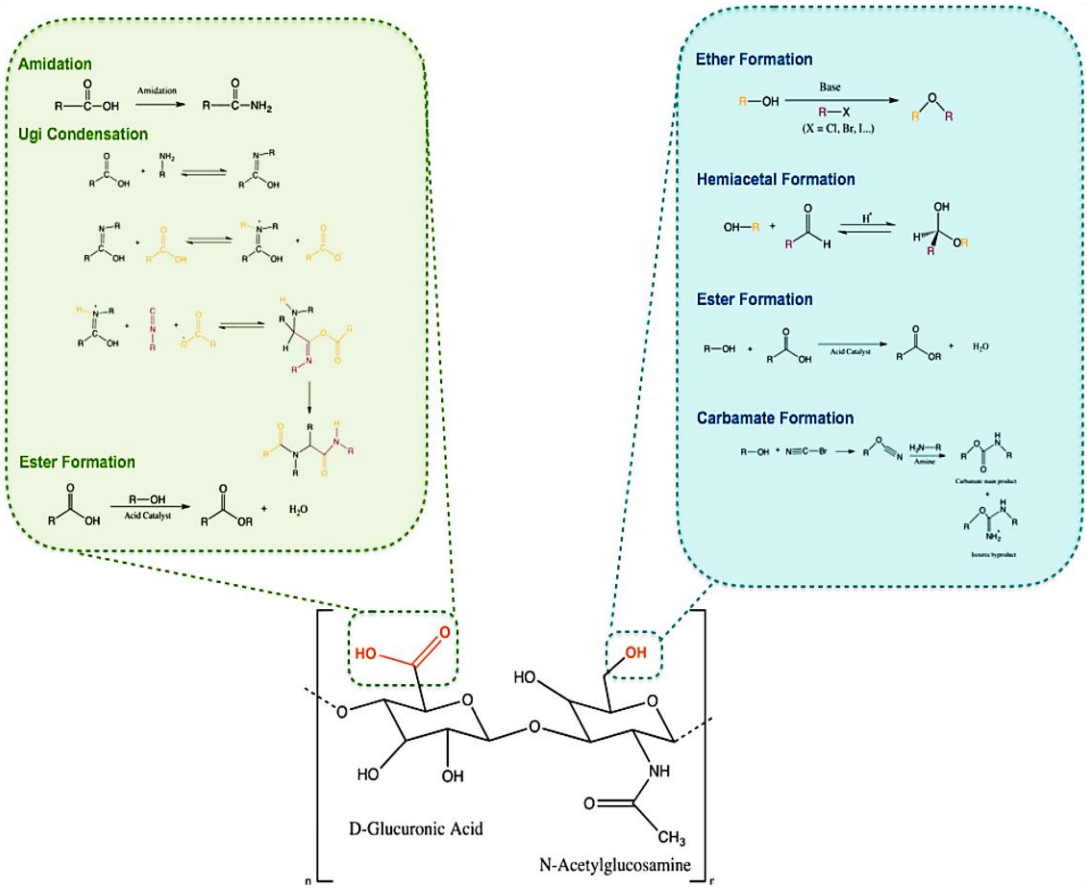

Figure 4.1. Chemical structure of HA and common modification reactions.

In tissue engineering, photo-initiated systems have been extensively utilized for cell encapsulation strategies (macro and microencapsulation). These hydrogels result mainly from the polymerization of water-soluble monomers in the presence of a multifunctional crosslinker by ultraviolet (UV) radiation (photo-crosslinking) or by the reaction between complementary groups (Bae et al., 2014, Choi et al., 2015). Although the rationale behind the development of these hydrogels is very simple, the resulting hydrogels commonly have increased structural stability, longer degradation and high swelling profiles (Collins and Birkinshaw, 2008a).

However, photo-polymerized hydrogels bring a few concerns relating to cell viability for cell encapsulation. Cell exposure to UV radiation increases the cellular production of reactive oxygen species (ROS) such as superoxide (O_2-) and hydrogen peroxide (H_2O_2).

They may induce lipoperoxidation and damage to DNA (Markovitsi et al., 2010) of cells and increase the oxidative degradation of HA (Valachova et al., 2016, Valachova et al., 2015). The use of photo initiators (such as Irgacure 2959, 2,2-dimethoxy-2-phenylacetophenone – DMPA, lithium phenyl-2,4,6-trimethylbenzoylphosphinate - LAP and eosin Y) in HA gelation have been well described (Poldervaart et al., 2017, Jha et al., 2010, Gwon et al., 2017, Rosales et al., 2017). However, it is known that these photo-initiators are cytotoxic in a time and concentration dependent manner (Xu et al., 2015b), although LAP is shown to be the most benign (Kessler et al., 2017).

In relation to the use of photo-initiators in HA gelation processes for cell encapsulation strategies, the cell type being encapsulated can influence the construct outcome. For instance, different cell types respond differently to photo-initiator's toxicity. This is thought to be due to the variable intracellular anti-oxidative machinery that different cell types use to quench ROS (Williams et al., 2005). For example, pancreatic β-cells are particularly sensitive to oxidative stress because of their low antioxidant capacity (Drews et al., 2010). Therefore, when using photo-polymerization in HA gelation processes for cell encapsulation applications, additional protective measures from oxidative stress, such as antioxidants and scavenger enzymes, should be put in place to ensure the maintenance of β-cell viability (Weaver and Stabler, 2015, Asami et al., 2013).

Therefore, the development of other covalent crosslinking chemistries is needed to tailor the structural stability of HA and produce novel HA derivates that provide more biocompatible alternatives to harmful effects associated to, for example, covalent photo-crosslinking reactions.

A number of chemical modifications have been developed as an alternative to photo-polymerization. For nanoencapsulation, for example, the sequential deposition of layers can be achieved by guest-host assemblies. For instance, HA has been conjugated to cyclodextrin (host) and adamantane or azobenzene (guest), curcubit(6)uril (host) and polyamine (guest), such as spermine and 1,6-diaminohexane, to self-assemble into hydrogels (Rodell et al., 2013, Park et al., 2012b, Rosales et al., 2018). The non-covalent character of guest-host networks confers to hydrogels full reversibility under shear, allowing association or self-healing when shear is removed.

Other smart hydrogels are also under the spotlight because they can be crosslinked *in situ* through covalent crosslinking by click chemistry reactions between polymers with

complementary functional groups or by enzymatic crosslinking under physiological conditions and showing minimal toxicity. *In situ* click chemistry crosslinking was reported for azide-modified HA and cyclooctyne-modified HA and for tyramine conjugated-HA hydrogels formed by the oxidative coupling of tyramines catalysed by H_2O_2 and horseradish peroxidase (Takahashi et al., 2013, Ni et al., 2015, Abu-Hakmeh et al., 2016, Xu et al., 2015a, Khanmohammadi et al., 2016).

HA modification through thiolation has been developed, aiming to create reversible hydrogels via thiol/disulphide bond crosslinking reaction (Shu et al., 2002). Converting thiol groups into disulphide bonds can be achieved by thiol oxidation and disulphide exchange mechanism (Figure 4.2).

In disulphide exchange mrechanism, aqueous solutions in neutral pH have the conjugated base (OH^-) as the predominant form, which is strong enough to effectively deprotonate any acid with p*K*a below 16 (p*K*a of thiol groups are around 9). Thus, the thiol groups of the polymer (HA-SH) are ionized to form thiolate anions ($-S^-$). The thiolate is a nucleophile (thus being named S^-_{nuc}) that attacks the sulphur atom (central sulphur or S_c) of the disulphide moiety of the pyridine-modified polymer (HA-PD). It forms a transition state before cleaving the original bond and creating the new one. The leaving sulphur (S_{lg}) belongs to the pyridine. This mechanism allows the formation of coating layers under normal physiological conditions (Fernandes and Ramos, 2004).

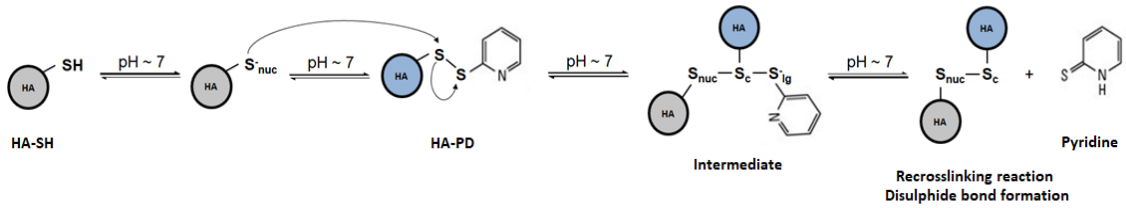

Figure 4.2. Disulphide exchange mechanism representation between HA-PD and HA-SH derivates.

4.2.HA in the Aid of Pancreatic Islet Immunoisolation

The physicochemical properties and biological functions of HA can be modulated to match the requirements for addressing the cell-specificity delivery needs in cell encapsulation strategies. Recent works have reported that HA can efficiently promote functional insulin-secreting cells and reduce adverse immune reactions after

transplantation. Table 4.1 outlines the most relevant studies and outcomes where HA has been used to encapsulate insulin-producing cells for T1DM treatment.

Table 4.1. HA in cell encapsulation therapies for T1DM.

HA MW	Other materials	Cell type	Outcome
	Alginate	Insulin-producing cells	Alginate-HA microcapsules enhanced cell viability, reduced early apoptosis and decreased membrane damage (Cañibano-Hernández et al., 2019a)
1 MDa	Methacrylate and thiolate HA in 3.4 kDa polyethylene glycol diacrylate (PEGDA)	Canine pancreatic islets	Microspheres reversed diabetes in NOD mice (Harrington et al., 2020)
	Alginate	MSC differentiated into insulin-producing cells	The addition of HA in alginate microcapsules enhanced the insulin release from insulin-producing cells (Cañibano-Hernández et al., 2019b)
	Alginate	Neonatal rat pancreatic islets	Both the insulin secretion values and the viability of HA embedded islets were higher than of alginate embedded islets (Velten et al., 1999)
	Collagen	Rat pancreatic islets	Allogenic transplantation of encapsulated islets reversed long-term diabetes and prevented graft rejection in all animals. Explanted grafts revealed viable islets in the transplant site as well as intact hydrogel, with little or no evidence of fibrotic overgrowth or cellular rejection (Harrington et al., 2017a)
Not informed		Pancreatic islets	Photo-crosslinked microcapsules (Smeds et al., 1999)
Not informed	Butyric acid and retinoic acid	Human adipose stem cells and pancreatic islets	Encapsulation showed graft revascularization after intrahepatic transplantation in

			syngeneic diabetic rats (Cavallari et al., 2012)
1,680 kDa		HIT-T15 cells	This study suggests that HA-coating increases the insulin secretion of HIT-T15 cells by the enhancement of expression of connexin 43-mediated gap-junctional intercellular communications (Li et al., 2006)
Not informed	Collagen	Isolated pancreatic islets from rats	HA-collagen hydrogel showed improved cell viability in comparison to alginate only hydrogels (Harrington et al., 2017b)

4.2.1. Intrinsic Pro-angiogenic Capacity of HA in Vascularization

The post-transplantation success of cell transplantation strategies will rely on the vascularization and oxygenation of the graft. Thus, the incorporation of pro-angiogenic materials or moieties should be considered. The influence of HA on the angiogenic process was reported in the early 1980's (West et al., 1985). While native HMW HA was reported as an angiogenic inhibitor, LMW HA are highly bioactive and stimulate the angiogenesis process (Gao et al., 2019). The size of these HA oligomers also influences the pro-angiogenic nature of the fragments. Oligomers with 6 to 10 saccharide units were shown to be proangiogenic (Wang et al., 2019) while fragments with only 4 saccharide units were unable to prompt a pro-angiogenic response (Cui et al., 2009).

In the endothelium, HA interacts with endothelial cells that line the interior surface of blood and lymphatic vessels. This angiogenic capacity comes from receptor-mediated interactions of HA oligomers with the CD44 and hyaluronan-mediated motility receptor (RHAMM) of endothelial cells, which triggers endothelial cell proliferation, migration, collagen synthesis and cell sprouting (Pardue et al., 2008). A new mechanism has been proposed for HA-promoted angiogenesis (Figure 4.3), where HA binds to CD44, promoting PKCδ activation. Upon activation, protein kinase C (PKCδ) leads to RHAMM and extracellular signal-regulated kinase (ERK) activation. This leads to the transactivation of transforming growth factor β receptor I (TGFβR1). This activation is closely related with a decrease on histone deacetylase 3 (HDAC3) expression, responsible for the induction of plasminogen activator-inhibitor-1 (PAI-1) and MMP-2.

Both PAI-1 and MMP-2 will promote angiogenesis (Park et al., 2012a). Recently, Olivares et al. showed that by inhibiting HA synthesis it was possible to supress angiogenesis in endometriotic lesions, highlighting the key role of HA in the vascularization process (Olivares et al., 2016).

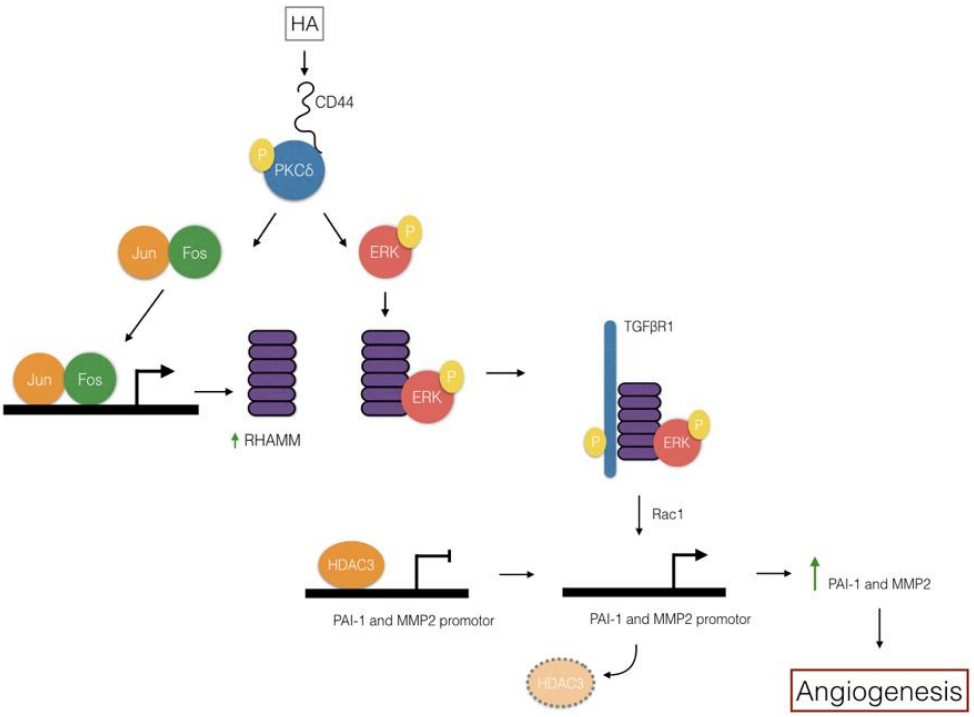

Figure 4.3. Proposed signalling cascade of HA-promoted angiogenesis. Adapted from (Park et al., 2012a).

As a result, HA oligomers have been used to increase the angiogenic capacity, and consequent vascularization, of other biomaterials (Silva et al., 2016b, Perng et al., 2011), and also to enhance wound healing strategies (Wang et al., 2016b). A recent clinical trial demonstrated that HA hydrogels enabled the vascularization of free gingival grafts and functioned as a scaffold between the recipient's transplantation bed and the gingival graft, reducing graft shrinkage (Cankaya et al., 2020). Another study showed that HA is able to sequester growth factors and enables endothelial cells derived from human induced pluripotent stem cells to form stable, capillary-like networks (Natividad-Diaz et al., 2019). In addition, HA-based matrices were also reported to selectively bind to VEGF (Lim et al., 2016) and release VEGF by mediated MMP degradation (Jha et al., 2016).

Other studies also show that HA hydrogels also upregulated the expression of angiogenic markers such as VEGF and fibroblast growth factor 2 (FGF-2) in endothelial cells and fibroblasts, respectively, resulting in a neovascular response *in vitro* (Ciccone et al., 2019). Scaffolds made of a microfibrous blend of poly(L-lactide-co-ε-caprolactone) and HA also increased CD34 expression of endothelial cells, resulting in the formation of small vessels (Kenar et al., 2019). Endothelial cells also increased their CD31 expression [also called platelet endothelial cell adhesion molecule (PECAM-1)] when cultured on HA-modified collagen nanofibers for a vascular tissue-engineered scaffold (Kang et al., 2019). Furthermore, higher expression of CD31 by endothelial cells, when exposed to HA, shows immunomodulatory properties, as it inhibits the circulation of leukocytes (Lertkiatmongkol et al., 2016). HA-modified collagen nanofibers also promoted lymphatic endothelium formation by increasing the expression of lymph vessel endothelial hyaluronan receptor-1 (LYVE-1) (Gao et al., 2019).

4.2.2. Intrinsic Immunomodulatory Capacity of HA

The immune system is a defence mechanism against environmental threats and pathogens, it can be divided in the innate and adaptive immune system. When the immune system experiences a biological imbalance, several chronic and acute inflammatory conditions can be triggered, as well as the development of several autoimmune conditions (Zamboni et al., 2018a).

The immune system also plays and important role in the success of cell and organ transplantation. Normally, when an injured or failing organ needs to be repaired or replaced using allogenic and xenogeneic sources available, these foreign cellular sources are recognized by the host immune system leading to its rejection. However, the immune system is not the only player during the inflammation process, the remodelling of the ECM plays also an important role by promoting immune cell activation, tissue invasion and destruction (Hallmann et al., 2015, Sorokin, 2010).

In healthy human islets, HA is located outside the endocrine cells. HMW HA, over 1,000 kDa, are contained in the pericellular matrix of pancreatic islets. It presents anti-inflammatory, filling, and hydrating functions, thus protecting β-cells from leukocyte-mediated death.

In addition, HA can be crosslinked into stable structures that impact leukocyte function by the interaction with a diverse group of HA-binding proteins, known as hyaladherins.

Tumour necrosis factor stimulated gene 6 (TSG-6) is a hyaladherin that has an important function in preventing HA degradation by inhibiting HYALs and enhancing HA binding to the cell surface receptor CD44 on lymphocytic cell lines (Baranova et al., 2011).

The effect of TSG-6 in the development of diabetes has shown to delay autoimmunity and enhance tolerogenicity of cells (Kota et al., 2013). When HMW HA alone or in association to hyaladherins bind to CD44 receptors on Tregs, it promotes its immune suppressive capacity by increasing the transcription factor Foxp3 expression and increasing the production of anti-inflammatory cytokines, such as interleukin (IL) 10 (Ruppert et al., 2014). For instance, HMW HA hydrogels have been shown to decrease leucocyte infiltration while increasing angiogenesis at the site of a dental extraction (Gocmen et al., 2015). Moreover, HMW HA hydrogels have been reported to increase lymphocyte and T helper cell proliferation and activation into an anti-inflammatory state. T helper cells increased the secretion of IL-10, a known anti-inflammatory cytokine, while decreasing the secretion of IL-2 and IFNγ, known pro-inflammatory cytokines. In addition, they also increased monocyte differentiation into M2 macrophage subtype (Gomez-Aristizabal et al., 2016).

However, in T1DM, HA accumulates along the islet microvessels and in regions of insulitis, where it forms a network around inflammatory cells. LMW HA, ~250 kDa, is highly angiogenic, immune-stimulatory and inflammatory (Jiang et al., 2011, Rayahin et al., 2015). For instance, it has been shown that LMW HA fragments activate TLR to stimulate inflammatory cells (Jiang et al., 2011). HA is also implicated to be remodelled by hyperglycaemia during diabetes. It is hypothesized that during hyperglycaemia, thrombospondin-1 activates HAS-2, increasing plasma levels of HA in diabetic patients (Vigetti et al., 2014), where platelets are responsible for HA cleavage into LMW HA fragments by HYAL-2. These HA fragments would promote leukocyte recruitment and adhesion, enhancing the inflammatory milieu within the microvasculature (Shakya et al., 2015).

Since neutrophil migration *in vivo* is a marker for transplant rejection, and it occurs through hyaluronate-rich connective tissue matrices, the relevance of studying the mechanisms of HA modulation on neutrophil populations is important. Studies have shown that exogenous HA (of a minimum MW of $1x10^4$) inhibits neutrophil aggregation in a dose-dependent manner, where processes such as inflammation and wound healing could be modulated with the application of HA of different MW sizes (Forrester and

Lackie, 1981). HA has also shown to inhibit lysozyme release from aggregated IgG stimulated neutrophils (Pisko et al., 1983). Soluble HMW HA has also shown to induce apoptosis of inflammatory neutrophils and macrophages. Moreover, macrophages which immobilized HMW HA were able to be polarized into M2 subtype upon LPS/TLR ligation (He et al., 2013).

4.2.2.1.Modulation of Platelet Activation

Platelets are one of the main cellular effectors of haemostasis, but they also possess a plethora of intracellular mediators (i.e. cytokines, chemokines) as well as surface receptors (i.e. integrins, CD44, TLR). These are known for their involvement in inflammatory and immune responses as outlined in section 1 (Iannacone, 2016). It is known following injury that platelets rapidly interact with the exposed ECM of the vessel wall and the surrounding tissues. Since platelets are involved with immunological responses and ECM interactions, the influence that HA could potentially have over platelet modulation can give new insights into immunomodulation.

Interestingly, it is reported that platelets enzymatically degrade HA, via HYAL-2, from the surfaces of activated endothelial cells into fragments capable of inducing immune responses. Platelet activation causes the immediate translocation of HYAL-2 from a distinctive population of α-granules to the surface membrane where it exerts a catalytic activity (Albeiroti et al., 2014).

In diabetes, hyperglycaemia is shown to induce a reduction of the glycocalyx of the endothelial cells from the blood vessels which may promote platelet adhesion and aggregation. The subsequent HA fragments generated by platelet-derived HYAL-2 initiate inflammatory and angiogenic signalling by stimulating mononuclear leukocytes in the immediate microenvironment to produce pro-inflammatory cytokines, such as IL-6 and IL-8 (Shakya et al., 2015).

4.2.2.2.Modulation of Complement Activation

The complement system is part of the innate immune system and comprises a series of proteins that are activated in response to a pathogen to enhance the ability of antibodies (adaptive immune system) and phagocytic cells (innate immune system) to fight a threat. Its modulation can be linked to autoimmunity and transplant rejection. Thus, it is important to establish whether HA plays a role in complement activation and if HA could modulate the complement system. GAGs have the ability to modulate complement

activation, which is highly dependent on sulphate and negative charge content (Meri and Pangburn, 1994). For example, it has been observed that highly sulphated GAGs can promote C3 activation while little or no effect was seen with negatively charged GAGs. Studies have also suggested that non-modified HA seems to have relatively weak anticomplementary activity (Hallgren et al., 1989).

4.2.3. Structure:Function Properties of HA Hydrogels in Cell Encapsulation Coatings

In Figure 4.4. it can be seen that the relationship between structure and functional properties of hydrogels are closely dependent on polymeric molecular weight, concentration, degree of substitution, backbone chemistry, and crosslinking density (Collins, 2010). For example, topography, capsule size, mechanical rigidity, charge distribution, and hydrophobicity of nano coatings are parameters that influence islet function and host response following transplantation (Ernst et al., 2019).

In terms of fouling proclivity alone, it has been suggested that the strength and degree of hydration layer around the polymer may be negatively correlated with protein adsorption. Polymer chain flexibility is also negatively correlated with fibrotic response because of steric repulsion. The implant geometry also influences the foreign body reaction (FBR). In spherical microcapsules larger spheres (greater than 1500 μm) resist fibrotic deposition to a greater degree than smaller spheres. It has also been suggested that smooth-contoured implants induce weaker FBR than those with rough edges. Material stiffness also positively correlates with the FBR magnitude (Ernst et al., 2019).

The reestablishment of vasculature is a major limiting factor in attempts to replace or regenerate defective tissues. Vascularization is considered one of the greatest challenges in tissue engineering. Biomaterials can promote vascularization by changing surface roughness, porosity, factor release, and cellular tethering. Surface roughness tends to positively correlate with increased vasculature in bulk encapsulation (macro- and micro) and larger pores sizes can act as effective scaffolding for vascular sprouting (Ernst et al., 2019). Hydrogel stiffness can also impact cell attachment and spreading. Generally, HA hydrogels with relatively lower storage modulus (G') are required to achieve spreading of a 3D culture, and if stiffer gels are used, micron-sized pores must be introduced for cellular attachment and spreading (Lam et al., 2014).

Hydrogel network mesh size is also an important parameter considering permeability. Permeation is a vital factor to consider for the success of tissue engineered constructs in

order to avoid graft rejection (Nafea et al., 2011b). It will prevent the inflow of molecules such as antibodies as small as IgG (150 kDa), cytokines and chemokines such as IL-1 (17.5 kDa) and MCP-1 (8 kDa), respectively, while allowing the diffusion of oxygen, CO_2 (44 Da) and glucose (180 Da), which are essential for cellular survival and function. For example, higher polymer and crosslink concentrations correlate to decreased pore sizes, which creates matrices with smaller molecular weight cut-off (MWCO) and slower diffusion rates (Weber et al., 2009, Bal et al., 2014).

Higher crosslinking densities in HA hydrogels reduce the mesh size and consequently the MWCO, but they also implicate in lower degrees of degradation (Lai, 2014). The stability of the cell encapsulating structure can also impact the immune response, as degradation can release damage-associated molecular patterns (DAMPs), such as LMW HA fragments to the cell surrounding environment (Shakya et al., 2015).

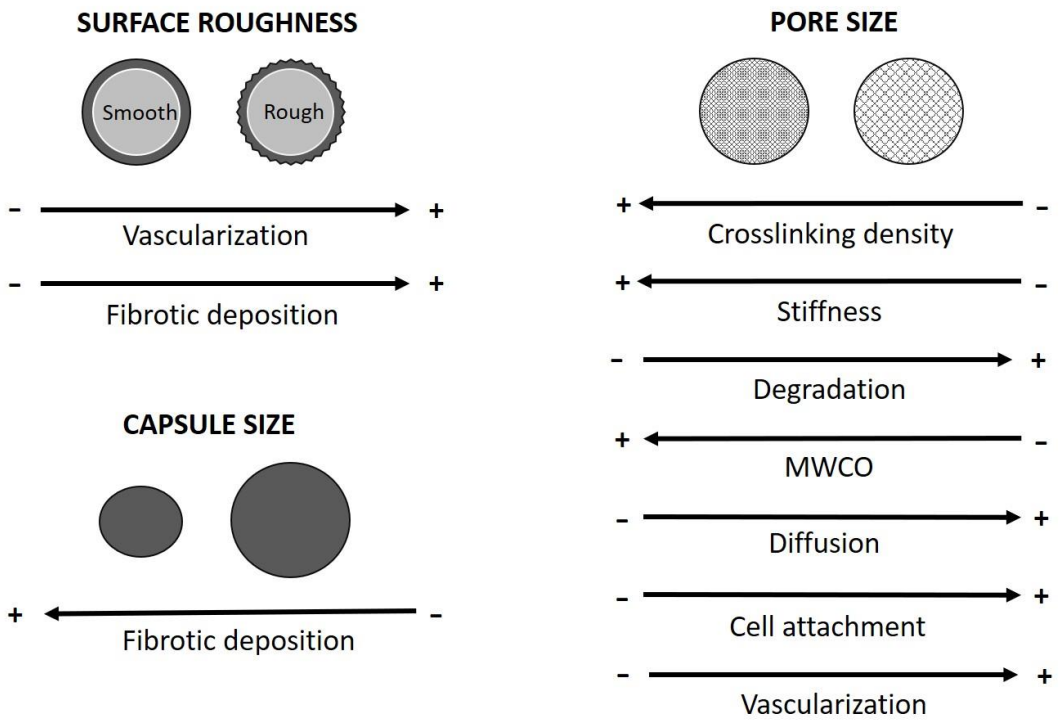

Figure 4.4. Structure-function properties of HA encapsulation systems.

4.2.4. Intrinsic Antimicrobial Activity of HA

Implantable device-related infections pose a huge financial burden on healthcare services and are associated with increased patient morbidity and mortality (VanEpps and Younger, 2016). For patients, infections are commonly associated with pain, inflammation, fever, and often long-term antimicrobial treatment regimen. However, in some cases the

infection can lead to a second operation, resulting in removal of the implant. These infections can also lead to more serious conditions, such as the risk of sepsis (spread of infection to blood and other organs) which can sometimes be fatal. The development of tissue engineered substitutes that possess intrinsic antimicrobial activity against the three main classes of microbes (bacteria, fungi, and virus) is vital for the success of implantable devices.

Reduction of bacterial burden at the implantation site may improve the clinical outcome for regenerative therapy. In the surgical setting, *S. aureus* is the leading cause of infection associated with implantable biomaterials. Treatment requires long term antibiotic administration often with additional surgeries, in order to remove the infected components (Ibberson et al., 2016). Several investigators have been interested in the interaction between HA and bacteria, particularly relating to invasion and virulence.

Amongst various polymers tested for antibacterial coatings, HA and its derivates offer long-term safety and proven ability to reduce bacterial adhesion and biofilm formation (Romanò et al., 2017, Zamboni et al., 2021). HA has been shown to exert bacteriostatic, but not bactericidal, dose-dependent effects on different microorganisms in the planktonic phase. For example, HMW HA (1.8 MDa) has been demonstrated to decrease the proliferation of Gram-positive bacteria such as streptococcus and enterococcus species (Ardizzoni et al., 2011). Gram-negative bacteria, such as *Escherichia coli*, was also negatively affected by HMW HA (del Hoyo-Gallego et al., 2016, Pérez-Álvarez et al., 2019).

Unlike the extensive study of the antimicrobial activity of HA, only a few studies have been conducted to assess the activity of HA in fungi. However, intrinsic antifungal dose-dependent properties of HMW HA (1.8 MDa) were demonstrated against *Candida glabrata* and *Candida parapsilosis* (Ardizzoni et al., 2011).

Although viral infections in surgical setups are not as problematic as those from bacteria and fungi, the potential antiviral activity of HA has been studied. HMW HA (1.800 KD) demonstrated strong antiviral activity against Coxsackievirus B5, mumps virus and influenza virus A (H1N1). Mild antiviral activity was shown against human simplex virus and porcine parvovirus. However, HA did not demonstrate any activity against Adenovirus 5, human Herpesvirus-6, porcine reproductive and respiratory syndrome virus. In all cases, no virucidal activity of HA was observed (Cermelli et al., 2011).

4.3. Final Considerations

HA shows great potential to address many of the challenges associated with the development of a functional β cell encapsulation system for the treatment of T1DM patients, which include:

- Possesses antimicrobial activity;
- Promotes angiogenesis;
- Downregulates the immune response;
- Possesses insulinotropic effects;
- Forms stable hydrated networks;
- Can be crosslinked in physiological conditions;
- Can form ultra-thin coatings by the sequential deposition of several polymeric layers.

In this context, the rationale of *in situ* crosslinking of low and high molecular weight HA with varying crosslinking densities on the surface pancreatic β cells will create a bio-functional multi-layered nano coating. This coating will support an immune protective and immunomodulatory environment to decrease transplant rejection, while enabling appropriate stability, stiffness, and mass transport of molecules (MWCO and diffusion) to support cell viability, functionality and restore insulin competence in T1DM patients after transplantation.

Chapter 5: A Novel Mechanism to Crosslink HA: Isocyanate-Based Crosslinker Uses HA Hydroxyl Groups to Form Urethane Bonds

The contents of the following chapter are adapted from the original research article published in the Carbohydrate Polymers journal.

Zamboni, F., Ryan, E., Culebras, M., Collins, M. N. (2020) Labile crosslinked hyaluronic acid via urethane formation using bis(β-isocyanatoethyl) disulphide with tuneable physicochemical and immunomodulatory properties. Carbohydrate Polymers v. 245, 2020.

DOI: 10.1016/j.carbpol.2020.116501

Abstract

BIED, a di-isocyanate crosslinker, was synthesized based on the reactivity of its isocyanate groups for HA hydroxyl moieties. HA with varying molecular weights were crosslinked by homogenous and heterogenous methods using BIED. Later, carbon nanofibres (CNF) were incorporated to the HA solutions prior to heterogeneous gelation to produce films with improved mechanical properties. HA gels were analysed in terms of chemical, physical, thermal, and mechanical characteristics. Rheological, swellability, and permeability profiles were studied. Results show that BIED successfully crosslinks HA. Moreover, the additional disulphide bond centring the crosslinker molecule gives these HA gels extra moiety with redox capabilities that can be further exploited in self-healing and reversible gels for conformal crosslinking approaches.

Keywords: Hyaluronic Acid, Isocyanate, Crosslinking, Carbon Nanofibres

5.1. Introduction

HA is a biocompatible polymer best known for its intrinsic hydrating properties, which acts as a space filler, lubricant, and osmotic buffer in the ECM of many tissues in the body (Zamboni et al., 2017). Nonetheless, HA is readily degraded in physiological conditions due to hydrolysis and enzymatic digestion (Pandey and Weigel, 2014, Collins and Birkinshaw, 2007a, Valachova et al., 2016). The rapid turnover of HA in biological systems requires HA to be chemically modified to improve its structural stability. This facilitates the use of HA in many pharmaceutical and biomedical applications (Burdick and Prestwich, 2011). Crosslinking strategies create more robust gels with low degradation rates, and the incorporation of inorganic nanoparticles (clay, graphene, carbon nanotubes, or silica) improve the mechanical toughness of the HA gels (Huang et al., 2018).

Up to date, there is little literature on HA gel formation using isocyanate crosslinkers, although there is an increased interest in crosslinking carbohydrate polymers with this group of crosslinkers (Sonker et al., 2018b). The main advantage of using isocyanates such as BIED is related to their excellent reactivity towards hydroxyl groups which result in the formation of urethane linkages (Koniev and Wagner, 2015).

BIED is a linear di-isocyanate that contains two isocyanate groups in total, one at each end of the molecule backbone. BIED is categorized as an alkyl-based isocyanate, which is known to be significantly slower to degrade by hydrolysis than more conventional aryl-based isocyanates (Brown et al., 1987). These linear isocyanates also produce upon reaction with hydroxyl groups, more stable urethane linkages against thermal degradation (Chattopadhyay and Webster, 2009). Alkyl-based isocyanates are also shown to pose very little to no cytotoxic effects in comparison with cyclic isocyanates (Touchet and Cosgriff-Hernandez, 2016). Moreover, BIED contains a central disulphide group in its molecular backbone. Upon covalently crosslinking HA, these redox-sensitive moieties can be interconverted between disulphide and dithiol groups. This dynamic interconversion generates a potential self-healing and reversible crosslinking application for these gels (Griesser et al., 2018, Pepels et al., 2013).

The production of nanocomposite HA hydrogels via the incorporation of CNFs can improve the overall mechanical, electrical, and thermal properties of the gels (Feng et al., 2014). CNFs also offer benefits for wound healing applications as they absorb exudates

and regulate wound moisture. This is attributed to their surface area, and porous structure (Eatemadi et al., 2016). Interestingly, CNFs are also shown to possess antimicrobial properties depend on their structural characteristics, which are also beneficial for wound healing applications (Song et al., 2015).

Herein, HA gels containing covalent crosslinks using BIED have been developed where the hydroxyl groups present in the N-acetylglucosamine moiety of HA react with the isocyanates to form carbamate linkages. The combination of CNFs embedded in HA hydrogel networks have been shown to produce nanocomposite films with improved mechanical performance. The CNFs serve as physical cross-linkers as well as reinforcing nanofillers in the HA hydrogel films. In the present work we anticipate that homogeneously crosslinked HA gels and heterogeneously crosslinked CNF-reinforced HA films result in gels with tuneable physical, mechanical, and biochemical properties.

5.2. Materials and Methods

5.2.1. Materials

HA, with an average molecular weight (MW) of 1.20 MDa and 0.1 MDa, was kindly supplied by Shanghai Easier Industrial Development Co. LTD. (Shanghai, China) as dry powder. 3,3'-dithiodipropionic acid, hydrazine monohydrate, sodium nitrite, dimethyl sulphoxide (DMSO), dithiothreitol (DTT) were purchased from Lennox Laboratories Supplies (Dublin, Ireland). The dialysis kit (Pur-A-Lyzer^{TM} Mega 1000), deuterium oxide (D_2O), Ellman's Reagent (5,5'-dithio-bis-(2-nitrobenzoic acid), fluorescein isothiocyanate (FITC) dextranes, phosphate buffered saline (PBS), and all other reagents used in this work were of analytical grade purchased from Sigma Aldrich (St. Louis, MO, USA).

5.2.2. BIED Synthesis

The synthesis of BIED can be divided into three steps. First, 3,3'-dithiodipropionic acid (10 g) and ethanol in excess (22 g) were dissolved in toluene (100 mL) with ρ-toluene sulfonic acid (2.5%) as the reaction catalyst. The reaction was heated up to boiling and temperature was constantly monitored using a thermocouple. The reaction was performed under reflux for 5 hours using a Dean-Stark trap to produce diethyl 3-3'-thiodipropionate. The yield of the product was obtained by the evaporation of toluene using a rotary evaporator (Rotavapor R-210, Buchi, Switzerland), giving a yield of 90%. In the second

step, diethyl 3-3'-thiodipropionate (10 g) and hydrazine monohydrate in excess (12 g) were dissolved in methanol (13 mL) and heated for 4h under reflux to obtain dithiodipropionate dihydrazine after crystalization in an ice bath. The yield of the product was obtained by the evaporation of methanol using a Gallenkamp vacuum oven at a temperature of 40°C overnight, yield of 97%. In the third step, dithiodipropionate dihydrazine (10 g) was dissolved in 60 mL of hydrochloric acid (HCl 2.5 M) and stirred in an ice bath. 16 mL of a sodium nitrite aqueous solution (76%) was added drop wise to avoid an extreme exothermic reaction. After, toluene (100 mL) is added to the solution, and this induced a phase separation using a separation funnel. The toluene phase contained an intermediate product that upon heating produces BIED by curtius rearrangement. The toluene is then refluxed for 10 minutes to completely convert acid hydrazine into isocyanate (pale yellow liquid). Toluene (boiling point: 110°C) is removed from BIED (boiling point: 148°C) by using a rotary evaporator (BUCHI, Switzerland) at 40°C and 29 mbar for 2 hours (yield of 38%). The overall yield was calculated to be 33.17%.

5.2.3. HA Crosslinking

BIED was used as a HA crosslinker and the crosslinking reaction was performed via two distinct methods. In the first method, the crosslinking reaction occurs when all the reactants are dispersed in the same phase (DMSO solvent), namely homogenous crosslinking. In the second method, the crosslinking reaction occurs when the reactants are in two separate phases (the crosslinker has to diffuse through HA films for the reaction to occur), namely heterogenous crosslinking.

5.2.3.1.Homogeneous Crosslinking

BIED (49.3 $mg.mL^{-1}$) was added to HA 1.20 MDa or 0.1 MDa solutions (70 $mg.mL^{-1}$) dissolved in DMSO. HCl 1M was used to adjust the pH to 4. The crosslinking reaction proceeded upon stirring.

5.2.3.2.Heterogeneous Crosslinking

HA solutions of 1.2 MDa 3% (w/v) and 0.1 MDa 3% (w/v) in water were prepared overnight at 25°C and 100 RPM. For HA-CNF blends, 2.9 wt.% of HA and 0.25 wt.% of CNF were dissolved in distilled water and homogenized using ultrasound-assisted dispersion at an amplitude of 10 microns for 10 minutes. The CNFs used in this project

are 98% carbon-based, measuring 100 nm in diameter and 20−200 μm in length. Figure 5.1 shows the SEM image of the CNFs using a TM-1000 tabletop microscope (Hitachi, Japan).

The HA and HA-CNF films were prepared via casting their respective aqueous solution onto a clean petri dish, followed by drying at 25°C for 120 hours. The resulting films were then cut in pieces of 1 cm^2 and subsequently placed in the vacuum oven at 40°C (1000 psi) for 3 hours, more details on the films are shown in Table 5.1.

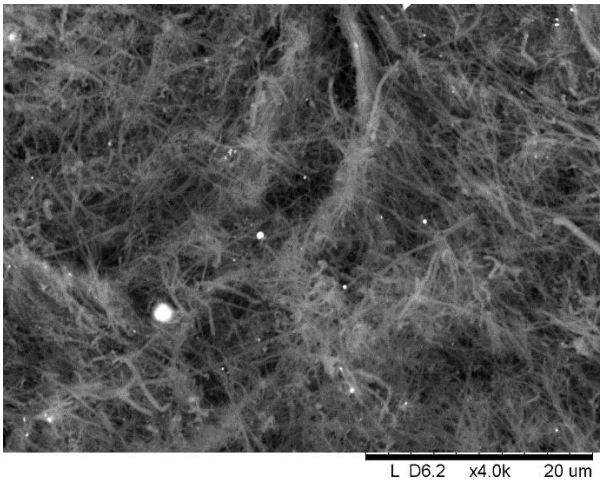

Figure 5.1. SEM image of CNFs used to reinforce HA gels.

Table 5.1. Cast-moulded HA and HA-CNF films with 1 cm^2.

Film	Thickness (mm)	Average Surface Roughness (nm)
HA (0.1 MDa)	0.035 (± 0.005774)	6.5 (± 1.3)
HA (1.2 MDa)	0.0575 (± 0.017078)	15.5 (± 3.7)
HA-CNF (0.1 MDa)	0.1125 (± 0.03304)	64.2 (± 8.5)
HA-CNF (1.2 MDa)	0.14 (± 0.08124)	89.4 (± 8.5)

± S.D.

Heterogeneous crosslinking was performed on the vacuum dried HA and HA-CNF films. The films (1 cm^2) were placed in 10 mL of acetone-water solution (80:20 by volume

respectively) containing 400 mg.mL^{-1} of BIED, pH was adjusted using 2.0 M hydrochloric acid (pH of 3.0). The crosslinking reaction was allowed to proceed for 72 hours at RT. Crosslinked films were washed with deionized water several times before being dried for 3 hours at 35°C in a fan oven.

5.2.4. Surface Roughness Analysis of HA Films

The surface roughness and topology of the films were recorded, in contact mode at room temperature, using a Thorlabs EDU-AFM1/M atomic force microscope (New Jersey, USA). The measurements were performed using monolithic silicon AFM probe with aluminum reflective coating (ContAl-G, Budgetsensors), in the same room, at room temperature and ambient pressure. The experiments were conducted on square areas of 20 mm x 20 mm, in 100 x 100 pixels resolution, at a scan speed of 100 pixels/s. The AFM micrographs were analysed using the Gwyddion 2.56 software. The average surface roughness value was calculated from three lines drawn across the AFM image for each sample.

5.2.5. Chemical Characterization

All spectra were recorded on a Perkin Elmer spectrum 100 FT-IR spectrometer operating in Attenuated Total Reflectance (ATR) mode (Perkin Elmer, MA, USA). Each FT-IR spectrum was scanned twenty times with a resolution of 2 cm^{-1}. The ranges used were from 4000 cm^{-1} to 650 cm^{-1}.

5.2.6. Mechanical Characterization

The rheological properties of HA gels produced from homogenous crosslinking were evaluated by the Discovery Hybrid Rheometer (DHR-2) (TA Instruments, DE, USA) using parallel plate geometry of 25 mm at 25°C. Prior to oscillatory frequency measurements, a strain sweep analysis was performed using a strain range of 0.01-0.1-1-10-100-1000%, at a fixed frequency of 1 Hz to obtain the linear viscoelstic region of the gels (0.01-1%). Then, a frequency sweep was conducted in the frequency range of 0.1-10 Hz.

HA films produced from heterogeneous crosslinking were dried in the vacuum oven at 40^{o}C (1000 psi) for 2 hours and their mechanical properties analysed using dynamic mechanical analysis (DMA) Q800 1535 (TA Instruments, DE, USA), operating in the DMA Controlled Force mode with a gauge length of 12.74 mm. The stress/strain test was

performed on samples maintained at an isothermal temperature of 25°C, and a force ramp rate of 3.0 N.minute^{-1} to an upper force limit of 18.0 N.

5.2.7. Swelling Profile

HA gels were prepared as described previously and dried in an oven at 70°C for 24 hours. The HA dry samples were weighed and incubated in 4 mL of PBS with pH 7.4 at RT. Hydrogels were removed at various time intervals; excess solution was wiped off and sample weights were recorded. Swelling ratios (SR) were calculated as follows:

$$SR = \frac{Ws}{Wd}$$

where *W*d is the dry weight and *W*s is the weight of the sample after the incubation time. All swelling measurements were carried out in triplicate.

5.2.7.1.Crosslinking Density

HA hydrogels were dried in an oven at 70°C, overnight. The dried gels were subsequently swollen in PBS until they reached their equilibrium water content. Crosslink densities were assessed by measuring volumetric swelling and applying a simplified version of the Flory-Rehner equation as described by Collins *et al* (Collins and Birkinshaw, 2008a).

$$\bar{M}_c \cong \frac{\left[1 + \frac{\rho\rho}{\rho s}(QM - 1)\right]^{5/3} * V_1}{\left(1/2 - \chi\right)\bar{v}}$$

where M_c is the average molecular weight between crosslinks, ρ_p is the density of the dry polymer (1.229 g/cm^3) and ρ_s is the density of PBS. Q_M is the swelling ratio determined experimentally by comparing the mass of the material before and after immersion, $\bar{v}$ is the specific volume of the dry polymer as the inverse of density, V_1 is the molar volume of the solvent (18 cm^3/mol for PBS), and χ is the Flory polymer solvent interaction parameter (0.473).

The effective crosslink density, *ve*, was then calculated as follows:

$$v_e = \frac{\rho\rho}{\bar{M}_c}$$

5.2.7.2.Mesh Size

The swollen hydrogel mesh size ξ (nm), was determined with the following equation adapted from Collins *et al* (Collins and Birkinshaw, 2008a):

$$\xi = 0.1748\sqrt{\bar{M}_c}\left[1 + \frac{\rho\rho}{\rho s}(QM - 1)\right]^{1/3}$$

5.2.8. Degree of Substitution of HA Gels

HA gels (MW 1.2 MDa and 0.1 MDa) were reduced to produced HA derivates bearing free thiol groups (HA-SH). First, gels had their pH adjusted to 7 using a solution of sodium hydroxide (NaOH 1 M), and then treated with DTT at a 1:1 ratio in comparison to BIED used to crosslink the gels. Samples were heated for 20 minutes at 90°C under stirring conditions to reduce the disulphide bonds of the gels. Gels gradually changed into a solution. HA-SH was precipitated from the solution using acetone in a ratio 2:1. The precipitate was re-dissolved in DMSO and dialysed against deionized water for 3 days at RT. Deionized water was changed every day to promote constant diffusion of DTT and DMSO out of the dialysis chamber. HA was freeze dried to obtain a lyophilized powder. Briefly, the dialysed sample was placed in a shelf freeze dryer (AdVantage BenchTop Freeze Dryer by Virtis, USA) and let to freeze at -40°C overnight before drying. Drying was conducted in four temperature stages. The temperature was held at -20°C for 6 hours under vacuum (200 mTorr), then the temperature was increased to -10°C for 1.5 hours, following another temperature increase to 5°C for 2 hours. This finally reached 25°C, after which HA-SH was obtained as a white powder. HA-SH was then stored under nitrogen in the freezer at -20°C.

The lyophilized powder of HA bearing free thiol groups was analyzed regarding the degree of thiolation using the Ellman's Reagent. Briefly, a stardant curve of L-cysteine was prepared using a solution buffer (0.1 M Na_2PO_4, 1 mM EDTA, pH 8.0). Then, aliquots of the standard curve samples were incubated with Ellman's solution for 15 minutes. HA samples were prepared the same way as the standard curve and they were all read using a microplate reader at 412 nm. Absorvances were used to create a linear regresion euqation, of which the concentration of free thiol groups in the HA samples were obtained.

The lyophilized powder of HA bearing free thiol groups was analysed regarding the degree of substitution using Proton Liquid Nuclear Magnetic Resonance (NMR). Jeol ECX 400 NMR (Jeol USA, Inc) was used to analyse the samples. Samples were diluted in 1 mL of D_2O. 128 scans were performed under RT with a 15 Hz sample spinning and 45° tip angle.

5.2.9. Permeability Test

For the permeability test, 0.1 and 1.2 MDa films were heterogeneously crosslinked using BIED. The permeability experiment consists of HA-BIED crosslinked films separating the donor solution from the acceptor solution. The donor solution contains 2 $mg.mL^{-1}$ of three distinct FITC-dextranes with molecular weights of 4,000 Da and 150,000 Da, whereas PBS 1X is used as the acceptor solution. An in-house permeation chamber made of polylactic acid (PLA) was 3D printed for these experiments using 3D printer MakerGear M3ID (USA) and Simplify3D software as shown in Figure 5.2. The two 3D-printed parts clip the gel in the middle, separating the top chamber (with the donor solution) from the bottom chamber (with the acceptor solution). Both chambers hold a volume of 261 μL. The detection of FITC-dextran in the acceptor solution is measured at time intervals of 15 minutes, 30 minutes, 1 hour, 3 hours and 6 hours using a fluorescence plate reader (SynergyMx, BioTek, EUA). with an excitation wavelength of 485 nm and emission of 535 nm. A standard curve (0.066, 0.0032, 0.0016, 0.0008, 0.0004, 0.0002 mg/mL) for each FITC-dextran was measured and the linear eqution was obtained to convert the fluorescence from the acceptor solution into equivalent concentration. from All tests were executed at RT (Hsu et al., 2018). The calculation of the permeability coefficient was determined according the equation below:

$$\frac{dCA}{dt} = P * A * \frac{CD}{VA}$$

Where dC_A/dt is the exchange of the concentration of the substance within the acceptor side over time (the slope); C_D is the concentration of the donor solution; P is the permeability coeficient; A is the permeation surface; and V_A is the volume of the acceptor solution. This equation is derived from Fick's First Law and can only be applied whe $C_D >> C_A$.

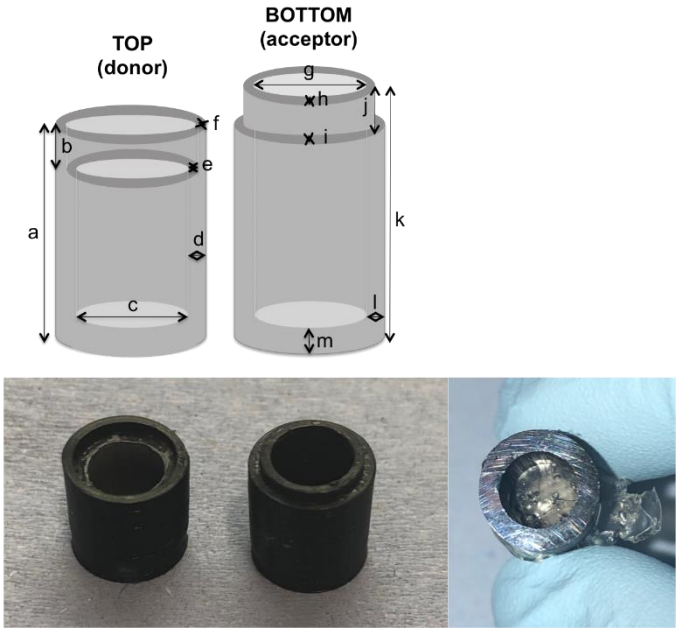

Figure 5.2. 3D-printed permeation chambers. Dimensions: a=11.27mm, b=0.9mm, c=5.5mm, d=1.55mm, e=0.7mm, f=0.7mm, g=5.5mm, h=0.7mm, i=0.7mm, j=0.9mm, k=13mm, l=1.55mm, m=2mm.

5.2.10. Thermo-chemical Characterization

The non-crosslinked and crosslinked HA and HA-CNF films were dried in the vacuum oven at 40^{o}C (1000 psi) for 2 hours and analysed using a differential scanning calorimeter (Perkin Elmer DSC 6). The experiment was carried out at 20 cc.mm^{-1} of nitrogen gas flow with an increasing temperature from 0^{o}C to 200^{o}C at a rate of 10^{o}C.minute^{-1}. Triplicate samples were tested to ensure reproducibility.

5.2.11. Statistical Analysis

Data are presented as mean ± standard deviation (s.d.) and analysed using two-way analysis of variance (ANOVA). *p-value* < 0.05 (*) was considered significant.

5.3. Results and Discussion

5.3.1. BIED Synthesis

The stepwise chemical reactions leading to BIED synthesis is shown in Figure 5.3. At every reaction step, products have been chemically confirmed using FT-IR. In Figure 5.4, each spectrum shows the characteristic bands from each reaction product. For example, in step 1 the starting material is a carboxylic acid that is converted into an ester. The bands for carboxylic acid do not appear following the completion of the reaction (O-H broad stretching band between 3,300-2,500 cm^{-1}) and the characteristic band for the ester, such

as the C=O stretch band at 1,735 cm^{-1} becomes apparent. In step 2, the characteristic ester band now disappears, and new bands relating to the product appear. These bands are related to N-H stretch 3,400-2,800 cm^{-1} overlapping with the primary amine (-NH_2) stretch band at 3,180 cm^{-1} and 3,320 cm^{-1} and the carbonyl of the acylamino at 1,622 (Xu et al., 2017). Step 2a involves a reaction between the dithiodipropionate dihydrazine and nitrous acid (which is formed in situ between the reaction of sodium nitrite and hydrochloric acid) producing an intermediate compound called acyl azide. The azide (-N_3) asymmetric stretching vibration band is shown in Figure 5.4 and was previously described in the literature at 2,162 nm (Tanver et al., 2015). After the acyl azide compound is extracted from the aqueous solution using toluene via phase separation, it is subsequently heated and converted into BIED by the Curtius rearrangement mechanism. BIED shows a characteristic broad and strong band at 2,262 cm^{-1} associated to isocyanates (Beck et al., 2009).

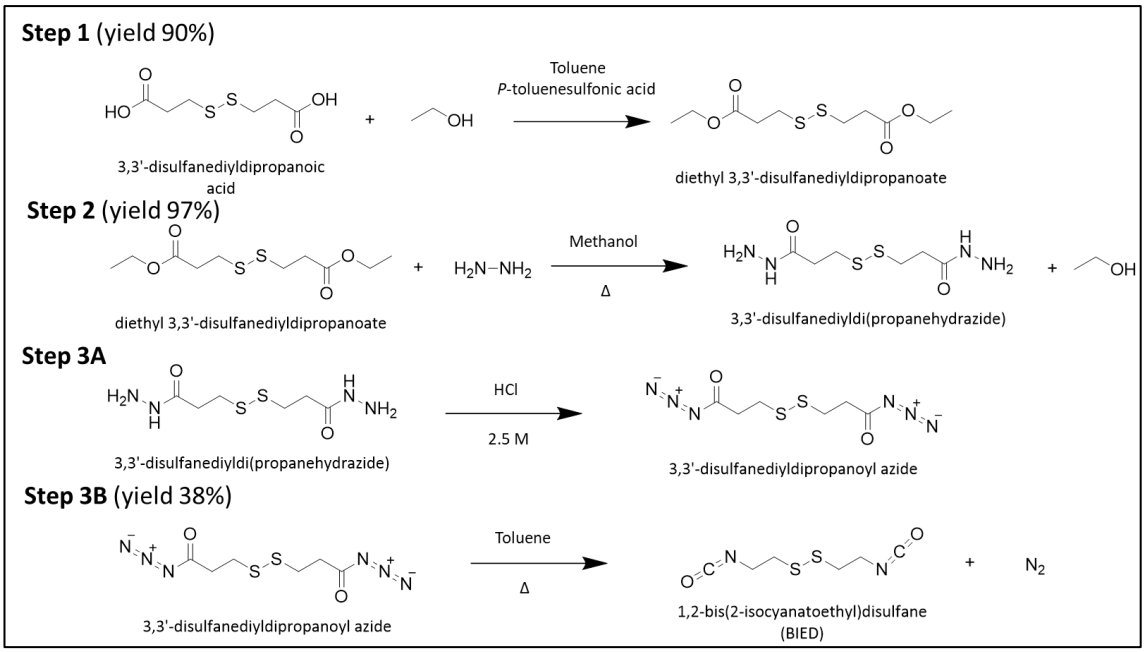

Figure 5.3. Stepwise synthesis reaction to produce BIED.

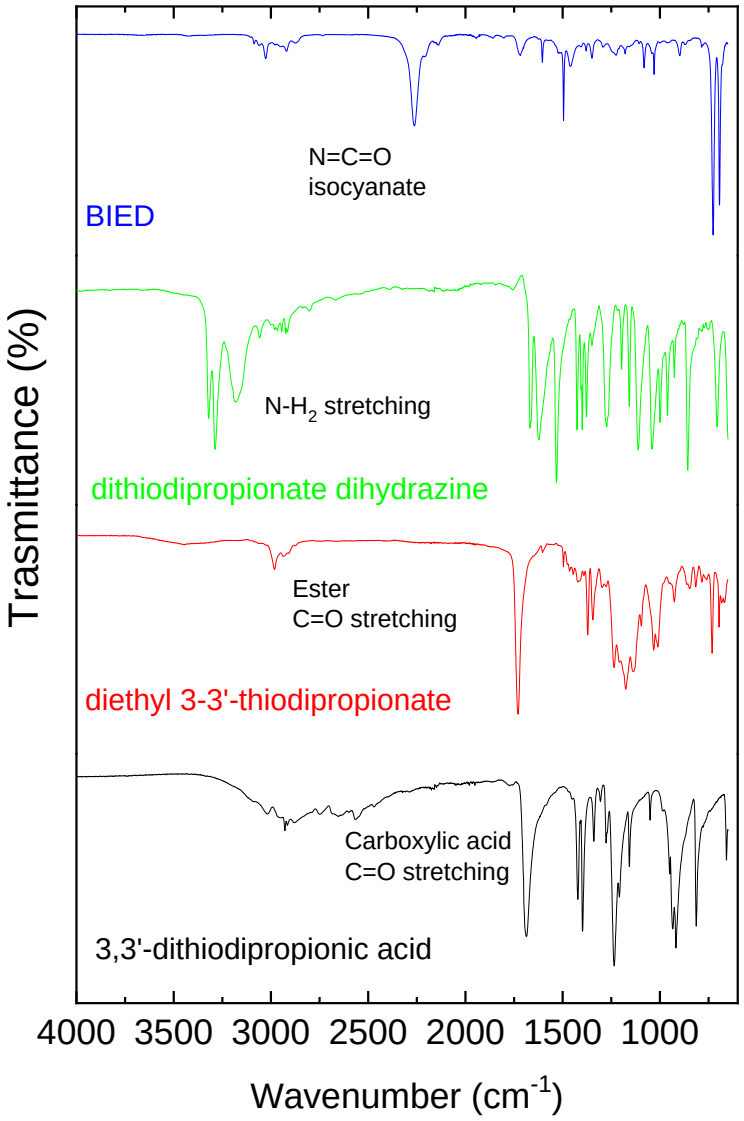

Figure 5.4. FT-IR spectra of the reaction products from the BIED synthesis. 3,3'-dithiodipropionic acid, diethyl 3-3'-thiodipropionate dithiodipropionate dihydrazine and BIED.

5.3.2. HA crosslinking

The synthesized di-isocyanate compound was then used to react with HA either by homogenous (bulk gel formation) or heterogenous crosslinking (film gelation), shown in Figure 5.5. The hydroxyl groups of the N-acetylglucosamine moiety of HA are targeted by the isocyanate to form urethane linkages as shown in the schematic reaction in Figure 5.6A. The formation of these urethane linkages is verified by FT-IR and confirms covalent crosslinking (Figure 5.6B).

Figure 5.5. Representative image of BIED-crosslinked HA gels. Homogenously crosslinked gels (a). Heterogeneously crosslinked HA films (b) and CNF-reinforced HA films (c).

The FT-IR spectrum of BIED clearly depicts spectral bands at 2270 cm^{-1} which is characteristic of the isocyanate functional group (C-N-O), 1731 cm^{-1} which indicates an ester carbonyl group (C=O) stretching, 1516.2 cm^{-1} (C=C bond), 1260.3 (O-H bending) and 1030 cm^{-1} (C-N group) in accordance with the literature. The FT-IR spectra of non-crosslinked HA and HA-CNF clearly shows the characteristic OH vibration band at 3346 cm^{-1} and the broad carbonyl band of the amide-carbonyl functional group at 1618 cm^{-1} (Dhanasingh et al., 2010). Once the crosslinking reaction with BIED occurs, HA crosslinked gels show the appearance of the characteristic carbonyl urethane group (C=O stretching) at 1729 cm^{-1}, carbamate group (C-N) at 1564 cm^{-1}, and C-O-C at 1228 cm^{-1} (Wong and Badri, 2012). The carbonyl band at 1729 cm^{-1} is regarded to be free of hydrogen bonding (Bahadur et al., 2016). Furthermore, the absence of the characteristic isocyanate band at 2262 cm^{-1} indicates a fully crosslinked HA, where there was no unreacted isocyanate groups (Sonker et al., 2018a).

A)

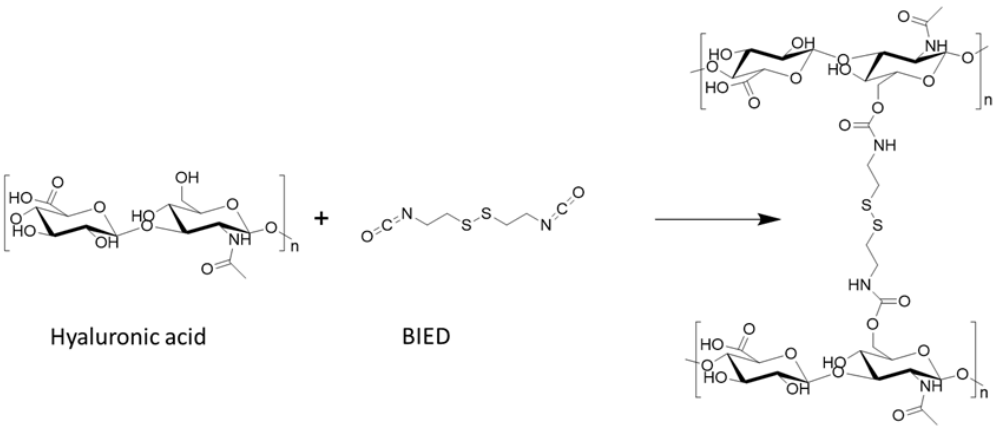

B)

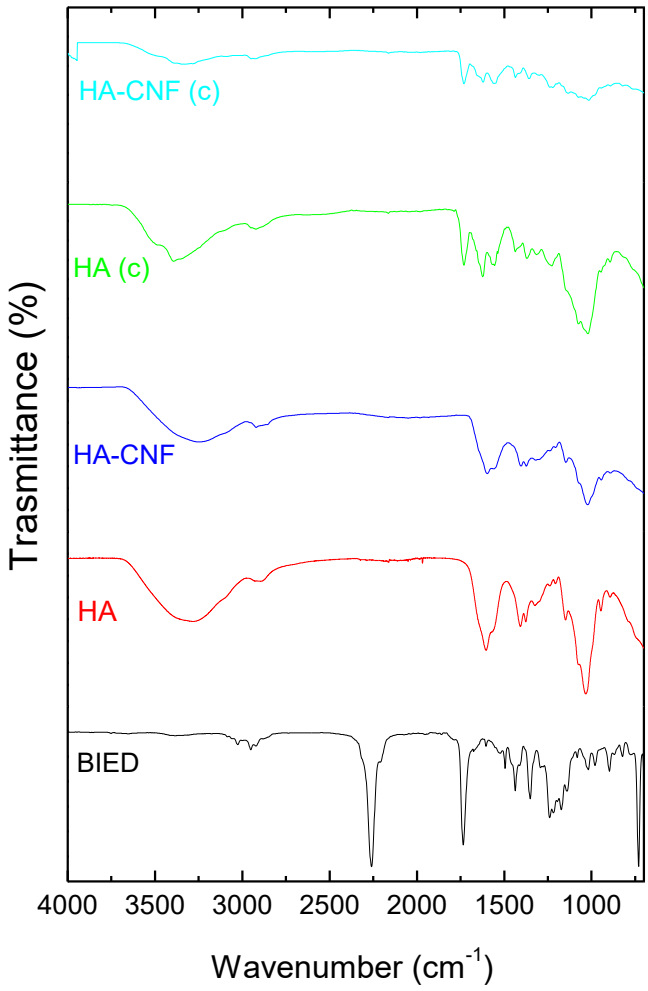

Figure 5.6. A) Schematic reaction of BIED crosslinking HA via urethane linkages. B) Representative FT-IR spectra of BIED in black, HA not crosslinked in red, HA crosslinked (c) in green, HA-CNF not crosslinked in blue, and HA-CNF crosslinked (c) in turquoise.

The thermal behaviour of HA and HA-CNF gels are shown in Figure 5.7. Unmodified HA is used as a control group and it shows the presence of a broad endothermic peak around 110°C, which is associated with the loss of moisture remaining after the initial drying procedure and an exothermic peak representing degradation around 230°C, in agreement with the literature (Collins and Birkinshaw, 2007b). On the other hand, the thermal behaviour of HA-CNF blend not crosslinked revealed the presence of two narrow exothermic peaks at around 230°C and 260°C, which indicates that the degradation of HA is disrupted by the interaction with CNF.

The thermal behaviour of both crosslinked HA and HA-CNF films shows a sharp endothermic peak at around 195°C and 185°C, respectively which is attributed to the scission of the disulphate bond.

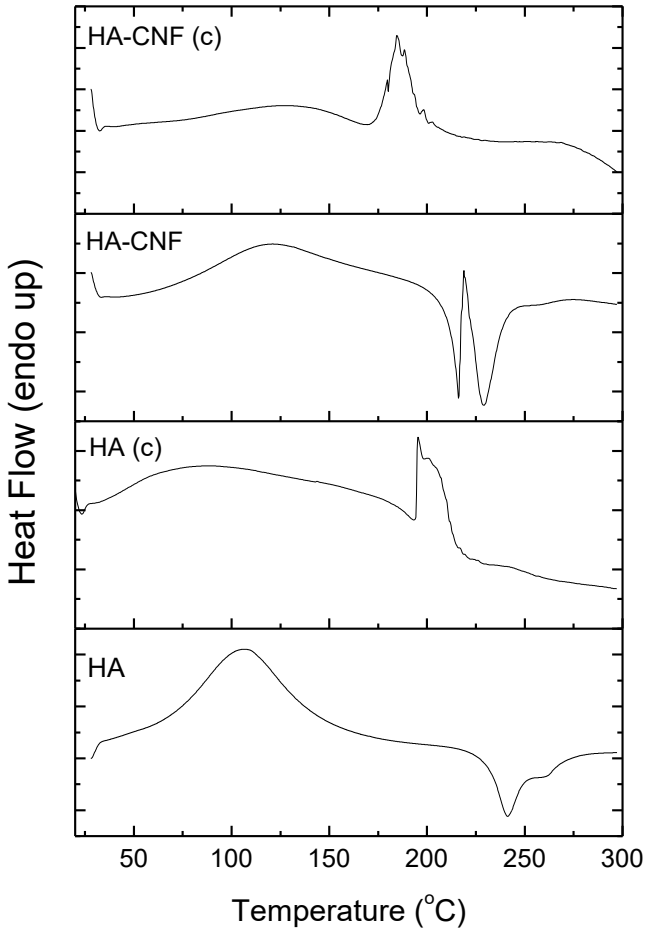

Figure 5.7. Representative DSC thermograms of HA not crosslinked, HA crosslinked (c), HA-CNF not crosslinked, and HA-CNF crosslinked (c).

5.3.2.1. Viscoelastic Profile of Homogenously Crosslinked HA Gels

The stiffness of homogenously crosslinked HA hydrogels was evaluated by the determination of the storage (G') and loss moduli (G''), where G' represents the elastic component of the gel and G" represents the viscous component of the gel (Figure 5.8). All gels produced in this study show G'>G", indicating they were successfully crosslinked. Results show that 0.1 MDa gels have higher storage modulus (20 KPa) while 1.2 MDa gels have lower storage modulus (2 KPa). This significant difference between the storage

modulus of gels was also observed by other studies. They show that gels with higher MW in fact decreases G' and stiffness (Amorim et al., 2020).

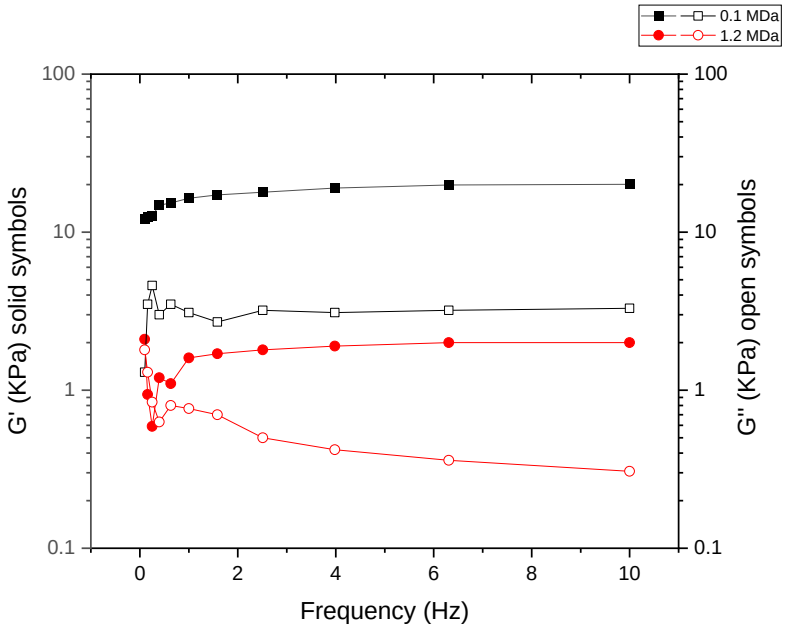

Figure 5.8. Rheological profile of BIED-crosslinked HA gels with 0.1 MDa and 1.2 MDa.

5.3.2.2. Mechanical Profile of Heterogeneously Crosslinked HA Films

For the tensile test results the films were subjected to the same test conditions and representative stress-strain plots of each film are shown in Figure 5.9 A and B. The Young's moduli for all films were calculated and results are shown in Figure 5.9C. As expected, HA MW strongly influences the mechanical properties of the films. High MW HA films (1.2 MDa) show decreased Young's modulus, in comparison to low MW HA films (0.1 MDa). Other studies have also observed the same tendency of HA films to decrease stiffness as a function of MW size (Amorim et al., 2020).

Although, for all samples, crosslinking the films with BIED, drastically increased the mechanical strength of the films. The low MW HA-CNF (C) films have the highest modulus, due to the reinforcing effect of CNF combined with BIED crosslinking to HA.

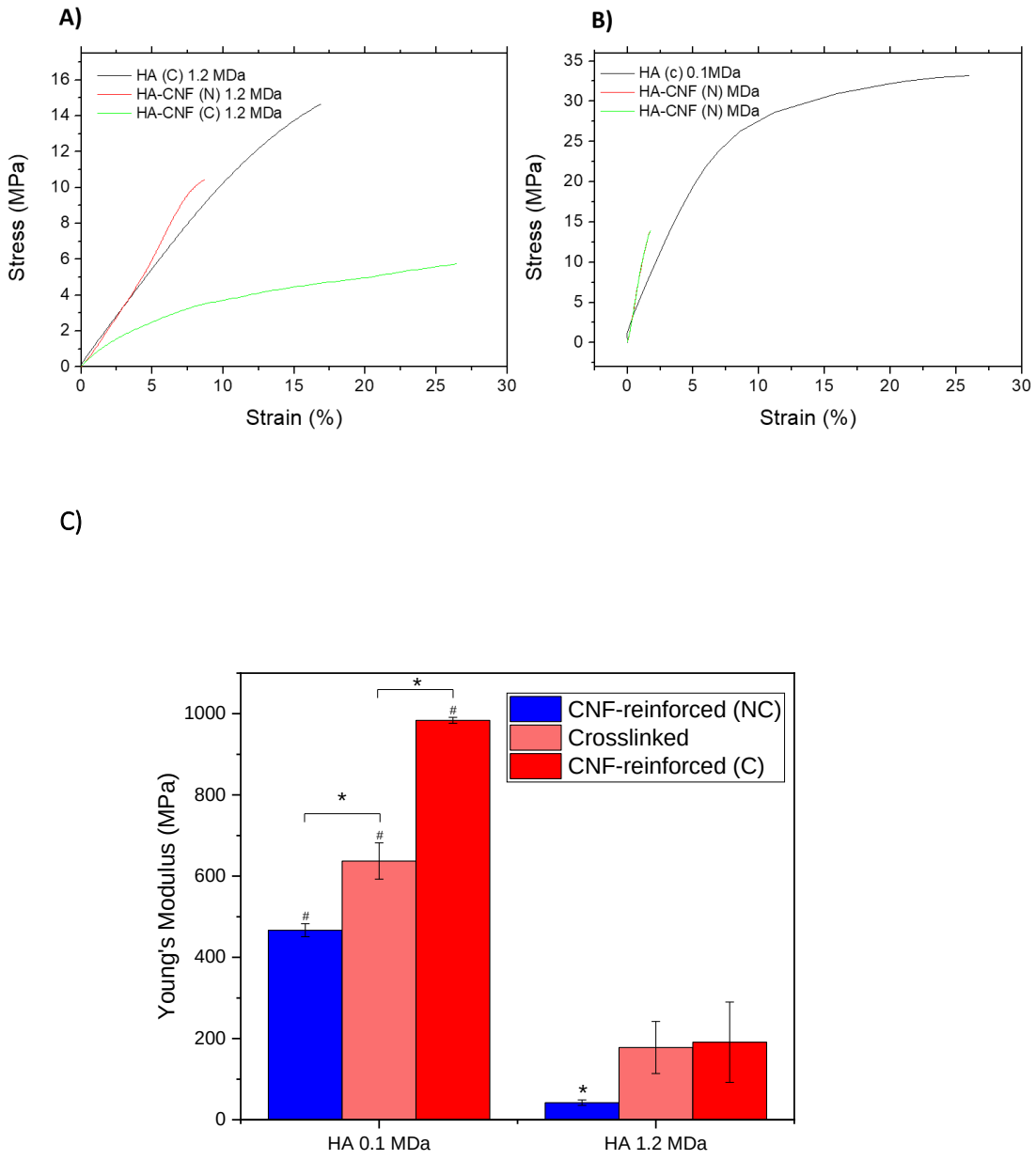

Figure 5.9: Representative stress-strain plots of various HA films A) 1.2 MDa, B) 0.1MDa and C) Young's modulus of 0.1 and 1.2 MDa HA films. Statistical analysis was performed using ANOVA followed by post-hoc Tukey's HSD test where p-value < 0.05 shows statistical difference between groups (#) and within groups (*).

5.3.2.3. Analysis of the Degree of Substitution

Due to the disulphide bond located in the centre of the crosslinker chain, the gel can be reduced back into a solution by the conversion of the disulphide bond into free thiol groups using DTT (Figure 5.10). The product of this reduction generates HA derivates carrying free thiol groups (HA-SH), which can be assessed for the degree of thiolation.

The degree of thiolation for homogeneously crosslinked HA 0.1 MDa was 594.3 $\mu M.mg^{-1}$ (± 198) of HA as opposed to 166.15 $\mu M.mg^{-1}$ (± 14.04) from homogeneously crosslinked HA 1.2 MDa, therefore explaining the difference in crosslink densities and subsequently gel stiffness (~ 20 kPa for 0.1 MDa and ~ 2 kPa for 1.2 MDa). It is hypothesised that the thiolation degree decreases with increasing molecular weight because the longer a single polymeric chain is, it increases the formation of hydrogen bonding resulting in higher viscosity. Also, longer polymeric chains are more likely to become entangled, which makes the sites for crosslinking difficult to reach, thus, causing lower reaction activity (Cao et al., 2019).

Confirmatory NMR analysis of HA derivates after the reduction of the disulphide bonds of HA gels are shown in Figure 5.11. NMR spectra shows the appearance of peaks at approximately 2.75 ppm for CH_2 groups related to the $-CH_2CH_2SH$ radical of the urethane linkages. The control CH_3 group of HA appears at approximately 2.05 ppm. The spectrum is in accordance with the literature (Bian et al., 2016).

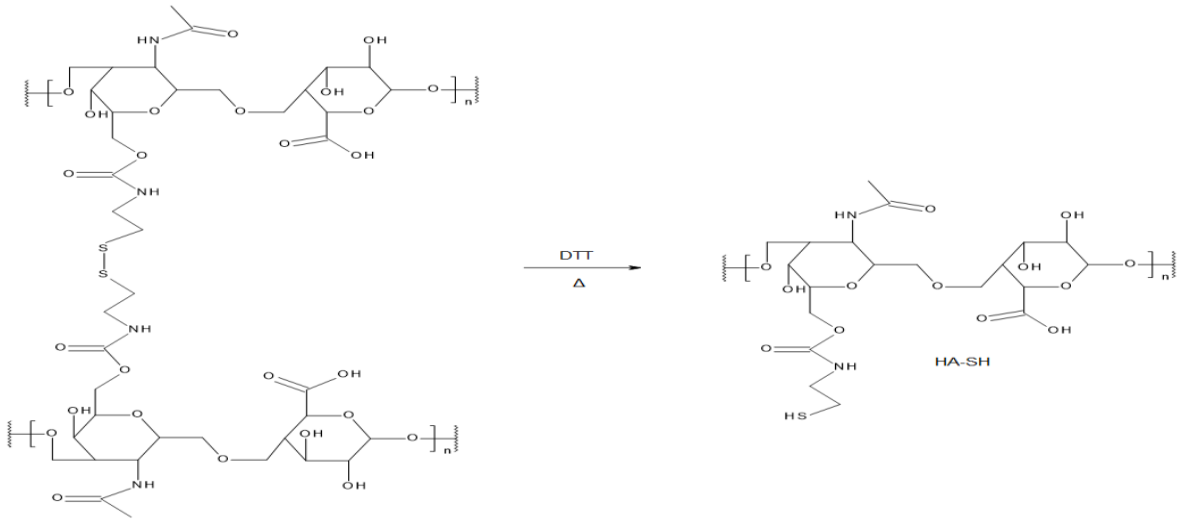

Figure 5.10. Schematic reduction reaction of the disulphide bond of the crosslinked HA into HA bearing free thiol groups

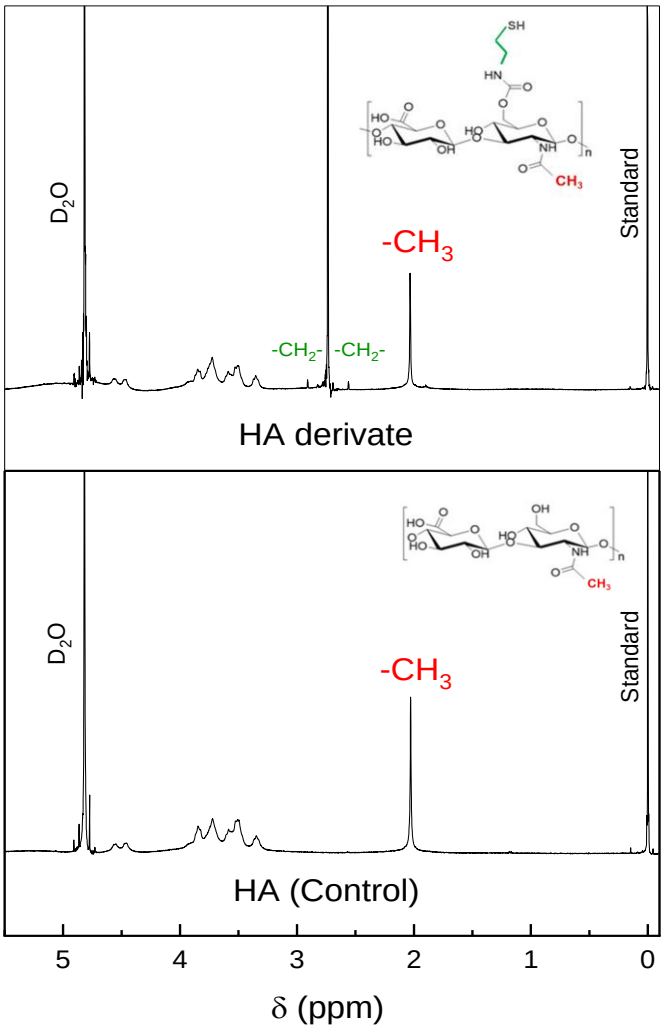

Figure 5.11. Representative NMR spectra for pure HA (control) and HA-SH derivate.

5.3.2.4. Swelling Characterization

The speed at which gels swell to their equilibrium water content is presumed to be a function of crosslink density and polymeric concentration (Figure 5.12).

When comparing crosslinking density, it is observed that LMW HA gels show lower swelling ratio than HMW HA gels, this is mainly attributed to the fact that LMW HA gels are more efficiently crosslinked than HMW HA gels, as shown by the quantification of thiol groups and the theoretical calculation of crosslinking density (Table 5.2). A similar influence of crosslinking density was also observed in other studies, although they utilized other chemical crosslinkers than isocyanates (Shimojo et al., 2015).

Overall, hydrogel swelling ratios decrease with decreasing molecular weight, which is due to increased crosslinking density and the formation of tighter network structures with an increasing number of covalent crosslinks (Hegger et al., 2017). However, although low molecular weight hydrogels (0.1 MDa) display higher crosslinking densities, they are also faster to degrade due to smaller and less entangled polymeric chains where glycosidic bonds are more likely be exposed and degraded by hydrolysis than in HMW HA gels (Cao et al., 2019).

The gels initially turned white in colour, and then a colourless swelling front moved inwards, separating the highly swollen surface from the less swollen core of the gel and gradually the entire gel turned colourless and was swollen evenly. This colour phenomenon was also described by (Collins and Birkinshaw, 2008b) and it is presumed to be due to molecular rearrangement as the water diffuses through the material.

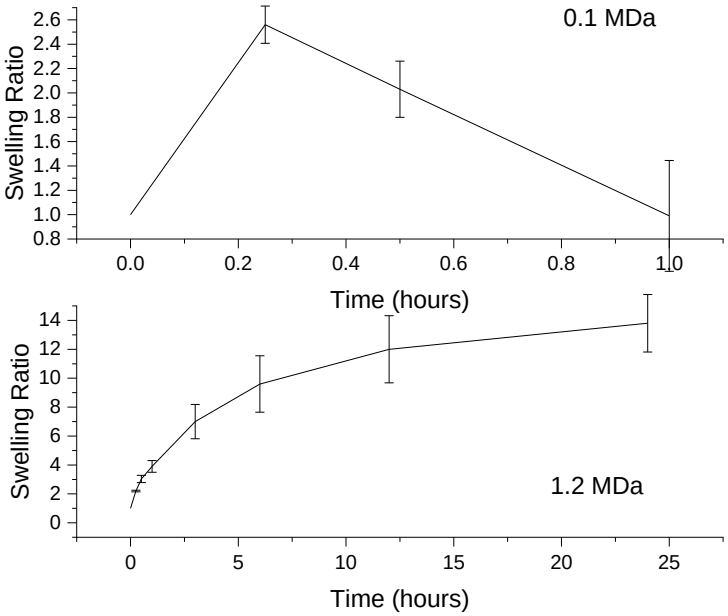

Figure 5.12. Swelling profiles of BIED-crosslinked HA gels with 0.1 MDa and 1.2 MDa.

5.3.2.4. Matrix Characterization

In general, increasing effective crosslinking density decreases mesh size and average MW between crosslinks (Collins and Birkinshaw, 2010) and produces hydrogel matrices with smaller MWCO and slower permeation rates (Weber et al., 2009, Bal et al., 2014). Hence, knowing these matrix parameters (shown in Table 5.2) is imperative for applications such as drug delivery and cellular scaffolding. Here, the characterization of homogeneous

BIED-crosslinked HA gels shows that LMW HA gels display much smaller mesh sizes than HMW HA due to their higher crosslink densities resulting from their higher degrees of thiolation. As mentioned, BIED in HMW HA has lower reaction activity due to the longer polymeric chains that are more likely to become entangled, which makes the sites for crosslinking difficult to reach (Cao et al., 2019).

It is envisaged that the homogeneous crosslinking carried out in this study can potentially be used to encapsulate drugs. Additionally, the use of DMSO can pose little constraint for drug encapsulation, as DMSO dissolves a large variety of polar and non-polar small molecules, making it an important drug solvent for topical pharmaceutical formulations (Tetko et al., 2013). Furthermore, DMSO possesses permeabilizing properties which enhance drug delivery though the skin without harmful effects (Marren, 2011). DMSO is also largely used in cryobiology as the cryoprotectant of choice for most animal cell systems. Nevertheless, cell exposure to DMSO show apparent cell toxicity specifically associated with plasma membrane changes, such as membrane fluidity and dysfunction, leading to programmed cell death (Awan et al., 2020).

Homogeneously crosslinked HA gels, due to the use of DMSO, are particularly difficult have DSMO removed from the gels through lyophilization and evaporation. The difficulty DMSO evaporation is due to its high boiling point (189 °C), limiting the use of these gels as cell scaffolds. However, to circumvent this issue, the conversion of these gels into solution by reducing the gel disulphide bond allows the purification of the HA-thiol derivates through dialysis (Black et al., 2014). Re-crosslinking the HA-thiol derivates can be facilitated by the oxidation of the thiol groups into disulphide bond for reversible or self-healing gel forming properties and are suitable for cell encapsulation (Fernandes and Ramos, 2004, Pepels et al., 2013). This is particularly interesting for the development of L-b-L coatings, which will be further discussed in chapters 8 and 9. As seen in Figure 5.10, the reduction of BIED-crosslinked HA is possible, and produces HA-bearing thiols. The degree of substitution of these HA derivates are shown in Table 5.2 and the results correlate to the calculated crosslinking density.

Table 5.2. Crosslinking parameters calculated for BIED-crosslinked HA gels.

HA MW (MDa)	Mesh size (nm)	Average MW between crosslinks ($g.mol^{-1}$)	Effective crosslinking density ($mol.cm^{-3}$)	Thiolation ($\mu M.mg^{-1}$ of HA)

0.1	17.3 ±0.9	4,900 (± 520.1)	0.00025 (± 2.6839E^{-05})	594.3 (± 198)
1.2	113.9 ±18.8	71,198.1 (± 22452)	0.000017 (± 6.65833E^{-06})	166.15 (± 14.04)

± SD

5.3.3.1.Permeability of HA Films

The MWCO determines the minimum molecular weight, correspondingly minimum size, of a solute that is completely excluded by the semipermeable membrane (Nafea et al., 2011a). MWCO is dictated by the mesh size and affects diffusion and permeation rates of molecules (such as antibodies and cytokines). Thus, the study of gel permeation rates to solutes of different sizes is particularly important to tissue engineering and drug delivery applications.

To mimic the penetration rate of IgG (150 kDa) and MCP-1 (8 kDa) through the HA hydrogel, two FITC-labelled dextranes of similar molecular weight were utilized to determine permeation rates through the LMW and HMW HA films. The results shown in Figure 5.13 demonstrate the delay of permeation of 150 KDa dextran in LMW HA gels ($p<0.05$) in comparison to HMW HA gels. Moreover, HMW HA gels were inefficient to delay the permeation of both 4 KDa and 150 KDa. The equal permeation rate for both dextranes means that the mesh size of the gels was significantly larger than the size of these two particles, thus both particles pass freely through the film.

IgG is the most abundant immunoglobulin (80%) in the body and previous studies have shown that membrane barriers for IgG are enough to prevent graft rejection in transplants. This indicates that blocking cytokines and chemokines may not be a requirement for immunosuppression in allotransplantation (Steele et al., 2014).

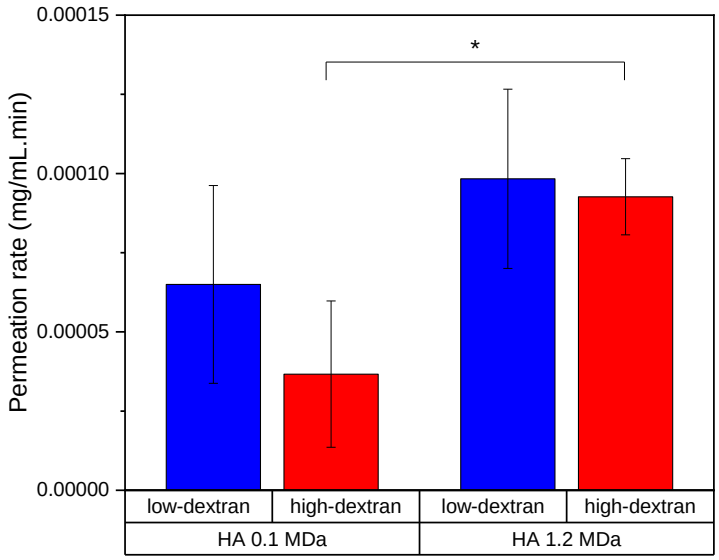

Figure 5.13. Permeation rate of low and high molecular weight dextranes through crosslinked HA films. Statistical analysis was performed using ANOVA followed by post-hoc Tukey's HSD test where p-value < 0.05 shows statistical difference (*).

5.3. Final Considerations

This study has demonstrated the novel use of crosslinking HA of both low and high molecular weights with the di-isocyanate BIED. This was achieved through the formation of urethane linkages between the HA chains, as described earlier in the chapter. The main advantage of using BIED over other isocyanate crosslinkers is that it has a disulphide bond in the middle of the molecule backbone, which can be reduced into free thiol groups, and possibly re-oxidized into disulphide bond for reversible or self-healing gel forming properties. This is particularly interesting for the development of L-b-L coatings, which will be further discussed in chapters 8 and 9.

Results have shown that gels can be tailored with mechanical and stability properties depending on HA content, HA molecular weight and crosslinking density. This is particularly useful when designing network systems which can be applied in a variety of uses for pharmaceutical applications. Specifically for drug delivery systems, the use of DMSO applied in the homogenous crosslinking methodology to create these can dissolves a large variety of polar and non-polar small molecules.

However, creating gels using aprotic solvents such as DMSO can pose limitations for bioengineering applications as tissue scaffolds. In this context, the heterogenous crosslinking of HA gels through BIED diffusion circumvents the associated limitation of DMSO use from homogenous crosslinking methods. Although heterogenous crosslinking is not as effective as the homogenous method, the mechanical properties of these gels can be improved through the inclusion of CNFs.

In the next chapter, focus will be given to the characterization of heterogeneously crosslinked HA gels regarding their suitability for biological applications. Biocompatibility and cell proliferation studies will be conducted, together with immunological response analysis via immune cell activation and pro-inflammatory cytokine production quantification. Lastly, the potential antimicrobial activity of HA and CNF will be assessed.

Chapter 6: Newly Crosslinked HA Hydrogels: Biological Function and Properties

The contents of the following chapter are adapted from the original research article published in the journal of Carbohydrate Polymers.

Zamboni, F., Okoroafor, C., Ryan, M. P., Pembroke, T., Strozyk, M., Culebras, M., Collins, M. N. On the Bacteriostatic activity of hyaluronic acid composite films. Carbohydrate Polymers, v. 260, 2021.

DOI: https://doi.org/10.1016/j.carbpol.2021.117803

Abstract

Herein, the biological characterization of the heterogeneously crosslinked HA films is assessed. HA films with varying molecular weights were crosslinked using BIED, a di-isocyanate-based crosslinker, which is highly reactive for the hydroxyl moieties of HA. These heterogenous-crosslinked films are envisaged to support cell growth as they do not require toxic solvents involved in their production, contrary for those crosslinked through homogenous reactions. Cell viability, cell proliferation, immune activation and antimicrobial activity assessments were performed. Results show that heterogenous-crosslinked HA films are biocompatible. Moreover, immunological, and antibacterial responses are dependent on HA molecular weight. In the future, these gels can be potentially exploited for a number of applications that include wound dressings, skin grafts, catheter coating for biofilm inhibition, cell encapsulation, and drug delivery.

Keywords: Hyaluronic Acid, Heterogenous Crosslinking, BIED, Immunomodulation, Bacteriostatic Activity

Graphical Abstract

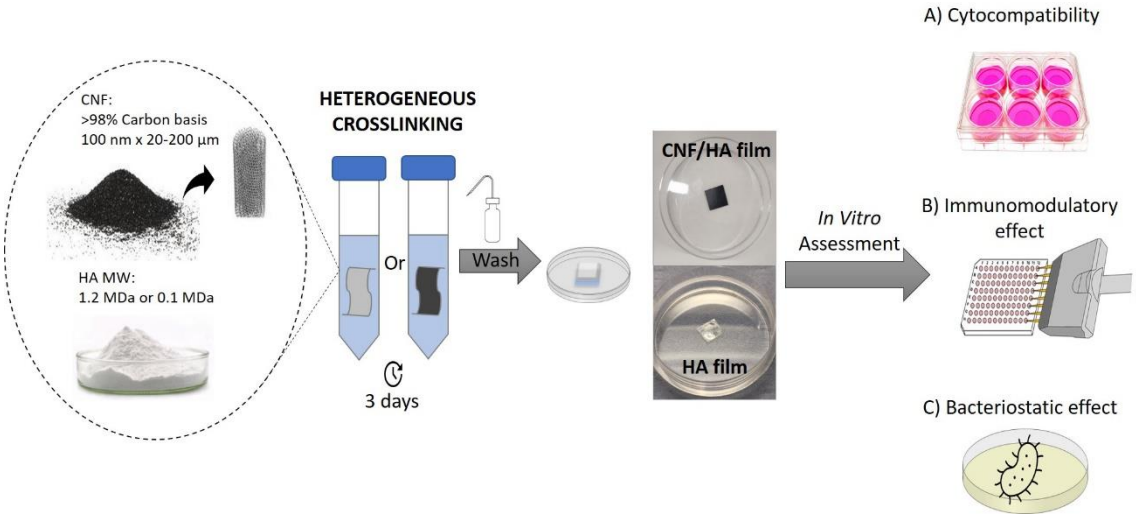

6.1. Introduction

HA is an important ECM component due to its hygroscopic nature it provides hydration and tumescence to all tissues in the body. Moreover, HA regulates a diversity of biological processes by triggering signalling pathways associated with the adhesion, proliferation, migration, and differentiation of cells (Amorim et al., 2021). Distinct cell responses are largely influenced by HA size, generated upon degradation by hyaluronidases or free radicals, and its interaction with different cell membrane receptors (Nusgens, 2010).

Due to its remarkable physicochemical properties and biological relevance, HA is being used in numerous biological applications concerning tissue repair (Liu et al., 2019b, Gokila et al., 2018). The ability of HA to modulate the immune system, which is primarily dependent on its molecular size, can be exploited for the development of HA-based biomaterials for enhanced bio integration and adequate tissue healing (Zamboni et al., 2018b). High MW HA is shown to elicit anti-inflammatory and immunosuppressive functions (Ruppert et al., 2014) while low MW HA is shown to be highly angiogenic, immune-stimulatory and pro-inflammatory (Jiang et al., 2011, Rayahin et al., 2015).

HA and its derivates also offer potential long-term safety and ability to reduce bacterial adhesion and biofilm formation (Romanò et al., 2017). HA is shown to be bacteriostatic, but not bactericidal, and exhibits dose-dependent effects on different microorganisms in the planktonic phase (Harris and Richards, 2004).

Staphylococcus aureus (S. aureus) is a Gram-positive, non-motile, non-spore forming facultative anaerobic coccid bacterium. The microorganism is approximately 0.5-1.5μm in diameter and in physiological conditions grows by aerobic respiration at a temperature range from 15^{o}C to 45^{o}C (Jorgensen et al., 2015). They are normally found on the skin and mucous membranes of the nose in 30% of the healthy human population, normally displaying no symptoms (Bhattacharya et al., 2015). These bacteria are transmitted via contaminated surfaces, air-borne and direct contact to predisposed humans. They are also easily spread in hospitals, particularly in surgical wards (Forster et al., 2013).

S. aureus are usually detected in the top layer of wounds and are the most common bacterium isolated from chronic wounds (Gjodsbol et al., 2006). The interaction between keratinocytes, fibroblasts, Langerhans cells and endothelial cells during wound healing remodelling promotes colonization of Gram-positive bacteria such as *S. aureus* (Serra et

al., 2015). They are also opportunistic pathogens that cause a variety of self-limiting to life-threatening diseases in humans. *S. aureus* as a bacterium is among the most common cause of staphylococcal infections and is responsible for various diseases including mild skin infections (impetigo and folliculitis), invasive diseases (wound infections and osteomyelitis, and toxin mediated diseases (such as food poisoning, scaled skin syndrome and toxic syndrome) (Bukowski et al., 2010, Mitchell and Howden, 2005). *S. aureus* infection largely impacts orthopaedics, trauma, and cardiology with treatment consisting of complex and long-term antibiotic courses (Ibberson et al., 2016).

In this context, it is necessary to evaluate the biocompatibility of the novel heterogeneously BIED-crosslinked HA films developed in Chapter 5. In the present work we anticipate that these gels are adequate for cell growth as they do not contain toxic solvents involved in their production in contrary to homogenously crosslinked HA gels.

Herein, the biological analysis of the heterogeneously crosslinked HA films is assessed. Cell viability, cell proliferation, immune activation and antimicrobial activities are performed, and the information obtained from these tests are imperative to ensure the biocompatibility of these gels. In the future, these gels can be potentially exploited for a number of applications that include wound dressings, skin grafts, catheter coating for biofilm inhibition, cell encapsulation, and drug delivery.

6.2. Materials and Methods

HA, with an average molecular weight (Mw) of 1.20 MDa and 0.1 MDa, was kindly supplied by Shanghai Easier Industrial Development Co. LTD. (Shanghai, China) as dry powder. 3,3'-dithiodipropionic acid, hydrazine monohydrate and sodium nitrite were purchased from Lennox Laboratories Supplies (Dublin, Ireland). Enzyme-linked immunosorbent assay (ELISA) tests for mouse GM-CSF and human TNFα were purchased from BioLegend. 4,6-Diamidino-2-phenylindole (DAPI), and dihydrochloride was purchased from ThermoFisher Scientific. CNFs, methanol, hydrazine monohydrate, 3,3'-dithiopropionic acid, sodium nitrite, concentrated sulfuric acid, hydrochloric acid, acetone, toluene, phosphate buffer saline (PBS), Alamar blue (AB), ethylenediaminetetraacetic acid disodium salt dihydrate (EDTA), sodium phosphate dibasic dihydrate, Dulbecco's modified Eagle Medium (DMEM), Roswell Park Memorial Institute (RPMI) medium, trypsin-EDTA 0.25%, foetal bovine serum (FBS), L-glutamine and antibiotics and all other reagents used in this work were of analytical

grade purchased from Sigma Aldrich (St. Louis, MO, USA). L929 fibroblast cell line derived from mouse was purchased from the European Collection of Authorized Cell Cultures (ECACC 85011425). NIH/3T3 fibroblast cell line derived from mouse (ATCC CRL-1658), THP-1 monocyte cell line derived from human (ATCC TIB-202), and *Staphylococcus aureus* (ATCC 29213) were purchased from the American Type Culture Collection.

6.2.2. Heterogenous Crosslinking of HA Films

The heterogeneous crosslinking of low MW (0.1 MDa) and high MW (1.2 MDa) HA films and CNF-reinforced HA films was previously described in section 5.2.3.2. Briefly, HA films of (1 cm^2) were placed in acetone-water (80:20 by volume respectively) solution containing 400 $mg.mL^{-1}$ of BIED. The crosslinking reaction was allowed to proceed at 25^oC for 72 hours at an acidic environment (pH 3.0). After the reaction, HA films were washed with distilled water and dried at room temperature, until further use. Prior to all biological tests, these films were sterilized using UV radiation for 1 hour each side within an aseptic environment using laminar flow. After sterilization, films were allowed to re-swell for 30 minutes at 37°C in the incubator using the appropriate cell growth medium.

6.2.3. Cell Culture

Fibroblast cells of L929 and NIH/3T3 lineages were cultured in DMEM, while monocytes of THP-1 lineage were cultured in RPMI media. Both media types were complemented with 10% FBS, 1% streptomycin-penicillin solution and 2 mM of L-glutamine. Cells were incubated at 37^oC with 5% CO_2 in a humidified atmosphere and medium was replenished every three days until 80% confluency was reached. Cells (where otherwise specified) were trypsinized and seeded into the various test conditions.

6.2.4. *In Vitro* Cell Viability and Proliferation Assessment

For the study, NIH/3T3 cells were assessed for viability/proliferation by a resazurin-based metabolic activity assay. Due to resazurin redox nature, in which the its oxidized form (substrate) contained in the medium is reduced (product) by the various components of the cellular respiration chain (when cells are dead, they lose the ability to convert the substrate into product), the reduced form of resazurin is proportional to the number of viable cells present in the different planes of a 3D microenvironment, being able to provide a quantitative analysis of cell viability and, assuming that the metabolic activity

maintains constant throughout the testing conditions, quantification of cell proliferation is also possible.

Cells at a concentration of 50.000 cells.mL^{-1} were seeded onto HA films of 0.1 MDa and 1.2 MDa, and CNF-reinforced HA films in a 24 well-plate. For the continuous monitoring of cell culture overtime, cells were incubated for 1 day, 3 days and 7 days, and then resazurin was added to the media at a concentration of 10%. The well plates were returned to the incubator and aliquots of the media were taken 20 minutes after resazurin addition as specified by the manufacturer. Fluorescence readings of the aliquots were performed in a 96 well-plate at the excitation and emission wavelengths of 540 nm and 590 nm, respectively, using a SynergyMx plate reader (BioTek, EUA).

Cells were incubated in growth medium containing CNF at concentrations of 0.25%, 0.1%, 0.05%, 0.01% and 0.005% (w/v) for 1 day, 3 days and 7 days. Resazurin was added as described above. After the incubation period, the fluorescence originated from the reduction of resazurin by the cells was read in a microplate reader (SynergyMx, BioTek, EUA) at the excitation and emission wavelengths of 535 nm and 615 nm, respectively.

6.2.3.3. *In Vitro* Cell Attachment Analysis

L929 cells, at a concentration of 50.000 cells.mL^{-1}, were seeded onto HA 1.2 MDa and 0.1 MDa crosslinked films for 24 hours and 48 hours. Cell nucleus was stained using DAPI. Cell fluorescence imaging was captured using cellSens software and the BX60 fluorescence microscope (Olympus, Japan).

Cell attachment analysis of NIH/3T3 cells in cell medium containing different concentrations of CNF (0.25%, 0.1%, 0.05%, 0.01% and 0.005% (w/v)) was assessed by optical microscopy at 1 day, 3 days and 7 days of incubation using a CKX41 Olympus inverted microscope (Tokyo, Japan) equipped with a DFK 31AU03 camera (The Imaging Source Europe GmbH, Germany) and IC Capture software (The Imaging Source Europe GmbH, Germany). For this test, NIH/3T3 cells, at a concentration of 50.000 cells.mL^{-1}, were seeded in 24 well-plates.

6.2.4. *In Vitro* Cytokine Quantification

For the immune activation analysis, L929 fibroblast cells at a density of 50,000 cell.mL^{-1} were seeded onto crosslinked films of HA 1.2 MDa and 0.1 MDa for 24, 48 and 72 hours. After the incubation period, supernatant was collected by centrifugations and

analysed for the production of GM-CSF, a cytokine that induce macrophage differentiation as part of the immune response chain, using an ELISA kit as described by the manufacturer (BioLegend). THP-1 cells at a density of 50,000 cell.mL^{-1} were seeded onto HA 1.2 MDa crosslinked films for 24 hours, with or without lipopolysaccharide (LPS) stimulation challenge (1:1000). After the incubation period, supernatant was collected by centrifugation and analysed for the production of TNF-alpha, a pro-inflammatory cytokine as described by the ELISA kit manufacturer (BioLegend).

Briefly, a 96-well plate was incubated with the respective capture antibody (mouse GM-CSF or human TNFα) overnight at 4°C. On the following day, the 96-well plate was washed with a washing buffer (PBS 1X + 0.05% Tween 20) for four times and residual buffer was blotted by firmly tapping the plate upside down on absorbent paper. All subsequent washes were performed similarly. Next, the 96-well plate was blocked for non-specific binding using the assay diluent and incubated at RT for one hour using a microplate shaker. While the plate was being blocked, the experimental samples and mouse GM-CSF or human TNFα standard solutions were prepared. Prior to their incubation, the 96-well plate was washed. The experimental samples and standard solutions were incubated for 2.5 hours at RT. Next, the plate was washed, and the detection antibody (mouse GM-CSF or human TNFα) was added to each well and incubated for an additional 1 hour at RT. After four wash cycles, avidin- horseradish peroxidase was added to the wells and incubated for 30 minutes at RT. After four washes, bound antibody complexes were developed using a freshly made tetramethylbenzidine (TMB) solution. TMB solution was incubated for 15 minutes at RT and protected from light. After that, a stop solution (1M H_2SO_4) was added to the wells to stop the developing reaction. Absorbance was measured at 450 and 570 nm using a SynergyMx plate reader (BioTek, EUA).

6.2.5. *In vitro* Antimicrobial Study

S. aureus was cultured in Luria Bertani (LB) Broth to monitor the growth kinetics by spectrophotometry. 10 g of LB broth was dissolved in a bottle containing 500 mL distilled water (according to manufacturer's specification) and sterilized via autoclaving. Then 5 mL of the sterilized LB Broth was poured into a set of sterile tubes and inoculated with inocula from sub-cultured strains of *S. aureus*. The vacuum dried non-crosslinked and crosslinked HA and HA-CNF films were sterilized via UV radiation for 1 hour prior to addition into the inoculated tubes and placed in the incubator at 37^{o}C to allow the

microorganisms to grow. Aliquots of 200 μL of the cultured media from each sample was added into cuvettes pre-filled with 800 μL of fresh medium, and the optical density (OD600) of each sample was recorded every hour for 4 hours.

Mean growth rate (MGR) was obtained as the slope of the linear region after plotting the ln OD x time for each sample, and the mean relative growth index (MRGI) was calculated from the equation below:

$$MRGI = \left(\frac{MGRsample}{MGR\ control}\right) x100$$

Where the MGR of *S. aureus* only is the control.

6.2.6. Statistical Analysis

Data are presented as mean ± standard deviation (s.d.) and analysed using one-way analysis of variance (ANOVA) followed by post-hoc Tukey's HSD test. P-values < 0.05 (*) were considered significant.

6.3. Results and Discussion

6.3.1. Biocompatibility

Previously in this study, HA was homogeneously crosslinked with BIED using DMSO as the solvent for the system reaction. This condition might not pose any constraint for the encapsulation of drugs, as drugs are normally hydrophobic, but for cellular applications, gels need to be free of organic solvents such as DMSO. In this instance, HA films were heterogeneously crosslinked with BIED via diffusion. These gels were easily dried, and solvents evaporated, which is a preferred method for cell seeding and analysis of biocompatibility.

As some isocyanates are shown to be cytotoxic, the evaluation of cytotoxicity of gels crosslinked with of isocyanates is imperative. In the literature, other materials such as PVA, PEG and agar were crosslinked with other isocyanates and showed no cytotoxic effects (Teramura et al., 2007, Qian et al., 2015, Xu et al., 2015c, Xu et al., 2015d, Sonker et al., 2018b). In recent years, different isocyanates were used to crosslink HA. For example, modified star-shaped poly(ethylene oxide-stat-propylene oxide) carrying reactive isocyanate functional groups at the distal ends of the arms and modified

polycaprolactone and polylactide acid bearing isocyanates were able to react with HA but no cytotoxicity evaluations were performed (Dhanasingh et al., 2010, Chen et al., 2010).

The incorporation of CNFs in HA hydrogel formulations allows the possibility to obtain very tough and electrically conductive hydrogels. However, there is a concern about the toxic effects of carbon nanotubes (CNTs) and, therefore, hydrogel biocompatibility. Studies have reported that CNF toxicity seems to be dose-dependent, but cytotoxicity could be reduced when CNFs are functionalized and/or incorporated in hydrogel networks (Mihajlovic et al., 2019). For this reason, a dose-dependent assessment of NIH/3T3 cell viability after exposure to cell medium solutions containing different concentrations of CNF was performed. In Figure 6.1A, all testing conditions show increased proliferation over time. Interestingly, the group with higher CNF concentration (0.25% w/v) showed a similar proliferation profile to the control group.

The proliferation of NIH/3T3 fibroblasts on different HA films is shown in Figure 7b. Overall, all samples increased proliferation over time. The reinforcement of HA films by the addition of CNF does not show negative effects on cell proliferation, which is supported by other publications (Steel et al., 2020, Bhattacharyya et al., 2008). However, it is observed that crosslinked films displayed a smaller increase in proliferation than their non-crosslinked counterparts. CNF and CNT have been shown to increase adhesion of different cell types to a variety of polymeric films (Salesa et al., 2020).

A)

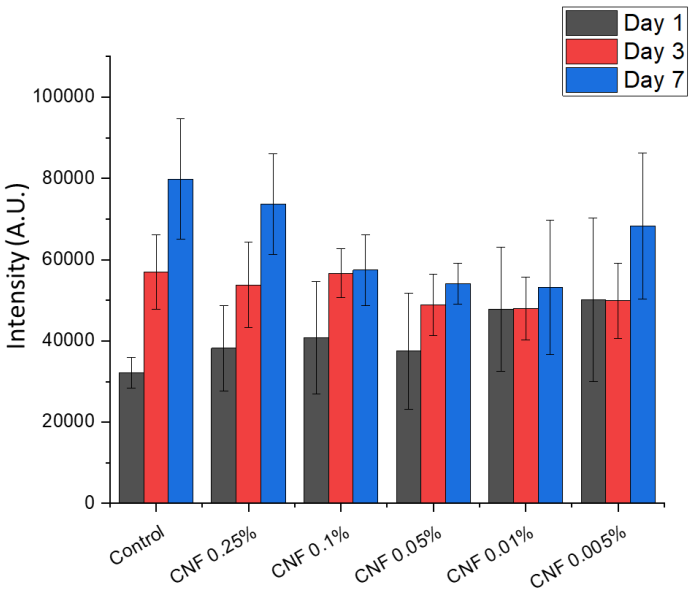

B)

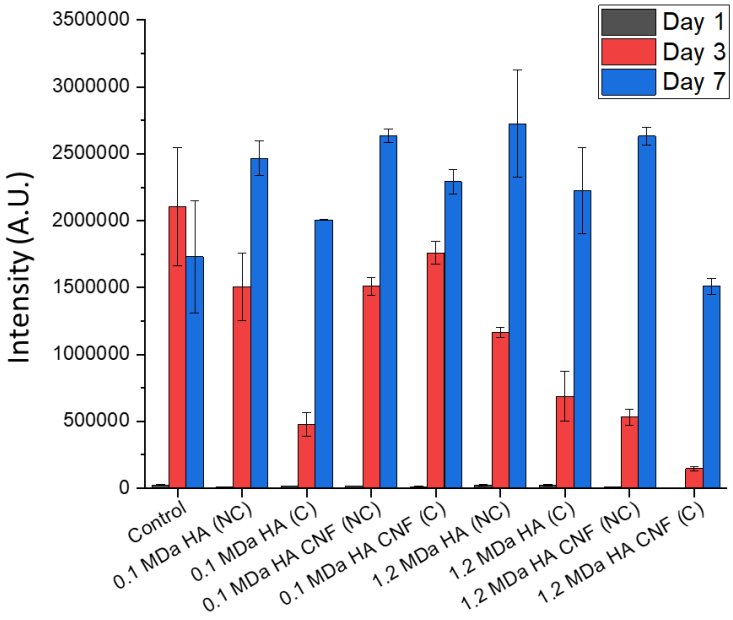

Figure 6.1. a) Cell viability of NIH/3T3 fibroblasts exposed to different concentrations of CNF suspended in cell culture medium using resazurin-based assay b) Continuous cell proliferation assessment of NIH/3T3 fibroblasts on different HA films with or without CNF reinforcement using resazurin-based assay. Not crosslinked (NC); Crosslinked (C).

Optical micrographs of the cell attachment to different substrates are shown in Figure 6.2. Interestingly, cell attachment does not seem to differ when CNF content in the cell culture medium is increased. For HA crosslinked films, it is observed that cells attach to the surface of the films independently of HA MW. This could be explained due to cell-mediated interactions via CD44 and RHAMM cell surface receptors on NIH/3T3 cells with HA crosslinked films (Zamboni et al., 2017). CNF-reinforced HA crosslinked films were unable to be photographed due to their opacity under the optical microscope.

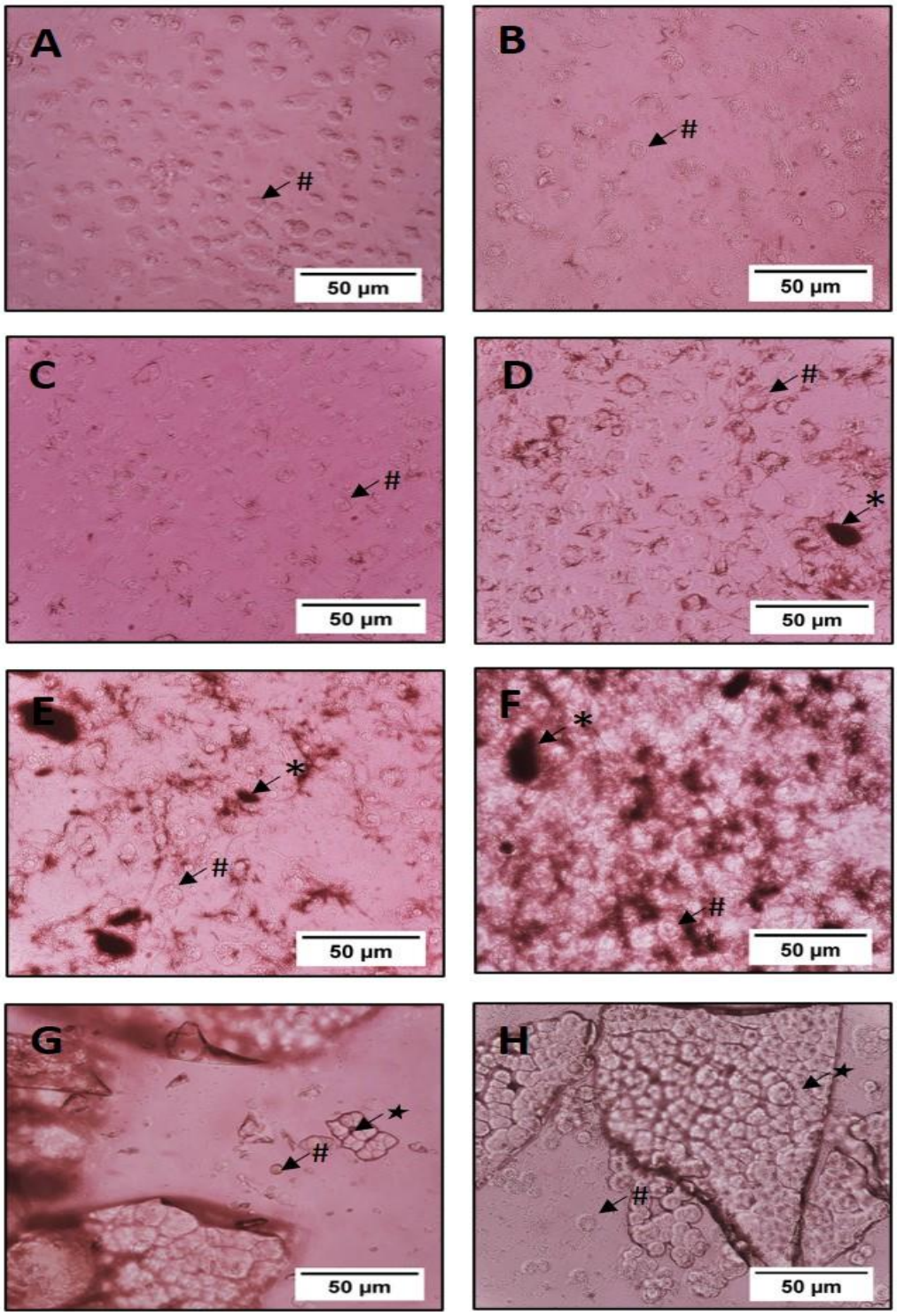

Figure 6.2. Cell attachment of NIH/3T3 cells after 7 days incubation on different substrates. A) Control; B) 0.005% CNF suspended in cell culture medium; C) 0.01% CNF suspended in cell culture medium; D) 0.05% CNF suspended in cell culture medium; E) 0.1% CNF suspended in cell culture medium; F) 0.25% CNF suspended in cell culture medium; G) 0.1 MDa HA crosslinked films; and H) 1.2 MDa HA crosslinked films. Arrows show: Cell attached to the well (#), cell attached to the

surface of the HA film (★), and CNF precipitate (*). Magnification 400X. Scale bar: 50 µm.

6.3.2. Immunomodulatory Analysis

For tissue engineering applications, it is also worth to analyse the response of the immune system to novel materials. In the literature, HA is said to be a material capable to modulate the immune system (Zamboni et al., 2018b). In Figure 6.3A and B, fibroblast activation was assessed by the quantification of cytokine production. Fibroblasts secrete GM-CSF, a cytokine that induce macrophage differentiation as part of the immune response chain. Figure 6.4 shows cells stained with fluorescent DAPI at 24 and 48 hours after being seeded onto crosslinked HA films. It can be noticed that the number of cells increase overtime.

Fibroblasts are present in all tissues but predominantly in connective tissues and are important producers and regulators of the ECM components. Moreover, fibroblasts also act as sentinels that elicit immunological responses by aiding the immune system. In Brief, fibroblasts act as sentinels to produce inflammatory mediators in response to several pathogens. Fibroblasts can express TLRs to sense microbial components and respond accordingly by synthesizing molecules that perform antimicrobial activity. Also, they can produce proinflammatory cytokines and chemokines to induce and recruit inflammatory cells (Bautista-Hernandez et al., 2017).

For this reason, this study decided to analyse the activation of fibroblasts and the production of GM-CSF, as it plays an important role in immune responses, survival, cancer pathogenesis, proliferation of macrophages, erythrocytes, eosinophils, megakaryocytes, and multipotent progenitors. The expression of GM-CSF is associated with inflammatory diseases, such as rheumatoid arthritis (Hamilton et al., 1992). Additionally, fibroblasts are well known to highly express CD44, which are receptors for HA (Quintanilla et al., 2014). Previous studies, were able to demonstrate that HA mediate GM-CSF mRNA expression and protein secretion via CD44 receptors on eosinophiles (Ohkawara et al., 2000). To date, there is no literature that has analysed the influence of HA nor CNF on GM-CSF production in fibroblasts.

CNF are also shown to decrease the production of nitric oxide and pro-inflammatory cytokines by macrophages (Khang, 2015). This auger well for the films produced in this study and their ability to potentially mitigate inflammatory reactions, especially when targeting wound healing and skin derivate applications.

Results show that GM-CSF production is concentration-dependent of CNF dispersed in the cell medium (Figure 6.3a). Solutions of CNF at 0.005% do not show increase GM-CSF production by L929 fibroblasts in comparison to the control group. Moreover, all HA films, independently of MW and CNF-reinforcement, show comparable GM-CSF production profiles to those observed by the control group (Figure 6.3b).

A)

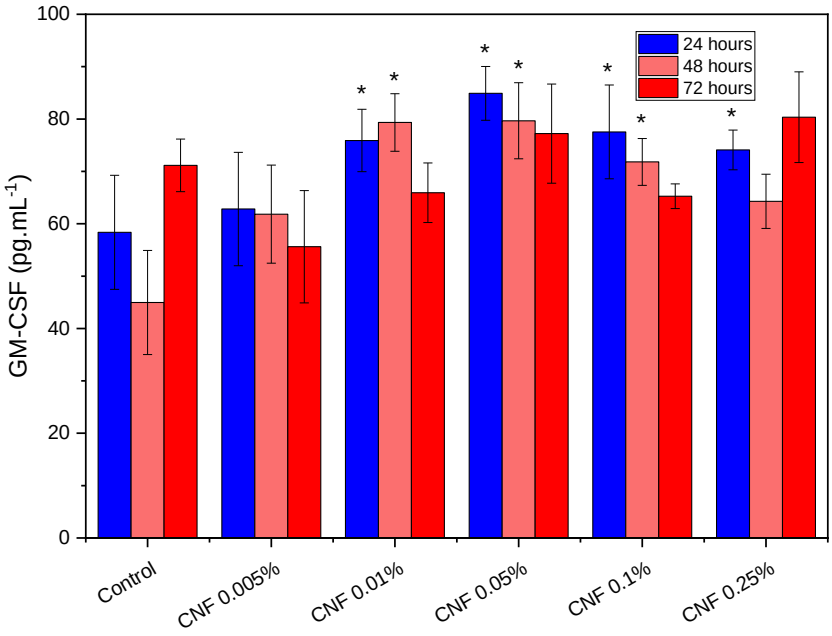

B)

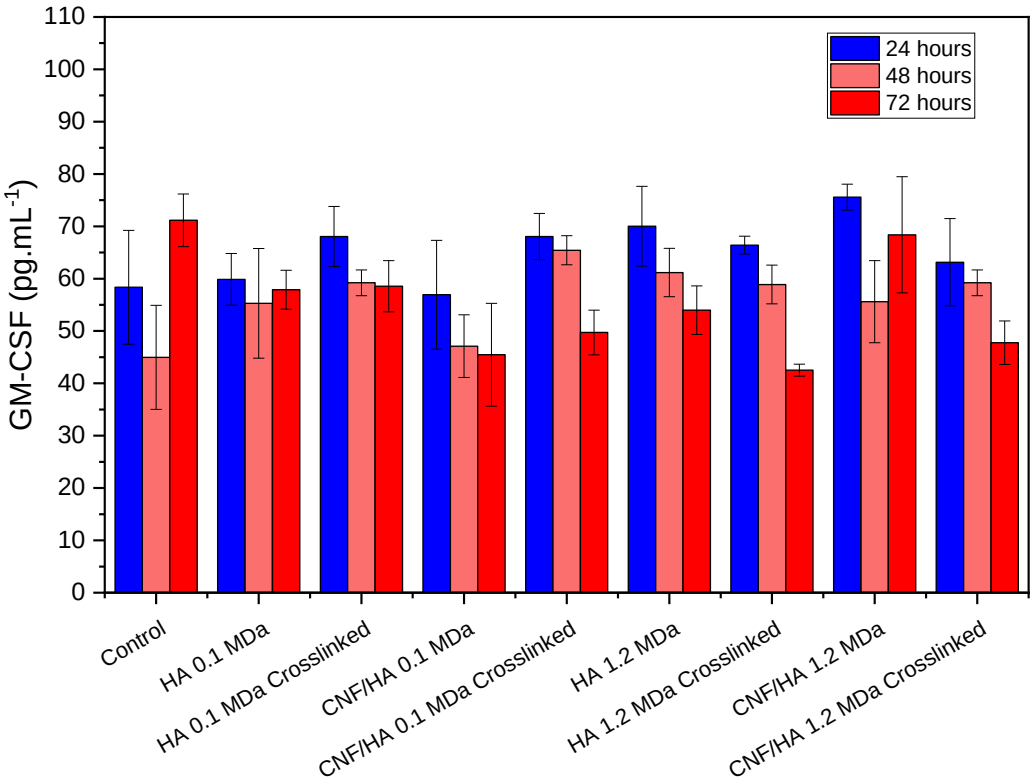

Figure 6.3. Modulation of L929 activation and production of GM-CSF through CNF content (a) and different HA films (b). Statistical analysis was performed using ANOVA followed by post-hoc Tukey's HSD test where p-value < 0.05 shows statistical difference (*) from control group.

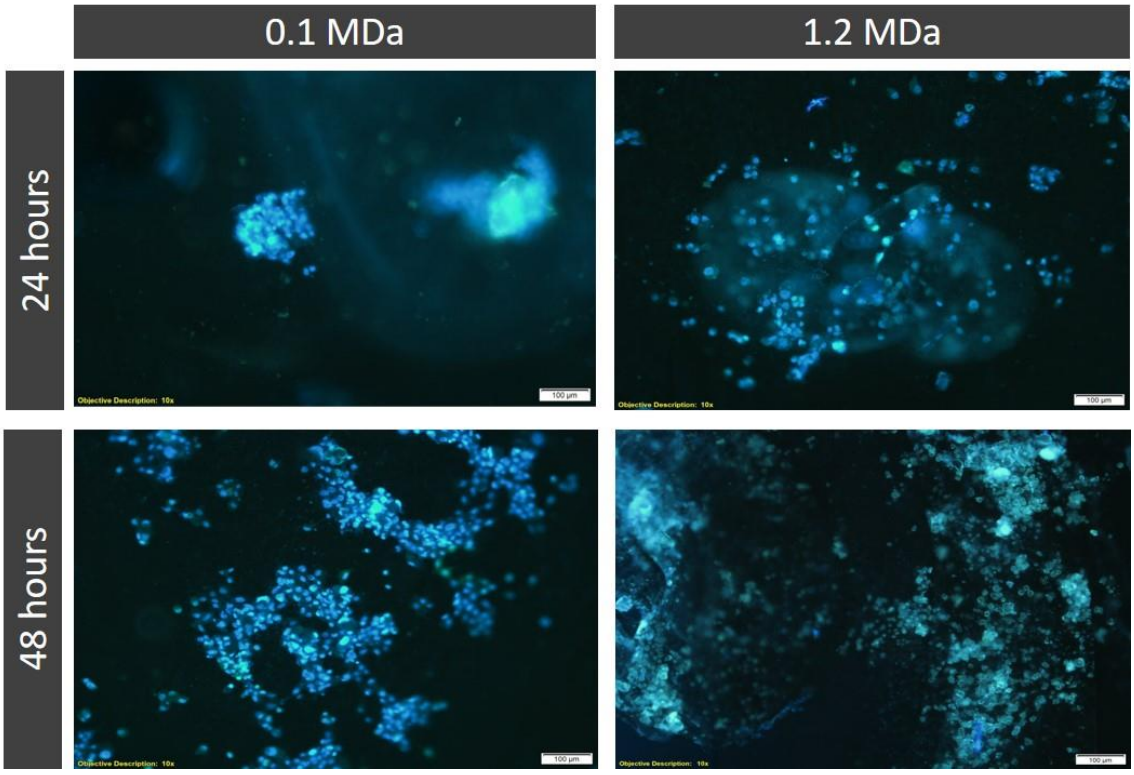

Figure 6.4. L929 cells fluorescently stained using DAPI. Cell attachment on the surface of 0.1 MDa and 1.2 MDa HA films crosslinked with BIED at 24 and 48 hours after incubation. Magnification 100X. Scale bar: 100 µm.

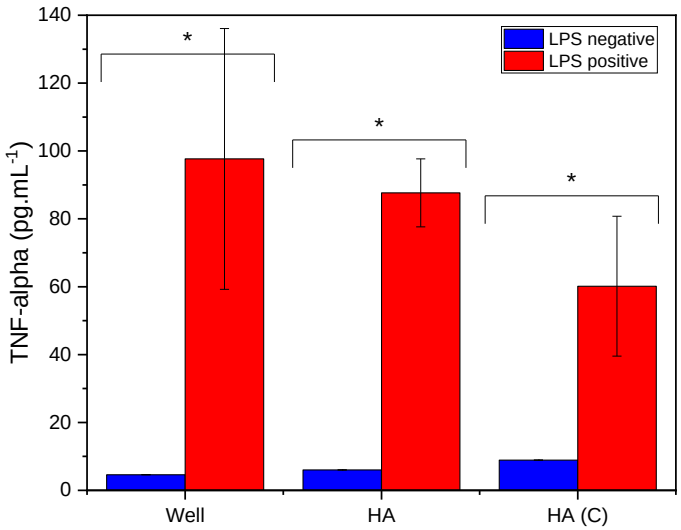

Figure 6.5. THP-1 monocyte activation and production of TNFα at 24 hours after incubation with HA 1.2 MDa. Statistical analysis was performed using ANOVA followed by post-hoc Tukey's HSD test where p-value < 0.05 shows statistical difference (*).

Further along the immunological response chain, monocytes are next in line. Within the first days of inflammation (acute), TNFα production in monocytes is observed during the first 24 hours. Once monocytes are activated, they differentiate into macrophages that can be further polarized into the M1 subset (pro-inflammatory) within 1-3 days or into the M2 subset (pro-healing and angiogenic) within 3-9 days (Yang et al., 2014).

Figure 6.5 shows the influence of HMW HA on the activation of monocytes to produce TNFα. It can be seen that no significant increase in TNFα secretion is observed for all test groups in comparison to the control group (well plate). Neither non-crosslinked nor BIED-crosslinked HA elicited TNFα production. Once monocytes are challenged with LPS, a significant ($p<0.05$) spike in TNFα is observed in all groups, however, BIED-crosslinked HMW HA shows to protect monocytes from LPS-induced TNFα production. Previous studies have already established that HMW HA has the ability to suppress inflammation due to LPS exposure in macrophages (Rayahin et al., 2015).

Interestingly, these results are able to give an insight on the modulation of the immune system by HA and HA crosslinked with isocyanates such as BIED. Going forward, there is a demand to continue to further study more complex approaches to elucidate the mechanism of immune modulation of these cells by HA. For the moment, these results can only give a hint of HA-BIED crosslinked immunomodulatory capacity and speculation of its applications. For example, cellular grafts of LMW HA-BIED crosslinked show decreased fibroblast production of GM-CSF, thus these grafts could be potentially transplanted into any tissues abundant of fibroblasts. On the other hand, cellular grafts of HMW HA-BIED crosslinked show no monocyte activation and TNFα production, even, slightly protecting LPS induction, thus being potentially transplanted in tissues with direct blood contact.

6.3.3. Antimicrobial Activity

The non-crosslinked and crosslinked HA and HA-CNF films show antimicrobial activity against *S. aureus*. The growth rate of *S. aureus* is shown in Figure 6.6.

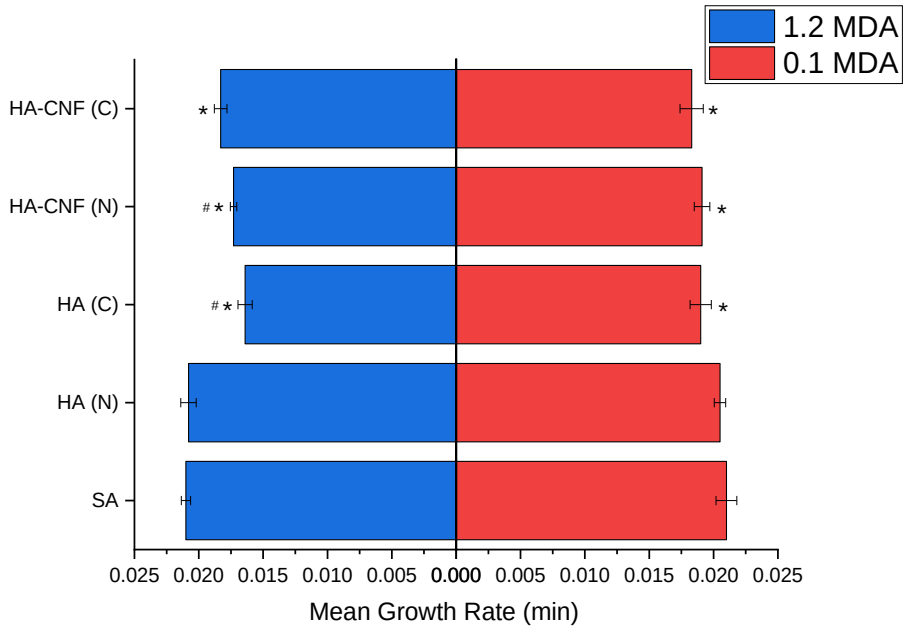

Figure 6.6. Mean growth rate of *S. aureus* for each HA hydrogel formulation. SA is the control group containing only S. aureus in LB broth. Statistical analysis was performed using ANOVA followed by post-hoc Tukey's HSD test where p-value < 0.05 shows statistical difference between groups (#) and within groups (*).

When comparing the MGR between the control (SA) group and the HA samples from both MWs tested, it shows that all crosslinked samples significantly decrease MGR

($p<0.05$), thus having a higher bacteriostatic activity. The decrease of MGR for crosslinked samples is not associated with the crosslinker itself. The MGR of *S. aureus* cultured in LB broth containing only BIED at the same concentration used to crosslink HA films is 0.0202 ($p>0.05$). Both 1.2 MDa and 0.1 MDa HA (N) films do not show bacteriostatic activity ($p>0.05$).

The bacteriostatic effect between low and high MW HA groups, shows that 1.2 MDa HA samples [HA (C) and HA-CNF (N)] present significant higher bacteriostatic effects than their low MW counterparts ($p<0.05$). Pointing out the highest decrease in MGR is related to crosslinked 1.2 MDa HA films (0.016 ± 0.00055). *S. aureus* produces hyaluronidase (a.k.a. hyaluronate lyases) encoded in the *hysA* gene, which cleaves the β-1,4 glycosidic bond of HA by β-elimination in a processive manner. This results in unsaturated disaccharides as the final product of complete digestion. It has been hypothesized that the bacteriostatic effect of HA is due to the saturation of the bacterial hyaluronidase owing to the excess of HA. This prevents the bacteria from proliferating, secondary to elevated levels of ECM component, which needs to be digested in turn affecting tissue permeability (Carlson et al., 2004). The increased bacteriostatic effect observed in the crosslinked HMW HA shows the dependency of the hyaluronate lyase to degrade the HMW HA network into small fragments, which is less evident for LMW HA. The addition of CNF to the HMW HA crosslinked network can decrease the number of interactions between HA and the bacteria, this compromises the digestion of HA through bacterial hyaluronate lyases, therefore reducing the bacteriostatic effect.

In table 6.1, the comparison between the mean growth indexes and mean doubling time are shown. The antibacterial findings of this research are in agreement with the earlier study of Pirnazar *et al*. This showed that the three different MW formulations of recombinant HA used in their experiment exhibited varied bacteriostatic effects on *S. aureus* depending on the MW and concentration of HA (Pirnazar et al., 1999).

Table 6.1. Bacteriostatic effects of various HA hydrogels.

HA MW	Groups	Mean Relative Growth Index	Mean Doubling Time (minutes)
	Control	100%	32.4
	HA (N)	97.6%	33.8

0.1 MDa	HA (C)	90.5%	36.5
	HA-CNF (N)	90.9%	36.2
	HA-CNF (C)	87.2%	37.9
1.2 MDa	HA (N)	99.1%	33.3
	HA (C)	78.1%	42.3
	HA-CNF (N)	82.4%	40.1
	HA-CNF (C)	85.7%	38.5

6.4. Final Considerations

Crosslinking HA films with BIED produced a gel-like biomaterial whose mechanical properties and functionality makes it suitable for various biomedical applications. More so, experimental tests revealed that the addition of CNFs (0.25 wt.%) to HA films significantly improved the film mechanical property and demonstrated no harmful cytotoxic effects.

Moreover, these films are able to modulate cells from the immune system. HA films did not elicit fibroblast activation through the evaluation of GM-CSF production. GM-CSF content in cell culture supernatant of various HA films tested was similar to the control group. Regarding the modulation of monocytes, HMW HA films were unable to activate these cells showing an anti-inflammatory effect, where the release of TNF-α (pro-inflammatory cytokine) from monocytes in culture with HMW HA films was absent.

Furthermore, the study of the antimicrobial activity of these films revealed that they possess bacteriostatic properties against *S. aureus*, where crosslinked HA-CNF films exhibited the highest antibacterial effect without any bactericidal effect.

In conclusion, the combined benefits of mechanical properties, together with fibroblast proliferation, immunomodulation and bacteriostatic activity of HA films crosslinked using BIED show their suitability as biomaterials for tissue engineering applications.

Chapter 7: Cell Surface Engineering of Pancreatic β Cells

The contents of the following chapter are being reformatted to be submitted as an original research article in the journal Biomaterials.

Authors: Fernanda Zamboni, Cristiana Rodrigues Carvalho, Raquel Maia, Rui L. Reis, Joaquim Miguel Oliveira, Maurice N. Collins

Abstract

Surface engineering the plasma membrane of cells creates tailored sites with specific functions that include anchorage sites for biomolecules, cell-tagging fluorophores, and cell encapsulation. Protein-anchorage or physical adsorption of fatty acid into the lipid bilayer are two of many approaches that have been developed to create these plasma membrane modifications. Herein, the plasma membrane of pancreatic β cells is engineered using Maleimide-PEG-Lipid (Mal-PEG-Lipid). Firstly, Mal-PEG-Lipid is synthesized by the reaction between maleimide-PEG-NHS and dipalmitoyl-glycerol-phosphatidyl ethanolamine (lipid) which has been confirmed by FT-IR analysis. Three different concentrations of Mal-PEG-Lipids (50, 250 and 500 $\mu g.mL^{-1}$) and two incubation times (30 minutes and 1 hour) were analysed for the optimization of single cell surface modification. Characterization of cell viability through live/dead assay, plasma membrane disruption through Annexin V assay, and Mal-PEG-Lipid membrane uptake and release were performed. Results show that cell viability analysed by calcein/propidium iodide staining does not significantly differ in all concentrations and incubation times tested. Plasma membrane disruption shows higher Annexin V binding to Mal-PEG-Lipid at 500 $\mu g.mL^{-1}$ for 1 hour, which correlates to higher Mal-PEG-Lipid uptake by the plasma membrane (confirmed by the fluorescence analysis of cells incubated with FITC-tagged Mal-PEG-Lipid). The stability of the Mal-PEG-Lipid at the plasma membrane shows that for all concentrations and incubation periods analysed, Mal-PEG-Lipid release to the cell medium did not increase over time, suggesting that palmitoyl hydrophobic insertion to the plasma membrane is stable. These results show that optimal Mal-PEG-Lipid surface engineering (500 $\mu g.mL^{-1}$ for 30 minutes) of the plasma membrane can provide anchorage-sites to a variety of molecules as the maleimide moiety reacts with primary amines and thiol groups to create stable conjugates.

7.1. Introduction

The transplantation of pancreatic β cells, pancreatic islets and whole pancreas has effectively improved the quality of life of end-stage renal failure type 1 diabetic patients (Light and Tucker, 2013). However, graft issues remain to be resolved in terms of improving graft survival, managing innate and adaptive immune responses, and decreasing life-long immunosuppressant drug therapy (Teramura et al., 2020). To enhance the function and improve the efficacy of cell-based therapeutics, a variety of cell surface engineering strategies have been developed to modify the surface of cells. A variety of materials have been studied which include therapeutic molecules, artificial receptors, and multifunctional nanomaterials (Abbina et al., 2017). Surface modification has the potential to create cell membrane synthetic sites mimicking surface receptors and proteins for the anchorage of specific biomolecules, cell-tagging fluorophores, and cell encapsulation coatings. The latter is particularly interesting in applications that envisage to hide the cell surface when exposed to immunological surveillance especially important in transplantation therapy.

Surface modification of the cellular plasma membrane can be achieved through chemical covalent conjugation and noncovalent physical bioconjugation. Noncovalent bioconjugation can be achieved through biotinylation, electrostatic interaction and lipid membrane fusion (Liu et al., 2019a). *In vitro* studies using biotin/streptavidin linker (biotinylation) are not appropriate for clinical applications. Xenogeneic proteins such as avidin and streptavidin are highly immunogenic *in vivo.* A less immunogenic alternative to biotinylation is PEG-maleimide, commonly referred to as PEGylation (Wang et al., 2015a). A study in 2016 reported that PEG molecular weight influences the immobilization and cellular uptake of bio-functional molecules. Low molecular weight PEG (1 kDa) was unable to prevent protein adsorption in contrast to 5 kDa PEG. Interestingly, high molecular weight PEG (40 kDa) was also unable to prevent protein adsorption and this was attributed to strong static repulsion of chains making them difficult to pack at high densities (Teramura et al., 2016).

In noncovalent bioconjugation, the selection of an appropriate fatty acid for lipid membrane fusion is based on three main variables: size of the hydrocarbon chain, saturation of hydrocarbon chain and the number of hydrocarbon chains. In the literature, using two long fatty acid chains to surface engineer the cell membrane has been described

to increase the anchorage and decrease the dissociation rates from the cell surface (Itagaki et al., 2015).

Herein, the plasma membrane of pancreatic β cells is engineered using Maleimide-PEG-conjugated with two palmitoyl fatty acid chains (Mal-PEG-Lipid). Mal-PEG-Lipid is an amphiphilic molecule designed to resemble a phospholipid, where the Mal-PEG portion is hydrophilic, and the lipid portion is hydrophobic. Mal-PEG-lipids are inserted in the cell membrane by lipophilic interactions. *In vitro* cell surface engineering of pancreatic β cells (MIN-6 line) is assessed for biocompatibility, membrane disruption and stability in order to determine optimal surface engineering using Mal-PEG-Lipid.

7.2. Materials and Methods

7.2.1. Materials

Maleimido propionyl-polyethylene glycol-n-hydroxysuccinimide ester (Mal-PEG-NHS), dipalmitoyl-glycerol-phosphatidyl ethanolamine (DPPE), FITC, L-cysteine, Live/Dead Viability/Cytotoxicity assay, were purchased from Sigma Aldrich (St. Louis, MO, USA). Annexin V-Alexa Fluor 568 was purchased from BD Life sciences (Berkshire, England, UK). All other consumables necessary for cell culture including cell culture medium, pipettes, flasks and plates were purchased from Thermofisher. Pancreatic MIN-6 cells were kindly donated by Dr. Joaquim Miguel Oliveira from the I3Bs Research Group at the University of Minho, Portugal.

7.2.2. Production of Mal-PEG-Lipids

Mal-PEG-NHS 50 mg is dissolved in chloroform together with 5 mg of DPPE to react under stirring for 24 hours at RT. The Mal-PEG-Lipid product is purified by precipitation in diethyl ether. Chemical characterization of Mal-PEG-Lipids was performed using FT-IR spectroscopy. All spectra were recorded on a Perkin Elmer spectrum 100 FT-IR spectrometer operating in Attenuated Total Reflectance (ATR) mode (Perkin Elmer, MA, USA). Each FT-IR spectrum was scanned twenty times with a resolution of 2 cm^{-1}. The ranges used were from 4000 cm^{-1} to 650 cm^{-1}.

Mal-PEG-lipids were labelled with FITC. Firstly, Mal-PEG-Lipid (25 mg) reacts with cysteine (0.6 mg) dissolved in a solution of acetone and ethanol (1:1) at a pH 6.5, overnight. The pH<7 favours the reaction between the maleimide and the thiol group of cysteine to form a thioether bond over the reaction of maleimide and the primary amine of cysteine. The Cys-Mal-PEG-Lipid product is purified by precipitation in diethyl ether. Then, Cys-Mal-PEG-Lipid reacts with 4 mg of FITC dissolved in acetone overnight. pH>5 is required for the amino group of cysteine to react with isothiocyanate to form a thiourea bond. The FITC-tagged Mal-PEG-Lipid is purified by precipitation in diethyl ether.

7.2.3. MIN-6 Culture

A cell number of $1x10^7$ cells were cultured in T75 flasks using high glucose DMEM, supplemented with 10% FBS, 1 % antibiotic/antimycotic, 10 mM sodium pyruvate and 50 µM β-mercaptoethanol. Cell media was replenished every 3 days until cell confluency was reached. MIN-6 cells at 30-40 passages were used.

7.2.4. Cell Surface Modification

MIN-6 cells at a density of $1x10^6 cells.mL^{-1}$ were incubated with Mal-PEG-Lipid in three concentrations (50, 250 and 500 $\mu g.mL^{-1}$) for two treatment times (0.5 and 1 hour). Right after Mal-PEG-Lipid incubation, cell viability was assessed using Live/Dead Viability/Cytotoxicity assay (calcein AM at 2 µM, ethidium homodimer-1 at 4 µM) and visualized using fluorescence microscopy.

7.2.5. Cell Surface Modification Stability

The stability of the surface modification was assessed using FITC-tagged Mal-PEG-Lipid. Cells were incubated with FITC-tagged Mal-PEG-Lipid as described above. After the incubation period, 45,000 cells were seeded in 24 well-plates. Over time, FITC-tagged Mal-PEG-Lipid can be released from the cell membrane to the medium, demonstrating a decrease in stability. The fluorescence intensity of free FITC-tagged Mal-PEG-Lipid released to the media at 0, 3 and 24 hours was measured in a 96-well plate by a plate reader with an emission of 570 nm and excitation of 490 nm. The release of FITC-tagged Mal-PEG-Lipid from the plasma membrane was also assessed by cell attachment to the well-plate at different time points (0, 3 and 24 hours) using a brightfield microscope.

7.2.6. Surface Integrity Evaluation

After surface modification of MIN-6 cells using Mal-PEG-Lipid, surface integrity of the plasma membrane was evaluated using Annexin V-Alexa Fluor 568. Negative control cells, positive apoptotic control cells (induced by heat-shock at 70°C for 5 minutes), and surface modified cells are incubated at a density of $1x10^6$ $cells.mL^{-1}$ in annexin-binding buffer (10 mM HEPES, 140 mM NaCl and 2.5 mM $CaCl_2$, pH 7.4). After, Annexin V-Alexa Fluor 568 (25 $\mu g.mL^{-1}$), sytox green (2 $\mu g.mL^{-1}$) are added to the cell suspension and incubated for 15 minutes at RT. After incubation, cells are washed with annexin-binding buffer. The combination of nuclear staining using sytox green distinguishes

necrotic (nuclear staining) from apoptotic cells. Cells were visualized using ImageXpress Micro Confocal and MetaXpress software (Molecular Devices, CA, USA).

7.2.7. Statistical Analysis

Data are presented as mean ± standard deviation (S.D.) and analysed using one-way analysis of variance (ANOVA) followed by post-hoc Tukey's HSD test. P-values < 0.05 (*) were considered significant.

7.3. Results and Discussion

7.3.1. Mal-PEG-Lipid Synthesis

Mal-PEG-NHS reacts with DPPE through a nucleophilic substitution reaction that occurs between the NHS and the primary amine from the ethanolamine. The primary amine is deprotonated and acts as a nucleophile (Figure 7.1).

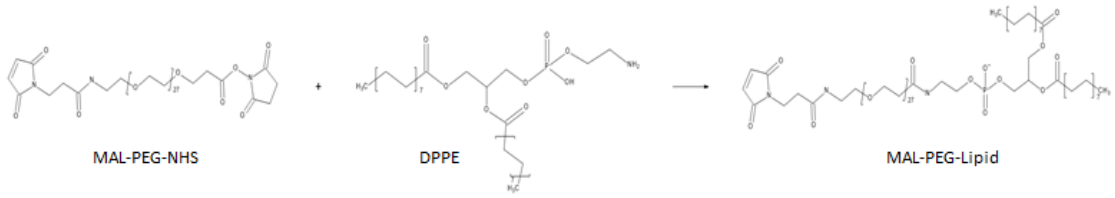

Figure 7.1. Reaction of MAL-PEG-NHS and DPPE. The nucleophilic substitution reaction occurs between the NHS and the primary amine from the ethanolamine forming MAL-PEG-Lipid.

DPPE is preferred for the synthesis of Mal-PEG-Lipid because it contains two chains of palmitoyl. Palmitoyl lipids have a saturated long fat acid chain (C16) that occurs naturally in the cell membrane (Freedman, 2012). It is also an important site for protein anchorage via protein palmitoylation (Guan and Fierke, 2011). The confirmatory FT-IR spectra of Mal-PEG-Lipid bond is shown in Figure 7.2. Mal-PEG-NHS spectrum shows characteristic NHS bands at around 1808, 1781, 1739 cm^{-1} and the ether band from PEG at 1109 cm^{-1} (Peng et al., 2010). Whereas DPPE shows characteristic primary amine stretch band at around 3600 cm^{-1} and NH bend band at around 1700 cm^{-1}. Upon the reaction between the primary amine of the ethanolamine from DPPE and the NHS group of Mal-PEG-NHS, a new band at around 1686 cm^{-1} appears, which is related to weak carbonyl stretch (Wang et al., 2015b).

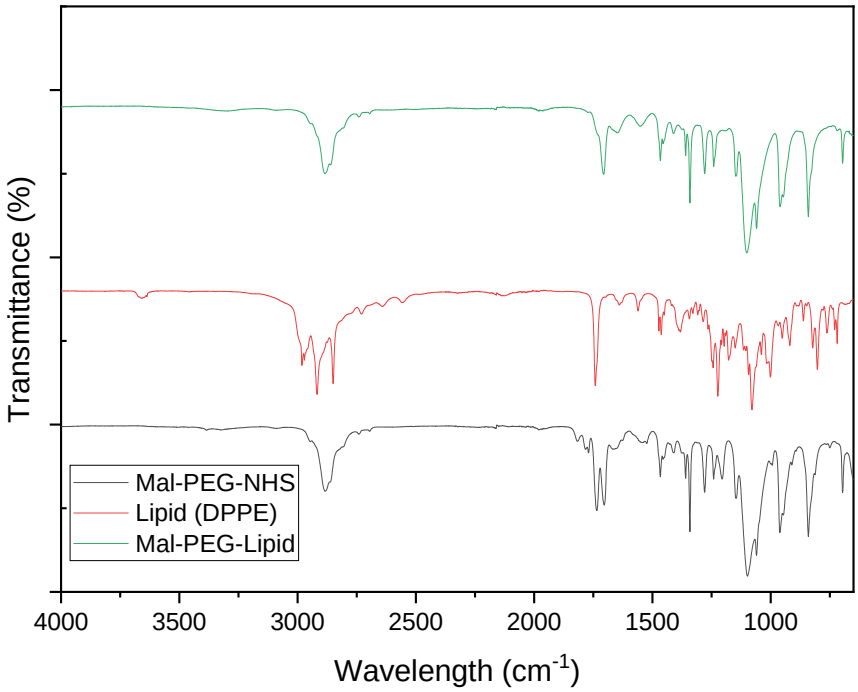

Figure 7.2. Chemical characterisation of Mal-PEG-Lipid through FT-IR Spectroscopy.

7.3.2. Cell Surface Modification

MIN-6 cells had their plasma membrane modified using a Mal-PEG-Lipid. After the surface modification, cell viability was assessed using Live/Dead assay (Figure 7.3). Cell viability was not affected by surface modification using the various concentrations and incubation times (Figure 7.4). Although cell surface modification is not accompanied by cell death, it is possible that plasma membrane can be potentially disrupted after surface engineering which can lead to an early apoptotic state. Plasma membrane disruption evaluation was performed using Annexin V. When plasma membrane disruption occurs, phosphatidylserine (only found in the inner leaflet of the plasma membrane) is externalized to the outer membrane and binds to Annexin V, demonstrating an early apoptotic state. The results shown in Figure 7.5 demonstrates that surface engineering the plasma membrane of MIN-6 cells with 50, 250, and 500 $\mu g.mL^{-1}$ of Mal-PEG-Lipids for 30 minutes or 1 hour does not disrupt the plasma membrane. The number of cells stained with Annexin V is comparable to the control group. Positive necrotic cells (Figure 7.5b) shows colocalization of fluorescence staining marked by sytox green (nucleus) and Annexin V (membrane) in red.

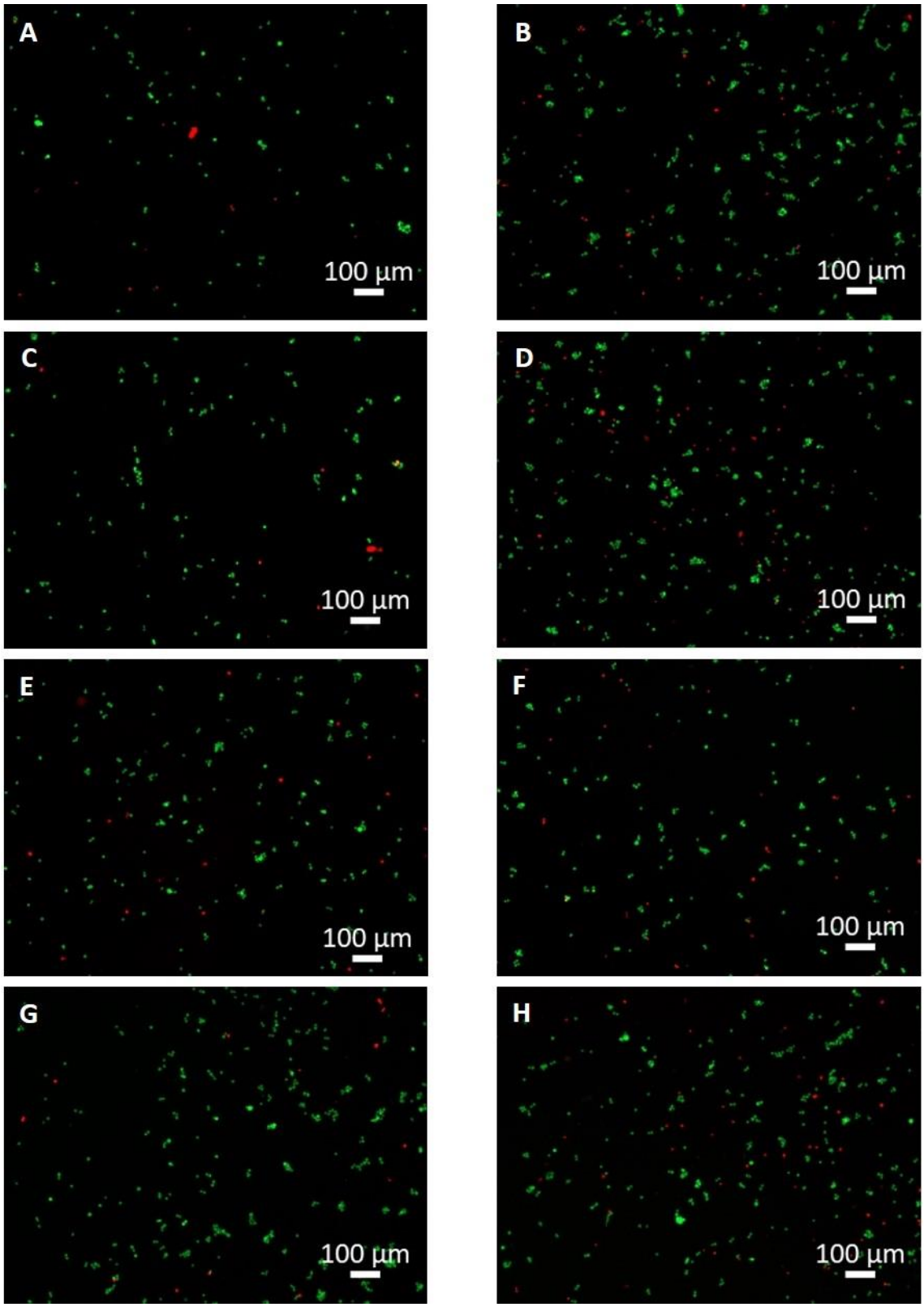

Figure 7.3. Cell viability by Live/Dead assay of surface modification using Mal-PEG-Lipids after incubation for 30 minutes at concentrations 50, 250 and 500 µg.mL^{-1} (C,E

and G respectively) and 1 hour at concentrations 50, 250 and 500 µg.mL^{-1} (D, F and H respectively). A and B are control cells with no surface modification.

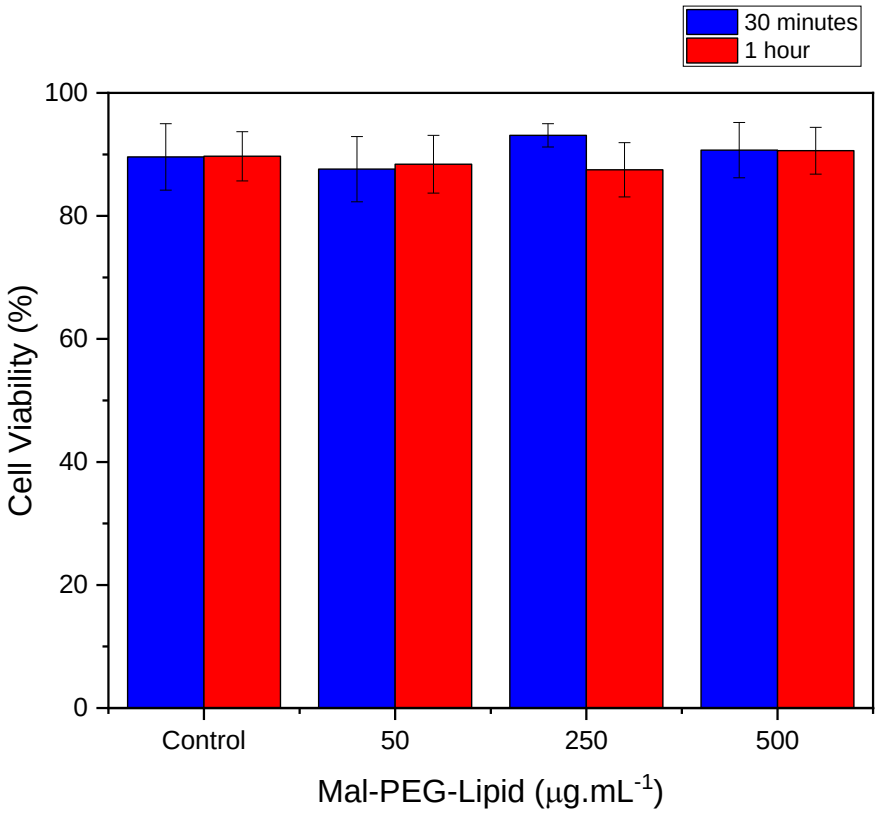

Figure 7.4. Viability of MIN-6 cells after surface modification using Mal-PEG-Lipid for 30 minutes and 1 hour at concentrations 50, 250 and 500 µg.mL^{-1}. Statistical analysis was performed using ANOVA followed by post-hoc Tukey's HSD test where p-value ≥ 0.05 showing no statistical difference between groups.

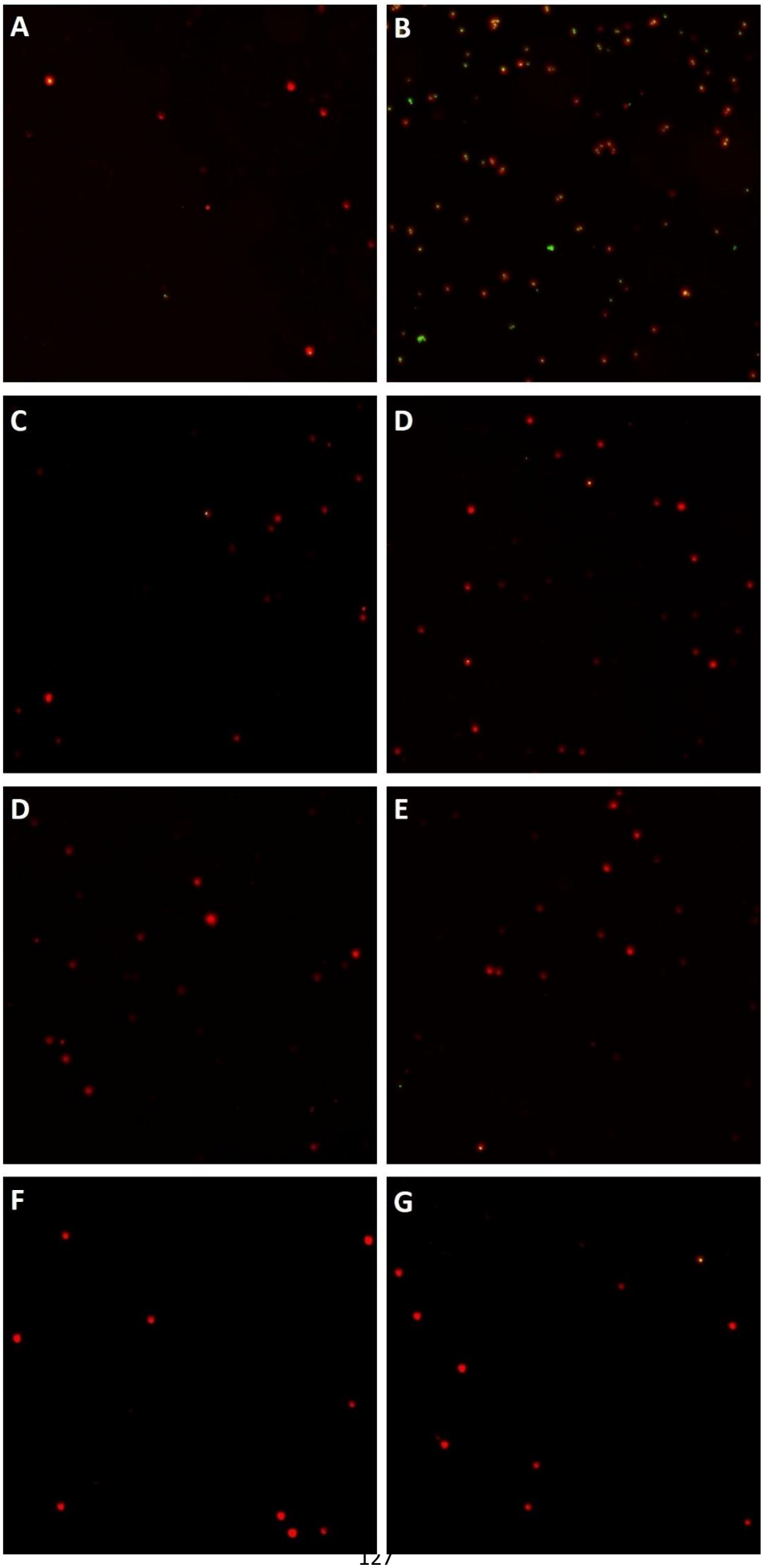
A
B
C
D
D
E
F
G

Figure 7.5. Plasma membrane disruption and early apoptosis assay using Annexin V after MIN-6 surface modification with Mal-PEG-Lipid. A) Control; B) Control dead cells; C) 50 µg.mL^{-1} for 30 minutes; D) 50 µg.mL^{-1} for 1 hour; E) 250 µg.mL^{-1} for 30 minutes; F) 250 µg.mL^{-1} for 1 hour; G) 500 µL µg.mL^{-1} for 30 minutes; and H) 500 µg.mL^{-1} for 1 hour. Magnification 4X.

7.3.3. Plasma Membrane Uptake of FITC-tagged Mal-PEG-Lipids

To show the incorporation of Mal-PEG-Lipids to the plasma membrane of MIN-6 cells, Mal-PEG-lipids were fluorescently tagged using FITC (Figure 7.6 and 7.7). All groups demonstrated homogenous fluorescence throughout their plasma membrane, which indicates that cell modification occurred evenly. In the control group, cell morphology is shown to be rounded and unattached to the culture plate at time 0, however after 24 hours cells start to attach to the bottom of the well plate and display elongated morphology. All groups incubated with FITC-tagged Mal-PEG-Lipid show rounded morphology and were unable to attach to the culture plate even after 24 hours.

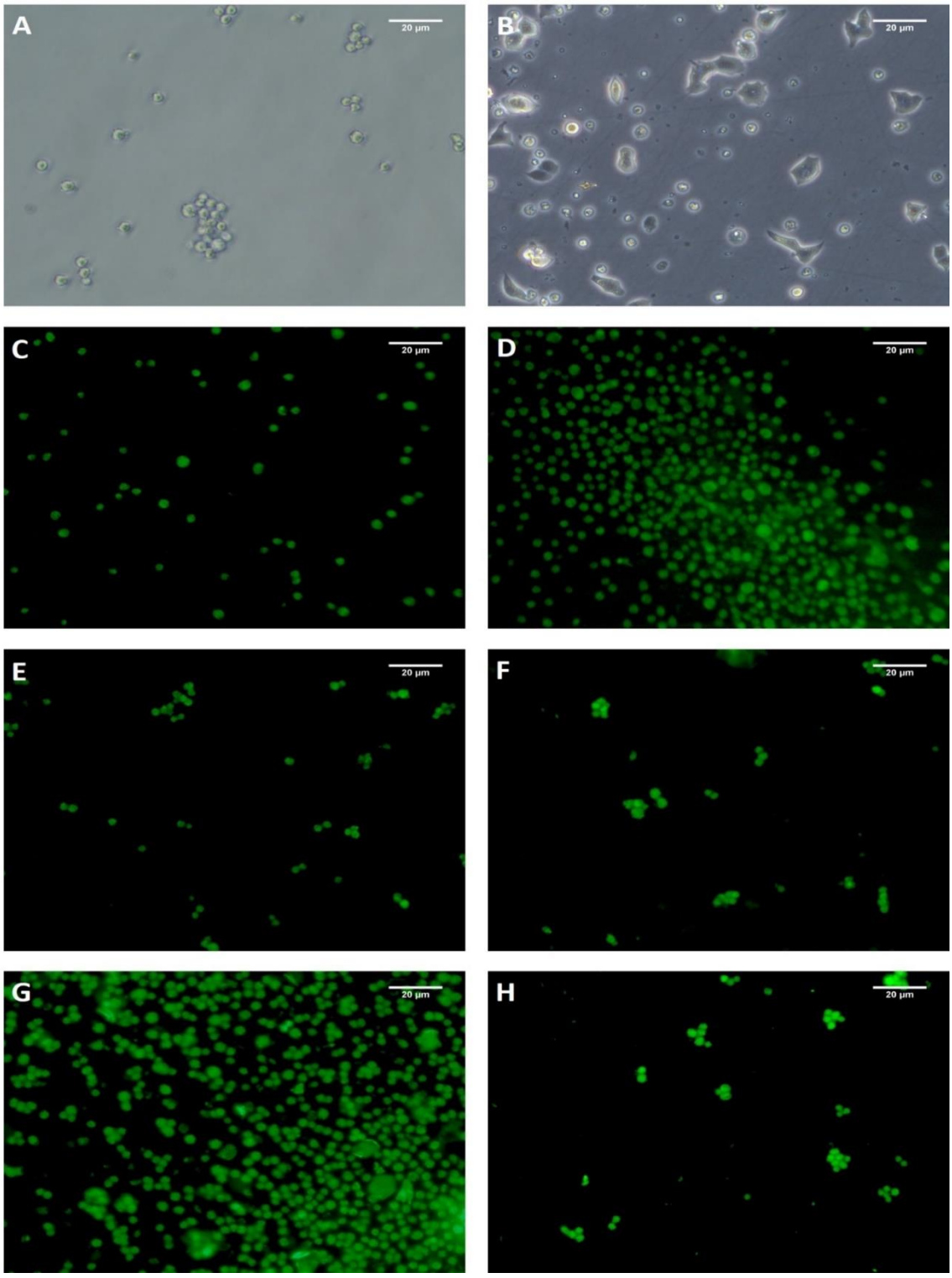

Figure 7.6. Surface modification of MIN-6 cells just after incubation with FITC-tagged Mal-PEG-Lipid for 30 minutes at 50, 250 and 500 µg.mL^{-1} (C, E and G, respectively) and at 24 hours after incubation with FITC-tagged Mal-PEG-Lipid for 30 minutes at 50, 250 and 500 µg.mL^{-1} (D, F and H, respectively). A and B are control cells with no surface modification at 0 and 24 hours, respectively.

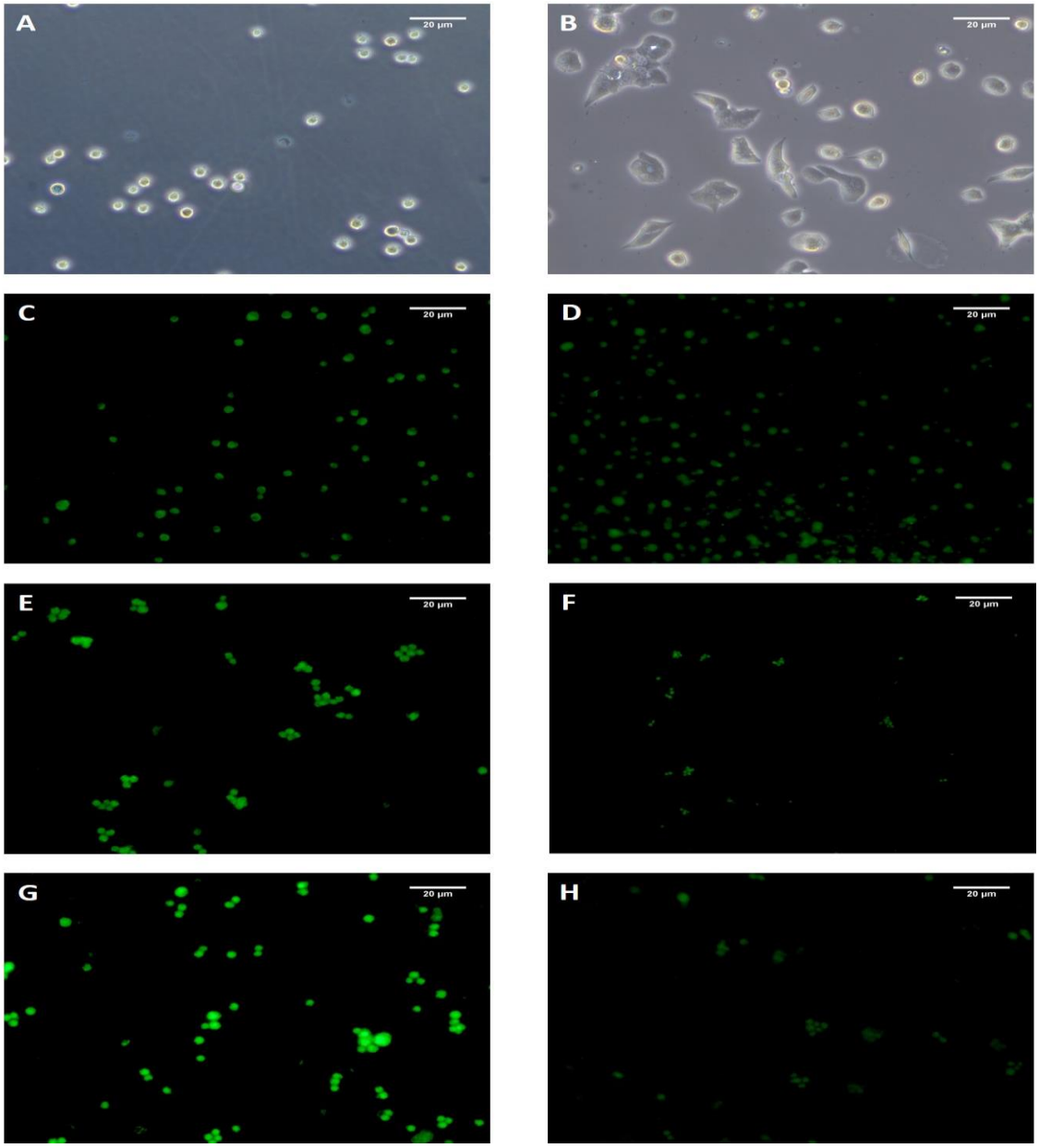

Figure 7.7. Surface modification of MIN-6 cells just after incubation with FITC-tagged Mal-PEG-Lipid for 1 hour at 50, 250 and 500 µg.mL^{-1} (C, E and G, respectively) and at 24 hours after incubation with FITC-tagged Mal-PEG-Lipid for 1 hour at 50, 250 and 500 µg.mL^{-1} (D, F and H, respectively). A and B are control cells with no surface modification at 0 and 24 hours, respectively.

7.3.4. Stability of FITC-tagged Mal-PEG-Lipid in the Plasma Membrane of MIN-6 Cells

The plasma membrane is a dynamic structure, where its components are in constant turnover. For this reason, the effect of incubation time and concentration on the stability of Mal-PEG-Lipid on the cell membrane of MIN-6 cells was evaluated by the release of FITC-tagged Mal-PEG-Lipid from the plasma membrane to the cell medium (Figure 7.8). In the first 24 hours after cell surface modification, there was no significant release of FITC-tagged Mal-PEG-Lipid over time for all groups. However, a trend can be observed from cells incubated with the lowest concentration (50 $\mu g.mL^{-1}$) of FITC-tagged Mal-PEG-Lipid that release of FITC-tagged Mal-PEG-Lipid is slightly higher for cells incubated for 30 minutes in comparison to cells incubated for 1 hour.

In the literature, structural differences in fatty acid chains influence the hydrophobic interactions within the cell membrane. A study comparing PEG-lipids carrying different fatty acid chains showed that as the chain becomes longer, an increase in anchorage and a decrease in the dissociation rates from the cell surface is observed. Moreover, PEG-lipids containing double fatty acid chains showed better anchorage and dissociation rates than PEG-lipids containing single chains. Regarding the degree of unsaturation, it was observed that unsaturated fatty acids on the cell surface are more stable than saturated fatty acids with the same alkyl chain length (Itagaki et al., 2015). This highlights that long-lasting cell surface engineering is still a significant challenge. Other factors contributing to the lifespan of surface engineered cells include: the dynamic nature of the plasma membrane by continuous lipid and protein internalization and degradation to be later resynthesized by *de novo* synthesis (Stephan and Irvine, 2011). Also, when pancreatic β cells are exposed to increasing concentrations of palmitic acid, these lipids are incorporated in the plasma membrane, and this triggers the activation of cell functions and various biosynthesis routes such as for ceramide, phospholipid, sphingolipid synthesis (Maulucci et al., 2016).

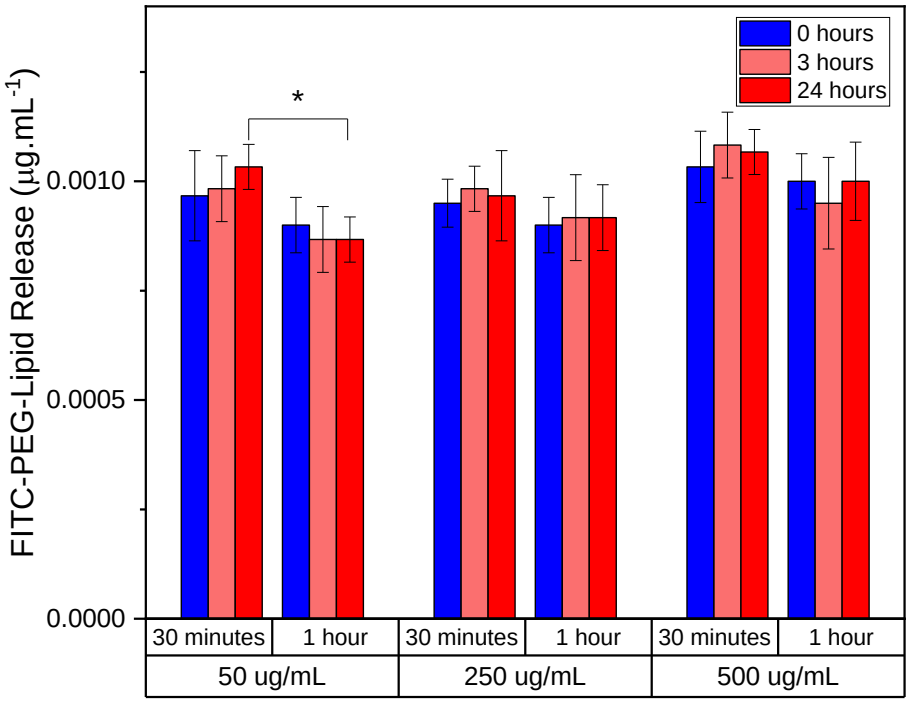

Figure 7.8. The effect of incubation time and concentration on the stability of FITC-tagged Mal-PEG-Lipid on the cell membrane of MIN-6 cells evaluated by the release of FITC-tagged Mal-PEG-Lipid to cell medium. Statistical analysis was performed using ANOVA followed by post-hoc Tukey's HSD test where p-value < 0.05 shows statistical difference (*).

When analysing the fluorescence intensity of MIN-6 cells after incubation with FITC-tagged Mal-PEG-Lipid at 50, 250 and 500 µg.mL^{-1} for 30 minutes and 1 hour (Figure 7.9). It can be seen that immediately after incubation of FITC-tagged Mal-PEG-Lipid, the higher the concentration of FITC-tagged Mal-PEG-Lipid used, the higher is the cellular uptake shown by the higher fluorescence intensity. When the time of incubation is compared, increasing the incubation period from 30 minutes to 1 hour shows that fluorescence intensity also increases related to higher cellular uptake. The practical significance of these results leads to the surface engineering optimization of the plasma membrane of MIN-6 cells, where a balance between concentration and incubation time (500 µg.mL^{-1} for 30 minutes) demonstrates high cell surface uptake, minimal surface damage, and higher stability. This is particularly important for the L-b-L and conformal coatings, where the Mal-PEG-Lipids serve as anchorage-sites to a variety of molecules

as the maleimide moiety reacts with primary amines and thiol groups to create stable conjugates. This approach will be further discussed in the next chapter.

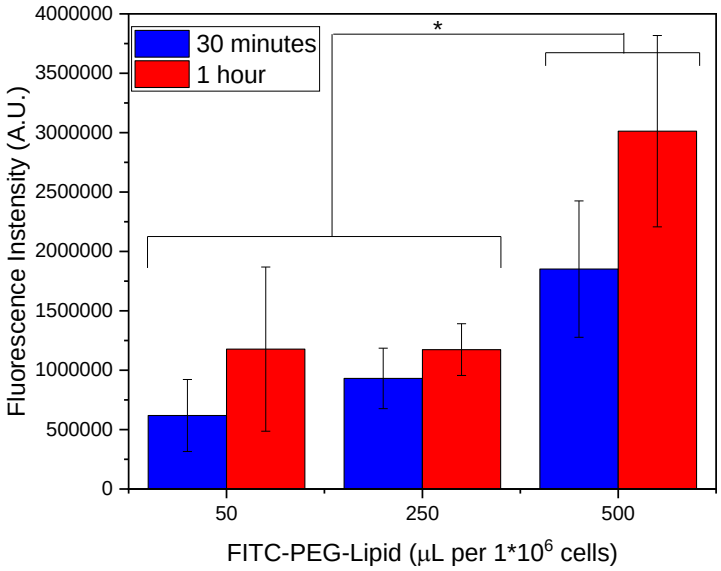

Figure 7.9. Fluorescence intensity of MIN-6 cells after incubation with FITC-tagged Mal-PEG-Lipid at 50, 250 and 500 µg.mL^{-1} per 1x10^{6} cells for 30 minutes and 1 hour. Statistical analysis was performed using ANOVA followed by post-hoc Tukey's HSD test where p-value < 0.05 shows statistical difference between groups (*).

7.4. Final Considerations

The surface modification of single cells was successfully performed through the insertion Mal-PEG-Lipid into the plasma membrane of MIN-6 cells. The results showed that Mal-PEG-Lipid did not induce cell toxicity. Moreover, little plasma membrane disruption was observed by the Annexin V assay. The stability of the Mal-PEG-Lipid also showed that two chains of palmitoyl fatty acids attached to Mal-PEG-NHS improved the molecule insertion to the plasma membrane where release of the molecule from the cell surface to the medium was not observed. For future work, the optimal Mal-PEG-Lipid concentration and incubation time for surface engineering was selected as 500 $\mu g.mL^{-1}$ for 30 minutes. Overall, surface engineering the plasma membrane of cells with Mal-PEG-Lipids can provide anchorage-sites to a variety of molecules that contain primary amines and thiol groups into their structure, as maleimide moiety reacts with these groups to create stable conjugates. This is particularly interesting for the development of L-b-L coatings, which will be further discussed in chapter 8.

Chapter 8: *In Vitro* Conformal Multilayer Encapsulation of Pancreatic β Cells

The contents of the following chapter are being reformatted to be submitted as an original research article in the journal Biomaterials.

Authors: Fernanda Zamboni and Maurice N. Collins

Abstract

In the previous chapter, it has been shown that the plasma membrane of pancreatic β cells can be engineered using Mal-PEG-Lipid at a concentration of 500 μg.mL^{-1} for 30 minutes. Earlier it has also been shown that HA with 0.1 and 1.2 MDa molecular weights can be modified to produce derivates carrying free thiol (HA-SH) and pyridine groups (HA-PD). Here, cell encapsulation is carried out by the successive deposition of HA-SH and HA-PD derivates onto the surface of the modified pancreatic β cells, where Mal-PEG-Lipid serves as an anchorage site in the plasma membrane for the HA layers as described in the previous chapter. Each HA layer is crosslinked with the next layer via a bimolecular nucleophilic substitution (S_N2) reaction until forming a 2, 6, and 10-layered coatings. The inner layers of the coating contained LMW HA derivates with higher degrees of substitution to produce membranes with smaller mesh sizes, while the outer layers used HMW HA derivates to induce anti-inflammatory responses. *In vitro* characterization of the cell encapsulation coating was assessed regarding stability, cytocompatibility, glucose challenge and insulin release. Results showed cell encapsulation does not hamper pancreatic β cell viability. Moreover, results show that the 10-layered cell coating is permeable to the diffusion of glucose and insulin, where cells were able to release insulin in response to glucose concentration variations. In conclusion, this novel multi-layered HA coating has shown suitability for the encapsulation of pancreatic β cells providing an appropriate environment for cell function and protection from mediated-immune cell attack.

Keywords: Surface Engineering, Cell Encapsulation, Layer-by-Layer, Hyaluronic Acid

Graphical Abstract

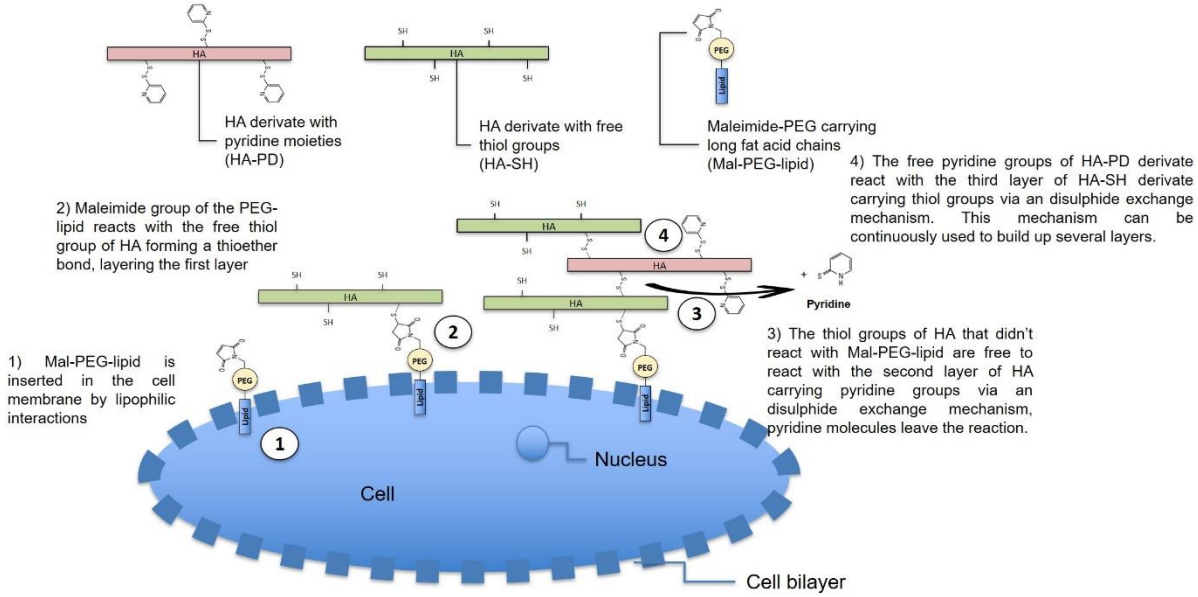

8.1. Introduction

Together with surface engineering, pancreatic β cell encapsulation is a promising strategy to improve graft survival and decrease alloreactivity and xenoreactivity after transplantation (Knopf-Marques et al., 2016). Pancreatic β cells, such as MIN-6 cells, have been encapsulated in a variety of encapsulation methods using many biomaterials including natural polymers (alginate, chitosan, agarose, collagen) and synthetic polymers (PEG and PVA) (de Vos et al., 2014, Iacovacci et al., 2016).

However, little research has been conducted in the encapsulation of pancreatic MIN-6 cells using HA. For example, MIN-6 cells have been encapsulated by a droplet-generating microfluidic device using various combinations of dextran-tyramine gels, one of which included HA in its composition (Kamperman et al., 2017a, Kamperman et al., 2017b). In another study, MIN-6 cells were encapsulated in alginate microgels, which were embedded within a HA matrix for the development of a responsive microneedle system for the physiological delivery of insulin (Gu and Ye, 2019). HA was also used to develop a synthetic insulin-secreting cell with glucose responsive nano particles containing insulin. The biocompatibility study for these synthetic cells were performed using MIN-6 cells, showing no toxicity of HA microgels in all concentrations used (Di et al., 2015). Pseudo islets from MIN-6 cells were PEGylated and embedded within a gel containing HA and other ECM components for increased vascularization (Marchioli et al., 2017).

Nonetheless, to achieve long-lasting immunoisolating coatings, HA structural stability needs to be improved through chemical modifications. These chemical modifications include the utilization of numerous crosslinking methods, such as, chemical crosslinking by covalent bonds, physical crosslinking by non-covalent interactions or crosslinked by a combination of both (Buwalda et al., 2014, Collins and Birkinshaw, 2008b). In this landscape, thiolation of HA can confer moieties that can be crosslinked under physiological conditions, with proper gelation kinetics and absence of toxic by-products (Xu et al., 2012). This becomes more critical to cells with low proliferation capacities, such as pancreatic islets and β cells (Drews et al., 2010). While, it has been shown in Chapter **5** that, the thiol groups of HA derivates can be oxidized to form disulphide bonds by a disulphide exchange mechanism. This mechanism allows the sequential deposition of several ultra-thin polymeric layers on the surface of pancreatic β cells and islets (Teramura et al., 2007).

Herein, HA derivates carrying free thiol (HA-SH) and pyridine groups (HA-PD) are developed aiming to create multiple nano coatings for cell encapsulation of MIN-6 cells. The successive deposition of HA-SH and HA-PD derivates is possible due to prior surface engineering of MIN-6 cells utilizing Mal-PEG-Lipids. These Mal-PEG-Lipids serve as anchorage sites on the plasma membrane for the HA layers.

8.2. Materials and Methods

8.2.1. Materials

HA, with an average molecular weight (MW) of 1.20 MDa and 0.1 MDa, was kindly supplied by Shanghai Easier Industrial Development Co. LTD. (Shanghai, China) as dry powder. Mal-PEG-NHS, DPPE, 2,2'-dithiodipyridine, DTT, lactate dehydrogenase (LDH), 3-aminopropyltriethoxysilane (APTES), D_2O and human serum (from male AB plasma, USA origin) were purchased from Sigma Aldrich (St. Louis, MO, USA). Rat/mouse insulin ELISA kit was purchased from EDM Millipore Corporation (Billerica, MA, USA). Annexin V-Alexa Fluor 568 was purchased from BD Life sciences (Berkshire, England, UK). All other consumables necessary for cell culture including cell culture medium, pipettes, flasks and plates were purchased from Thermofisher. Pancreatic MIN-6 cells were kindly donated by Dr. Joaquim Miguel Oliveira from the I3Bs Research Group at the University of Minho, Portugal.

8.2.2. Production of Mal-PEG-Lipids

Mal-PEG-NHS 50 mg is dissolved in chloroform together with 5 mg of DPPE to react under stirring for 24 hours at room temperature. While the Mal-PEG-Lipid product is purified by precipitation in diethyl ether.

8.2.3. Production of HA Derivates

As previously described in Chapter 5, HA is first crosslinked using BIED, where the hydroxyl groups of the N-acetylglucosamine moiety of HA are targeted by the isocyanate to form urethane linkages. HA (0.1 MDa and 1.2 MDa) was dissolved in DMSO for a final concentration of 70 $mg.mL^{-1}$ and reacted with BIED (49.3 $mg.mL^{-1}$). HCl 1M was used to adjust the pH to 4. The crosslinking reaction proceeds upon stirring. Then, the disulphide bond of these gels is reduced using DTT to form HA derivates bearing free thiol groups (HA-SH).

HA-pyridine derivate (HA-PD) was produced from the reaction of HA-SH derivates with 2,2'-dithiodipyridine. Briefly, 2,2'-dithiodipyridine (20mg) is added to HA-SH (0.1 and 1.2 MDa) dissolved in methanol. The solutions are stirred for 12 hours at 4°C under nitrogen atmosphere to produce HA-PD. Then they are dialysed against PBS 1X for 3 days at room temperature where PBS is changed every day. HA-PD was freeze dried to obtain a lyophilized powder. Briefly, the dialysed sample was placed in a shelf freeze

dryer (AdVantage BenchTop Freeze Dryer by Virtis, USA) and let to freeze at -40°C overnight before drying. Drying was conducted in four temperature stages. The temperature was held at -20°C for 6 hours under vacuum (200 mTorr), then the temperature was increased to -10°C for 1.5 hours, following another temperature increase to 5°C for 2 hours. This finally reached 25°C, after which HA-PD was obtained as a white powder. HA-PD was then stored under nitrogen in the freezer at -20°C.

Chemical characterization of HA derivates was performed using FT-IR spectroscopy. All spectra were recorded on a Perkin Elmer spectrum 100 FT-IR spectrometer operating in Attenuated Total Reflectance (ATR) mode. Each FT-IR spectrum was scanned twenty times with a resolution of 2 cm^{-1}. The ranges used were from 4000 cm^{-1} to 650 cm^{-1}.

8.2.4. MIN-6 Culture

MIN-6 cells ($1x10^7$ cells) between 30-40 passages, were cultured in T75 flasks using high glucose DMEM, supplemented with 10% FBS, 1 % antibiotic/antimycotic, 10 mM sodium pyruvate and 50 µM β-mercaptoethanol. Cell media was replenished every 3 days until cell confluency was reached.

8.2.5. Conformal Cell Coating

MIN-6 cells at a density of $1x10^6.mL^{-1}$ were incubated with Mal-PEG-Lipid at 500 $\mu g.mL^{-1}$ for 30 minutes. After cells were centrifuged at 1,000 RPM and washed with PBS 1X, and the supernatant was removed. Cells were incubated in solutions containing 1.8 $mg.mL^{-1}$ of different HA derivates in DMEM. The first conformal layer was deposited onto the surface of the cells by incubating HA-SH 0.1 MDa for 10 minutes. After, cells were centrifuged and washed with PBS 1X they were incubated with HA-PD 1.2 MDa for 10 minutes. This first cycle produces the first bilayer. For the second bilayer, cells were incubated with HA-SH 0.1 MDa for 10 minutes. After, cells were centrifuged and washed with PBS 1X as before and they were incubated with HA-PD 1.2 MDa for 10 minutes. For the third bilayer, cells were incubated with HA-SH 1.2 MDa for 10 minutes. After, cells were centrifuged and washed with PBS 1X and incubated with HA-PD 1.2 MDa for 10 minutes. For the fourth and fifth bilayers, cells were incubated with HA-SH 1.2 MDa for 10 minutes. After, cells were centrifuged and washed with PBS 1X and incubated with HA-PD 1.2 MDa for 10 minutes. After cell encapsulation, cell viability was assessed using trypan blue.

8.2.6. Multilayer Contact Angle and Stiffness Measurements

Glass slides were carefully cleaned with detergent (5% by volume), flushed thoroughly and ultrasonicated in distilled water for 10 minutes. Then, the slides had their surface etched using freshly prepared piranha solution (37% H_2SO_4 + 30% H_2O_2 + distilled water) (1:1:5 by volume) for 3 minutes. Glass slides were rinsed with distilled water and immersed in a freshly prepared solution of 37% HCl, 30% H_2O_2 and distilled water (1:1:5 by volume) for 5 minutes for the oxidation of the surface. Subsequently, the slides were washed thoroughly with distilled water, ethanol and acetone, one after another. After the glass slides were dried in an oven at 110°C for 1 hour, they were immediately modified by immersion in a 5% APTES solution in anhydrous toluene for 5 minutes. After several rinsing washes with toluene and acetone, the modified glass slides were dried in an oven at 110°C for 1 hour. Mal-PEG-NHS and HA multi-layer coating deposition on the surface of silanization-treated glass slides follows the protocol described previously in section 7.2.9. Briefly, NH_2-bearing glass slides were dipped in a solution of Mal-PEG-NHS (500 $\mu g.mL^{-1}$) for 30 minutes. NHS reacts with primary amines to form a stable thioester bond. After three cycles of washes in distilled water, glass slides were dipped in solutions containing 1.8 $mg.mL^{-1}$ of different HA derivates in distilled water for 10 minutes to create coatings of 1, 3 and 5 bilayers.

KSV contact angle test apparatus together with CAM software were used to calculate the contact angles of 1µL droplets of water in the surface of unmodified and modified glass slides prior to Mal-PEG-NHS and HA multi-layer coating deposition. 8 measurements were performed per sample. Stiffness of the different coatings was measured using a Thorlabs EDU-AFM1/M atomic force microscope (New Jersey, USA). The measurements were performed using monolithic silicon AFM probe with aluminum reflective coating (ContAl-G, Budgetsensors), at room temperature and ambient pressure. Force of adhesion was calculated as follows:

$$Fad = K * Cp * \Delta zp$$

Where K is the cantilever spring constant (0.2 $N.m^{-1}$), Cp is a factor ($0.26*10^{-6}$ $m.V^{-1}$), and Δzp is the deflection of the cantilever from snap-in to pull-off point.

8.2.7. *In Vitro* Cell Encapsulation Protection Against Cytokine-Mediated Cytotoxicity

Human blood serum and heat inactivated blood serum (56°C for 30 minutes) were diluted at a ratio of 1:4 in FBS-free DMEM. Diluted serums were incubated with MIN-6 naked cells (control), surface engineered cells (Mal-PEG-Lipid only), and encapsulated cells (1 bilayer, 3 bilayers and 5 bilayers) for 24 hours at 37°C. After incubation, encapsulated cells were washed thrice with PBS 1X. Encapsulated MIN-6 cells were assessed for viability. Supernatant was assessed for LDH activity. The percentage of LDH released from encapsulated MIN-6 cells to the culture medium was calculated as described by the manufacturer.

8.2.8. Glucose Challenge and Insulin Release

Surface modified and encapsulated MIN-6 cells were exposed to static glucose stimulation at specified time points. Cells were placed in a low glucose concentration medium (2.5 mM) for 40 minutes followed by incubation in a high glucose concentration medium (25 mM) for 40 minutes. Cells in high glucose media were tested for insulin release profile by using a mouse insulin ELISA kit as described by the manufacturer. Briefly, an anti-mouse insulin pre-coated 96-well plate was incubated with the experimental samples and standard insulin solutions for 2.5 hour at RT. Next, the plate was washed four times with washing buffer and the biotin-conjugated monoclonal anti-insulin antibody was added to each well (1:80 dilution) and incubated for an additional 1 hour at 37°C. After four wash cycles, horseradish peroxidase-conjugated streptavidin (1:400 dilution) was added to the wells and incubated for 45 minutes at RT. After four washes, bound antibody complexes were developed with TMB substrate for 15 minutes at RT and were protected from light. Absorbance was measured at 450 and 550 nm using a SynergyMx plate reader (BioTek, EUA).

8.2.9. Statistical Analysis

Data are presented as mean ± standard deviation (S.D.) and analysed using one-way analysis of variance (ANOVA) followed by post-hoc Tukey's HSD test. P-values < 0.05 (*) were considered significant.

8.3. Results and Discussion

8.3.1. Production of HA Derivates

HA derivates carrying free thiol (HA-SH) were developed from the reduction of disulphide bonds of BIED-crosslinked HA gels, shown in chapter 5 (Figure 5.10). HA-bearing pyridine groups (HA-PD) on the other hand, were developed from the reaction of HA-SH derivates with dithiodipyridine, as shown in Figure 8.1. The confirmatory chemical characterization of the HA derivates was performed using FT-IR analysis. Figure 8.2 shows that HA-PD presents the characteristic C=C and C=N bands of pyridine at around 1750 cm^{-1} and 1550 cm^{-1}, respectively.

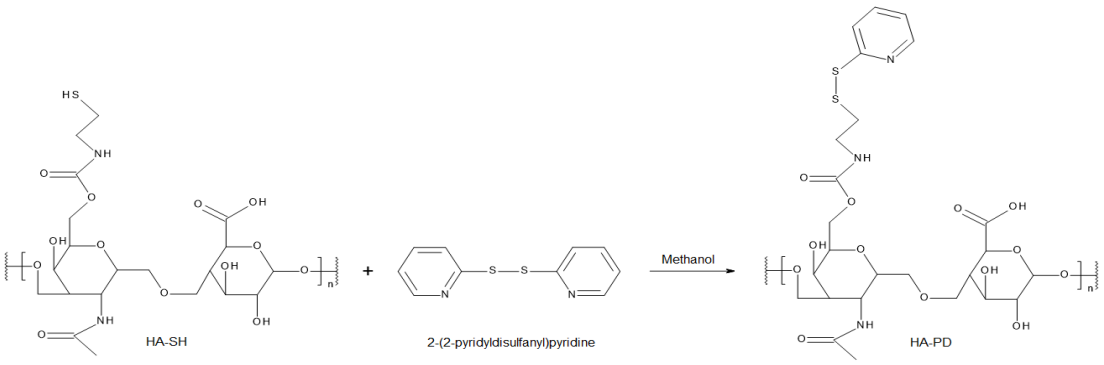

Figure 8.1. Formation of HA-PD derivates via disulphide exchange mechanism.

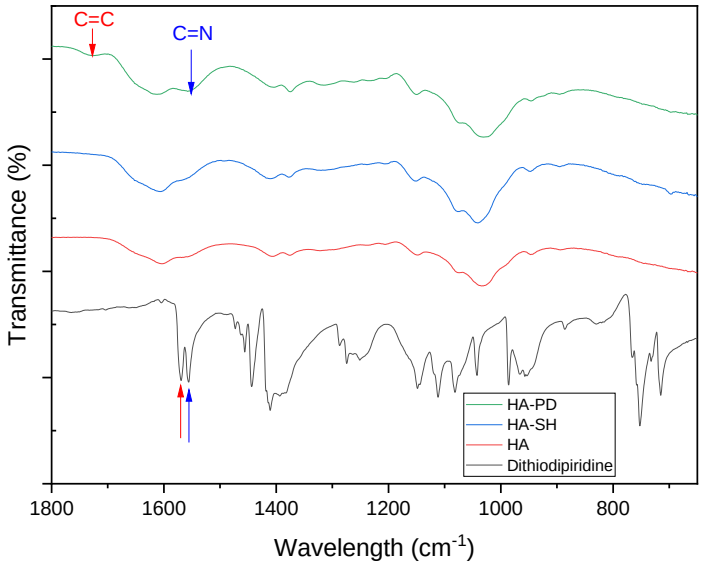

Figure 8.2. FT-IR spectra of pure HA, dithiodipyridine, and HA derivates containing thiol and pyridine moieties (HA-SH and HA-PD, respectively).

8.3.2. Multilayer Conformal Coating

Prior to the successive deposition of HA-SH and HA-PD derivates, the plasma membrane of MIN-6 cells was engineered utilizing Mal-PEG-Lipids. The maleimide group of the Mal-PEG-Lipid is located outside the plasma membrane, and it is free to react with the thiol groups of HA-SH derivate. This reaction forms a thioether bond and adheres the first HA layer (Figure 8.3). For the implementation of the second HA layer, pyridine groups of HA-PD derivate react with the remaining free thiol groups of HA-SH derivate that did not react with Mal-PEG-Lipid in the first layer. This reaction occurs via a disulphide exchange mechanism that utilizes a bimolecular nucleophilic substitution (S_N2) reaction that allows the formation of crosslinks between the HA-SH and HA-PD in physiological conditions (aqueous medium and neutral pH) (Fernandes and Ramos, 2004). The two HA chains connect with each other through the formation of a disulphide bridge, where pyridine molecules leave the reaction. This mechanism can be continuously used to build up several layers.

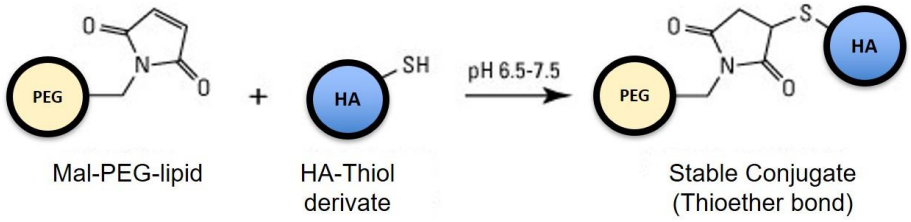

Figure 8.3. Maleimide reaction with free thiol groups of HA-SH derivate forming stable thioether bonds.

8.3.3. Characterization of Multilayer Conformal Coatings

Conformal coating techniques are based on the interfacial polymerization of biomaterials to form a thin (< 500 nm) and crosslinked coating network on the surface of islets and β cells (Zhi et al., 2013). This cyclic stepwise deposition method can tailor the final number of layers and coating thickness, thus, dictating the permeability and robustness of the coating (Silva et al., 2016a). Due to the nanometric size of the coatings, direct assessment of contact angle, thickness, and stiffness is difficult to obtain from encapsulated cells. In this regard, the stepwise deposition of multiple layers mimicking the cell encapsulation was performed using pre-treated silanized glass slides (Figure 8.4a). Silanization of glass is performed to modify the surface of glass slices by the introduction of primary amines. APTES covalently binds to the surface of glass slides creating a silane bond. The

introduction of the primary amine to glass slides can be further exploited for conjugation with Mal-PEG-NHS. NHS reacts with primary amines to create stable amide bonds. The sequential deposition of HA layers via disulphide exchange mechanism is performed as usual on the surface of Mal-PEG-glass slides.

Silanization of glass slides is an efficient way to insert amine moieties on the surface of the glass slides, this technique has been extensively described in the literature for a variety of applications that include immobilization and detection of IgG antigens, DNA microarrays, etc (Huan et al., 2017, Phaner-Goutorbe et al., 2011).

Contact angles measurements of untreated, pre-treated silanized glass slides, Mal-PEG-coated glass slides, and HA coated glass slides with different number of layers (1 bilayer, 3 bilayers and 10 bilayers) are shown in Figure 8.4b. The contact angle of glass slides significantly increased after silanization, making the glass slide more hydrophobic. This confirms successful silanization treatment of glass slides (Huan et al., 2017). Moreover, the sequential deposition of HA on the surface of treated glass slides greatly decreased contact angle in comparison to Mal-PEG-NHS coating. Coating the glass slides with either 1, 3 and 5 bilayers of HA returned the hydrophilicity of the glass slide to those of untreated values.

A)

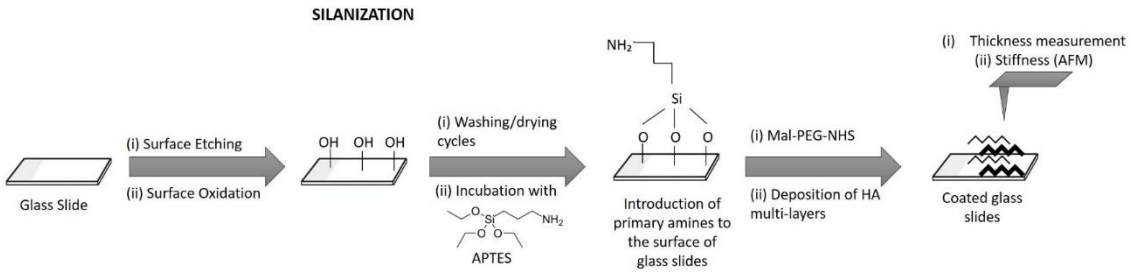
SILANIZATION
Glass Slide
(i) Surface Etching
(ii) Surface Oxidation
OH OH OH
(i) Washing/drying cycles
(ii) Incubation with
APTES
NH2
Si
O O O
Introduction of primary amines to the surface of glass slides
(i) Mal-PEG-NHS
(ii) Deposition of HA multi-layers
(i) Thickness measurement
(ii) Stiffness (AFM)
Coated glass slides

B)

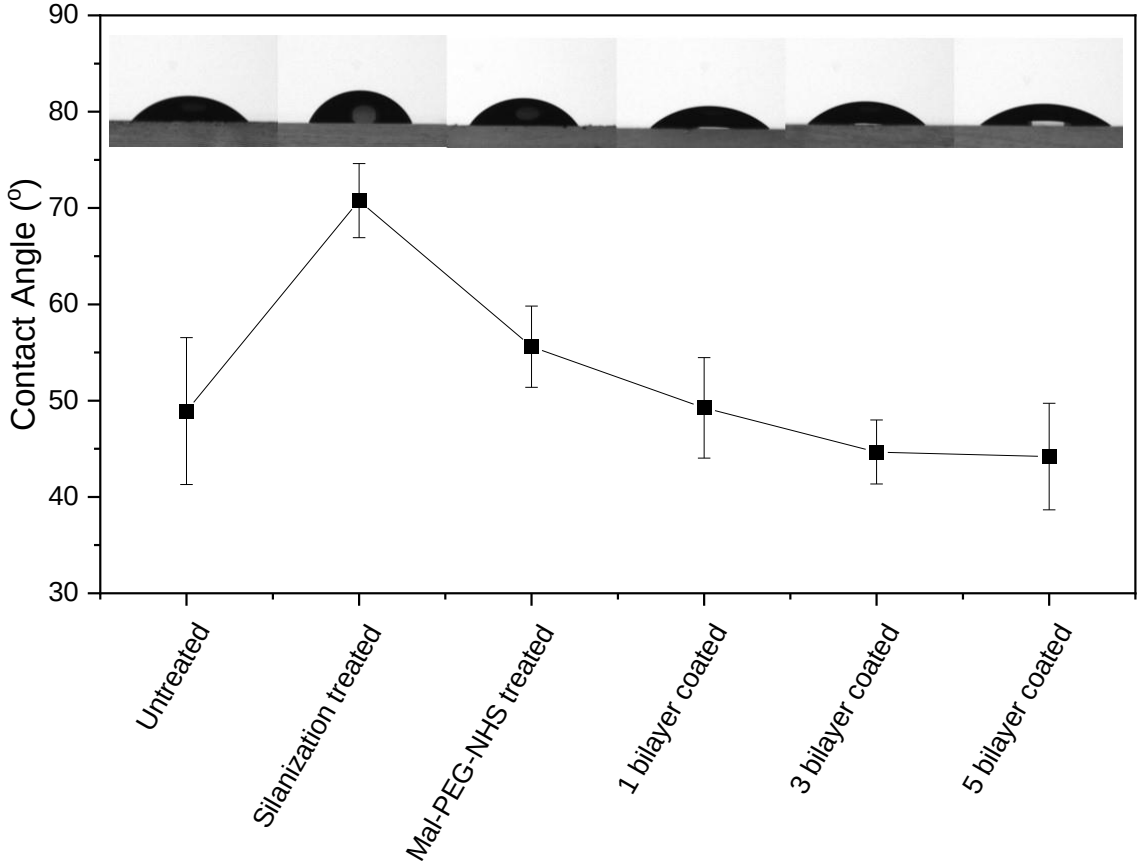
Contact Angle (°)
90
80
70
60
50
40
30
Untreated
Silanization treated
Mal-PEG-NHS treated
1 bilayer coated
3 bilayer coated
5 bilayer coated

C)

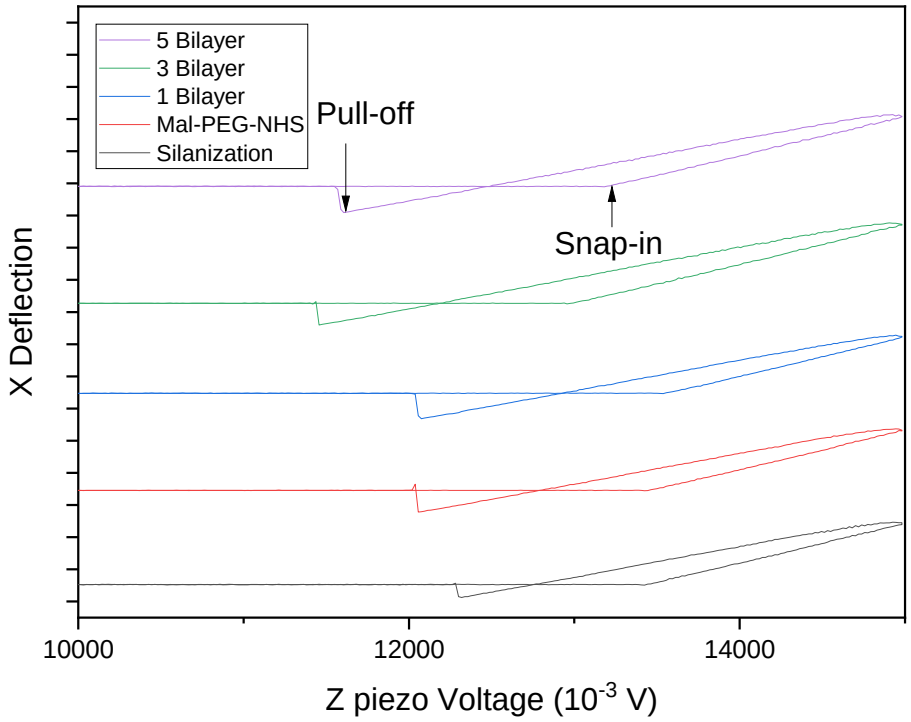

Figure 8.4 a) Surface modification of glass slides through silanization. NH_2-bearing glass slides react with Mal-PEG-NHS for the deposition of multi-layers of HA to mimic cell encapsulation. Contact angle (b) and Force-Distance Curves (c) of treated glass slides mimicking multilayer conformal cell coating protocol.

The sequential deposition of multiple coatings on the surface of pre-treated glass slides enabled the analysis of different coatings via AFM. In Figure 8.4c, the force-distance curves of the coatings were recorded and the points of interest for the calculation of stiffness measurements are highlighted as the snap-in and pull-off points. In Table 8.1, the calculated force of adhesion for the different coatings are shown. All coatings show significantly higher force of adhesion when compared to uncoated glass slides (pre-treated silanized glass slides).

Table 8.1. Force of adhesion measurements obtained from AFM Force-Distance curves.

Surface Treatment	Force of Adhesion (nN)
Silanization-treated Glass	62 ± 0.86

Mal-PEG-NHS coated Glass	75 ± 3.05
1 Bilayer-coated Glass	76 ± 4.44
3 Bilayer-coated Glass	73 ± 7.95
5 Bilayer-coated Glass	77 ± 7.84

± S.D.

8.3.4. *In vitro* Multilayer Conformal Cell Encapsulation

Differing molecular weights of HA were used to build the coatings of MIN-6 cells. In Chapter 5, it was demonstrated that LMW HA (0.1 MDa) gels have higher degrees of modification 594.3 $\mu M.mg^{-1}$ (± 198) of HA as opposed to HMW HA 166.15 $\mu M.mg^{-1}$ (± 14.04). This in turn produces gels with lower mesh size and higher mechanical moduli (Zamboni et al., 2020). However, LMW HA when degraded produce pro-inflammatory cues that are detrimental to transplants (Jiang et al., 2011).

With this rational in mind, cells were encapsulated in two, three or five HA bilayers. The deposition of the coatings was designed to have the inner layers containing LMW HA and outer layers containing HMW HA (Figure 8.5). The inner layer inherent purpose is to produce smaller mesh sizes which contributes to block inflammatory cell recognition and cytokine infiltration through the coating, while the outer layers containing HMW HA induce anti-inflammatory responses, a perfect match to protect the cellular graft and decrease graft rejection upon transplantation.

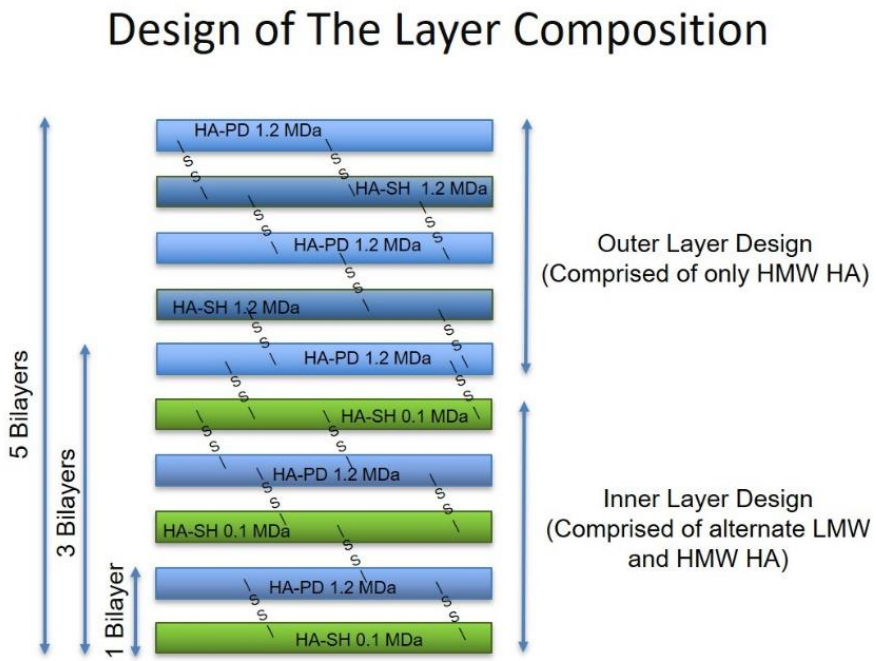

Figure 8.5. Composition design of the encapsulation coating layers.

In order to analyse the viability of cells after encapsulation, trypan blue cell count was performed (shown in Figure 8.6). The decrease in viability after the cell encapsulation is significant for all three groups (1, 3 and 5 bilayers) in comparison to the control group. However, the decrease of viability is still acceptable, and it is above 80%.

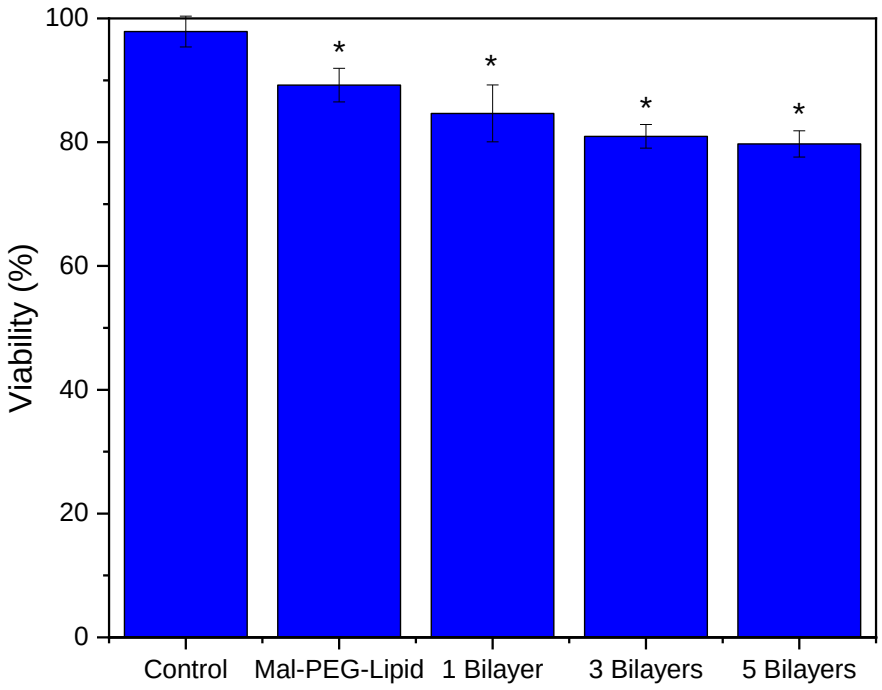

Figure 8.6. Viability of MIN-6 cells after surface modification using 500 µg.mL^{-1} Mal-PEG-Lipids for 30 minutes, and cell encapsulation using 1, 3 and 5 bilayers of HA. Statistical analysis was performed using ANOVA followed by post-hoc Tukey's HSD test where p-value < 0.05 shows statistical difference between groups (*) and control.

The functionality of the encapsulated cells was examined in terms of their ability to diffuse glucose through the coating and secrete insulin accordingly. As shown in figure 8.7, the static low glucose stimulation of encapsulated cells and control cells (naked cells) at day 1, day 7 and day 14 after encapsulation resulted in similar insulin secretion (not significant change). However, very distinct insulin secretion patterns are observed for high glucose challenge. On day 1 after encapsulation, all groups show similar insulin secretion, with the exception of the HA 5 bilayers group, which shows significant smaller insulin secretion content than the other groups. However, on day 7 after transplantation, the encapsulated cell group containing 5 bilayers shows spike in insulin secretion in comparison to the other groups. By day 14 after transplantation, the insulin secretion of all encapsulated groups is significantly lower than the control group.

There are two main reasons for immortal cell lines to lose the ability to secrete insulin. Sudden loss of glucose-induced insulin secretion can occur following several passages.

MIN-6 cells at low passage (between 30-40) present optimal insulin response, in contrary to high passage cells (between passage 60-70). High passage MIN-6 cells lose their ability to secrete insulin possibly due to an outgrowth of cells with a poor response to glucose and decrease in gene expression of *Sirt3* and *Nampt.* These metabolic changes contribute to decreased glucose and lipid oxidation (Cheng et al., 2012b). Functional loss, measured by glucose-stimulated insulin secretion, can also be correlated with decreased cell-cell interactions (Giraldo et al., 2010).

The higher insulin secretion content of the control group is sought to be a consequence of β cell aggregation. It is well known that MIN-6 cells attach to the well only a few hours after cell seeding. During culture, these cells have a different spreading profile than other adherent cell types (i.e. fibroblasts). MIN-6 cells will aggregate in clusters mimicking the formation of islets. The cell-cell interaction within these cell clusters boost insulin release by these cells at day 14, in contrary to encapsulated cells which maintain a single cell structure.

A)

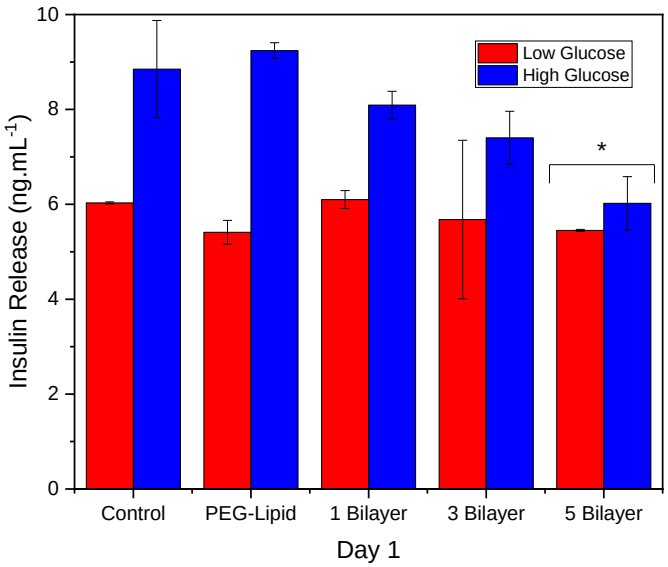

B)

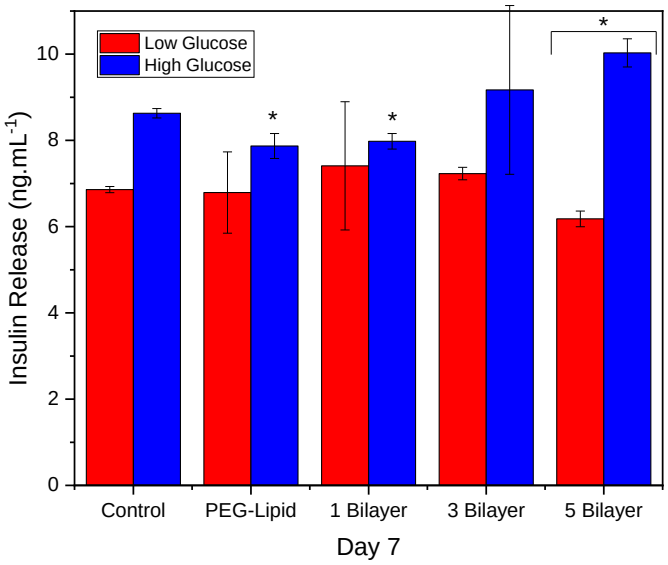

C)

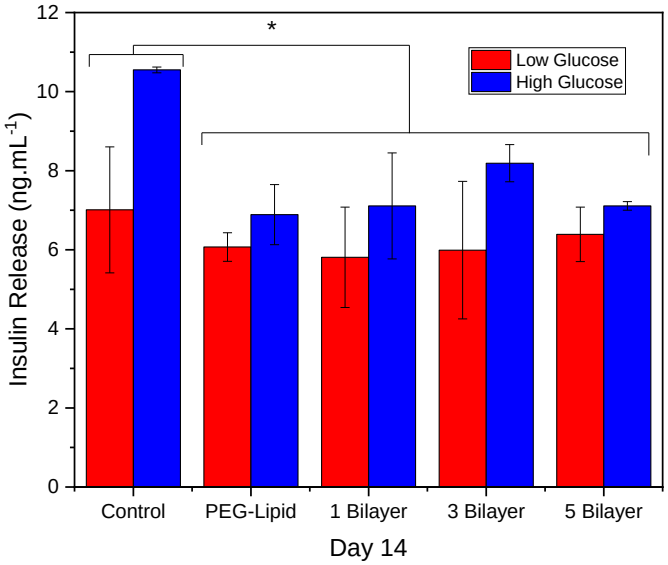

Figure 8.7. Glucose stimulated insulin release from MIN-6 cells encapsulated using 500 μg.mL^{-1} Mal-PEG-Lipids for 30 minutes, 1, 3 and 5 bilayers of HA at day 1 (a), day 7 (b) and day 14 (c) after encapsulation. Statistical analysis was performed using ANOVA followed by post-hoc Tukey's HSD test where p-value < 0.05 shows statistical difference between groups (*) and control.

The immunoisolation of pancreatic β cells requires a biocompatible semi-permeable membrane encapsulating cells to protect them from direct contact with the host's immune

system. As discussed in previous chapters, direct immune cell recognition of allogenic and xenogeneic cellular grafts can lead to transplant rejection. Moreover, small biological molecules such as antibodies, cytokines and chemokines can also induce graft failure by cellular death. However, studies have shown that membrane barriers for IgG are enough to prevent graft rejection in transplants. This indicates that blocking cytokines and chemokines may not be a requirement for immunosuppression in allotransplantation (Steele et al., 2014).

In this regard, the different cell coatings developed in this project were examined to test their ability to protect MIN-6 cells against cytokine-mediated cytotoxicity. Encapsulated cells were incubated with human blood serum (mismatched species to induce xenogeneic recognition) and cellular death was quantified by the release of the intracellular enzyme, lactate dehydrogenase, to the cell medium. As shown in Figure 8.8, cytokine-mediated cytotoxicity was observed in all groups incubated with complete serum in comparison to heat-inactivated human serum. However, at day 7 and day 14 post-encapsulation, the 5-bilayered encapsulation coating was the only group able to significantly reduce cell death, proportional to a decrease of LDH content in the medium, in comparison to the control group. This finding corroborates the significance of encapsulating pancreatic β cells in multi-layered nano-coatings. As expected, the higher the number of layers in a coating, the higher is the protection against the components of the immune system.

A)

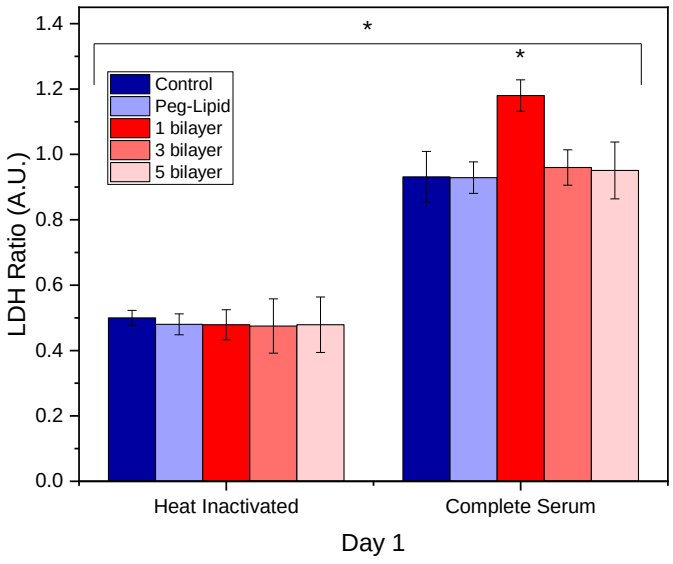

B)

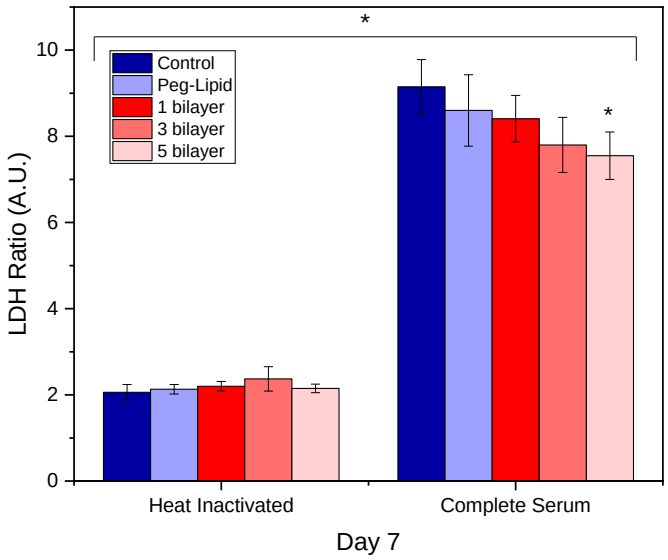

C)

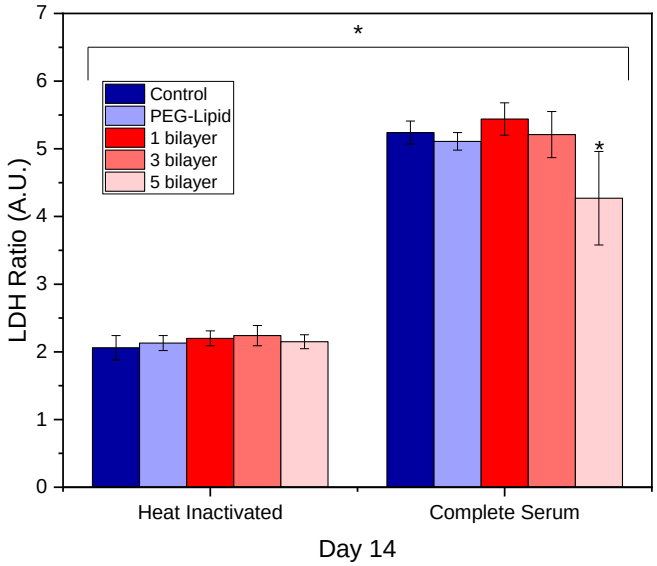

Figure 8.8. Viability of MIN-6 cells was assessed after exposure to heated inactivated and complete human serum at day 1 (a), day 7 (b) and day 14 (c) after encapsulation using LDH activity assay. Statistical analysis was performed using ANOVA followed by post-hoc Tukey's HSD test where p-value < 0.05 shows statistical difference (*).

8.3. Final Considerations

HA derivates carrying free thiol (HA-SH) and pyridine groups (HA-PD) were successfully developed from the reduction of disulphide bonds of BIED-crosslinked HA gels. Prior to the successive deposition of HA-SH and HA-PD derivates, the plasma membrane of MIN-6 cells was engineered utilizing Mal-PEG-Lipids. Lipids are inserted in the plasma membrane of MIN-6 cells while the hydrophilic Mal-PEG portion of the molecule serve as anchorage sites for the HA layers. Maleimide reacts with the thiol group of HA-SH derivates and create a stable thioether bond. The next layer of HA-PD is deposited on the surface of MIN-6 cells and reacts with the remaining free thiol groups of HA-SH through disulphide exchange mechanism. The successive deposition of HA-SH and HA-PD creates multiple nano coatings for cell encapsulation of MIN-6 cells.

As observed from the results shown in this chapter, the 1-layered, 3-layered and 5-layered coatings have acceptable cell viability decrease following single cell encapsulation. Moreover, insulin secretion in response to glucose stimulation in all three coatings are similar to the control group at day 7 after encapsulation. A decrease of insulin secretion is observed for cells encapsulated within 5-layered coatings at day 14 after encapsulation, however an increase in cell protection is observed against cytokine-mediated cytotoxicity from cells encapsulated within 5-layered coatings.

Overall, the cell encapsulation of MIN-6 cells through disulphide exchange mechanism of HA-SH and HA-PD derivates enables a novel safe encapsulation method that can be tailored regarding HA MW and number of coatings. The balance between the structure:function properties of these coatings suggests that improved immunoisolation is achieved through a minimum of 5 bilayers, but the insulin secretion might be delayed due to the increased thickness of the coatings. This is especially true to single-cell encapsulation. Further studies should be carried out to assess the appropriate structure:function properties of these coatings if encapsulating pancreatic islets or pseudo islet aggregates.

In the next chapter, the *in vivo* evaluation of the functionality and graft survival of MIN-6 cells encapsulated within a 5-bilayered coating through the transplantation in the renal capsule of female diabetic mice will be discussed.

Chapter 9: Hyaluronic Acid-Encapsulated MIN-6 Cells Transplanted in the Kidney of STZ-induced Diabetic Female Mice

The contents of the following chapter are being reformatted to be submitted as an original research article in the journal Biomaterials.

Authors: Fernanda Zamboni, Ibrahim Fatih Cengiz, Gil Castro, Rui L. Reis, Joaquim Miguel Oliveira, Maurice N. Collins

Abstract

Female mice (Black 6 strain) (C57BL/6) aged 6 weeks were subjected to low dose streptozotocin (STZ) treatment for five consecutive days to mimic T1DM with insulitis. At two weeks, evaluation of the elevated glucose levels was used to confirm diabetes. The diabetic mice were then subject to the transplantation of pancreatic β cells (MIN-6 line). Four groups of mice were studied. The first group were injected with saline-only (SHAM group), the second and third groups were injected with MIN-6 single cells and Mal-PEG-lipid modified MIN-6 single cells (500 $\mu g.mL^{-1}$ for 30 minutes), respectively, while the fourth group were injected with HA-coated MIN-6 single cells (5 bilayers). At seven- and fourteen-days following transplantation, the mice were euthanized. The renal and pancreatic tissues were then collected and histologically analysed. The induction of diabetes in female mice, through five daily STZ injections resulted in inconsistent hyperglycaemia, where 20% of mice were unable to achieve hyperglycaemia (blood glucose levels falling between 100-149 mg/dL), 32% of the mice displayed little increase in blood glucose levels (150-199 mg/dL), and 48% of the mice successfully presenting high blood glucose levels above 200 mg/dL (hyperglycaemia). Moreover, surface-modified cells and encapsulated cells were unable to revert diabetes, failing to decrease blood glucose hyperglycaemia into the physiological range. In conclusion, incomplete diabetes induction in female mice is associated with sex dimorphism and hormonal interferences. Furthermore, transplant failure of encapsulated cells may be associated with deprived cell-cell interaction, which leads decreased β cells functionality, where insulin secretion is dependent on cell-cell interaction.

Keywords: Diabetes induction, Animal model, Transplantation, Kidney capsule

Graphical Abstract

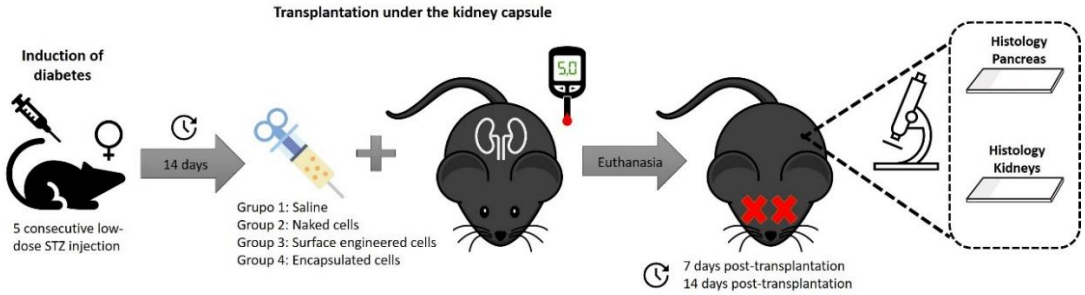

9.1. Introduction

Streptozotocin STZ is a broad-spectrum antibiotic with unique toxic selectivity for β cells in the pancreas, being used clinically for the treatment of metastatic insulinomas. STZ uptake into rodent pancreatic β cells is mediated by GLUT2 receptor. STZ is equally diabetogenic whether administered to fed or fastened mice (Chaundhry et al., 2013), showing no competition with glucose for the GLUT2 receptor.

Outside its therapeutic application, STZ has been used since early 1960's in diabetes research in order to induce hyperglycaemia in rodents via selective destruction of β cells. This effect is attributed to the nitroso moiety in STZ. Once inside the cell, this nitroso group act as a nitric oxide (NO) donor to create reactive oxygen species and induce cell death.

However, the cell death pathway greatly differs by the STZ posology adopted for the induction of hyperglycaemia in mice. When delivered by intraperitoneal injection as a single high dose (180-190 mg/kg body weight), STZ causes massive β cell necrosis within 2-3 days after administration. One moderate dose (150 mg/kg body weight) in conjunction of high fat diet can also accelerate β cell endoplasmic reticulum stress which mimics T2DM with high toxicity and mortality rate. Whereas multiple low dose of STZ mimics T1DM with insulitis and no important toxicity (Chaundhry et al., 2013).

Different doses and administration routes are used according to the rodent strain and gender. STZ response from different mouse strains shows hierarchical response as following: DBA > C57BL/6 > MRL/MP > 129/SvEv > BALB/c. Strain variability is attributed to differences in immune response. C57BL/6 immune response is Th1 dependent, while BALB/c is Th2 dependent. Islets of STZ induced C57BL/6 mouse produce INF-γ and TNF-α (Th1 type cytokine) and have reduced IL-4 and IL-10 levels (Th2 type cytokine), while opposite findings are reported for BALB/c (Cantarelli et al., 2013).

STZ protocols for diabetes induction produce a reliable T1DM animal model, specifically applied in pre-clinical research related to the transplantation of allogenic and xenogeneic pancreatic β cells. However, from the array of immortal pancreatic β cell lines available for transplantation, MIN-6 cells originated from transgenic C57BL/6 mouse insulinoma and expressing an insulin-promoter/SV40 T-antigen construct are one of the few immortal cell lines to retain glucose-stimulated insulin release (Kinoshita et al., 2001).

Herein, the administration of a low dose STZ injection for five consecutive days is selected for the induction of pancreatic β cell destruction which resembles autoimmune T1DM in female C57BL/6 mice leading to hyperglycaemia. The transplantation of single-encapsulated cellular grafts developed in the previous chapters is key to assess the *in vivo* suitability of HA conformal multi-layered nano coatings. These coatings are designed to protect pancreatic β cell from the host immune system, while maintaining cell functionality and physiological insulin secretion patterns in response to blood glucose concentrations. The ultimate aim of these cell coatings is to decrease hyperglycaemia and reverse diabetes.

9.2.Materials and Methods

9.2.1. Animals

Female mice of Black 6 strain (C57BL/6) aged 6 weeks were housed in ventilated cages of no more than 5 mice per cage and were housed with free access to food and water, at a controlled temperature of 23°C with 12 hours light-dark cycles. Mice were kept at the Life and Health Sciences Research Institute at the University of Minho, Portugal. All procedures were performed in accordance with the European Directive 86/609/EEC and approved by the University of Minho Animal Ethics Committee (SECVS 074/2016) and the Portuguese National Authority (DGAV 014072).

9.2.2. Model for Diabetes Induction

All mice were subjected to low dose STZ treatment to mimic T1DM with insulitis. An STZ solution was freshly prepared using sodium citrate pH 4.5 prior to be administered intraperitoneally (50 mg/kg of body weight) once a day for five consecutive days. At the time of the injections, mice were kept *ad libitum* fed regimen. Diabetes development was assessed by the measurement of blood glucose levels (Freestyle Precision Neo, Abbott).

9.2.3. MIN-6 Graft Transplantation

Diabetic mice were subject to the transplantation of pancreatic β cells (MIN-6 line). Four groups of mice were used. Mice injected with saline-only (SHAM group), mice injected with MIN-6 single cells, mice injected with Mal-PEG-Lipid modified MIN-6 single cells, and mice injected with HA-coated MIN-6 single cells with 5 bilayers.

Prior to the surgery, intramuscular (IM) injection (100 µl) of 90 mg/kg ketamine (Imalgen; Meriel, Lyon, France) in combination with 0.65 mg/kg of the α2 adrenergic receptor agonist medetomidine (Domitor; Pfizer, Paris, France) were used for anaesthesia and sedation, respectively. Shaving and incision under the left rib was performed. The left kidney was injected with 10 µL of saline or cell suspension preparations with cell density of 750,000 cells per mice. Mice were sutured and they were given an IM injection (50 µl) of atipanezole 1 mg/kg (Antisedant; Pfizer, Paris, France) as a sedative reversor. In post-operatory recovery, mice were kept resting under warm light.

9.2.4. Blood Glucose Control

Mice were assessed for up to 14 days post-transplantation to analyse diabetes reversion through the measurement of blood glucose levels twice a week. Blood samples were collected from pricking the cheek with a needle. The blood droplet was placed in a glucose strip and measured using a glucometer (Freestyle Precision Neo, Abbott). After follow-up, mice were sacrificed for renal and pancreas dissection and histological analysis.

9.2.5. Dissection of Renal and Pancreatic Tissues

Mice were euthanized via CO_2 inhalation at different time points. 7 days and 14 days after transplantation mice from each group (n=5) were sacrificed for the collection of renal and pancreas tissues to determine leukocytic infiltration degree. Renal and pancreatic tissues were retrieved and fixed using 4% formalin solution. Fixed kidneys and pancreas were embedded in paraffin and cut in 5 µm thick sections using a microtome.

9.2.6. Histology

Haematoxylin and eosin were used to analyse graft-localized cell infiltration and inflammation. All images were acquired using a CKX41 Olympus inverted microscope (Tokyo, Japan) equipped with a DFK 31AU03 camera (The Imaging Source Europe GmbH, Germany) and IC Capture software (The Imaging Source Europe GmbH, Germany).

9.2.7. Statistical Analysis

Data are presented as mean ± standard deviation (s.d.) and analysed using one-way analysis of variance (ANOVA) followed by post-hoc Tukey's HSD test. P-values < 0.05 (*) were considered significant.

9.3.Results and Discussion

9.3.1. Animal Model for Diabetes Induction

Diabetes was induced in female mice by 5 consecutive STZ injections (Figure 9.1). In table 9.1, the blood glucose levels of the female mice after 14 days of the injections are shown. The blood glucose levels of 20% of all mice subjected to the induction were unable to achieve hyperglycaemia after 14 days of the last STZ injection, with blood

glucose levels falling between 100-149 mg/dL. 32% of the mice displayed little increase in blood glucose levels (150-199 mg/dL), however still falling into a non-diabetic category. 48% of the mice were successfully induced with diabetes, showing high blood glucose levels above 200 mg/dL (hyperglycaemia). These findings of incomplete diabetes induction in female mice are thought to be associated with sexual dimorphism assigned to oestradiol hormone.

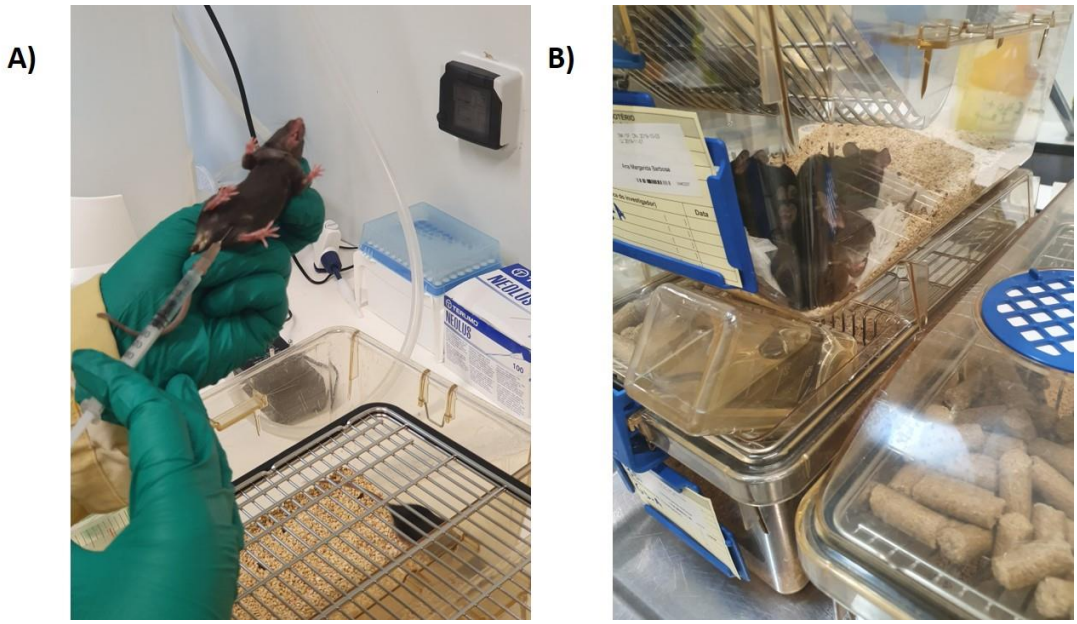

Figure 9.1. A) Intraperitoneal injection of STZ. B) Mice are kept in cages with *ad libidum* fed regimen.

Table 9.1. Blood glucose levels of mice at 14 days after STZ induction and before transplantation.

Blood glucose level	SHAM	Cells only	Cell encapsulation	Cell with surface modification	Total (%)
100-149 mg/dL	2	2	2	2	20
150-199 mg/dL	4	1	3	5	32
200-299 mg/dL	2	4	3	1	25
300-399 mg/dL	1	3	2	1	18
≥400 mg/dL	1	0	0	1	5

Sex differences in physiology begin early in development, due to a combination of genetic and hormonal cues which continue after puberty. In multiple rodent models of diabetes in which β cell failure occurs, sex dimorphism is observed. It has been shown that female mice of Black 6 strain (C57BL/6) are more resistant to become diabetic after induction with STZ. They will develop insulitis, with modest hyperglycaemia (around 200 mg/dL) after 14 days following the injections. While male mice develop diabetes with severe hyperglycaemia (> 400 mg/dL) during the course of the 5 days of injection (Leiter, 1982). Therefore, the extent of diabetes-associated hyperglycaemia is more pronounced in males than females (Chandramouli et al., 2018). In the literature, this difference is mainly assigned to Oestradiol, the major female oestrogen steroid hormone, which is presumed to protect β cell from oxidative stress-induced apoptosis (Cantarelli et al., 2013). Moreover, when male and female mice were transplanted with two different stages of pancreatic cells derived from human embryonic stem cells (endocrine progenitors and insulin-positive cells), the *in vivo* maturation of both cell populations into insulin-secreting cells was accelerated in female recipients than in male hosts. The oestradiol-2 (E2) hormone was the promoter of a faster β cell maturation (Gannon et al., 2018).

In humans, women tend to have an increased glucose-stimulated insulin secretion (GSIS) due to a higher GLP-1 production associated to the female E2 hormone (Gannon et al.,

2018). E2 hormone also influences the immune system, which plays a central role in the development of T1DM. The immunological effects of E2 on innate immune system show to be protective against innate immune pro-inflammatory responses and prevents apoptosis of islets. E2 also protect islets from the adaptive immune response, where E2 hormone promotes the expansion of immunosuppressive Treg cells. In ketosis-prone diabetes (KPD is a form of T2DM), a male predominance is also observed. Interestingly, the rare women developing KPD were in an anovulatory state, with decreased E2 levels (Gannon et al., 2018).

Endocrine pancreas cell composition is known to vary according to pancreatic anatomical location and amongst different species (Dolensek et al., 2015). Moreover, the proportion of different hormone-producing cells in the pancreas also differs between males and females of the same species, possibly also contributing to the female resistance to diabetes induction. Studies suggest that islets from women have an average of 6% more β cells than men, moreover, islet transplantation from female donors also show better outcomes than with islets obtained from male donors (Gannon et al., 2018).

Animal research across all disciplines predominantly uses male subjects instead of mixed or only female subjects. The incorporation of only male subjects in animal research is likely to lead to poorer treatment outcomes for women in the future, as studies have already revealed marked differences between male and females in many basic biological processes (Beery, 2018). The National Institute of Health (NIH) in the USA has been developing policies encouraging the use of both male and female animal research subjects and consideration of sex and biological variables (Clayton JA and Collins, 2014). Although the results shown in this project have great variability regarding diabetes induction and hyperglycaemia achievement, it corroborates that more research and adaptation of current protocols have to be changed in order to better characterize disease models in female subjects.

Moreover, the great variability of hyperglycaemia within female mice (reported in table 9.1) is sought to be a consequence of each individual rodent reproductive cycle. In rodents the reproductive cycle, called the estrous cycle, lasts approximately 4-5 days (in humans it is called the menstrual cycle, and lasts approximately 28 days). The estrous cycle has four stages (proestrus, estrus, metestrus, and diestrus). Each stage lasts for approximately one day (Byers et al., 2012). Proestrus stage corresponds to the pre-ovulatory day, when E2 increases and consequently, during the night, luteinizing hormone (LH) and follicle-

stimulating hormone (FSH) surge and ovulation occurs. In the estrus stage, E2 remains elevated throughout the morning and falls back to basal levels in the afternoon. In the metestrus stage, plasma E2 concentration is low. Finally, in the diestrus stage, E2 levels start to increase (Caligioni, 2009). Considering that 52% of all mice did not achieve hyperglycaemia, and 48% of the mice were successfully induced with diabetes, showing high blood glucose levels, it may be possible that the start of the estrous cycle (high E2 levels) coinciding with the start date of STZ injection, decreases the efficacy of STZ induction. While starting the STZ induction in the metestrus stage, where low levels of E2 are found, may increase STZ-induced cell toxicity and higher diabetes induction efficiency rates.

9.3.2. *In vivo* Transplantation in the Renal Subcapsular Space

In mice, the kidneys are located retroperitoneally, where the left kidney is readily visible and can be accessed more easily in comparison to the right kidney, which is located under the small intestine and adjacent to the liver (Delaney et al., 2018). In the kidneys, the adrenal glands are in close proximity to each renal cranial pole, and they can be distinguished by the light orange coloration due to steroid hormone production (La Perle and Dintzis, 2018). The kidneys in rodents are unilobular, unipapillary and unipyramidal, in contrast to human kidneys which are multilobular, multipapillary and multipyramidal. On a cross-section of the kidney, four main structures can be seen: the capsule, the cortex, the medulla, and the papilla which extends deep into the renal pelvis. The capsule is made of epithelial and fat tissue, In the renal cortex, the glomeruli (with an average diameter of 73.4 μm) and the proximal convoluted tubules can be found. In the medulla (pyramid) the medullary capillary plexus is found. Little interstitial connective tissue is found in the kidney of rodents in contrast to kidneys of humans (Delaney et al., 2018). In this study MIN-6 cells were injected into the sub-capsule membrane of the kidney as single-cell treatments as shown in Figure 9.2.

Five mice have died at day 3 post-transplantation. Of the ten mice for each group, three mice died from the group implanted with Mal-PEG-lipid cell surface modification, one mouse died from the group implanted with HA encapsulated cells, and one mouse died from the SHAM group. These demises are likely to be related to stitch opening and infection at the incision site. After the transplantation, mice had their blood glucose concentrations recorded until day 14 after transplantation (Figure 9.3).

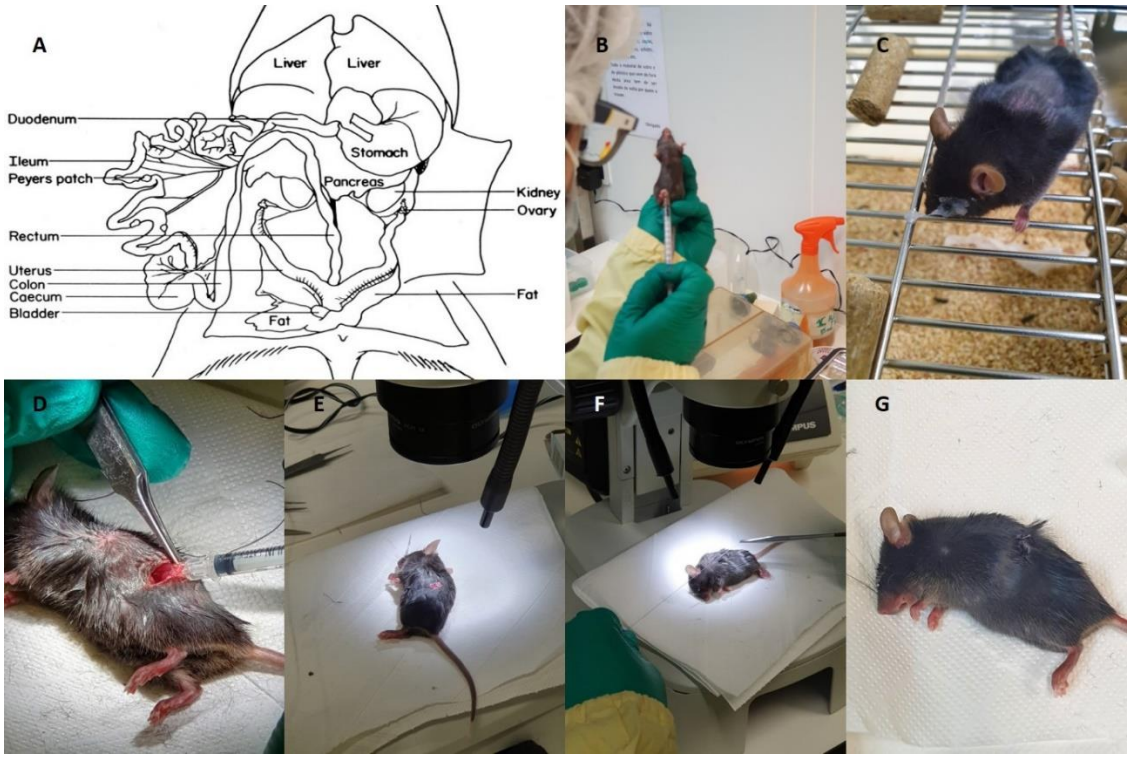

Figure 9.2. MIN-6 cell transplantation. A) Abdominal viscera of female mice (Cook, 1965). B) Intramuscular administration of anaesthetics. C) Topical application of Vaseline to protect eyes from drying during surgery, lateral hair removal for incision. D) Graft injection inside the kidney capsule. E-F) Suture and stiches. G) Post-operation recovery.

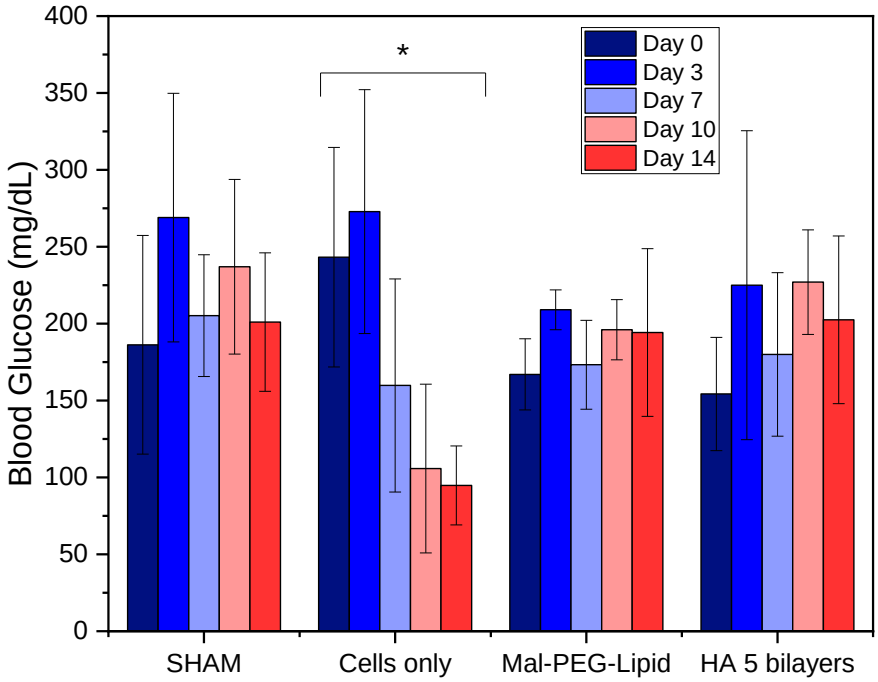

Figure 9.3. Post-transplantation blood glucose levels for mice groups euthanised at day 14. Statistical analysis was performed using ANOVA followed by post-hoc Tukey's HSD test where p-value < 0.05 shows statistical difference within cell only group (*) over time.

In figure 9.3, although there is no significant difference on blood glucose levels for the different groups over time (apart from cells only group), it can be seen that at day 0 (prior to transplantation) mice had reached mild hyperglycaemia (200-300 mg/dL), except for the cell surface modification group which was just below 200 mg/dL. However, if we observe the SHAM group on day 3 after transplantation, we can notice an ongoing rise on blood glucose levels. This result suggests that diabetes induced by STZ was not complete after 14 days as suggested by the literature (Leiter, 1982, Chandramouli et al., 2018). On day 7, we can observe a slight decrease of blood glucose level, which is associated with β cell recovery due to an incomplete β cell destruction (Cantarelli et al., 2013). When analysing the pancreas of mice, islets are unevenly distributed throughout the pancreas, and are present in both interlobular (Figure 9.4a) and periductal/perivascular (Figure 9.4b) locations (Liggitt and Dintzis, 2018). In the islets of mice, β cell populations

are typically clustered in the centre of the islet and surrounded by other islet cell types, whereas in humans all islet cells are homogenously intermingled (Liggitt and Dintzis, 2018).

Regarding the morphology of the islets after treatment with STZ, their architecture is expected to be largely disrupted (Micucci et al., 2014, Han et al., 2017). However, as seen in Figure 9.4, islets did not show morphological changes nor boundary irregularities. Moreover, no infiltration of immune cells was observed in the histological analysis of the pancreas of STZ-induced diabetic mice. In this scenario, considering the results presented, diabetes induction cannot be assured only 14 days after STZ injections. We should consider extending the induction for at least 21 days after STZ injections or increasing the daily dose of STZ.

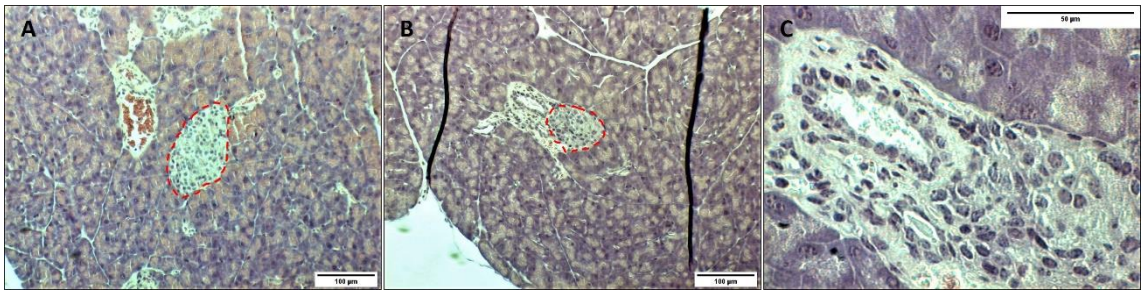

9.4. Histological images of pancreatic tissue from STZ induced diabetic female mice on day 7 (a) and day 14 (b) after transplantation, where (c) shows higher magnification for day 14 after transplantation. Islets are circled in red.

In figure 9.3, results show that non-encapsulated single cells (cells only group) were able to decrease hyperglycaemia over time to normal physiological levels (<200 mg/dL). This was not observed in mice transplanted with encapsulated and surface modified cells. We hypothesise that non-encapsulated cells were able to interact with each other and were probably able to form clusters to mimic a pseudo-islet. This hypothesis has been confirmed in the histological analysis of the renal tissue after transplantation. In Figure 9.5 a and b, the saline transplanted group (SHAM) shows the normal appearance of the renal capsule and the underlying renal cortex. In Figure 9.5 c and d, the histological analysis of the mice transplanted with naked cells, show that the MIN-6 cells are grouped and located between the renal capsule and the renal cortex. Images also show graft infiltration with leukocytes. Infiltration of immune cells have also been reported by other studies at the 2-week transplantation mark. The degree of leukocyte infiltration is

maximum at the first two weeks after transplantation and decreases after that (Plesner et al., 2005).

Unfortunately, MIN-6 cells were not able to be found in the histological images of various slices of the kidneys of mice transplanted with encapsulated and surface engineering cells. This finding confirms our hypothesis that surface modified and encapsulated cells were deprived from cell-cell interaction, unable to form clusters similar to islets. This has also implications in β cells functionality. Functional loss (measured by insulin expression, insulin content, and glucose-stimulated secretion) is correlated with decreased cell-cell interaction (Giraldo et al., 2010). Other studies have also demonstrated this pattern of functionality associated to MIN-6 cell aggregates and single cells. Encapsulation using poly(ethylene glycol) diacrylate (PEGDA) of either MIN-6 cell aggregates or MIN-6 single cells showed a 4-fold higher insulin secretion in response to glucose for aggregated MIN-6 cells when compared with encapsulated single cells (Bernard et al., 2012). Fukuda et al encapsulated MIN-6 single cells using fibronectin and gelatin by a L-b-L approach but only after the formation of 3D spheroids, the insulin secretion, and the expression of GLUT2 increased (Fukuda et al., 2018). Dispersed MIN-6 cells were encapsulated in dextran-tyramine microgels, and within one day of subsequent cell culture, cells centralized and aggregated. MIN-6 cells remained viable and functional (Kamperman et al., 2017b). Interestingly, the functionality of encapsulated MIN-6 aggregates is reported to be heavily reduced compared to free-floating aggregates (Marchioli et al., 2017). Another important point to highlight is that MIN-6 cells are anchorage dependent cells. When single cells are encapsulated, they are denied attaching to one-another or to surrounding ECM, which might trigger anoikis.

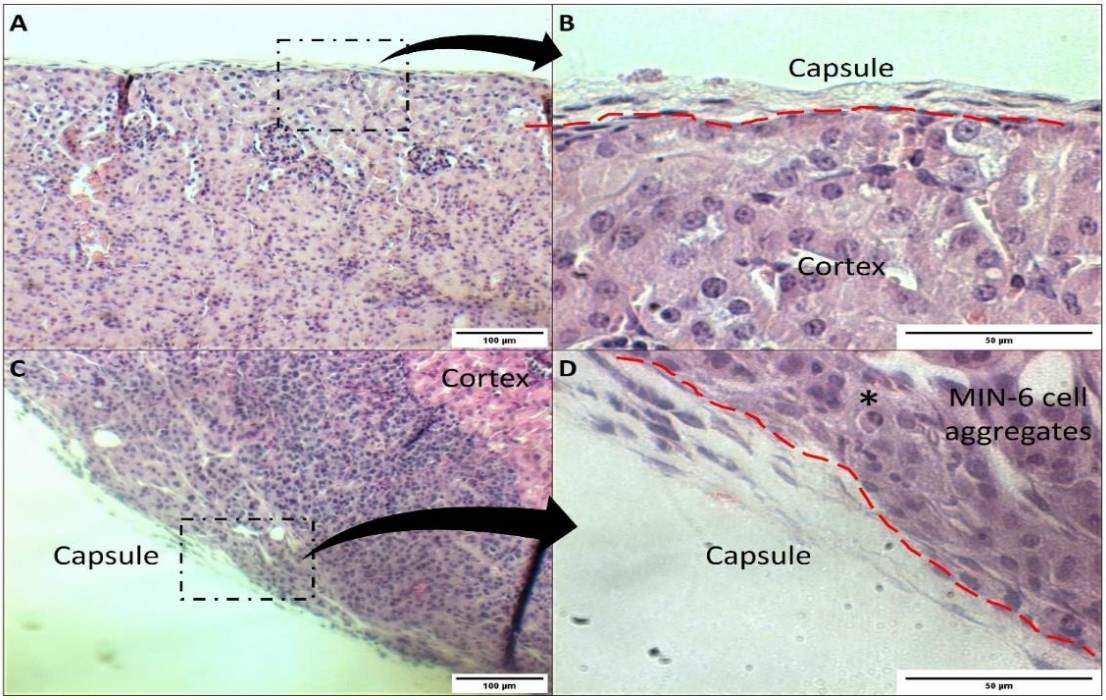

Figure 9.5. Histology analysis of the kidneys after 14 days post-transplantation of MIN-6 single cells. Saline group (A and B) and cells only group (C and D). Immune cell infiltration is shown (*). Lower magnification 10X, scale bar 100 µm. Higher magnification 40X, scale bar 50 µm.

9.4. Final considerations

Overall, studies have proposed that diabetes is achieved when levels of blood glucose are higher than 200 mg/dL. Reversion of diabetes and transplantation success is defined as the ability to reach non-fasting blood glucose levels under 250 mg/dL within five days after transplantation. Graft rejection is defined as two consecutive measurements above 300 mg/dL in mice after normoglycemia was achieved. If more detailed definitions are required, transplant function can be normalized for pre-transplant glycemia and the outcome can be classified as: 1) full function (non-fasting blood glucose concentration < 50% of pre-transplant concentration); 2) partial function (non-fasting blood glucose concentration between 50% and 80% of pre-transplant concentration); and 3) no function (non-fasting blood glucose concentration > 80% of the pre-transplant concentration) (Cantarelli et al., 2013).

T1DM induction disease protocols established using male mice do not demonstrate a viable option to induce diabetes in female mice. The results shown in this chapter agree that female mice are more resistant to diabetes induction through STZ administration. The levels of blood glucose shown in this project are not consistently raise above normal

physiological ranges. This result is hypothesized to be a consequence of sexual dimorphism characteristics and hormonal interferences. Nevertheless, the use of female subjects in this study is important to highlight sex-related deviations in protocols to induce diabetes in mice.

Moreover, during the procedure of injecting the cellular grafts into the kidney capsule, the gauge of the syringe left a sizeable puncture after retrieving the needle. It was observed leakage of some cell suspension outside the kidney capsule. This finding may also have contributed to the failure of reversing diabetes after transplantation of the cell grafts. In order to decrease graft loss during transplantation the use a gel foam or surgical glue is suggested to create a clog at the puncture site to prevent leakage.

Chapter 10: Conclusions, Limitations and Future Work

10.1. Conclusions and Limitations

In this project, the synthesis of BIED, a di-isocyanate crosslinker and the gelation of HA have been successfully conducted. It demonstrates an innovative crosslinking method through the formation of urethane linkages between isocyanate groups of the crosslinker and hydroxyl groups present in the HA chain. These HA gels have been developed through homogeneous and heterogenous crosslinking methodologies creating very distinct gels. These gels have potential to be further developed for applications that include drug release and skin wound dressings. The main advantage of using BIED over other isocyanate crosslinkers is that it possesses a disulphide bond in the middle of its molecular backbone. This feature enables the reduction of the disulphide bond into free thiol groups, its re-oxidation for reversible or self-healing gel forming properties.

In recent years, the role of biomaterials in cell encapsulation exceeds solely a barrier to provide immunoisolation. The role of biomaterials is now sought to modulate the interaction of the surrounding biological environment with the cellular graft in order to create long-lasting immune tolerance. In this landscape, HA, a known modulator of the immune system, has been successfully modified to create derivates capable to encapsulate pancreatic β cells for T1DM treatment.

The HA derivates developed in this project are able to assemble in nano-layers through a disulphide exchange mechanism, where disulphide bonds are recreated without the use of strong oxidizing agents and catalysts. This method utilizes a bimolecular nucleophilic substitution (S_N2) reaction that allows the formation of crosslinks between a thiol-modified and pyridine-modified polymeric material in physiological conditions (aqueous medium and neutral pH) (Fernandes and Ramos, 2004). Furthermore, this method also brings high tailorable interfaces, where the number and the composition of each layer can be specifically designed to improve cell encapsulation functionality. This method of encapsulation is biocompatible and provides stronger crosslinking bonds when compared to simple ionic interactions observed in L-b-L surface deposition of polyelectrolytes.

The *in vitro* encapsulation of MIN- 6 cells via surface modification using Mal-PEG-Lipid and through conformal deposition of nano-coatings of HA derivates was successfully performed. Results show neglectable detrimental effects to cells during the process of encapsulation. Moreover, encapsulated cells showed resistance to immune mediated cell death with increasing number of coating layers in comparison to the control group (naked

cells), while maintaining *in vitro* functionality. Cells were able to secrete insulin when stimulated with glucose. However, the *in vivo* studies assessing the transplantation of these cells under the kidney capsule of mice showed unsatisfactory results.

The diabetes induction of female mice through five daily STZ injections did not show consistent hyperglycaemia. This result is sought to be a consequence of sexual dimorphism and hormonal interferences. Using male mice could give more robust and reliable data, nevertheless, animal research using female mice can lead to better understanding of disease and treatment outcomes used to prevent or treat diabetes.

10.2. Future Work

This work presented insightful prospects regarding using female subjects in diabetes research and the transplantation of pancreatic β cells into the kidney capsule. However, further studies could be conducted to assess the optimization of disease-inducing protocols for female mice and the comparison of single-cell versus pseudo-islet aggregates encapsulation.

a) Design appropriate diabetes model for female mice. Suggested T1DM inducing protocol modifications:

    - Increase the daily dose of STZ above 50 mg/kg. Optimization of the dose has to be conducted regarding hyperglycaemia development;
    - If maintaining the 50 mg/kg dose a day, it may be advisable to increase the number of induction days above the 5 consecutive daily injections;
    - In order to guarantee complete diabetes induction without β recovery, the post-induction period should be increased from 14 days to 21 days;
    - Assess the interference of the estrus cycle in the efficacy of STZ induction of diabetes in female mice.

b) Lack of cell-cell interaction may affect transplantation outcome and diabetes reversion, where deficient insulin secretion is unable to control hyperglycaemia. To confirm the hypothesis of the decreased functionality of encapsulated single-cells due to lack of cell-cell and cell-ECM interactions:

    - Development of pseudo-islet aggregates using MIN-6 cells;

- Encapsulation of pseudo-islet;
- Assessment of glucose-induced insulin secretion;
- Transplantation of encapsulated pseudo-islet;
- Histological assessment of pseudo-islet aggregates under the kidney capsule of female mice.

Fundamental materials research has been completed in this project, showing great scope for project expansion. Where these novel HA derivates can be studied for many other applications that include wound healing dressings with antimicrobial properties, scaffolds for skin grafts, gels for anti-inflammatory drug delivery, and cell encapsulation of many other cell types.

Appendices

Appendix A: List of Achievements Obtained in the Last 5 Years

Awards

- Irish Research Council Post-Doctoral Fellowship Scheme 2021 - Progression to Inner International Assessment Board
- PhD Scholar Bursary 2021 – University of Limerick, Ireland
- Best publication of the year - Bernal Research Day 2020, University of Limerick, Ireland
- Open Access grant award 2020 – Health Research Institute, University of Limerick, Ireland
- Open Access grant award 2019 – Health Research Institute, University of Limerick, Ireland
- Silver President Volunteer Award 2018-2019, University of Limerick, Ireland
- Bronze President Volunteer Award, 2017-2018, University of Limerick, Ireland
- Erasmus Plus Traineeship, 2019
- PhD Postgraduate Scholarship, 2015-2019, Irish Research Council

Project Dissemination (Podcast and Conference Presentations)

- Cahill, D., Zamboni, F., Collins, M. N. (2021) Role of imaging in pancreatic islet transplantation. ESGAR 2021 Virtual Congress, June 15-18.
- Cahill, D., Zamboni, F., Collins, M. N. (2021) Prospective role of PET-CT, SPECT, and MRI in monitoring pancreatic islet cells in post-transplant patients. European Society of Gastrointestinal and Abdominal Radiology (ESGAR) 2021 Virtual Congress, June 15-18.
- Zamboni, F., Collins, M. N. (2021) Pancreatic beta cell transplantation in Type 1 Diabetes Mellitus-induced female mice. Shannon Region Postgraduate Researcher Conference, Virtual, May 18-19.
- Zamboni, F. (2021) The PhD Podcast Series 1. Released by the UL Graduate and Professional Studies & the UL Postgraduate Student's Union.

- Zamboni, F., Okoroafor, C., Collins, M. N. (2020) Bacteriostatic activity of hyaluronic acid films. World Biomaterials Congress, Virtual.
- Zamboni, F., Collins, M. N. (2019) Women in Science: A retrospective gender analysis through publication. Limerick Postgraduate Research Conference (LPRC), Kemmy Business School
- Zamboni, F., Ryan, E., McGourty, K., Collins, M. N. (2019) Immunomodulatory Hyaluronic Acid Gels for Cell Encapsulation Strategies. TERMIS EU, 27th to 31st of May 2019, Rhodes, Greece
- Zamboni, F. & Collins, M. N. (2019) Immunomodulatory properties of hyaluronic acid derivates. 25th Annual Conference of the Section of Bioengineering of the Royal Academy of Medicine in Ireland, Ireland
- Zamboni, F. & Collins, M. N. (2018) Engineering the plasma membrane of pancreatic beta cells for a cell-based treatment in T1DM. 1st TERMIS-AM Workshop, Brazil
- Zamboni, F. & Collins, M. N. (2018) Rational crosslinking of hyaluronic acid into multi-layered networks. 24th Annual Conference of the Section of Bioengineering of the Royal Academy of Medicine in Ireland, Ireland
- Zamboni, F. & Collins, M. N. (2017) BIED-modified hyaluronic acid for conformal nanoencapsulation of pancreatic beta cells for an integrated bioengineered cell-based therapy in type 1 diabetes mellitus. 28th Annual Conference of the European Society of Biomaterials, Athens
- Zamboni, F. & Collins, M. N. (2017) Development of a Cell-based Therapy for Type 1 Diabetes Mellitus using a Novel Hyaluronic Acid Derivate. Health Research Symposium, Ireland
- Zamboni, F. & Collins, M. N. (2016) Hyaluronic Acid Coated Poly (Lactic-co-Glycolic Acid) Scaffolds for Tissue Engineering Applications. NUIG-UL Postgraduate Research Day, Ireland
- Zamboni, F.; Keays, M.; Collins, M. N. (2016) Cellular Carriers for Medical Diagnostic Applications. Frontiers of Pharmaceutical Sciences in the Omics Era, Brazil
- Zamboni, F. & Collins, M. N. (2016) The Immunoprotection of Pancreatic Beta Cells Via Layer-By-Layer Encapsulation with Hyaluronic Acid. AIChE Annual Meeting, San Francisco

Published Articles and Book Chapters

- Zamboni, F., Carvalho, C. R., Oliveira, J. M., Collins, M. MIN-6 pancreatic beta cell nano-encapsulation for diabetes treatment (planned)

- Zamboni, F., Fatih, I., Oliveira, J. M., Castro, A. G., Collins, M. Pancreatic beta cell transplantation under the kidney capsule of mice (planned)

- Ren, G., Culebras, M., Zamboni, F., O'Driscoll, J., O'Dwyer, J., Mackey, M., Carmody, M., Dowling, A., Ryan, E., Collins, M. N. Curcumin nanoparticles embedded hydrogel for on-site immunoregulation (planned)

- Collins, M. N., Zamboni, F., Serafin, A., Ren, G., Thanusha, A.V., Culebras, M. (in print) The role of Hyaluronic Acid in Tissue Engineering, in Oliveira, J. M., Radhouani, H., Reis, R. L. (editors) *Polysaccharides of Microbial Origin: Biomedical Applications.* Springer International Publishing. e-Reference ISBN 978-3-030-42215-8.

- Zamboni, F., Okoroafor, C., Ryan, M. P., Pembroke, T., Culebras, M., Strozyk, M., Collins, M. N. (2021) On the Bacteriostatic activity of hyaluronic acid composite films, Carbohydrate Polymers (OPEN ACESS) (Quartile 1, JCR Impact factor 7.182)

- Zamboni, F., Ryan, E., Culebras, M., Collins, M. N. (2020) Labile crosslinked hyaluronic acid via urethane formation using bis(β-isocyanatoethyl) disulphide with tuneable physicochemical and immunomodulatory properties. Carbohydrate Polymers v. 245, 2020. (OPEN ACESS) (Quartile 1, JCR Impact factor 7.182)

- Cahill, D., Zamboni, F., Collins, M. Radiological Advances in Pancreatic Islet Transplantation. Journal Academic Radiology, 26 (11) 1536-1543, 2019. (Quartile 2, JCR Impact factor 2.488)

- Zamboni, F.; Vieira, S.; Reis, R. L.; Oliveira, J. M. and Collins, M. N. The Potential of Hyaluronic acid in Immunoprotection and Immunomodulation: Chemistry, Processing and Function. Progress in Materials Science v. 97, p. 97-122, 2018. (Quartile 1, JCR Impact factor 31.560)

- Zamboni, F. and M.N. Collins, Cell Based Therapeutics in Type 1 Diabetes Mellitus. Int J Pharm, 2017. 521(1-2): p. 346-356. (Quartile 1, JCR Impact factor 4.845)

Total Citations: 285

H-index: 10

References

2020a. 2. Classification and Diagnosis of Diabetes: Standards of Medical Care in Diabetes—2020. *Diabetes Care,* 43**,** S14-S31.

2020b. 5. Facilitating Behavior Change and Well-being to Improve Health Outcomes: Standards of Medical Care in Diabetes—2020. *Diabetes Care,* 43**,** S48-S65.

2020c. 6. Glycemic Targets: Standards of Medical Care in Diabetes—2020. *Diabetes Care,* 43**,** S66-S76.

2020d. 7. Diabetes Technology: Standards of Medical Care in Diabetes—2020. *Diabetes Care,* 43**,** S77-S88.

2020e. 9. Pharmacologic Approaches to Glycemic Treatment: Standards of Medical Care in Diabetes—2020. *Diabetes Care,* 43**,** S98-S110.

2020f. 11. Microvascular Complications and Foot Care: Standards of Medical Care in Diabetes−2020. *Diabetes Care,* 43**,** S135-S151.

2020g. 13. Children and Adolescents: Standards of Medical Care in Diabetes−2020. *Diabetes Care,* 43**,** S163-S182.

ABBINA, S., SIREN, E. M., MOON, H. & KIZHAKKEDATHU, J. N. 2017. Surface Engineering for Cell-based Therapies: Techniques for Manipulating Mammalian Cell Surfaces. *ACS Biomaterials Science & Engineering,* 4**,** 20.

ABU-HAKMEH, A., KUNG, A., MINTZ, B. R., KAMAL, S., COOPER, J. A., LU, X. L. & WAN, L. Q. 2016. Sequential gelation of tyramine-substituted hyaluronic acid hydrogels enhances mechanical integrity and cell viability. *Med Biol Eng Comput*.

ABUID, N. J., GATTÁS-ASFURA, K. M., SCHOFIELD, E. A. & STABLER, C. L. 2019. Layer-by-Layer Cerium Oxide Nanoparticle Coating for Antioxidant Protection of Encapsulated Beta Cells. *Advanced Healthcare Materials,* 8**,** 1801493.

ACHARYA, P. S., MAJUMDAR, S., JACOB, M., HAYDEN, J., MRASS, P., WENINGER, W., ASSOIAN, R. K. & PURE, E. 2008. Fibroblast migration is mediated by CD44-dependent TGF beta activation. *J Cell Sci,* 121**,** 1393-402.

AIHW 2012. Insulin pump use in Australia. *Diabetes series no.18. Cat. no. CVD 58.* Canberra: Australian Institute of Health and Welfare.

AKERBLOM, H. K. & GRP, T. T. S. 2011. The Trial to Reduce IDDM in the Genetically at Risk (TRIGR) study: recruitment, intervention and follow-up. *Diabetologia,* 54**,** 627-633.

ALBEIROTI, S., AYASOUFI, K. & DE LA MOTTE, C. 2014. The role of platelet activation in the expression and function of platelet hyaluronidase-2. *Faseb Journal,* 28.

ALEXANDER, V. & GREENE, S. 2009. Insulin pumps for children. *Paediatrics and Child Health,* 19**,** 316-320.

AMERICAN DIABETES, A. 2013. Standards of medical care in diabetes--2013. *Diabetes Care,* 36 Suppl 1**,** S11-66.

AMORIM, S., PASHKULEVA, I., REIS, C. A., REIS, R. L. & PIRES, R. A. 2020. Tunable layer-by-layer films containing hyaluronic acid and their interactions with CD44. *Journal of Materials Chemistry B,* 8**,** 3880-3885.

AMORIM, S., REIS, C. A., REIS, R. L. & PIRES, R. A. 2021. Extracellular Matrix Mimics Using Hyaluronan-Based Biomaterials. *Trends in Biotechnology,* 39**,** 90-104.

ARDIZZONI, A., NEGLIA, R. G., BASCHIERI, M. C., CERMELLI, C., CARATOZZOLO, M., RIGHI, E., PALMIERI, B. & BLASI, E. 2011. Influence of hyaluronic acid on bacterial and fungal species, including clinically relevant opportunistic pathogens. *Journal of Materials Science: Materials in Medicine,* 22**,** 2329.

ASAMI, K., INAGAKI, A., IMURA, T., SEKIGUCHI, S., FUJIMORI, K., MASUTANI, H., YODOI, J., SATOMI, S., OHUCHI, N. & GOTO, M. 2013. Thioredoxin-1 Attenuates Early Graft Loss after Intraportal Islet Transplantation in Mice. *Plos One,* 8.

ASHCROFT, F. M. & ASHCROFT, S. J. H. 1992. *Insulin : molecular biology to pathology,* Oxford ; New York, IRL Press at Oxford University Press.
ATKINSON, M. A. & EISENBARTH, G. S. 2001. Type 1 diabetes: new perspectives on disease pathogenesis and treatment. *Lancet,* 358**,** 221-9.
AVOLIO, E., ALVINO, V. V., GHORBEL, M. T. & CAMPAGNOLO, P. 2016. Perivascular cells and tissue engineering: Current applications and untapped potential. *Pharmacol Ther*.
AWAN, M., BURIAK, I., FLECK, R., FULLER, B., GOLTSEV, A., KERBY, J., LOWDELL, M., MERICKA, P., PETRENKO, A., PETRENKO, Y., ROGULSKA, O., STOLZING, A. & STACEY, G. N. 2020. Dimethyl sulfoxide: a central player since the dawn of cryobiology, is efficacy balanced by toxicity? *Regenerative Medicine,* 15**,** 1463-1491.
BAE, M. S., OHE, J. Y., LEE, J. B., HEO, D. N., BYUN, W., BAE, H., KWON, Y. D. & KWON, I. K. 2014. Photo-cured hyaluronic acid-based hydrogels containing growth and differentiation factor 5 (GDF-5) for bone tissue regeneration. *Bone,* 59**,** 189-98.
BAHADUR, A., SHOAIB, M., SAEED, A. & IQBAL, S. 2016. FT-IR spectroscopic and thermal study of waterborne polyurethane-acrylate leather coatings using tartaric acid as an ionomer. *E-Polymers,* 16**,** 463-474.
BAL, T., KEPSUTLU, B. & KIZILEL, S. 2014. Characterization of protein release from poly(ethylene glycol) hydrogels with crosslink density gradients. *J Biomed Mater Res A,* 102**,** 487-95.
BALTZINGER, P., MOREAU, F., GREGET, M., BEDAT, B., BERNEY, T. & KESSLER, L. 2016. Unexpected Massive Hemothorax After Pancreatic Islet Transplantation: A Case Report. *Transplantation Proceedings,* 48**,** 285-287.
BANERJEE, A., PONS, T., LEQUEUX, N. & DUBERTRET, B. 2016. Quantum dots-DNA bioconjugates: synthesis to applications. *Interface Focus,* 6**,** 20160064.
BANTING, F. G. & BEST, C. H. 1922. *The internal secretion of the pancreas,* Toronto, The University Library: pub. by the librarian.
BANTING, F. G., BEST, C. H., COLLIP, J. B., CAMPBELL, W. R. & FLETCHER, A. A. 1922. Pancreatic Extracts in the Treatment of Diabetes Mellitus. *Can Med Assoc J,* 12**,** 141-6.
BARANOVA, N. S., NILEBACK, E., HALLER, F. M., BRIGGS, D. C., SVEDHEM, S., DAY, A. J. & RICHTER, R. P. 2011. The inflammation-associated protein TSG-6 cross-links hyaluronan via hyaluronan-induced TSG-6 oligomers. *J Biol Chem,* 286**,** 25675-86.
BARNETT, B. P., AREPALLY, A., KARMARKAR, P. V., QIAN, D., GILSON, W. D., WALCZAK, P., HOWLAND, V., LAWLER, L., LAUZON, C., STUBER, M., KRAITCHMAN, D. L. & BULTE, J. W. 2007. Magnetic resonance-guided, real-time targeted delivery and imaging of magnetocapsules immunoprotecting pancreatic islet cells. *Nat Med,* 13**,** 986-91.
BAUTISTA-HERNANDEZ, L. A., GOMEZ-OLIVARES, J. L., BUENTELLO-VOLANTE, B. & MANUEL BAUTISTA-DE LUCIO, V. 2017. Fibroblasts: The Unknown Sentinels Eliciting Immune Responses against Microorganisms. *European Journal of Microbiology and Immunology,* 7**,** 151-157.
BECK, J. B., KILLOPS, K. L., KANG, T., SIVANANDAN, K., BAYLES, A., MACKAY, M. E., WOOLEY, K. L. & HAWKER, C. J. 2009. Facile Preparation of Nanoparticles by Intramolecular Cross-Linking of Isocyanate Functionalized Copolymers. *Macromolecules,* 42**,** 5629-5635.
BEERY, A. K. 2018. Inclusion of females does not increase variability in rodent research studies. *Current Opinion in Behavioral Sciences,* 23**,** 7.
BERNARD, A. B., LIN, C. C. & ANSETH, K. S. 2012. A microwell cell culture platform for the aggregation of pancreatic beta-cells. *Tissue Eng Part C Methods,* 18**,** 583-92.
BESSAOUD, K., BOUDRAA, G., DE ROPOLO, M. M., DE SEREDAY, M., MARTI, M. L., MOSER, M., LAPERTOSA, S., DAMIANO, M., VERGE, C., HOWARD, N., SCHOBER, E., JORDAN, O., WEETS, I., GORUS, F., COECKELBERGHS, M., ROOMAN, R., VAN GAAL, L., FRANCO, L. J., FERREIRA, S. R. G., LISBOA, H. P. K., KURTZ, L. A., GRAEBIN, R., KUTZKE, L., RODRIGES, C., SAVOVA, R., CHRISTOV, V., IOTOVA, V., TZANEVA, V., PACAUD, D., TOTH, E., TAN, M. H., CARRASCO, E., PEREZ, F., ZE, Y., BO, Y., CHEN, S., FU, L., DENG, L., SHEN, S., TENG, K., WANG, C., JIAN, H., JU, J., YAN, C., ZE, Y., DENG, Y., LI, C., ZHANG, Y., LIU, Y.,

LONG, X., ZHEN, Z., SUN, Z., WANG, B., WONG, G., ORREGO, O. V., ASCHNER, P., DIAZ-DIAZ, O., DE ACOSTA, O. M., CINEK, O., VAVRINEC, J., OLSEN, B. S., SVENDSEN, A. J., KREUTZFELDT, J., LUND, E., TULL, E. S., SELMAN-GEARA, A., ALMONTE, A. S., PODAR, T., TUOMILEHTO, J., KARVONEN, M., NOTKOLA, I. L., MOLTCHANOVA, E., TASKINEN, O., LEVY-MARCHAL, C., CZERNICHOW, P., KOCAVA, M., NEU, A., EHEHALT, S., ROSENBAUER, J., GIANI, G., ICKS, A., BARTSOCAS, C., VAZEOU, A., SOLTESZ, G., LARON, Z., GORDON, O., ALBAG, Y., SHAMIS, I., PURRELLO, F., ARPI, M., FICHERA, G., MANCUSO, M., LUCENTI, C., CHIUMELLO, G., BRUNO, G., PAGANO, G., SONGINI, M., CASU, A., MARINARO, A., FRONGIA, P., et al. 2006. Incidence and trends of childhood Type 1 diabetes worldwide 1990-1999. *Diabetic Medicine,* 23**,** 857-866.

BHATTACHARYA, M., WOZNIAK, D. J., STOODLEY, P. & HALL-STOODLEY, L. 2015. Prevention and treatment of Staphylococcus aureus biofilms. *Expert Rev Anti Infect Ther,* 13**,** 1499-516.

BHATTACHARYYA, S., GUILLOT, S., DABBOUE, H., TRANCHANT, J.-F. & SALVETAT, J.-P. 2008. Carbon Nanotubes as Structural Nanofibers for Hyaluronic Acid Hydrogel Scaffolds. *Biomacromolecules,* 9**,** 505-509.

BIAN, S. Q., HE, M. M., SUI, J. H., CAI, H. X., SUN, Y., LIANG, J., FAN, Y. J. & ZHANG, X. D. 2016. The self-crosslinking smart hyaluronic acid hydrogels as injectable three-dimensional scaffolds for cells culture. *Colloids and Surfaces B-Biointerfaces,* 140**,** 392-402.

BISCEGLIE, V. 1934. Über die antineoplastische Immunität. *Zeitschrift für Krebsforschung,* 40**,** 122-140.

BLACK, S. P., SANDERS, J. K. M. & STEFANKIEWICZ, A. R. 2014. Disulfide exchange: exposing supramolecular reactivity through dynamic covalent chemistry. *Chemical Society Reviews,* 43**,** 1861-1872.

BOGDANI, M., KORPOS, E., SIMEONOVIC, C. J., PARISH, C. R., SOROKIN, L. & WIGHT, T. N. 2014. Extracellular matrix components in the pathogenesis of type 1 diabetes. *Curr Diab Rep,* 14**,** 552.

BORG, D. J. & BONIFACIO, E. 2011. The Use of Biomaterials in Islet Transplantation. *Current Diabetes Reports,* 11**,** 434-444.

BOWMAN, S., AWAD, M. E., HAMRICK, M. W., HUNTER, M. & FULZELE, S. 2018. Recent advances in hyaluronic acid based therapy for osteoarthritis. *Clinical and Translational Medicine,* 7**,** e6.

BOZKURT, N. C., PEIXOTO, E. M. L., FROUD, T., HERRADA, E., CORRALES, A., RICORDI, C. & ALEJANDRO, R. 2013. Hepatic hematoma after islet cell transplantation. *Transplantation Reviews,* 95**,** 5.

BRENNAN, D. C., KOPETSKIE, H. A., SAYRE, P. H., ALEJANDRO, R., CAGLIERO, E., SHAPIRO, A. M. J., GOLDSTEIN, J. S., DESMARAIS, M. R., BOOHER, S. & BIANCHINE, P. J. 2016. Long-Term Follow-Up of the Edmonton Protocol of Islet Transplantation in the United States. *American Journal of Transplantation,* 16**,** 509-517.

BRODIN, P. & DAVIS, M. M. 2017. Human immune system variation. *Nat Rev Immunol,* 17**,** 21-29.

BROWN, H., SANGER, F. & KITAI, R. 1955. The structure of pig and sheep insulins. *Biochem J,* 60**,** 556-65.

BROWN, W. E., GREEN, A. H., CEDEL, T. E. & CAIRNS, J. 1987. Biochemistry of Protein-Isocyanate Interactions - a Comparison of the Effects of Aryl Vs Alkyl Isocyanates. *Environmental Health Perspectives,* 72**,** 5-11.

BUKHARI, S. N. A., ROSWANDI, N. L., WAQAS, M., HABIB, H., HUSSAIN, F., KHAN, S., SOHAIL, M., RAMLI, N. A., THU, H. E. & HUSSAIN, Z. 2018. Hyaluronic acid, a promising skin rejuvenating biomedicine: A review of recent updates and pre-clinical and clinical investigations on cosmetic and nutricosmetic effects. *International Journal of Biological Macromolecules,* 120**,** 1682-1695.

BUKOWSKI, M., WLADYKA, B. & DUBIN, G. 2010. Exfoliative toxins of Staphylococcus aureus. *Toxins (Basel),* 2**,** 1148-65.

BURDICK, J. A. & PRESTWICH, G. D. 2011. Hyaluronic acid hydrogels for biomedical applications. *Adv Mater,* 23**,** H41-56.

BUWALDA, S. J., BOERE, K. W. M., DIJKSTRA, P. J., FEIJEN, J., VERMONDEN, T. & HENNINK, W. E. 2014. Hydrogels in a historical perspective: From simple networks to smart materials. *Journal of Controlled Release,* 190**,** 254-273.

BYERS, S. L., WILES, M. V., DUNN, S. L. & TAFT, R. A. 2012. Mouse Estrous Cycle Identification Tool and Images. *PLOS ONE,* 7**,** e35538.

CAHILL, D., ZAMBONI, F. & COLLINS, M. N. 2019. Radiological Advances in Pancreatic Islet Transplantation. *Acad Radiol,* 26**,** 1536-1543.

CALAFIORE, R. 2018. Microencapsulation for cell therapy of type 1 diabetes mellitus: The interplay between common beliefs, prejudices and real progress. *Journal of diabetes investigation,* 9**,** 231-233.

CALAFIORE, R., BASTA, G., LUCA, G., LEMMI, A., RACANICCHI, L., MANCUSO, F., MONTANUCCI, M. P. & BRUNETTI, P. 2006. Standard technical procedures for microencapsulation of human islets for graft into nonimmunosuppressed patients with type 1 diabetes mellitus. *Transplantation Proceedings,* 38**,** 1156-1157.

CALIGIONI, C. S. 2009. Assessing reproductive status/stages in mice. *Current protocols in neuroscience,* Appendix 4**,** Appendix-4I.

CAÑIBANO-HERNÁNDEZ, A., SAENZ DEL BURGO, L., ESPONA-NOGUERA, A., ORIVE, G., HERNÁNDEZ, R. M., CIRIZA, J. & PEDRAZ, J. L. 2019a. Hyaluronic acid enhances cell survival of encapsulated insulin-producing cells in alginate-based microcapsules. *International Journal of Pharmaceutics,* 557**,** 192-198.

CAÑIBANO-HERNÁNDEZ, A., SAENZ DEL BURGO, L., ESPONA-NOGUERA, A., ORIVE, G., HERNÁNDEZ, R. M., CIRIZA, J. & PEDRAZ, J. L. 2019b. Hyaluronic Acid Promotes Differentiation of Mesenchymal Stem Cells from Different Sources toward Pancreatic Progenitors within Three-Dimensional Alginate Matrixes. *Molecular Pharmaceutics,* 16**,** 834-845.

CANKAYA, Z. T., GURBUZ, S., BAKIRARAR, B. & KURTIS, B. 2020. Evaluation of the Effect of Hyaluronic Acid Application on the Vascularization of Free Gingival Graft for Both Donor and Recipient Sites with Laser Doppler Flowmetry: A Randomized, Examiner-Blinded, Controlled Clinical Trial. *Int J Periodontics Restorative Dent,* 40**,** 233-243.

CANTARELLI, E., CITRO, A., MARZORATI, S., MELZI, R., SCAVINI, M. & PIEMONTI, L. 2013. Murine animal models for preclinical islet transplantation: No model fits all (research purposes). *Islets,* 5**,** 79-86.

CAO, W., SUI, J., MA, M., XU, Y., LIN, W., CHEN, Y., MAN, Y., SUN, Y., FAN, Y. & ZHANG, X. 2019. The preparation and biocompatible evaluation of injectable dual crosslinking hyaluronic acid hydrogels as cytoprotective agents. *Journal of Materials Chemistry B,* 7**,** 4413-4423.

CARLSON, G. A., DRAGOO, J. L., SAMIMI, B., BRUCKNER, D. A., BERNARD, G. W., HEDRICK, M. & BENHAIM, P. 2004. Bacteriostatic properties of biomatrices against common orthopaedic pathogens. *Biochemical and Biophysical Research Communications,* 321**,** 472-478.

CAVALLARI, G., OLIVI, E., BIANCHI, F., NERI, F., FORONI, L., VALENTE, S., LA MANNA, G., NARDO, B., STEFONI, S. & VENTURA, C. 2012. Mesenchymal stem cells and islet cotransplantation in diabetic rats: improved islet graft revascularization and function by human adipose tissue-derived stem cells preconditioned with natural molecules. *Cell Transplant,* 21**,** 2771-81.

CERMELLI, C., CUOGHI, A., SCURI, M., BETTUA, C., NEGLIA, R. G., ARDIZZONI, A., BLASI, E., IANNITTI, T. & PALMIERI, B. 2011. In vitro evaluation of antiviral and virucidal activity of a high molecular weight hyaluronic acid. *Virology Journal,* 8**,** 141.

CHANDRAMOULI, C., REICHELT, M. E., CURL, C. L., VARMA, U., BIENVENU, L. A., KOUTSIFELI, P., RAAIJMAKERS, A. J. A., DE BLASIO, M. J., QIN, C. X., JENKINS, A. J., RITCHIE, R. H., MELLOR, K. M. & DELBRIDGE, L. M. D. 2018. Diastolic dysfunction is more apparent in

STZ-induced diabetic female mice, despite less pronounced hyperglycemia. *Sci Rep,* 8**,** 2346.
CHATTOPADHYAY, D. K. & WEBSTER, D. C. 2009. Thermal stability and flame retardancy of polyurethanes. *Progress in Polymer Science,* 34**,** 1068-1133.
CHAUNDHRY, Z. Z., MORRIS, D. L., MOSS, D. R., SIMS, E. K., CHIONG, Y., KONO, T. & EVANS-MOLINA, C. 2013. Streptozotocin is equally diabetogenic whether administered to fed or fasted mice. *Laboratory Animals,* 47**,** 9.
CHEN, H., TERAMURA, Y. & IWATA, H. 2011a. Co-immobilization of urokinase and thrombomodulin on islet surfaces by poly(ethylene glycol)-conjugated phospholipid. *Journal of Controlled Release,* 150**,** 229-234.
CHEN, H., TERAMURA, Y. & IWATA, H. 2011b. Immobilization of anticoagulant-loaded liposomes on cell surfaces by DNA hybridization. *Biomaterials,* 32**,** 7971-7.
CHEN, J.-H., TSAI, B.-H., CHANG, H.-T., CHEN, M.-L., CHEN, Y.-H., JAN, S.-H. & LIU, M.-J. 2010. *Biodegradable Hyaluronic Acid Derivate and Biodegrable Polymeric Micelle Composition*. 10/992,387.
CHEN, J. Q., SZODORAY, P. & ZEHER, M. 2016. Toll-Like Receptor Pathways in Autoimmune Diseases. *Clin Rev Allergy Immunol,* 50**,** 1-17.
CHENG, J. Y., WHITELOCK, J. & POOLE-WARREN, L. 2012a. Syndecan-4 is associated with beta-cells in the pancreas and the MIN6 beta-cell line. *Histochem Cell Biol,* 138**,** 933-44.
CHENG, K., DELGHINGARO-AUGUSTO, V., NOLAN, C. J., TURNER, N., HALLAHAN, N., ANDRIKOPOULOS, S. & GUNTON, J. E. 2012b. High passage MIN6 cells have impaired insulin secretion with impaired glucose and lipid oxidation. *PLoS One,* 7**,** e40868.
CHIARELLI, F., GIANNINI, C. & PRIMAVERA, M. 2019. Prediction and prevention of type 1 diabetes in children. *Clinical pediatric endocrinology : case reports and clinical investigations : official journal of the Japanese Society for Pediatric Endocrinology,* 28**,** 43-57.
CHOH, S. Y., CROSS, D. & WANG, C. 2011. Facile synthesis and characterization of disulfide-cross-linked hyaluronic acid hydrogels for protein delivery and cell encapsulation. *Biomacromolecules,* 12**,** 1126-36.
CHOI, S. C., YOO, M. A., LEE, S. Y., LEE, H. J., SON, D. H., JUNG, J., NOH, I. & KIM, C. W. 2015. Modulation of biomechanical properties of hyaluronic acid hydrogels by crosslinking agents. *J Biomed Mater Res A,* 103**,** 3072-80.
CICCONE, V., ZAZZETTA, M. & MORBIDELLI, L. 2019. Comparison of the Effect of Two Hyaluronic Acid Preparations on Fibroblast and Endothelial Cell Functions Related to Angiogenesis. *Cells,* 8.
CLAYTON JA & COLLINS, F. 2014. Policy: NIH to balance sex in cell and animal studies. *Nature,* 509**,** 1.
CLEGG, T. E., CABORN, D. & MAUFFREY, C. 2013. Viscosupplementation with hyaluronic acid in the treatment for cartilage lesions: a review of current evidence and future directions. *European Journal of Orthopaedic Surgery & Traumatology,* 23**,** 119-124.
COLLINS, M. N. & BIRKINSHAW, C. 2007a. Comparison of the effectiveness of four different crosslinking agents with hyaluronic acid hydrogel films for tisslue-culture applications. *Journal of Applied Polymer Science,* 104**,** 3183-3191.
COLLINS, M. N. & BIRKINSHAW, C. 2007b. Comparison of the effectiveness of four different crosslinking agents with hyaluronic acid hydrogel films for tissue-culture applications. *Journal of Applied Polymer Science,* 104**,** 3183-3191.
COLLINS, M. N. & BIRKINSHAW, C. 2008a. Investigation of the swelling behavior of crosslinked hyaluronic acid films and hydrogels produced using homogeneous reactions. *Journal of Applied Polymer Science,* 109**,** 923-931.
COLLINS, M. N. & BIRKINSHAW, C. 2008b. Physical properties of crosslinked hyaluronic acid hydrogels. *Journal of Materials Science-Materials in Medicine,* 19**,** 3335-3343.
COLLINS, M. N. & BIRKINSHAW, C. 2010. Morphology of crosslinked hyaluronic acid porous hydrogels. *Journal of Applied Polymer Science,* 120**,** 10.

COLLINS, M. N. & BIRKINSHAW, C. 2013a. Hyaluronic acid based scaffolds for tissue engineering-A review. *Carbohydrate Polymers,* 92**,** 1262-1279.
COLLINS, M. N. & BIRKINSHAW, C. 2013b. Hyaluronic acid solutionsA processing method for efficient chemical modification. *Journal of Applied Polymer Science,* 130**,** 145-152.
COLLINS, M. N. B., C. 2010. Morphology of crosslinked hyaluronic acid porous hydrogels. *Journal of Applied Polymer Science,* 120**,** 1040-1049.
COLTON, C. K. 2014. Oxygen supply to encapsulated therapeutic cells. *Adv Drug Deliv Rev,* 67-68**,** 93-110.
COOK, M. J. 1965. *The anatomy of the laboratory mouse,* London, New York,, Academic Press.
CRAWFORD, M. P., SINHA, S., RENAVIKAR, P. S., BORCHERDING, N. & KARANDIKAR, N. J. 2020. CD4 T cell-intrinsic role for the T helper 17 signature cytokine IL-17: Effector resistance to immune suppression. *Proceedings of the National Academy of Sciences,* 117**,** 19408-19414.
CUI, X., XU, H., ZHOU, S., ZHAO, T., LIU, A., GUO, X., TANG, W. & WANG, F. 2009. Evaluation of angiogenic activities of hyaluronan oligosaccharides of defined minimum size. *Life Sci,* 85**,** 573-7.
DA ROCHA FERNANDES, J., OGURTSOVA, K., LINNENKAMP, U., GUARIGUATA, L., SEURING, T., ZHANG, P., CAVAN, D. & MAKAROFF, L. E. 2016. IDF Diabetes Atlas estimates of 2014 global health expenditures on diabetes. *Diabetes Research and Clinical Practice,* 117**,** 48-54.
DA SILVA XAVIER, G. 2018. The Cells of the Islets of Langerhans. *J Clin Med,* 7.
DAJKOVICH, G. & BARKLEY, T. W. 2015. Understanding Insulin Pump Therapy. *Journal of Community Health Nursing,* 32**,** 131-140.
DANG, T. T., THAI, A. V., COHEN, J., SLOSBERG, J. E., SINIAKOWICZ, K., DOLOFF, J. C., MA, M., HOLLISTER-LOCK, J., TANG, K. M., GU, Z., CHENG, H., WEIR, G. C., LANGER, R. & ANDERSON, D. G. 2013. Enhanced function of immuno-isolated islets in diabetes therapy by co-encapsulation with an anti-inflammatory drug. *Biomaterials,* 34**,** 5792-801.
DAVIS, C. L. 2004. Transplant: immunology and treatment of rejection. *American Journal of Kidney Diseases,* 43**,** 1116-1134.
DE TATA, V. 2014. Age-Related Impairment of Pancreatic Beta-Cell Function: Pathophysiological and Cellular Mechanisms. *Frontiers in Endocrinology,* 5.
DE VOS, P., LAZARJANI, H. A., PONCELET, D. & FAAS, M. M. 2014. Polymers in cell encapsulation from an enveloped cell perspective. *Adv Drug Deliv Rev,* 67-68**,** 15-34.
DEL HOYO-GALLEGO, S., PÉREZ-ÁLVAREZ, L., GÓMEZ-GALVÁN, F., LIZUNDIA, E., KURITKA, I., SEDLARIK, V., LAZA, J. M. & VILA-VILELA, J. L. 2016. Construction of antibacterial poly(ethylene terephthalate) films via layer by layer assembly of chitosan and hyaluronic acid. *Carbohydrate Polymers,* 143**,** 35-43.
DEL TORO-ARREOLA, A., ROBLES-MURILLO, A. K., DANERI-NAVARRO, A. & RIVAS-CARRILLO, J. D. 2016. The role of endothelial cells on islet function and revascularization after islet transplantation. *Organogenesis,* 12**,** 28-32.
DELANEY, M. A., KOWALEWSKA, J. & TREUTING, P. M. 2018. 16 - Urinary System. *In:* TREUTING, P. M., DINTZIS, S. M. & MONTINE, K. S. (eds.) *Comparative Anatomy and Histology (Second Edition).* San Diego: Academic Press.
DHANASINGH, A., SALBER, J., MOELLER, M. & GROLL, J. 2010. Tailored hyaluronic acid hydrogels through hydrophilic prepolymer cross-linkers. *Soft Matter,* 6**,** 618-629.
DI, J., YU, J., YE, Y., RANSON, D., JINDAL, A. & GU, Z. 2015. Engineering Synthetic Insulin-Secreting Cells Using Hyaluronic Acid Microgels Integrated with Glucose-Responsive Nanoparticles. *Cellular and Molecular Bioengineering,* 8**,** 445-454.
DOLENSEK, J., RUPNIK, M. S. & STOZER, A. 2015. Structural similarities and differences between the human and the mouse pancreas. *Islets,* 7**,** e1024405.
DONG, H., FAHMY, T. M., METCALFE, S. M., MORTON, S. L., DONG, X., INVERARDI, L., ADAMS, D. B., GAO, W. & WANG, H. 2012. Immuno-isolation of pancreatic islet allografts using

pegylated nanotherapy leads to long-term normoglycemia in full MHC mismatch recipient mice. *PLoS One,* 7**,** e50265.
DREWS, G., KRIPPEIT-DREWS, P. & DUFER, M. 2010. Oxidative stress and beta-cell dysfunction. *Pflugers Archiv-European Journal of Physiology,* 460**,** 703-718.
DUFRANE, D. & GIANELLO, P. 2012. Pig islet for xenotransplantation in human: structural and physiological compatibility for human clinical application. *Transplantation Reviews,* 26**,** 183-188.
EATEMADI, A., DARAEE, H., ZARGHAMI, N., MELAT YAR, H. & AKBARZADEH, A. 2016. Nanofiber: Synthesis and biomedical applications. *Artif Cells Nanomed Biotechnol,* 44**,** 111-21.
EISENBARTH, G. S. 1986. Type I diabetes mellitus. A chronic autoimmune disease. *N Engl J Med,* 314**,** 1360-8.
ERIKSSON, O., SELVARAJU, R., EICH, T., WILLNY, M., BRISMAR, T. B., CARLBOM, L., AHLSTROM, H., TUFVESSON, G., LUNDGREN, T. & KORSGREN, O. 2016. Positron Emission Tomography to Assess the Outcome of Intraportal Islet Transplantation. *Diabetes,* 65**,** 2482-9.
ERLICH, H., VALDES, A. M., NOBLE, J., CARLSON, J. A., VARNEY, M., CONCANNON, P., MYCHALECKYJ, J. C., TODD, J. A., BONELLA, P., FEAR, A. L., LAVANT, E., LOUEY, A., MOONSAMY, P. & TYPE 1 DIABETES GENETICS, C. 2008. HLA DR-DQ haplotypes and genotypes and type 1 diabetes risk: analysis of the type 1 diabetes genetics consortium families. *Diabetes,* 57**,** 1084-92.
ERNST, A. U., BOWERS, D. T., WANG, L.-H., SHARIATI, K., PLESSER, M. D., BROWN, N. K., MEHRABYAN, T. & MA, M. 2019. Nanotechnology in cell replacement therapies for type 1 diabetes. *Advanced drug delivery reviews,* 139**,** 116-138.
ETER, W. A., BOS, D., FRIELINK, C., BOERMAN, O. C., BROM, M. & GOTTHARDT, M. 2015. Graft revascularization is essential for non-invasive monitoring of transplanted islets with radiolabeled exendin. *Sci Rep,* 5**,** 15521.
FAN, C. B., WANG, Y., WANG, Q. P., DU, K. L., WEN, D. G. & OUYANG, J. 2015. Alloantigen-specific T-cell hyporesponsiveness induced by dnIKK2 gene-transfected recipient immature dendritic cells. *Cell Immunol,* 297**,** 100-7.
FEDERATION, I. D. 2015. *IDF Diabetes Atlas*

[Online]. Brussels, Belgium: International Diabetes Federation Available: http://www.diabetesatlas.org [Accessed 27th january 2016].
FEENER, E. P. & KING, G. L. 1997. Vascular dysfunction in diabetes mellitus. *The Lancet,* 350**,** S9-S13.
FENG, L., XIE, N. & ZHONG, J. 2014. Carbon Nanofibers and Their Composites: A Review of Synthesizing, Properties and Applications. *Materials (Basel),* 7**,** 3919-3945.
FERNANDES, P. A. & RAMOS, M. J. 2004. Theoretical insights into the mechanism for thiol/disulfide exchange. *Chemistry-a European Journal,* 10**,** 257-266.
FOLDVARI, M., CHEN, D. W., NAFISSI, N., CALDERON, D., NARSINENI, L. & RAFIEE, A. 2016. Non-viral gene therapy: Gains and challenges of non-invasive administration methods. *J Control Release,* 240**,** 165-190.
FORRESTER, J. V. & LACKIE, J. M. 1981. Effect of hyaluronic acid on neutrophil adhesion. *J Cell Sci,* 50**,** 329-44.
FORSTER, A. J., OAKE, N., ROTH, V., SUH, K. N., MAJEWSKI, J., LEEDER, C. & VAN WALRAVEN, C. 2013. Patient-level factors associated with methicillin-resistant Staphylococcus aureus carriage at hospital admission: a systematic review. *Am J Infect Control,* 41**,** 214-20.
FORTUNE, M. D., GUO, H., BURREN, O., SCHOFIELD, E., WALKER, N. M., BAN, M., SAWCER, S. J., BOWES, J., WORTHINGTON, J., BARTON, A., EYRE, S., TODD, J. A. & WALLACE, C. 2015. Statistical colocalization of genetic risk variants for related autoimmune diseases in the context of common controls. *Nat Genet,* 47**,** 839-46.
FOSTER, D. W. & MCGARRY, J. D. 1983. The Metabolic Derangements and Treatment of Diabetic Ketoacidosis. *New England Journal of Medicine,* 309**,** 159-169.

FRANTZ, C., STEWART, K. M. & WEAVER, V. M. 2010. The extracellular matrix at a glance. *J Cell Sci,* 123**,** 4195-200.

FREDERIKSEN, B., KROEHL, M., LAMB, M. M., SEIFERT, J., BARRIGA, K., EISENBARTH, G. S., REWERS, M. & NORRIS, J. M. 2013. Infant Exposures and Development of Type 1 Diabetes Mellitus The Diabetes Autoimmunity Study in the Young (DAISY). *Jama Pediatrics,* 167**,** 808-815.

FREEDMAN, J. C. 2012. Chapter 3 - Cell Membranes. *In:* SPERELAKIS, N. (ed.) *Cell Physiology Source Book (Fourth Edition).* San Diego: Academic Press.

FUKUDA, Y., AKAGI, T., ASAOKA, T., EGUCHI, H., SASAKI, K., IWAGAMI, Y., YAMADA, D., NODA, T., KAWAMOTO, K., GOTOH, K., KOBAYASHI, S., MORI, M., DOKI, Y. & AKASHI, M. 2018. Layer-by-layer cell coating technique using extracellular matrix facilitates rapid fabrication and function of pancreatic beta-cell spheroids. *Biomaterials,* 160**,** 82-91.

GALLO DE MORAES, A. & SURANI, S. 2019. Effects of diabetic ketoacidosis in the respiratory system. *World journal of diabetes,* 10**,** 16-22.

GANNON, M., KULKARNI, R. N., TSE, H. M. & MAUVAIS-JARVIS, F. 2018. Sex differences underlying pancreatic islet biology and its dysfunction. *Mol Metab,* 15**,** 82-91.

GAO, Y., SUN, Y., YANG, H., QIU, P., CONG, Z., ZOU, Y., SONG, L., GUO, J. & ANASTASSIADES, T. P. 2019. A Low Molecular Weight Hyaluronic Acid Derivative Accelerates Excisional Wound Healing by Modulating Pro-Inflammation, Promoting Epithelialization and Neovascularization, and Remodeling Collagen. *Int J Mol Sci,* 20.

GASPERINI, L., MANO, J. F. & REIS, R. L. 2014. Natural polymers for the microencapsulation of cells. *Journal of The Royal Society Interface,* 11**,** 20140817-20140817.

GATTÁS-ASFURA, K. M., ABUID, N. J., LABRADA, I. & STABLER, C. L. 2020. Promoting Dendrimer Self-Assembly Enhances Covalent Layer-by-Layer Encapsulation of Pancreatic Islets. *ACS Biomaterials Science & Engineering,* 6**,** 2641-2651.

GATTAS-ASFURA, K. M. & STABLER, C. L. 2013. Bioorthogonal Layer-by-Layer Encapsulation of Pancreatic Islets via Hyperbranched Polymers. *Acs Applied Materials & Interfaces,* 5**,** 9964-9974.

GERICH, J. E. 1988. Glucose Counterregulation and Its Impact on Diabetes Mellitus. *Diabetes,* 37**,** 1608-1617.

GHATAK, A., PAUL, P., HAWCUTT, D. B., WHITE, H. D., FURLONG, N. J., SAUNDERS, S., MORRISON, G., LANGRIDGE, P. & WESTON, P. J. 2015. UK service level audit of insulin pump therapy in paediatrics. *Diabet Med,* 32**,** 1652-7.

GHOLIPOURMALEKABADI, M., ZHAO, S., HARRISON, B. S., MOZAFARI, M. & SEIFALIAN, A. M. 2016. Oxygen-Generating Biomaterials: A New, Viable Paradigm for Tissue Engineering? *Trends Biotechnol,* 34**,** 1010-1021.

GIRALDO, J., WEAVER, J. & STABLER, C. 2010. Enhancing Clinical Islet Transplantation through Tissue Engineering Strategies. *Journal of diabetes science and technology,* 4**,** 1238-47.

GJODSBOL, K., CHRISTENSEN, J. J., KARLSMARK, T., JORGENSEN, B., KLEIN, B. M. & KROGFELT, K. A. 2006. Multiple bacterial species reside in chronic wounds: a longitudinal study. *Int Wound J,* 3**,** 225-31.

GOCMEN, G., GONUL, O., OKTAY, N. S., YARAT, A. & GOKER, K. 2015. The antioxidant and anti-inflammatory efficiency of hyaluronic acid after third molar extraction. *J Craniomaxillofac Surg,* 43**,** 1033-7.

GOKILA, S., GOMATHI, T., VIJAYALAKSHMI, K., ALSHARANI, F. A., ANIL, S. & SUDHA, P. N. 2018. Development of 3D scaffolds using nanochitosan/silk-fibroin/hyaluronic acid biomaterials for tissue engineering applications. *International Journal of Biological Macromolecules,* 120**,** 876-885.

GOMEZ-ARISTIZABAL, A., KIM, K. P. & VISWANATHAN, S. 2016. A Systematic Study of the Effect of Different Molecular Weights of Hyaluronic Acid on Mesenchymal Stromal Cell-Mediated Immunomodulation. *PLoS One,* 11**,** e0147868.

GOWER, R. M., BOEHLER, R. M., AZARIN, S. M., RICCI, C. F., LEONARD, J. N. & SHEA, L. D. 2014. Modulation of leukocyte infiltration and phenotype in microporous tissue engineering scaffolds via vector induced IL-10 expression. *Biomaterials,* 35**,** 2024-31.

GRAÇA, M. F. P., MIGUEL, S. P., CABRAL, C. S. D. & CORREIA, I. J. 2020. Hyaluronic acid—Based wound dressings: A review. *Carbohydrate Polymers,* 241**,** 116364.

GRANICKA, L. H., ANTOSIAK-IWAŃSKA, M., GODLEWSKA, E., STRAWSKI, M., SZKLARCZYK, M., MARANOWSKI, B., KOWALEWSKI, C. & WIŚNIEWSK, J. 2011. Conformal Nano-Thin Modified Polyelectrolyte Coatings for Encapsulation of Cells. *Artificial Cells, Blood Substitutes, and Biotechnology,* 39**,** 274-280.

GRAPIN-BOTTON, A. 2005. Ductal cells of the pancreas. *Int J Biochem Cell Biol,* 37**,** 504-10.

GRAS, S., KJER-NIELSEN, L., CHEN, Z., ROSSJOHN, J. & MCCLUSKEY, J. 2011. The structural bases of direct T-cell allorecognition: implications for T-cell-mediated transplant rejection. *Immunology & Cell Biology,* 89**,** 388-395.

GRIESSER, J., HETENYI, G. & BERNKOP-SCHNURCH, A. 2018. Thiolated Hyaluronic Acid as Versatile Mucoadhesive Polymer: From the Chemistry Behind to Product Developments-What Are the Capabilities? *Polymers,* 10.

GU, Z. & YE, Y. 2019. *Methods and compositions related to physiologically responsive microneedle delivery systems*. USA patent application 15/999,770.

GUAN, X. & FIERKE, C. A. 2011. Understanding Protein Palmitoylation: Biological Significance and Enzymology. *Science China. Chemistry,* 54**,** 1888-1897.

GUTIERREZ-ARCELUS, M., RICH, S. S. & RAYCHAUDHURI, S. 2016. Autoimmune diseases - connecting risk alleles with molecular traits of the immune system. *Nat Rev Genet,* 17**,** 160-74.

GWON, K., KIM, E. & TAE, G. 2017. Heparin-hyaluronic acid hydrogel in support of cellular activities of 3D encapsulated adipose derived stem cells. *Acta Biomaterialia,* 49**,** 284-295.

HAGOPIAN, W. A., LERNMARK, A., REWERS, M. J., SIMELL, O. G., SHE, J. X., ZIEGLER, A. G., KRISCHER, J. P. & AKOLKAR, B. 2006. TEDDY- The environmental determinants of diabetes in the young - An observational clinical trial. *Immunology of Diabetes Iv: Progress in Our Understanding,* 1079**,** 320-326.

HALLGREN, R., SAMUELSSON, T., LAURENT, T. C. & MODIG, J. 1989. Accumulation of Hyaluronan (Hyaluronic-Acid) in the Lung in Adult Respiratory-Distress Syndrome. *American Review of Respiratory Disease,* 139**,** 682-687.

HALLMANN, R., ZHANG, X., DI RUSSO, J., LI, L., SONG, J., HANNOCKS, M. J. & SOROKIN, L. 2015. The regulation of immune cell trafficking by the extracellular matrix. *Curr Opin Cell Biol,* 36**,** 54-61.

HAMILTON, J. A., PICCOLI, D. S., CEBON, J., LAYTON, J. E., RATHANASWANI, P., MCCOLL, S. R. & LEIZER, T. 1992. Cytokine Regulation of Colony-Stimulating Factor (Csf) Production in Cultured Human Synovial Fibroblasts .2. Similarities and Differences in the Control of Interleukin-1 Induction of Granulocyte-Macrophage Csf and Granulocyte-Csf Production. *Blood,* 79**,** 1413-1419.

HAN, X., TAO, Y. L., DENG, Y. P., YU, J. W., CAI, J., REN, G. F., SUN, Y. N. & JIANG, G. J. 2017. Metformin ameliorates insulitis in STZ-induced diabetic mice. *PeerJ,* 5**,** e3155.

HAQUE, M. R., JEONG, J. H. & BYUN, Y. 2016. Combination strategy of multi-layered surface camouflage using hyperbranched polyethylene glycol and immunosuppressive drugs for the prevention of immune reactions against transplanted porcine islets. *Biomaterials,* 84**,** 144-56.

HAQUE, M. R., KIM, J., PARK, H., LEE, H. S., LEE, K. W., AL-HILAL, T. A., JEONG, J.-H., AHN, C.-H., LEE, D. S., KIM, S. J. & BYUN, Y. 2017. Xenotransplantation of layer-by-layer encapsulated non-human primate islets with a specified immunosuppressive drug protocol. *Journal of Controlled Release,* 258**,** 10-21.

HARJUTSALO, V., SJOBERG, L. & TUOMILEHTO, J. 2008. Time trends in the incidence of type 1 diabetes in Finnish children: a cohort study. *Lancet,* 371**,** 1777-82.

HARRINGTON, S., OTT, L., KARANU, F., RAMACHANDRAN, K. & STEHNO-BITTEL, L. 2020. A Versatile Microencapsulation Platform for Hyaluronic Acid and Polyethylene Glycol. *Tissue Engineering Part A,* 0**,** null.

HARRINGTON, S., WILLIAMS, J., RAWAL, S., RAMACHANDRAN, K. & STEHNO-BITTEL, L. 2017a. Hyaluronic Acid/Collagen Hydrogel as an Alternative to Alginate for Long-Term Immunoprotected Islet Transplantation. *Tissue Engineering Part A,* 23**,** 1088-1099.

HARRINGTON, S., WILLIAMS, S. J., RAWAL, S., RAMACHANDRAN, K. & STEHNO-BITTEL, L. 2017b. Hyaluronic Acid/Collagen Hydrogel as an Alternative to Alginate for Long-Term Immunoprotected Islet Transplantation. *Tissue Eng Part A*.

HARRIS, L. G. & RICHARDS, R. G. 2004. Staphylococcus aureus adhesion to different treated titanium surfaces. *J Mater Sci Mater Med,* 15**,** 311-4.

HATHOUT, E., CHAN, N. K., TAN, A., SAKATA, N., MACE, J., PEARCE, W., PEVERINI, R., CHINNOCK, R., SOWERS, L. & OBENAUS, A. 2009. In vivo imaging demonstrates a time-line for new vessel formation in islet transplantation. *Pediatr Transplant,* 13**,** 892-7.

HE, H., ZHANG, S., TIGHE, S., SON, J. & TSENG, S. C. G. 2013. Immobilized heavy chain-hyaluronic acid polarizes lipopolysaccharide-activated macrophages toward M2 phenotype. *The Journal of biological chemistry,* 288**,** 25792-25803.

HE, X. W. & MA, N. 2014. An overview of recent advances in quantum dots for biomedical applications. *Colloids and Surfaces B-Biointerfaces,* 124**,** 118-131.

HEGGER, P. S., KUPKA, J., MINSKY, B. B., SCHÄDEL, N., PETRI, N., LASCHAT, S. & BOEHM, H. 2017. Charge Matters: Modulating Secondary Interactions in Hyaluronan Hydrogels. *ChemistrySelect,* 2**,** 7701-7705.

HEINONEN, M. T., MOULDER, R. & LAHESMAA, R. 2015. New Insights and Biomarkers for Type 1 Diabetes: Review for Scandinavian Journal of Immunology. *Scand J Immunol,* 82**,** 244-53.

HELLER, A. & FELDMAN, B. 2008. Electrochemical glucose sensors and their applications in diabetes management. *Chem Rev,* 108**,** 2482-505.

HILAL-DANDAN, R., BRUNTON, L. L. & GOODMAN, L. S. 2014. *Goodman and Gilman's manual of pharmacology and therapeutics, editors Randa Hilal-Dandan, Laurence L. Brunton,* New York, McGraw-Hill.

HILL, A. B., CHEN, M., CHEN, C. K., PFEIFER, B. A. & JONES, C. H. 2016. Overcoming Gene-Delivery Hurdles: Physiological Considerations for Nonviral Vectors. *Trends Biotechnol,* 34**,** 91-105.

HIRSCH, I. B. 2005. Insulin Analogues. *New England Journal of Medicine,* 352**,** 174-183.

HOTAMISLIGIL, G. S. 2017. Inflammation, metaflammation and immunometabolic disorders. *Nature,* 542**,** 177-185.

HSU, H. H., KRACHT, J. K., HARDER, L. E., RUDNIK, K., LINDNER, G., SCHIMEK, K., MARX, U. & PORTNER, R. 2018. A Method for Determination and Simulation of Permeability and Diffusion in a 3D Tissue Model in a Membrane Insert System for Multi-well Plates. *Jove-Journal of Visualized Experiments*.

HUAN, Y., PARK, S. J., GUPTA, K. C., PARK, S. Y. & KANG, I. K. 2017. Slide cover glass immobilized liquid crystal microdroplets for sensitive detection og an IgG antigen. *Royal Society of Chemistry Advances,* 7**,** 14.

HUANG, S., ZHAO, Z., FENG, C., MAYES, E. & YANG, J. 2018. Nanocellulose reinforced P(AAm-co-AAc) hydrogels with improved mechanical properties and biocompatibility. *Composites Part A: Applied Science and Manufacturing,* 112**,** 395-404.

IACOVACCI, V., RICOTTI, L., MENCIASSI, A. & DARIO, P. 2016. The bioartificial pancreas (BAP): Biological, chemical and engineering challenges. *Biochem Pharmacol,* 100**,** 12-27.

IANNACONE, M. 2016. Platelet-mediated modulation of adaptive immunity. *Seminars in Immunology,* 28**,** 555-560.

IBBERSON, C. B., PARLET, C. P., KWIECINSKI, J., CROSBY, H. A., MEYERHOLZ, D. K. & HORSWILL, A. R. 2016. Hyaluronan Modulation Impacts Staphylococcus aureus Biofilm Infection. *Infection and immunity,* 84**,** 1917-1929.

IDF 2015. IDF Diabetes Atlas

7th ed. Brussels, Belgium: International Diabetes Federation

IM, B. H., JEONG, J. H., HAGUE, M. R., LEE, D. Y., AHN, C. H., KIM, J. E. & BYUN, Y. 2013. The effects of 8-arm-PEG-catechol/heparin shielding system and immunosuppressive drug, FK506 on the survival of intraportally allotransplanted islets. *Biomaterials,* 34**,** 2098-2106.

ITAGAKI, T., ARIMA, Y., KUWABARA, R., KITAMURA, N. & IWATA, H. 2015. Interaction between cells and poly(ethylene glycol)-lipid conjugates. *Colloids and Surfaces B-Biointerfaces,* 135**,** 765-773.

IVERSON, N. M., BISKER, G., FARIAS, E., IVANOV, V., AHN, J., WOGAN, G. N. & STRANO, M. S. 2016. Quantitative Tissue Spectroscopy of Near Infrared Fluorescent Nanosensor Implants. *J Biomed Nanotechnol,* 12**,** 1035-47.

JACKSON, S., MAGER, D. R., BHARGAVA, R., ACKERMAN, T., IMES, S., HUBERT, G., KOH, A., SHAPIRO, A. M. & SENIOR, P. A. 2013. Long-term follow-up of hepatic ultrasound findings in subjects with magnetic resonance imaging defined hepatic steatosis following clinical islet transplantation: a case-control study. *Islets,* 5**,** 16-21.

JANSSON, L., BARBU, A., BODIN, B., DROTT, C. J., ESPES, D., GAO, X., GRAPENSPARR, L., KÄLLSKOG, Ö., LAU, J., LILJEBÄCK, H., PALM, F., QUACH, M., SANDBERG, M., STRÖMBERG, V., ULLSTEN, S. & CARLSSON, P.-O. 2016. Pancreatic islet blood flow and its measurement. *Upsala journal of medical sciences,* 121**,** 81-95.

JEONG, J. H., HONG, S. W., HONG, S., YOOK, S., JUNG, Y., PARK, J. B., KHUE, C. D., IM, B. H., SEO, J., LEE, H., AHN, C. H., LEE, D. Y. & BYUN, Y. 2011. Surface camouflage of pancreatic islets using 6-arm-PEG-catechol in combined therapy with tacrolimus and anti-CD154 monoclonal antibody for xenotransplantation. *Biomaterials,* 32**,** 7961-70.

JEONG, J. H., YOOK, S., LEE, H., AHN, C. H., LEE, D. Y. & BYUN, Y. 2013. Effects of surface camouflaged islet transplantation on pathophysiological progression in a db/db type 2 diabetic mouse model. *Biochemical and Biophysical Research Communications,* 433**,** 513-518.

JHA, A. K., MALIK, M. S., FARACH-CARSON, M. C., DUNCAN, R. L. & JIA, X. Q. 2010. Hierarchically structured, hyaluronic acid-based hydrogel matrices via the covalent integration of microgels into macroscopic networks. *Soft Matter,* 6**,** 5045-5055.

JHA, A. K., THARP, K. M., BROWNE, S., YE, J., STAHL, A., YEGHIAZARIANS, Y. & HEALY, K. E. 2016. Matrix metalloproteinase-13 mediated degradation of hyaluronic acid-based matrices orchestrates stem cell engraftment through vascular integration. *Biomaterials,* 89**,** 136-47.

JIA, Y., DUAN, L. & LI, J. B. 2016. Hemoglobin-Based Nanoarchitectonic Assemblies as Oxygen Carriers. *Advanced Materials,* 28**,** 1312-1318.

JIANG, D., LIANG, J. & NOBLE, P. W. 2011. Hyaluronan as an immune regulator in human diseases. *Physiol Rev,* 91**,** 221-64.

JIMENEZ-DALMARONI, M. J., GERSWHIN, M. E. & ADAMOPOULOS, I. E. 2016. The critical role of toll-like receptors--From microbial recognition to autoimmunity: A comprehensive review. *Autoimmun Rev,* 15**,** 1-8.

JODAL, A., SCHIBLI, R. & BEHE, M. 2017. Targets and probes for non-invasive imaging of beta-cells. *European Journal of Nuclear Medicine and Molecular Imaging,* 44**,** 712-727.

JOHNSON, P. R., WHITE, S. A., ROBERTSON, G. S., KOPPIKER, N., BURDEN, A. C., DENNISON, A. R. & LONDON, N. J. 1999. Pancreatic islet autotransplantation combined with total pancreatectomy for the treatment of chronic pancreatitis--the Leicester experience. *J Mol Med (Berl),* 77**,** 130-2.

JOHNSON, S. R., COOPER, M. N., JONES, T. W. & DAVIS, E. A. 2013. Long-term outcome of insulin pump therapy in children with type 1 diabetes assessed in a large population-based case-control study. *Diabetologia,* 56**,** 2392-2400.

JORGENSEN, J. H., PFALLER, M. A. & CARROLL, K. C. 2015. *Manual of Clinical Microbiology*, ASM Press.

JUNG, Y. S., JEONG, J. H., YOOK, S., IM, B. H., SEO, J., HONG, S. W., PARK, J. B., YANG, V. C., LEE, D. Y. & BYUN, Y. 2012. Surface modification of pancreatic islets using heparin-DOPA conjugate and anti-CD154 mAb for the prolonged survival of intrahepatic transplanted islets in a xenograft model. *Biomaterials,* 33**,** 295-303.

KAIDO, T., YEBRA, M., CIRULLI, V. & MONTGOMERY, A. M. 2004. Regulation of human beta-cell adhesion, motility, and insulin secretion by collagen IV and its receptor alpha1beta1. *J Biol Chem,* 279**,** 53762-9.

KAMPERMAN, T., HENKE, S., VISSER, C. W., KARPERIEN, M. & LEIJTEN, J. 2017a. Centering Single Cells in Microgels via Delayed Crosslinking Supports Long-Term 3D Culture by Preventing Cell Escape. *Small,* 13.

KAMPERMAN, T., HENKE, S., ZOETEBIER, B., RUITERKAMP, N., WANG, R., POURAN, B., WEINANS, H., KARPERIEN, M. & LEIJTEN, J. 2017b. Nanoemulsion-induced enzymatic crosslinking of tyramine-functionalized polymer droplets. *J Mater Chem B,* 5**,** 4835-4844.

KANAK, M. A., TAKITA, M., KUNNATHODI, F., LAWRENCE, M. C., LEVY, M. F. & NAZIRUDDIN, B. 2014. Inflammatory Response in Islet Transplantation. *International Journal of Endocrinology,* 2014**,** 451035.

KANG, A., PARK, J., JU, J., JEONG, G. S. & LEE, S. H. 2014. Cell encapsulation via microtechnologies. *Biomaterials,* 35**,** 2651-63.

KANG, L., JIA, W., LI, M., WANG, Q., WANG, C., LIU, Y., WANG, X., JIN, L., JIANG, J., GU, G. & CHEN, Z. 2019. Hyaluronic acid oligosaccharide-modified collagen nanofibers as vascular tissue-engineered scaffold for promoting endothelial cell proliferation. *Carbohydr Polym,* 223**,** 115106.

KAPUSTIN, J. 2008. Latent Autoimmune Diabetes in Adults. *The Journal for Nurse Practitioners,* 4**,** 681-687.

KAWAHARA, T., KIN, T. & SHAPIRO, A. M. 2012. A comparison of islet autotransplantation with allotransplantation and factors elevating acute portal pressure in clinical islet transplantation. *J Hepatobiliary Pancreat Sci,* 19**,** 281-8.

KELLY, S. H., SHORES, L. S., VOTAW, N. L. & COLLIER, J. H. 2017. Biomaterial strategies for generating therapeutic immune responses. *Adv Drug Deliv Rev*.

KENAR, H., OZDOGAN, C. Y., DUMLU, C., DOGER, E., KOSE, G. T. & HASIRCI, V. 2019. Microfibrous scaffolds from poly(l-lactide-co-epsilon-caprolactone) blended with xeno-free collagen/hyaluronic acid for improvement of vascularization in tissue engineering applications. *Mater Sci Eng C Mater Biol Appl,* 97**,** 31-44.

KENDALL, F. E., HEIDELBERGER, M. & DAWSON, M. H. 1937. A SEROLOGICALLY INACTIVE POLYSACCHARIDE ELABORATED BY MUCOID STRAINS OF GROUP A HEMOLYTIC STREPTOCOCCUS. *Journal of Biological Chemistry,* 118**,** 61-69.

KESSLER, L., GEHRKE, S., WINNEFELD, M., HUBER, B., HOCH, E., WALTER, T., WYRWA, R., SCHNABELRAUCH, M., SCHMIDT, M., KUCKELHAUS, M., LEHNHARDT, M., HIRSCH, T. & JACOBSEN, F. 2017. Methacrylated gelatin/hyaluronan-based hydrogels for soft tissue engineering. *J Tissue Eng,* 8**,** 2041731417744157.

KHANG, D. 2015. Real time macrophage migration analysis and associated pro-inflammatory cytokine release on transparent carbon nanotube/polymer composite nano-film. *Nanotechnology,* 26**,** 325101.

KHANMOHAMMADI, M., SAKAI, S., ASHIDA, T. & TAYA, M. 2016. Production of hyaluronic-acid-based cell-enclosing microparticles and microcapsules via enzymatic reaction using a microfluidic system. *Journal of Applied Polymer Science,* 133.

KIM, H.-O., LEE, S. H., NA, W., LIM, J.-W., PARK, G., PARK, C., LEE, H., KANG, A., HAAM, S., CHOI, I., KANG, J.-T. & SONG, D. 2020. Cell-mimic polymersome-shielded islets for long-term immune protection of neonatal porcine islet-like cell clusters. *Journal of Materials Chemistry B,* 8**,** 2476-2482.

KIM, J. C. & TAE, G. 2015. Recent Advances in Cell surface Engineering Focused on Cell Therapy. *Bulletin of the Korean Chemical Society,* 36**,** 59-65.

KIM, J. H., OH, B. J., LEE, H. N., PARK, H. S., PARK, S. G. & PARK, K. S. 2011. Endothelial Colony-Forming Cell Coating of Pig Islets Prevents Xenogeneic Instant Blood-Mediated Inflammatory Reaction. *Cell Transplantation,* 20**,** 1805-1815.

KINASIEWICZ, J., ANTOSIAK-IWANSKA, M. & SABAT, M. 2011. Histomorphometrical Analysis of Porcine Islets of Langerhans. *Transplantation Proceedings,* 43**,** 3105-3106.

KINOSHITA, N., ECHIGO, Y., SHINOHARA, S., GU, Y., MIYAZAKI, J., INOUE, K. & IMAMURA, M. 2001. Regulation of cell proliferation using tissue engineering in MIN6 cells. *Cell Transplant,* 10**,** 473-7.

KITAMURA, N., NAKAI, R., KOHDA, H., FURUTA-OKAMOTO, K. & IWATA, H. 2013. Labeling of islet cells with iron oxide nanoparticles through DNA hybridization for highly sensitive detection by MRI. *Bioorg Med Chem,* 21**,** 7175-81.

KNOPF-MARQUES, H., PRAVDA, M., WOLFOVA, L., VELEBNY, V., SCHAAF, P., VRANA, N. E. & LAVALLE, P. 2016. Hyaluronic Acid and Its Derivatives in Coating and Delivery Systems: Applications in Tissue Engineering, Regenerative Medicine and Immunomodulation. *Adv Healthc Mater,* 5**,** 2841-2855.

KOHI, S., SATO, N., KOGA, A., HIRATA, K., HARUNARI, E. & IGARASHI, Y. 2016. Hyaluromycin, a Novel Hyaluronidase Inhibitor, Attenuates Pancreatic Cancer Cell Migration and Proliferation. *Journal of Oncology,* 2016**,** 9063087.

KONIEV, O. & WAGNER, A. 2015. Developments and recent advancements in the field of endogenous amino acid selective bond forming reactions for bioconjugation (vol 44, pg 5495, 2015). *Chemical Society Reviews,* 44**,** 5743-5743.

KORDONOURI, O., LAUTERBORN, R. & DEISS, D. 2002. Lipohypertrophy in Young Patients With Type 1 Diabetes. *Diabetes Care,* 25**,** 634-634.

KOTA, D. J., WIGGINS, L. L., YOON, N. & LEE, R. H. 2013. TSG-6 Produced by hMSCs Delays the Onset of Autoimmune Diabetes by Suppressing Th1 Development and Enhancing Tolerogenicity. *Diabetes,* 62**,** 2048-2058.

KRISCHER, J. 2007. The environmental determinants of diabetes in the young (TEDDY) study: study design. *Pediatric Diabetes,* 8**,** 286-298.

KRISHNAN, R., ALEXANDER, M., ROBLES, L., FOSTER 3RD, C. E. & LAKEY, J. R. T. 2014. Islet and Stem Cell Encapsulation for Clinical Transplantation. *The Review of Diabetic Studies : RDS,* 11**,** 84-101.

LA PERLE, K. M. D. & DINTZIS, S. M. 2018. 15 - Endocrine System. *In:* TREUTING, P. M., DINTZIS, S. M. & MONTINE, K. S. (eds.) *Comparative Anatomy and Histology (Second Edition).* San Diego: Academic Press.

LAI, J. Y. 2014. Relationship between structure and cytocompatibility of divinyl sulfone cross-linked hyaluronic acid. *Carbohydr Polym,* 101**,** 203-12.

LAM, J., TRUONG, N. F. & SEGURA, T. 2014. Design of cell-matrix interactions in hyaluronic acid hydrogel scaffolds. *Acta Biomaterialia,* 10**,** 1571-1580.

LARSSON, H. E. 2008. *Type 1 Diabetes in Children - Risk Factors and Prediction - Results from the DiPiS study.* Doctoral Doctoral Dissertation, Lund University.

LAURENT, T. C., LAURENT, U. B. & FRASER, J. R. E. 1996. The structure and function of hyaluronan: An overview. *Immunology and Cell Biology,* 74**,** A1-A7.

LAVERNIA, F., ADKINS, S. E. & SHUBROOK, J. H. 2015. Use of oral combination therapy for type 2 diabetes in primary care: Meeting individualized patient goals. *Postgraduate Medicine,* 127**,** 808-817.

LECHLEITNER, M. & HOPPICHLER, F. 2011. Insulin therapy. *Wien Med Wochenschr,* 161**,** 300-4.

LEE, K. Y. & MOONEY, D. J. 2012. Alginate: Properties and biomedical applications. *Progress in Polymer Science,* 37**,** 106-126.

LEE, S. H., HAO, E., SAVINOV, A. Y., GERON, I., STRONGIN, A. Y. & ITKIN-ANSARI, P. 2009. Human beta-Cell Precursors Mature into Functional Insulin-Producing Cells in an Immunoisolation Device: Implications for Diabetes Cell Therapies. *Diabetes,* 58**,** A499-A499.

LEHNINGER, A. L., NELSON, D. L. & COX, M. M. 2013. *Lehninger principles of biochemistry,* New York, W.H. Freeman.
LEITER, E. H. 1982. Multiple low-dose streptozotocin-induced hyperglycemia and insulitis in C57BL mice: influence of inbred background, sex, and thymus. *Proc Natl Acad Sci U S A,* 79**,** 630-4.
LERTKIATMONGKOL, P., LIAO, D., MEI, H., HU, Y. & NEWMAN, P. J. 2016. Endothelial functions of platelet/endothelial cell adhesion molecule-1 (CD31). *Curr Opin Hematol,* 23**,** 253-9.
LEVENE, P. A. & LÓPEZ-SUÁREZ, J. 1918. MUCINS AND MUCOIDS. *Journal of Biological Chemistry,* 36**,** 105-126.
LI, X., MENG, Q. & ZHANG, L. 2018. The Fate of Allogeneic Pancreatic Islets following Intraportal Transplantation: Challenges and Solutions. *Journal of Immunology Research,* 2018**,** 2424586.
LI, Y., NAGIRA, T. & TSUCHIYA, T. 2006. The effect of hyaluronic acid on insulin secretion in HIT-T15 cells through the enhancement of gap-junctional intercellular communications. *Biomaterials,* 27**,** 1437-43.
LI, Y., XUE, W., LIU, H., FAN, P., WANG, X., DING, X., TIAN, X., FENG, X., PAN, X., ZHENG, J., TIAN, P., DING, C. & FAN, X. 2013. Combined strategy of endothelial cells coating, Sertoli cells coculture and infusion improves vascularization and rejection protection of islet graft. *PLoS One,* 8**,** e56696.
LIGGITT, D. & DINTZIS, S. M. 2018. 14 - Pancreas. *In:* TREUTING, P. M., DINTZIS, S. M. & MONTINE, K. S. (eds.) *Comparative Anatomy and Histology (Second Edition).* San Diego: Academic Press.
LIGHT, J. & TUCKER, M. 2013. Simultaneous pancreas kidney transplants in diabetic patients with end-stage renal disease: 20 year experience. *Clinical Transplantation,* 27**,** 8.
LIM, D. K., WYLIE, R. G., LANGER, R. & KOHANE, D. S. 2016. Selective binding of C-6 OH sulfated hyaluronic acid to the angiogenic isoform of VEGF(165). *Biomaterials,* 77**,** 130-138.
LIM, F. & SUN, A. M. 1980. Microencapsulated islets as bioartificial endocrine pancreas. *Science (New York, N.Y.),* 210**,** 908-910.
LIU, H. Q., TANG, W., LI, C., LV, P. L., WANG, Z., LIU, Y. L., ZHANG, C. L., BAO, Y., CHEN, H. Y., MENG, X. Y., SONG, Y., XIA, X. L., PAN, F., CUI, D. X. & SHI, Y. Q. 2015. CdSe/ZnS Quantum Dots-Labeled Mesenchymal Stem Cells for Targeted Fluorescence Imaging of Pancreas Tissues and Therapy of Type 1 Diabetic Rats. *Nanoscale Research Letters,* 10**,** 1-12.
LIU, L., HE, H. & LIU, J. 2019a. Advances on Non-Genetic Cell Membrane Engineering for Biomedical Applications. *Polymers,* 11**,** 2017.
LIU, Y., WANG, Y., YANG, J., ZHANG, H. & GAN, L. 2019b. Cationized hyaluronic acid coated spanlastics for cyclosporine A ocular delivery: Prolonged ocular retention, enhanced corneal permeation and improved tear production. *Int J Pharm,* 565**,** 133-142.
LOW, G., JAREMKO, J. L. & LOMAS, D. J. 2015. Extravascular complications following abdominal organ transplantation. *Clin Radiol,* 70**,** 898-908.
LUAN, N. M., TERAMURA, Y. & IWATA, H. 2011. Layer-by-layer co-immobilization of soluble complement receptor 1 and heparin on islets. *Biomaterials,* 32**,** 6487-92.
LUDWIG, B. & LUDWIG, S. 2015. Transplantable bioartificial pancreas devices: current status and future prospects. *Langenbecks Archives of Surgery,* 400**,** 531-540.
MADOFF, D. C., GABA, R. C., WEBER, C. N., CLARK, T. W. & SAAD, W. E. 2016. Portal Venous Interventions: State of the Art. *Radiology,* 278**,** 333-53.
MAEDE, L. T. & RUSHTON, W. E. 2013. Optimizing Insulin Pump. *The Diabetes Educator,* 39**,** 841-847.
MAFFI, P. & SECCHI, A. 2015. Clinical results of islet transplantation. *Pharmacological Research,* 98**,** 86-91.
MALOSIO, M. L., ESPOSITO, A., BRIGATTI, C., PALMISANO, A., PIEMONTI, L., NANO, R., MAFFI, P., DE COBELLI, F., DEL MASCHIO, A. & SECCHI, A. 2015. MR imaging monitoring of

iron-labeled pancreatic islets in a small series of patients: islet fate in successful, unsuccessful, and autotransplantation. *Cell Transplant,* 24**,** 2285-96.
MANGINO, M., ROEDERER, M., BEDDALL, M. H., NESTLE, F. O. & SPECTOR, T. D. 2017. Innate and adaptive immune traits are differentially affected by genetic and environmental factors. *Nat Commun,* 8**,** 13850.
MARCHIOLI, G., ZELLNER, L., OLIVEIRA, C., ENGELSE, M., KONING, E., MANO, J., KARPERIEN, APELDOORN, A. V. & MORONI, L. 2017. Layered PEGDA hydrogel for islet of Langerhans encapsulation and improvement of vascularization. *J Mater Sci Mater Med,* 28**,** 195.
MARÍN-PEÑALVER, J. J., MARTÍN-TIMÓN, I., SEVILLANO-COLLANTES, C. & DEL CAÑIZO-GÓMEZ, F. J. 2016. Update on the treatment of type 2 diabetes mellitus. *World journal of diabetes,* 7**,** 354-395.
MARKOVITSI, D., GUSTAVSSON, T. & BANYASZ, A. 2010. Absorption of UV radiation by DNA: Spatial and temporal features. *Mutation Research-Reviews in Mutation Research,* 704**,** 21-28.
MARREN, K. 2011. Dimethyl Sulfoxide: An Effective Penetration Enhancer for Topical Administration of NSAIDs. *Physician and Sportsmedicine,* 39**,** 75-82.
MATHIEU, C., GILLARD, P. & BENHALIMA, K. 2017. Insulin analogues in type 1 diabetes mellitus: getting better all the time. *Nature Reviews Endocrinology,* 13**,** 385-399.
MAULUCCI, G., COHEN, O., DANIEL, B., SANSONE, A., PETROPOULOU, P. I., FILOU, S., SPYRIDONIDIS, A., PANI, G., DE SPIRITO, M., CHATGILIALOGLU, C., FERRERI, C., KYPREOS, K. E. & SASSON, S. 2016. Fatty acid-related modulations of membrane fluidity in cells: detection and implications. *Free Radic Res,* 50**,** S40-S50.
MCCALL, M. & SHAPIRO, A. M. J. 2012. Update on Islet Transplantation. *Cold Spring Harbor Perspectives in Medicine,* 2.
MCCRIMMON, R. J. & SHERWIN, R. S. 2010. Hypoglycemia in type 1 diabetes. *Diabetes,* 59**,** 2333-2339.
MEDAROVA, Z., VALLABHAJOSYULA, P., TENA, A., EVGENOV, N., PANTAZOPOULOS, P., TCHIPASHVILI, V., WEIR, G., SACHS, D. & MOORE, A. 2009. In vivo imaging of autologous islet grafts in the liver and under the kidney capsule in non-human primates. *Transplantation,* 87**,** 1659-66.
MERANI, S., TOSO, C., EMAMAULLEE, J. & SHAPIRO, A. M. 2008a. Optimal implantation site for pancreatic islet transplantation. *Br J Surg,* 95**,** 1449-61.
MERANI, S., TOSO, C., EMAMAULLEE, J. & SHAPIRO, A. M. J. 2008b. Optimal implantation site for pancreatic islet transplantation. *British Journal of Surgery,* 95**,** 1449-1461.
MERI, S. & PANGBURN, M. K. 1994. Regulation of Alternative Pathway Complement Activation by Glycosaminoglycans - Specificity of the Polyanion Binding-Site on Factor-H. *Biochemical and Biophysical Research Communications,* 198**,** 52-59.
MEYER, K. & PALMER, J. W. 1934. THE POLYSACCHARIDE OF THE VITREOUS HUMOR. *Journal of Biological Chemistry,* 107**,** 629-634.
MICUCCI, C., ORCIARI, S. & CATALANO, A. 2014. Hyperglycemia promotes K-Ras-induced lung tumorigenesis through BASCs amplification. *PLoS One,* 9**,** e105550.
MIHAJLOVIC, M., MIHAJLOVIC, M., DANKERS, P. Y. W., MASEREEUW, R. & SIJBESMA, R. P. 2019. Carbon Nanotube Reinforced Supramolecular Hydrogels for Bioapplications. *Macromolecular Bioscience,* 19**,** 1800173.
MITCHELL, D. H. & HOWDEN, B. P. 2005. Diagnosis and management of Staphylococcus aureus bacteraemia. *Intern Med J,* 35 Suppl 2**,** S17-24.
MOBERG, L., KORSGREN, O. & NILSSON, B. 2005. Neutrophilic granulocytes are the predominant cell type infiltrating pancreatic islets in contact with ABO-compatible blood. *Clin Exp Immunol,* 142**,** 125-31.
MOHANTY, R. & DAS, S. 2017. Inhaled Insulin - Current Direction of Insulin Research. *Journal of Clinical and Diagnostic Research,* 11**,** OE01-OE02.

NAFEA, E. H., MARSON, A., POOLE-WARREN, L. A. & MARTENS, P. J. 2011a. Immunoisolating semi-permeable membranes for cell encapsulation: focus on hydrogels. *J Control Release,* 154**,** 110-22.

NAFEA, E. H., POOLE-WARREN, A. M. L. A. & MARTENS, P. J. 2011b. Immunoisolating semi-permeable membranes for cell encapsulation: Focus on hydrogels. *Journal of Controlled Release.*

NAFTANEL, M. A. & HARLAN, D. M. 2005. Pancreatic Islet Transplantation. *PLOS Medicine,* 1**,** e58.

NAGARAJU, S., BOTTINO, R., WIJKSTROM, M., TRUCCO, M. & COOPER, D. K. C. 2015. Islet xenotransplantation: what is the optimal age of the islet-source pig? *Xenotransplantation,* 22**,** 7-19.

NASREEN, N., MOHAMMED, K. A., HARDWICK, J., VAN HORN, R. D., SANDERS, K., KATHURIA, H., LOGHMANI, F. & ANTONY, V. B. 2002. Low molecular weight hyaluronan induces malignant mesothelioma cell (MMC) proliferation and haptotaxis: role of CD44 receptor in MMC proliferation and haptotaxis. *Oncol Res,* 13**,** 71-8.

NATIVIDAD-DIAZ, S. L., BROWNE, S., JHA, A. K., MA, Z., HOSSAINY, S., KUROKAWA, Y. K., GEORGE, S. C. & HEALY, K. E. 2019. A combined hiPSC-derived endothelial cell and in vitro microfluidic platform for assessing biomaterial-based angiogenesis. *Biomaterials,* 194**,** 73-83.

NI, Y. L., TANG, Z. R., CAO, W. X., LIN, H., FAN, Y. J., GUO, L. K. & ZHANG, X. D. 2015. Tough and elastic hydrogel of hyaluronic acid and chondroitin sulfate as potential cell scaffold materials. *International Journal of Biological Macromolecules,* 74**,** 367-375.

NICHOLLS, A. & PARTRIDGE, H. L. 2015. An introduction to insulin pump therapy. *Prescriber***,** 11-14.

NUSGENS, B. V. 2010. [Hyaluronic acid and extracellular matrix: a primitive molecule?]. *Ann Dermatol Venereol,* 137 Suppl 1**,** S3-8.

OHKAWARA, Y., TAMURA, G., IWASAKI, T., TANAKA, A., KIKUCHI, T. & SHIRATO, K. 2000. Activation and transforming growth factor-beta production in eosinophils by hyaluronan. *American Journal of Respiratory Cell and Molecular Biology,* 23**,** 444-451.

OLIVARES, C. N., ALANIZ, L. D., MENGER, M. D., BARANAO, R. I., LASCHKE, M. W. & MERESMAN, G. F. 2016. Inhibition of Hyaluronic Acid Synthesis Suppresses Angiogenesis in Developing Endometriotic Lesions. *PLoS One,* 11**,** e0152302.

OLIVEIRA, M. B., HATAMI, J. & MANO, J. F. 2016. Coating Strategies Using Layer-by-layer Deposition for Cell Encapsulation. *Chemistry-an Asian Journal,* 11**,** 1753-1764.

OLIVEIRA, R. L., CHAGASTELLES, P. C., SESTERHEIM, P. & PRANKE, P. 2017. In Vivo Immunogenic Response to Allogeneic Mesenchymal Stem Cells and the Role of Preactivated Mesenchymal Stem Cells Cotransplanted with Allogeneic Islets. *Stem Cells Int,* 2017**,** 9824698.

OPDENAKKER, G., PROOST, P. & VAN DAMME, J. 2016. Microbiomic and Posttranslational Modifications as Preludes to Autoimmune Diseases. *Trends Mol Med,* 22**,** 746-57.

ORGANIZATION, W. H. 2011. Use of Glycated Haemoglobin (HbA1c) in the Diagnosis of Diabetes Mellitus *In:* WHO (ed.). Switzerland: Geneva: Word Health Organization.

OWEN, O. E., TRAPP, V. E., SKUTCHES, C. L., MOZZOLI, M. A., HOELDTKE, R. D., BODEN, G. & REICHARD, G. A. 1982. Acetone Metabolism During Diabetic Ketoacidosis. *Diabetes,* 31**,** 242-248.

OWEN, R. J., RYAN, E. A., O'KELLY, K., LAKEY, J. R., MCCARTHY, M. C., PATY, B. W., BIGAM, D. L., KNETEMAN, N. M., KORBUTT, G. S., RAJOTTE, R. V. & SHAPIRO, A. M. 2003. Percutaneous transhepatic pancreatic islet cell transplantation in type 1 diabetes mellitus: radiologic aspects. *Radiology,* 229**,** 165-70.

PAGLIUCA, F. W. & MELTON, D. A. 2013. How to make a functional β-cell. *Development,* 140**,** 2472-2483.

PALUMBO, F. S., DI STEFANO, M., PICCIONELLO, A. P., FIORICA, C., PITARRESI, G., PIBIRI, I., BUSCEMI, S. & GIAMMONA, G. 2014. Perfluorocarbon functionalized hyaluronic acid derivatives as oxygenating systems for cell culture. *Rsc Advances,* 4**,** 22894-22901.

PANDEY, M. S. & WEIGEL, P. H. 2014. Hyaluronic acid receptor for endocytosis (HARE)-mediated endocytosis of hyaluronan, heparin, dermatan sulfate, and acetylated low density lipoprotein (AcLDL), but not chondroitin sulfate types A, C, D, or E, activates NF-kappaB-regulated gene expression. *J Biol Chem,* 289**,** 1756-67.

PARDUE, E. L., IBRAHIM, S. & RAMAMURTHI, A. 2008. Role of hyaluronan in angiogenesis and its utility to angiogenic tissue engineering. *Organogenesis,* 4**,** 203-14.

PARK, D., KIM, Y., KIM, H., KIM, K., LEE, Y. S., CHOE, J., HAHN, J. H., LEE, H., JEON, J., CHOI, C., KIM, Y. M. & JEOUNG, D. 2012a. Hyaluronic acid promotes angiogenesis by inducing RHAMM-TGFbeta receptor interaction via CD44-PKCdelta. *Mol Cells,* 33**,** 563-74.

PARK, K. M., YANG, J. A., JUNG, H., YEOM, J., PARK, J. S., PARK, K. H., HOFFMAN, A. S., HAHN, S. K. & KIM, K. 2012b. In Situ Supramolecular Assembly and Modular Modification of Hyaluronic Acid Hydrogels for 3D Cellular Engineering. *Acs Nano,* 6**,** 2960-2968.

PARK, S. Y., KIM, J., KIM, B. W., WANG, H. J., KIM, S. S., CHEONG, J. Y., CHO, S. W. & WON, J. H. 2014. Embolization of percutaneous transhepatic portal venous access tract with N-butyl cyanoacrylate. *British Journal of Radiology,* 87.

PATTERSON, C., GUARIGUATA, L., DAHLQUIST, G., SOLTESZ, G., OGLE, G., SILINK, M. & ATLAS, I. D. 2014. Diabetes in the young - a global view and worldwide estimates of numbers of children with type 1 diabetes. *Diabetes Research and Clinical Practice,* 103**,** 161-175.

PATTERSON, C. C., DAHQUIST, G. G., GYURUS, E., GREEN, A., SOLTESZ, G. & GRP, E. S. 2009. Incidence trends for childhood type 1 diabetes in Europe during 1989-2003 and predicted new cases 2005-20: a multicentre prospective registration study. *Lancet,* 373**,** 2027-2033.

PEDRAZA, E., CORONEL, M. M., FRAKER, C. A., RICORDI, C. & STABLER, C. L. 2012. Preventing hypoxia-induced cell death in beta cells and islets via hydrolytically activated, oxygen-generating biomaterials. *Proceedings of the National Academy of Sciences of the United States of America,* 109**,** 4245-4250.

PENG, H. T., HUANG, H., PANG, N. S., CHABONNEAU, S. & BLOSTEIN, M. 2010. Pegylation of Melittin: Structural Characterization and Hemostatic Effects. *Journal of Bioactive and Compatible Polymers,* 25.

PENNO, M. A., COUPER, J. J., CRAIG, M. E., COLMAN, P. G., RAWLINSON, W. D., COTTERILL, A. M., JONES, T. W., HARRISON, L. C. & GROUP, E. S. 2013. Environmental determinants of islet autoimmunity (ENDIA): a pregnancy to early life cohort study in children at-risk of type 1 diabetes. *BMC Pediatr,* 13**,** 124.

PEPELS, M., FILOT, I., KLUMPERMAN, B. & GOOSSENS, H. 2013. Self-healing systems based on disulfide-thiol exchange reactions. *Polymer Chemistry,* 4**,** 4955-4965.

PÉREZ-ÁLVAREZ, L., RUIZ-RUBIO, L., AZUA, I., BENITO, V., BILBAO, A. & VILAS-VILELA, J. L. 2019. Development of multiactive antibacterial multilayers of hyaluronic acid and chitosan onto poly(ethylene terephthalate). *European Polymer Journal,* 112**,** 31-37.

PERNG, C. K., WANG, Y. J., TSI, C. H. & MA, H. 2011. In vivo angiogenesis effect of porous collagen scaffold with hyaluronic acid oligosaccharides. *J Surg Res,* 168**,** 9-15.

PEROGLIO, M., GRAD, S., MORTISEN, D., SPRECHER, C. M., ILLIEN-JUNGER, S., ALINI, M. & EGLIN, D. 2012. Injectable thermoreversible hyaluronan-based hydrogels for nucleus pulposus cell encapsulation. *Eur Spine J,* 21 Suppl 6**,** S839-49.

PHANER-GOUTORBE, M., DUGAS, V., CHEVOLOT, Y. & SOUTEYRAND, E. 2011. Silanization of silica and glass slides for DNA microarrays by impregnation and gas phase protocol: A comparative study. *Materials Science and Engineering: C,* 31**,** 7.

PHELPS, E. A., TEMPLEMAN, K. L., THULE, P. M. & GARCIA, A. J. 2015. Engineered VEGF-releasing PEG-MAL hydrogel for pancreatic islet vascularization. *Drug Deliv Transl Res,* 5**,** 125-36.

PIRNAZAR, P., WOLINSKY, L., NACHNANI, S., HAAKE, S., PILLONI, A. & BERNARD, G. W. 1999. Bacteriostatic Effects of Hyaluronic Acid. *Journal of Periodontology,* 70**,** 370-374.

PISKO, E. J., TURNER, R. A., SODERSTROM, L. P., PANETTI, M., FOSTER, S. L. & TREADWAY, W. J. 1983. Inhibition of neutrophil phagocytosis and enzyme release by hyaluronic acid. *Clin Exp Rheumatol,* 1**,** 41-4.

PLESNER, A., LISTON, P., TAN, R., KORNELUK, R. G. & VERCHERE, C. B. 2005. The X-Linked Inhibitor of Apoptosis Protein Enhances Survival of Murine Islet Allografts. *Diabetes,* 54**,** 2533.

POLDERVAART, M. T., GOVERSEN, B., DE RUIJTER, M., ABBADESSA, A., MELCHELS, F. P. W., ONER, F. C., DHERT, W. J. A., VERMONDEN, T. & ALBLAS, J. 2017. 3D bioprinting of methacrylated hyaluronic acid (MeHA) hydrogel with intrinsic osteogenicity. *Plos One,* 12.

QIAN, J. M., XU, M. H., SUO, A. L., XU, W. J., LIU, T., LIU, X. F., YAO, Y. & WANG, H. J. 2015. Folate-decorated hydrophilic three-arm star-block terpolymer as a novel nanovehicle for targeted co-delivery of doxorubicin. and Bcl-2 siRNA in breast cancer therapy. *Acta Biomaterialia,* 15**,** 102-116.

QUINTANILLA, R. H., ASPRER, J. S. T., VAZ, C., TANAVDE, V. & LAKSHMIPATHY, U. 2014. CD44 Is a Negative Cell Surface Marker for Pluripotent Stem Cell Identification during Human Fibroblast Reprogramming. *Plos One,* 9.

RAMASAMY, R., YAN, S. F. & SCHMIDT, A. M. 2006. Glycation and RAGE: Common Links in the Pathogenesis of Microvascular and Macrovascular Complications of Diabetes. *CANADIAN JOURNAL OF DIABETES,* 30**,** 422-429.

RAYAHIN, J. E., BUHRMAN, J. S., ZHANG, Y., KOH, T. J. & GEMEINHART, R. A. 2015. High and low molecular weight hyaluronic acid differentially influence macrophage activation. *ACS Biomater Sci Eng,* 1**,** 481-493.

RESNIKOFF, S., PASCOLINI, D., ETYA'ALE, D., KOCUR, I., PARARAJASEGARAM, R., POKHAREL, G. P. & MARIOTTI, S. P. 2004. Global data on visual impairment in the year 2002. *Bulletin of the World Health Organization,* 82**,** 844-851.

RHEE, S. Y., KIM, H. J., KO, S. H., HUR, K. Y., KIM, N. H., MOON, M. K., PARK, S. O., LEE, B. W., CHOI, K. M., KIM, J. H. & COMMITTEE OF CLINICAL PRACTICE GUIDELINE OF KOREAN DIABETES, A. 2017. Monotherapy in Patients with Type 2 Diabetes Mellitus. *Diabetes & metabolism journal,* 41**,** 349-356.

ROBERTSON, M. & HAYES, P. 2015. Management of portal hypertension, Budd–Chiari syndrome and portal vein thrombosis. *Medicine,* 43**,** 5.

RODELL, C. B., KAMINSKI, A. L. & BURDICK, J. A. 2013. Rational design of network properties in guest-host assembled and shear-thinning hyaluronic acid hydrogels. *Biomacromolecules,* 14**,** 4125-34.

ROEP, B. O. 2020. Improving Clinical Islet Transplantation Outcomes. *Diabetes Care,* 43**,** 698.

ROMANÒ, C. L., DE VECCHI, E., BORTOLIN, M., MORELLI, I. & DRAGO, L. 2017. Hyaluronic Acid and Its Composites as a Local Antimicrobial/Antiadhesive Barrier. *Journal of bone and joint infection,* 2**,** 63-72.

ROSALES, A. M., RODELL, C. B., CHEN, M. H., MORROW, M. G., ANSETH, K. S. & BURDICK, J. A. 2018. Reversible Control of Network Properties in Azobenzene-Containing Hyaluronic Acid-Based Hydrogels. *Bioconjug Chem*.

ROSALES, A. M., VEGA, S. L., DELRIO, F. W., BURDICK, J. A. & ANSETH, K. S. 2017. Hydrogels with Reversible Mechanics to Probe Dynamic Cell Microenvironments. *Angew Chem Int Ed Engl,* 56**,** 12132-12136.

RUPPERT, S. M., HAWN, T. R., ARRIGONI, A., WIGHT, T. N. & BOLLYKY, P. L. 2014. Tissue integrity signals communicated by high-molecular weight hyaluronan and the resolution of inflammation. *Immunol Res,* 58**,** 186-92.

RYLE, A. P., SANGER, F., SMITH, L. F. & KITAI, R. 1955. The disulphide bonds of insulin. *Biochem J,* 60**,** 541-56.

SAKATA, N., YOSHIMATSU, G. & KODAMA, S. 2019. Development and Characteristics of Pancreatic Epsilon Cells. *Int J Mol Sci,* 20.

SAKATA, N., YOSHIMATSU, G., TSUCHIYA, H., EGAWA, S. & UNNO, M. 2012. Animal Models of Diabetes Mellitus for Islet Transplantation. *Experimental Diabetes Research*.

SALESA, B., LLORENS-GÁMEZ, M. & SERRANO-AROCA, Á. 2020. Study of 1D and 2D Carbon Nanomaterial in Alginate Films. *Nanomaterials (Basel),* 10.

SANGER, F., THOMPSON, E. O. & KITAI, R. 1955. The amide groups of insulin. *Biochem J,* 59**,** 509-18.

SCHANTE, C. E., ZUBER, G., HERLIN, C. & VANDAMME, T. F. 2011. Chemical modifications of hyaluronic acid for the synthesis of derivatives for a broad range of biomedical applications. *Carbohydrate Polymers,* 85**,** 469-489.

SCHARP, D. W. & MARCHETTI, P. 2014. Encapsulated islets for diabetes therapy: history, current progress, and critical issues requiring solution. *Adv Drug Deliv Rev,* 67-68**,** 35-73.

SCHUETZ, C. & MARKMANN, J. F. 2015. Immunogenicity of beta-cells for autologous transplantation in type 1 diabetes. *Pharmacological Research,* 98**,** 60-68.

SCOZZI, D., IBRAHIM, M., MENNA, C., KRUPNICK, A. S., KREISEL, D. & GELMAN, A. E. 2017. The Role of Neutrophils in Transplanted Organs. *Am J Transplant,* 17**,** 328-335.

SERRA, R., GRANDE, R., BUTRICO, L., ROSSI, A., SETTIMIO, U. F., CAROLEO, B., AMATO, B., GALLELLI, L. & DE FRANCISCIS, S. 2015. Chronic wound infections: the role of Pseudomonas aeruginosa and Staphylococcus aureus. *Expert Rev Anti Infect Ther,* 13**,** 605-13.

SHAKYA, S., WANG, Y., MACK, J. A. & MAYTIN, E. V. 2015. Hyperglycemia-Induced Changes in Hyaluronan Contribute to Impaired Skin Wound Healing in Diabetes: Review and Perspective. *Int J Cell Biol,* 2015**,** 701738.

SHAPIRO, A. M. J., LAKEY, J. R. T., RYAN, E. A., KORBUTT, G. S., TOTH, E., WARNOCK, G. L., KNETEMAN, N. M. & RAJOTTE, R. V. 2000. Islet transplantation in seven patients with type 1 diabetes mellitus using a glucocorticoid-free immunosuppressive regimen. *New England Journal of Medicine,* 343**,** 230-238.

SHAPIRO, A. M. J., RICORDI, C., HERING, B. J., AUCHINCLOSS, H., LINDBLAD, R., ROBERTSON, P., SECCHI, A., BRENDEL, M. D., BERNEY, T., BRENNAN, D. C., CAGLIERO, E., ALEJANDRO, R., RYAN, E. A., DIMERCURIO, B., MOREL, P., POLONSKY, K. S., REEMS, J. A., BRETZEL, R. G., BERTUZZI, F., FROUD, T., KANDASWAMY, R., SUTHERLAND, D. E. R., EISENBARTH, G., SEGAL, M., PREIKSAITIS, J., KORBUTT, G. S., BARTON, F. B., VIVIANO, L., SEYFERT-MARGOLIS, V., BLUESTONE, J. & LAKEY, J. R. T. 2006. International trial of the edmonton protocol for islet transplantation. *New England Journal of Medicine,* 355**,** 1318-1330.

SHIMOJO, A. A., PIRES, A. M., LICHY, R., RODRIGUES, A. A. & SANTANA, M. H. 2015. The crosslinking degree controls the mechanical, rheological, and swelling properties of hyaluronic acid microparticles. *J Biomed Mater Res A,* 103**,** 730-7.

SHU, X. Z., LIU, Y., LUO, Y., ROBERTS, M. C. & PRESTWICH, G. D. 2002. Disulfide cross-linked hyaluronan hydrogels. *Biomacromolecules,* 3**,** 1304-11.

SILVA, J. M., REIS, R. L. & MANO, J. F. 2016a. Biomimetic Extracellular Environment Based on Natural Origin Polyelectrolyte Multilayers. *Small,* 12**,** 4308-4342.

SILVA, L. P., PIRRACO, R. P., SANTOS, T. C., NOVOA-CARBALLAL, R., CERQUEIRA, M. T., REIS, R. L., CORRELO, V. M. & MARQUES, A. P. 2016b. Neovascularization Induced by the Hyaluronic Acid-Based Spongy-Like Hydrogels Degradation Products. *ACS Appl Mater Interfaces,* 8**,** 33464-33474.

SKELIN, M., RUPNIK, M. & CENCIC, A. 2010. Pancreatic beta cell lines and their applications in diabetes mellitus research. *ALTEX,* 27**,** 105-13.

SKRZYPEK, K., GROOT NIBBELINK, M., VAN LENTE, J., BUITINGA, M., ENGELSE, M. A., DE KONING, E. J. P., KARPERIEN, M., VAN APELDOORN, A. & STAMATIALIS, D. 2017.

Pancreatic islet macroencapsulation using microwell porous membranes. *Scientific reports,* 7**,** 9186-9186.
SMEDS, K., PFISTER-SERRES, A., HATCHELL, D. & GRINSTAFF, M. 1999. Synthesis of a novel polysaccharide hydrogel. *Journal of MACROMOLECULAR SCIENCE—PURE AND APPLIED CHEMISTRY,* 36**,** 981-989.
SMETS, Y. F. C., WESTENDORP, R. G. J., VAN DER PIJL, J. W., DE CHARRO, F. T., RINGERS, J., DE FIJTER, J. W. & LEMKES, H. H. P. J. 1999. Effect of simultaneous pancreas-kidney transplantation on mortality of patients with type-1 diabetes mellitus and end-stage renal failure. *The Lancet,* 353**,** 1915-1919.
SONG, J. E., KIM, M. J., YOON, H., YOO, H., LEE, Y. J., KIM, H. N., LEE, D., YUK, S. H. & KHANG, G. 2013. Effect of hyaluronic acid (HA) in a HA/PLGA scaffold on annulus fibrosus regeneration: In vivo tests. *Macromolecular Research,* 21**,** 1075-1082.
SONG, K., WU, Q., ZHANG, Z., REN, S., LEI, T., NEGULESCU, II & ZHANG, Q. 2015. Porous Carbon Nanofibers from Electrospun Biomass Tar/Polyacrylonitrile/Silver Hybrids as Antimicrobial Materials. *ACS Appl Mater Interfaces,* 7**,** 15108-16.
SONG, S. & ROY, S. 2016. Progress and challenges in macroencapsulation approaches for type 1 diabetes (T1D) treatment: Cells, biomaterials, and devices. *Biotechnology and bioengineering,* 113**,** 1381-1402.
SONKER, A. K., BELAY, M., RATHORE, K., JAHAN, K., VERMA, S., RAMANATHAN, G. & VERMA, V. 2018a. Crosslinking of agar by diisocyanates. *Carbohydrate Polymers,* 202**,** 454-460.
SONKER, A. K., BELAY, M., RATHORE, K., JAHAN, K., VERMA, S., RAMANATHAN, G. & VERMA, V. 2018b. Crosslinking of agar by diisocyanates. *Carbohydr Polym,* 202**,** 454-460.
SORELLE, J. A., KANAK, M. A., ITOH, T., HORTON, J. M., NAZIRUDDIN, B. & KANE, R. R. 2015. Comparison of surface modification chemistries in mouse, porcine, and human islets. *J Biomed Mater Res A,* 103**,** 869-77.
SOROKIN, L. 2010. The impact of the extracellular matrix on inflammation. *Nat Rev Immunol,* 10**,** 712-23.
SOUZA, Y. E. D. M., CHAIB, E., LACERDA, P. G., CRESCENZI, A., BERNAL-FILHO, A. & D'ALBUQUERQUE, L. A. C. 2011. Islet Transplantation in Rodents: Do encapsulated islets really work? *Archives of Gastroenterology,* 48**,** 7.
STEEL, E. M., AZAR, J.-Y. & SUNDARARAGHAVAN, H. G. 2020. Electrospun hyaluronic acid-carbon nanotube nanofibers for neural engineering. *Materialia,* 9**,** 100581.
STEELE, J. A., HALLE, J. P., PONCELET, D. & NEUFELD, R. J. 2014. Therapeutic cell encapsulation techniques and applications in diabetes. *Adv Drug Deliv Rev,* 67-68**,** 74-83.
STEG, H., BUIZER, A. T., WOUDSTRA, W., VELDHUIZEN, A. G., BULSTRA, S. K., GRIJPMA, D. W. & KUIJER, R. 2016. Oxygen-releasing poly(trimethylene carbonate) microspheres for tissue engineering applications. *Polymers for Advanced Technologies*.
STEINECK, I., CEDERHOLM, J., ELIASSON, B., RAWSHANI, A., EEG-OLOFSSON, K., SVENSSON, A. M., ZETHELIUS, B., AVDIC, T., LANDIN-OLSSON, M., JENDLE, J., GUDBJORNSDOTTIR, S. & REGISTER, S. N. D. 2015. Insulin pump therapy, multiple daily injections, and cardiovascular mortality in 18 168 people with type 1 diabetes: observational study. *Bmj-British Medical Journal,* 350.
STEPHAN, M. T. & IRVINE, D. J. 2011. Enhancing cell therapies from the outside in: Cell surface engineering using synthetic nanomaterials. *Nano Today,* 6**,** 309-325.
STERN, R. 2004. Hyaluronan catabolism: a new metabolic pathway. *European Journal of Cell Biology,* 83**,** 317-325.
STOCK, A. A., MANZOLI, V., DE TONI, T., ABREU, M. M., POH, Y.-C., YE, L., ROOSE, A., PAGLIUCA, F. W., THANOS, C., RICORDI, C. & TOMEI, A. A. 2020. Conformal Coating of Stem Cell-Derived Islets for β Cell Replacement in Type 1 Diabetes. *Stem Cell Reports,* 14**,** 91-104.
SUISSA, S., HUTCHINSON, T., BROPHY, J. M. & KEZOUH, A. 2006. ACE-inhibitor use and the long-term risk of renal failure in diabetes. *Kidney International,* 69**,** 913-919.
SUMI, S. 2011. Regenerative medicine for insulin deficiency: creation of pancreatic islets and bioartificial pancreas. *Journal of Hepato-Biliary-Pancreatic Sciences,* 18**,** 6-12.

SUSZYNSKI, T. M., WILHELM, J. J., RADOSEVICH, D. M., BALAMURUGAN, A. N., SUTHERLAND, D. E. R., BEILMAN, G. J., DUNN, T. B., CHINNAKOTLA, S., PRUETT, T. L., VICKERS, S. M., HERING, B. J., PAPAS, K. K. & BELLIN, M. D. 2014. Islet Size Index as a Predictor of Outcomes in Clinical Islet Autotransplantation. *Transplantation,* 97**,** 1286-1291.

SZABAT, M., LYNN, F. C., HOFFMAN, B. G., KIEFFER, T. J., ALLAN, D. W. & JOHNSON, J. D. 2012. Maintenance of β-cell maturity and plasticity in the adult pancreas: developmental biology concepts in adult physiology. *Diabetes,* 61**,** 1365-1371.

TAKAHASHI, A., SUZUKI, Y., SUHARA, T., OMICHI, K., SHIMIZU, A., HASEGAWA, K., KOKUDO, N., OHTA, S. & ITO, T. 2013. In Situ Cross-Linkable Hydrogel of Hyaluronan Produced via Copper-Free Click Chemistry. *Biomacromolecules,* 14**,** 3581-3588.

TANVER, A., HUANG, M.-H., LUO, Y., KHALID, S. & HUSSAIN, T. 2015. Energetic interpenetrating polymer network based on orthogonal azido–alkyne click and polyurethane for potential solid propellant. *RSC Advances,* 5**,** 64478-64485.

TAPIA, G., BOAS, H., DE MUINCK, E. J., CINEK, O., STENE, L. C., TORJESEN, P. A., RASMUSSEN, T. & RONNINGEN, K. S. 2015. Saffold Virus, a Human Cardiovirus, and Risk of Persistent Islet Autoantibodies in the Longitudinal Birth Cohort Study MIDIA. *Plos One,* 10.

TERAMURA, Y., EKDAHL, K. N., FROMELL, K., NILSSON, B. & ISHIHARA, K. 2020. Potential of Cell Surface Engineering with Biocompatible Polymers for Biomedical Applications. *Langmuir,* 36**,** 12088-12106.

TERAMURA, Y. & IWATA, H. 2008. Islets surface modification prevents blood-mediated inflammatory responses. *Bioconjugate Chemistry,* 19**,** 1389-1395.

TERAMURA, Y., KANEDA, Y. & IWATA, H. 2007. Islet-encapsulation in ultra-thin layer-by-layer membranes of poly(vinyl alcohol) anchored to poly(ethylene glycol)-lipids in the cell membrane. *Biomaterials,* 28**,** 4818-4825.

TERAMURA, Y., KUROYAMA, K. & TAKAI, M. 2016. Influence of molecular weight of PEG chain on interaction between streptavidin and biotin-PEG-conjugated phospholipids studied with QCM-D. *Acta Biomaterialia,* 30**,** 135-143.

TESFAYE, S. 2014. Neuropathy in diabetes. *Medicine (Baltimore),* 43**,** 26-32.

TETKO, I. V., NOVOTARSKYI, S., SUSHKO, I., IVANOV, V., PETRENKO, A. E., DIEDEN, R., LEBON, F. & MATHIEU, B. 2013. Development of Dimethyl Sulfoxide Solubility Models Using 163 000 Molecules: Using a Domain Applicability Metric to Select More Reliable Predictions. *Journal of Chemical Information and Modeling,* 53**,** 1990-2000.

THEOCHARIS, A. D., SKANDALIS, S. S., GIALELI, C. & KARAMANOS, N. K. 2016. Extracellular matrix structure. *Adv Drug Deliv Rev,* 97**,** 4-27.

TIAN, C., ANSARI, M. J., PAEZ-CORTEZ, J., BAGLEY, J., GODWIN, J., DONNARUMMA, M., SAYEGH, M. H. & IACOMINI, J. 2007. Induction of robust diabetes resistance and prevention of recurrent type 1 diabetes following islet transplantation by gene therapy. *J Immunol,* 179**,** 6762-9.

TIAN, K., PRESTGARD, M. & TIWARI, A. 2014. A review of recent advances in nonenzymatic glucose sensors. *Materials Science and Engineering: C,* 41**,** 100-118.

TOMEI, A. A., MANZOLI, V., FRAKER, C. A., GIRALDO, J., VELLUTO, D., NAJJAR, M., PILEGGI, A., MOLANO, R. D., RICORDI, C., STABLER, C. L. & HUBBELL, J. A. 2014. Device design and materials optimization of conformal coating for islets of Langerhans. *Proceedings of the National Academy of Sciences,* 111**,** 10514-10519.

TOSO, C., VALLEE, J. P., MOREL, P., RIS, F., DEMUYLDER-MISCHLER, S., LEPETIT-COIFFE, M., MARANGON, N., SAUDEK, F., JAMES SHAPIRO, A. M., BOSCO, D. & BERNEY, T. 2008. Clinical magnetic resonance imaging of pancreatic islet grafts after iron nanoparticle labeling. *Am J Transplant,* 8**,** 701-6.

TOUCHET, T. J. & COSGRIFF-HERNANDEZ, E. M. 2016. 1 - Hierarchal structure–property relationships of segmented polyurethanes. *In:* COOPER, S. L. & GUAN, J. (eds.) *Advances in Polyurethane Biomaterials.* Woodhead Publishing.

TSE, H. M., KOZLOVSKAYA, V., KHARLAMPIEVA, E. & HUNTER, C. S. 2015. Minireview: Directed Differentiation and Encapsulation of Islet beta-Cells-Recent Advances and Future Considerations. *Mol Endocrinol,* 29**,** 1388-99.

TUCH;, B. E. & KANNANGARA, K. 2008. Beta Cell Regeneration. *Drug Discovery Today: Therapeutic Strategies,* 5**,** 7.

TUOMILEHTO, J. 2013. The Emerging Global Epidemic of Type 1 Diabetes. *Current Diabetes Reports,* 13**,** 795-804.

VAGESJO, E., CHRISTOFFERSSON, G., WALDEN, T. B., CARLSSON, P. O., ESSAND, M., KORSGREN, O. & PHILLIPSON, M. 2015. Immunological shielding by induced recruitment of regulatory T-lymphocytes delays rejection of islets transplanted in muscle. *Cell Transplant,* 24**,** 263-76.

VALACHOVA, K., BANASOVA, M., TOPOL'SKA, D., SASINKOVA, V., JURANEK, I., COLLINS, M. N. & SOLTES, L. 2015. Influence of tiopronin, captopril and levamisole therapeutics on the oxidative degradation of hyaluronan. *Carbohydrate Polymers,* 134**,** 516-523.

VALACHOVA, K., TOPOL'SKA, D., MENDICHI, R., COLLINS, M. N., SASINKOVA, V. & SOLTES, L. 2016. Hydrogen peroxide generation by the Weissberger biogenic oxidative system during hyaluronan degradation. *Carbohydrate Polymers,* 148**,** 189-193.

VAN DER WINDT, D. J., BOTTINO, R., KUMAR, G., WIJKSTROM, M., HARA, H., EZZELARAB, M., EKSER, B., PHELPS, C., MURASE, N., CASU, A., AYARES, D., LAKKIS, F. G., TRUCCO, M. & COOPER, D. K. C. 2012. Clinical Islet Xenotransplantation How Close Are We? *Diabetes,* 61**,** 3046-3055.

VANEPPS, J. S. & YOUNGER, J. G. 2016. Implantable Device-Related Infection. *Shock (Augusta, Ga.),* 46**,** 597-608.

VELTEN, F., LAUE, C. & SCHREZENMEIR, J. 1999. The effect of alginate and hyaluronate on the viability and function of immunoisolated neonatal rat islets. *Biomaterials,* 20**,** 2161-2167.

VENTURINI, M., MAFFI, P., QUERQUES, G., AGOSTINI, G., PIEMONTI, L., SIRONI, S., DE COBELLI, F., FIORINA, P., SECCHI, A. & DEL MASCHIO, A. 2015a. Hepatic steatosis after islet transplantation: Can ultrasound predict the clinical outcome? A longitudinal study in 108 patients. *Pharmacological Research,* 98**,** 52-59.

VENTURINI, M., MAFFI, P., QUERQUES, G., AGOSTINI, G., PIEMONTI, L., SIRONI, S., DE COBELLI, F., FIORINA, P., SECCHI, A. & DEL MASCHIO, A. 2015b. Hepatic steatosis after islet transplantation: Can ultrasound predict the clinical outcome? A longitudinal study in 108 patients. *Pharmacol Res,* 98**,** 52-9.

VENTURINI, M., SALLEMI, C., COLANTONI, C., AGOSTINI, G., BALZANO, G., ESPOSITO, A., SECCHI, A., DE COBELLI, F., FALCONI, M., PIEMONTI, L., MAFFI, P. & DEL MASCHIO, A. 2016. Single-centre experience of extending indications for percutaneous intraportal islet autotransplantation (PIPIAT) after pancreatic surgery to prevent diabetes: feasibility, radiological aspects, complications and clinical outcome. *Br J Radiol,* 89**,** 20160246.

VIGETTI, D., VIOLA, M., KAROUSOU, E., DELEONIBUS, S., KARAMANOU, K., DE LUCA, G. & PASSI, A. 2014. Epigenetics in extracellular matrix remodeling and hyaluronan metabolism. *FEBS J,* 281**,** 4980-92.

VIRK, S. A., DONAGHUE, K. C., WONG, T. Y. & CRAIG, M. E. 2015. Interventions for Diabetic Retinopathy in Type 1 Diabetes: Systematic Review and Meta-Analysis. *American Journal of Ophthalmology,* 160**,** 1055-1064.

WANG, H. Y., HUA, X. W., JIA, H. R., LIU, P. D., GU, N., CHEN, Z. & WU, F. G. 2016a. Enhanced cell membrane enrichment and subsequent cellular internalization of quantum dots via cell surface engineering: illuminating plasma membranes with quantum dots. *Journal of Materials Chemistry B,* 4**,** 834-843.

WANG, N., LIU, C., WANG, X., HE, T., LI, L., LIANG, X., WANG, L., SONG, L., WEI, Y., WU, Q. & GONG, C. 2019. Hyaluronic Acid Oligosaccharides Improve Myocardial Function

Reconstruction and Angiogenesis against Myocardial Infarction by Regulation of Macrophages. *Theranostics,* 9**,** 1980-1992.
WANG, P., SCHUETZ, C., ROSS, A., DAI, G., MARKMANN, J. F. & MOORE, A. 2013. Immune rejection after pancreatic islet cell transplantation: in vivo dual contrast-enhanced MR imaging in a mouse model. *Radiology,* 266**,** 822-30.
WANG, Q., CHENG, H., PENG, H. S., ZHOU, H., LI, P. Y. & LANGER, R. 2015a. Non-genetic engineering of cells for drug delivery and cell-based therapy. *Advanced Drug Delivery Reviews,* 91**,** 125-140.
WANG, Y., HAN, G., GUO, B. & HUANG, J. 2016b. Hyaluronan oligosaccharides promote diabetic wound healing by increasing angiogenesis. *Pharmacol Rep,* 68**,** 1126-1132.
WANG, Z. & THURMOND, D. C. 2009. Mechanisms of biphasic insulin-granule exocytosis – roles of the cytoskeleton, small GTPases and SNARE proteins. *Journal of Cell Science,* 122**,** 893-903.
WANG, Z., ZHAO, Y., JIANG, Y., LV, W., WU, L., WANG, B., LV, L., XU, Q. & XIN, H. 2015b. Enhanced anti-ischemic stroke of ZL006 by T7-conjugated PEGylated liposomes drug delivery system. *Scientific reports,* 5**,** 12651.
WATKINS, P. J. 2003. *Diabetes and its management,* Malden, Mass., Blackwell Science.
WATKINS, P. J. & WATKINS, P. J. 2003. *Diabetes and its management,* Malden, Mass., Blackwell Science.
WATKINS, R. A., EVANS-MOLINA, C., BLUM, J. S. & DIMEGLIO, L. A. 2014. Established and emerging biomarkers for the prediction of type 1 diabetes: a systematic review. *Transl Res,* 164**,** 110-21.
WEAVER, J. D. & STABLER, C. L. 2015. Antioxidant cerium oxide nanoparticle hydrogels for cellular encapsulation. *Acta Biomaterialia,* 16**,** 136-144.
WEBER, L. M., LOPEZ, C. G. & ANSETH, K. S. 2009. The effects of PEG hydrogel crosslinking density on protein diffusion and encapsulated islet survival and function. *Journal of biomedical materials research. Part A,* 90**,** 720-729.
WEETS, I., DE LEEUW, I. H., DU CAJU, M. V. L., ROOMAN, R., KEYMEULEN, B., MATHIEU, C., ROTTIERS, R., DAUBRESSE, J.-C., ROCOUR-BRUMIOUL, D., PIPELEERS, D. G. & GORUS, F. K. 2002. The Incidence of Type 1 Diabetes in the Age Group 0–39 Years Has Not Increased in Antwerp (Belgium) Between 1989 and 2000. *Diabetes Care,* 25**,** 840.
WEIR, G. C. 2013. Islet encapsulation: advances and obstacles. *Diabetologia,* 56**,** 1458-61.
WEIR, M. R., BARTLETT, S. T. & DRACHENBERG, C. B. 2012. Eosinophilia as an early indicator of pancreatic allograft rejection. *Clinical Transplantation,* 26**,** 238-241.
WEN, D., PENG, Y., LIU, D., WEIZMANN, Y. & MAHATO, R. I. 2016. Mesenchymal stem cell and derived exosome as small RNA carrier and Immunomodulator to improve islet transplantation. *J Control Release,* 238**,** 166-75.
WEST, D. C., HAMPSON, I. N., ARNOLD, F. & KUMAR, S. 1985. Angiogenesis induced by degradation products of hyaluronic acid. *Science,* 228**,** 1324-6.
WHO/IDF 2006. Definition and diagnosis of diabetes mellitus and intermediate hyperglycemia: report of a WHO/IDF consultation. Switzerland: Geneva.
WILHELM, J. J., BELLIN, M. D., DUNN, T. B., BALAMURUGAN, A. N., PRUETT, T. L., RADOSEVICH, D. M., CHINNAKOTLA, S., SCHWARZENBERG, S. J., FREEMAN, M. L., HERING, B. J., SUTHERLAND, D. E. R. & BEILMAN, G. J. 2013. Proposed Thresholds for Pancreatic Tissue Volume for Safe Intraportal Islet Autotransplantation After Total Pancreatectomy. *American Journal of Transplantation,* 13**,** 3183-3191.
WILLCOX, A., RICHARDSON, S. J., BONE, A. J., FOULIS, A. K. & MORGAN, N. G. 2009. Analysis of islet inflammation in human type 1 diabetes. *Clinical and experimental immunology,* 155**,** 173-181.
WILLIAMS, C. G., MALIK, A. N., KIM, T. K., MANSON, P. N. & ELISSEEFF, J. H. 2005. Variable cytocompatibility of six cell lines with photoinitiators used for polymerizing hydrogels and cell encapsulation. *Biomaterials,* 26**,** 1211-8.

WILSON, J. T., HALLER, C. A., QU, Z., CUI, W., URLAM, M. K. & CHAIKOF, E. L. 2010. Biomolecular surface engineering of pancreatic islets with thrombomodulin. *Acta Biomater,* 6**,** 1895-903.

WOERNER, S. 2014. The benefits of insulin pump therapy in children and adolescents with type 1 diabetes. *J Pediatr Nurs,* 29**,** 712-3.

WONG, C. S. & BADRI, K. H. 2012. Chemical Analyses of Palm Kernel Oil-Based Polyurethane Prepolymer. *Materials Sciences and Applications,* 3**,** 9.

WU, J., YANG, X., CHEN, B. & XU, X. 2015. Pancreas beta cell regeneration and type 1 diabetes (Review). *Exp Ther Med,* 9**,** 653-657.

XU, K. M., NARAYANAN, K., LEE, F., BAE, K. H., GAO, S. J. & KURISAWA, M. 2015a. Enzyme-mediated hyaluronic acid-tyramine hydrogels for the propagation of human embryonic stem cells in 3D. *Acta Biomaterialia,* 24**,** 159-171.

XU, L. Y., SHEYBANI, N., YEUDALL, W. A. & YANG, H. 2015b. The effect of photoinitiators on intracellular AKT signaling pathway in tissue engineering application. *Biomaterials Science,* 3**,** 250-255.

XU, M. H., QIAN, J. M., SUO, A. L., CUI, N., YAO, Y., XU, W. J., LIU, T. & WANG, H. J. 2015c. Co-delivery of doxorubicin and P-glycoprotein siRNA by multifunctional triblock copolymers for enhanced anticancer efficacy in breast cancer cells. *Journal of Materials Chemistry B,* 3**,** 2215-2228.

XU, M. H., QIAN, J. M., SUO, A. L., LIU, T., LIU, X. F. & WANG, H. J. 2015d. A reduction-dissociable PEG-b-PGAH-b-PEI triblock copolymer as a vehicle for targeted co-delivery of doxorubicin and P-gp siRNA. *Polymer Chemistry,* 6**,** 2445-2456.

XU, X., JHA, A. K., HARRINGTON, D. A., FARACH-CARSON, M. C. & JIA, X. Q. 2012. Hyaluronic acid-based hydrogels: from a natural polysaccharide to complex networks. *Soft Matter,* 8**,** 3280-3294.

XU, X. N., GUAN, X. N., ZHOU, H. H. & ZHU, Y. F. 2017. One-Step Reduction and Surface Modification of Graphene Oxide by 3-Hydroxy-2-Naphthoic Acid Hydrazide and Its Polypropylene Nanocomposites. *Nanomaterials,* 7.

YANG, H. K. & YOON, K. H. 2015. Current status of encapsulated islet transplantation. *J Diabetes Complications,* 29**,** 737-43.

YANG, J., ZHANG, L., YU, C., YANG, X. F. & WANG, H. 2014. Monocyte and macrophage differentiation: circulation inflammatory monocyte as biomarker for inflammatory diseases. *Biomark Res,* 2**,** 1.

YEUNG, W. C. G., AL-SHABEEB, A., PANG, C. N. I., WILKINS, M. R., CATTEAU, J., HOWARD, N. J., RAWLINSON, W. D. & CRAIG, M. E. 2012. Children With Islet Autoimmunity and Enterovirus Infection Demonstrate a Distinct Cytokine Profile. *Diabetes,* 61**,** 1500-1508.

YOSHIMATSU, G., SAKATA, N., TSUCHIYA, H., MINOWA, T., TAKEMURA, T., MORITA, H., HATA, T., FUKASE, M., AOKI, T., ISHIDA, M., MOTOI, F., NAITOH, T., KATAYOSE, Y., EGAWA, S. & UNNO, M. 2015. The Co-Transplantation of Bone Marrow Derived Mesenchymal Stem Cells Reduced Inflammation in Intramuscular Islet Transplantation. *Plos One,* 10.

ZAMBONI, F. & COLLINS, M. N. 2017. Cell based therapeutics in type 1 diabetes mellitus. *Int J Pharm,* 521**,** 346-356.

ZAMBONI, F., KEAYS, M., HAYES, S., ALBADARIN, A. B., WALKER, G. M., KIELY, P. A. & COLLINS, M. N. 2017. Enhanced cell viability in hyaluronic acid coated poly(lactic-co-glycolic acid) porous scaffolds within microfluidic channels. *Int J Pharm,* 532**,** 595-602.

ZAMBONI, F., OKOROAFOR, C., RYAN, M. P., PEMBROKE, J. T., STROZYK, M., CULEBRAS, M. & COLLINS, M. N. 2021. On the bacteriostatic activity of hyaluronic acid composite films. *Carbohydrate Polymers,* 260**,** 117803.

ZAMBONI, F., RYAN, E., CULEBRAS, M. & COLLINS, M. N. 2020. Labile crosslinked hyaluronic acid via urethane formation using bis(β-isocyanatoethyl) disulphide with tuneable physicochemical and immunomodulatory properties. *Carbohydrate Polymers,* 245**,** 116501.

ZAMBONI, F., VIEIRA, S., REIS, R. L., MIGUEL OLIVEIRA, J. & COLLINS, M. N. 2018a. The potential of hyaluronic acid in immunoprotection and immunomodulation: Chemistry, processing and function. *Progress in Materials Science,* 97**,** 97-122.

ZAMBONI, F., VIEIRA, S., REIS, R. L., OLIVEIRA, J. M. & COLLINS, M. N. 2018b. The potential of hyaluronic acid in immunoprotection and immunomodulation: Chemistry, processing and function. *Progress in Materials Science,* 97**,** 25.

ZHANG, P., ZHANG, X., BROWN, J., VISTISEN, D., SICREE, R., SHAW, J. & NICHOLS, G. 2010. Global healthcare expenditure on diabetes for 2010 and 2030. *Diabetes Research and Clinical Practice,* 87**,** 293-301.

ZHANG, W. J. & HE, X. M. 2011. Microencapsulating and Banking Living Cells for Cell-Based Medicine. *Journal of Healthcare Engineering,* 2**,** 427-446.

ZHANG, Y. C., PILEGGI, A., AGARWAL, A., MOLANO, R. D., POWERS, M., BRUSKO, T., WASSERFALL, C., GOUDY, K., ZAHR, E., POGGIOLI, R., SCOTT-JORGENSEN, M., CAMPBELL-THOMPSON, M., CRAWFORD, J. M., NICK, H., FLOTTE, T., ELLIS, T. M., RICORDI, C., INVERARDI, L. & ATKINSON, M. A. 2003. Adeno-associated virus-mediated IL-10 gene therapy inhibits diabetes recurrence in syngeneic islet cell transplantation of NOD mice. *Diabetes,* 52**,** 708-16.

ZHI, Z. L., KERBY, A., KING, A. J., JONES, P. M. & PICKUP, J. C. 2012. Nano-scale encapsulation enhances allograft survival and function of islets transplanted in a mouse model of diabetes. *Diabetologia,* 55**,** 1081-90.

ZHI, Z. L., KHAN, F. & PICKUP, J. C. 2013. Multilayer nanoencapsulation: a nanomedicine technology for diabetes research and management. *Diabetes Res Clin Pract,* 100**,** 162-9.

ZHI, Z. L., LIU, B., JONES, P. M. & PICKUP, J. C. 2010. Polysaccharide multilayer nanoencapsulation of insulin-producing beta-cells grown as pseudoislets for potential cellular delivery of insulin. *Biomacromolecules,* 11**,** 610-6.

ZHI, Z. L., SINGH, J., AUSTIN, A. L., HOPE, D. C., KING, A. J., PERSAUD, S. J. & JONES, P. M. 2015. Assembly of bioactive multilayered nanocoatings on pancreatic islet cells: incorporation of alpha1-antitrypsin into the coatings. *Chem Commun (Camb),* 51**,** 10652-5.

ZHUO, F., ELIZABETH, R. G. & DONGMIN, L. 2013. Regulation of Insulin Synthesis and Secretion and Pancreatic Beta-Cell Dysfunction in Diabetes. *Current Diabetes Reviews,* 9**,** 25-53.

ZIEGLER, A. G., BONIFACIO, E. & GRP, B.-B. S. 2012. Age-related islet autoantibody incidence in offspring of patients with type 1 diabetes. *Diabetologia,* 55**,** 1937-1943.

ZIOLKOWSKI, A. F., POPP, S. K., FREEMAN, C., PARISH, C. R. & SIMEONOVIC, C. J. 2012. Heparan sulfate and heparanase play key roles in mouse beta cell survival and autoimmune diabetes. *J Clin Invest,* 122**,** 132-41.